The geomechanical behaviour of peat foundations below rail-track structures

A Thesis Submitted to the College of Graduate Studies and Research in Partial Fulfillment of the Degree of Doctor of Philosophy in the Department of Civil Engineering,

University of Saskatchewan, Saskatoon, Canada

By

Michael Thomson Hendry

Permission to Use

In presenting this thesis in partial fulfillment of the requirements for a Postgraduate degree from the University of Saskatchewan, I agree that the Libraries of this University may make it freely available for inspection. I further agree that the permission for copying of this thesis in any manner, in whole or in part, for the scholarly purposes may be granted by the professor or professors who supervised my thesis work or, in their absence, by the Head of the Department or the Dean of the College in which my thesis work was done. It is understood that any copying or publication or use of this thesis or parts thereof for financial gain shall not be allowed without my written permission. It is also understood that due recognition shall be given to me and the University of Saskatchewan in any scholarly use which may be made of any material in my thesis.

Requests for permission to copy or to make other use of material in this thesis in whole or part should be addressed to:

Head of the Department of Civil Engineering,
University of Saskatchewan,
Saskatoon, Saskatchewan
Canada, S7N 0W0

Abstract

This thesis presents the results of research conducted to define the response of peat foundations underlying railway embankments to heavy axle loads. Three field sites were investigated, two in Northern Alberta on Canadian National Railway's Edson and Lac-La-Biche subdivisions, and one on the Lévis subdivision in southern Quebec. The scope of this thesis is fourfold: the development and installation of instrumentation; the laboratory testing of peat specimens retrieved from each site; the development of a conceptual model for the behaviour of peat beneath an embankment subjected to heavy axle loads; and finally, the modelling of the strength of the peat foundations relative to the applied loads.

The first component of this research included the development and installation of instrumentation to measure *in situ* the distribution and magnitude of strain and pore pressure generation. The development included the assembly of instrumentation systems to measure all of the required parameters, and the development of the ShapeAccelArray^{TM} (SAA) from Measurand Inc. to measure horizontal cyclic motion under train loading. It was found the SAA, as provided by the manufacturer, was not able to provide accurate measurements of displacement. A method for determining the magnitude of cyclic displacement from the output of the MEMS accelerometers was developed from the laboratory testing data done as part of this study. This resulted in the ability to obtain a profile of cyclic displacement with depth.

The second component of the research was the laboratory testing of peat specimens retrieved from the sites. Consolidated undrained triaxial tests and direct shear tests were conducted on remoulded peat, remoulded peat fibre and Shelby specimens of peat to investigate the fundamental mechanisms which control the strength of peat. The results were analyzed within the frameworks of elastic behaviour of cross-anisotropic materials and shear strength of fibre-reinforced soil. The test results from samples collected at all three sites were compared and the influence of peat fibres on the undrained strength was explored.

The third component was the development of conceptual models for the undrained behaviour of peat, and peat foundations subjected to moving axle loads. A model for peat was developed from the cross-anisotropic response observed during the laboratory testing and correlations to fibre reinforced soil literature. This material model was then applied to the spatial distribution of stresses and orientation of principal stresses below embankments.

The final component of the project was an analysis of the field data collected from all three sites to provide the magnitude and distribution of strain and pore pressure generation developed within the peat foundations. Further analysis of the measured response was conducted with both with calculations of effective stress paths and finite element modelling to determine the distribution of stress, the locations of potential yielding within the foundations and to determine how close to yielding the peat is under the maximum applied stresses.

The results of this thesis provide new tools for the railway industry to evaluate the response and stability of railway embankments over peat foundations. The development of the SAA allows for the *in situ* measurement of the magnitude and distribution of displacement, and from this the strain, within soft soils under heavy axle loading. The conceptual models developed and applied to the undrained response of peat foundations provide a framework to evaluate the stability of railway embankments over soft foundations. The results of the application of this framework to the study sites included in this thesis provide context for further investigations.

Manuscript Based Thesis

This is a manuscript-style Ph.D. thesis; it has been assembled in the format determined by the Department of Civil & Geological Engineering Graduate Affairs Committee. The Department of Civil & Geological Engineering allows a PhD. Thesis in which several of the chapters have been written in journal manuscript format and have either been published, or intended for publication as peer-reviewed journal articles. At the time of the submission of this thesis the requirement that at least one of the papers should be accepted for publication has been met. In addition to the journal papers, additional chapters provide an introduction to the thesis, a review of the relevant literature and a summary of conclusions and recommendations. Due to the format of the thesis there is some repetition among the different manuscripts, and between the manuscripts and other chapters.

At the time of the publication of this thesis the status of the manuscripts are as follows:

"An evaluation of real-time deformation monitoring using motion capture instrumentation and its application in monitoring railway foundations." (Chapter 3; Manuscript #1). Status: published by the ASTM Journal of Geotechical Testing.

"Effect of fibre content and structure on anisotropic elastic stiffness and shear strength of peat." (Chapter 4; Manuscript #2). Status: accepted for publication by the Canadian Geotechnical Journal.

"The variability and net effect of the stiffness and strength derived from the fibrous nature of peat." (Chapter 5; Manuscript #3). Status: To be submitted to the Journal of Geotechnical and Geoenviromental Engineering. The contents of this Manuscript relies on the citation of the data and analysis conducted in Manuscript #2, and will be submitted upon the publication of Manuscript #2.

"The measurement of the cyclic response and strength of railway embankments and underlying soft peat foundations to heavy axle loads." (Chapter 6; Manuscript #4). Status: To be submitted to Geotechnique. The content of this Manuscript relies on the citation of the strength parameters and constitutive model developed in Manuscript #3, and will be submitted upon the publication of Manuscript #3.

Acknowledgements

The completion of this thesis would not have been made possible without the support and help of various organizations and people. In particular, the industry representatives involved with the Railway Ground Hazard Research Program: Chris Bunce (Canadian Pacific Railway), Tom Edwards (Canadian National Railway) and Mario Ruel (Canadian National Railway). This research was made possible through funding provided by the Natural Sciences and Engineering Research Council of Canada (NSERC), Canadian Pacific Railway, Canadian National Railway, and Transport Canada.

I owe special thanks Tom Edwards for his personal support and involvement with this project. Tom spent a lot of his time to make our site installations a success. Without Tom this research would not have happened.

I am grateful to both of my supervisors. To Dr. Lee Barbour patiently guided me through my graduate studies; and Dr. Derek Martin who has provided me with such great opportunities.

And of course, my family. My wife, Nadine, has always supported me in pursuing my unending education; and my career aspirations. My son, Daniel, whose arrival made me determined to wrap this up.

To my son Daniel "The End"

Table of Contents

List of Tables

Chapter Two

Chapter Four

Chapter Five

List of Figures

Chapter One

Chapter Two

Chapter Three

Chapter Four

Chapter Five

Chapter Six

Chapter One: Introduction

The majority of the existing railway structures in Canada have been in service for nearly a century. In the time since they were constructed railway loads have more than tripled, from 40 to 131.5 tonnes per axle for freight cars. These increasing loads have put increasing demands on the existing infrastructure, particularly the structures built upon weak foundations. The least understood of the weak foundation materials is peat.

Both of the major Canadian railways (Canadian National Railway and Canadian Pacific Railway) have experienced ongoing problems with embankments built over peat foundations. The recent reacquisition of the Athabasca Northern Railway from Lac-La-Biche to Fort McMurray, Alberta and the Mackenzie Northern Railway to Hay River, North West Territories by Canadian National Railway (CN) has made this problem more critical since both of these lines include large stretches of embankments over peat.

The current research program was initiated following the investigation of the failure of a railway embankment on peat foundations on the Lévis subdivision in south-western Quebec. This research program has been expanded to a total of three sites and includes field monitoring, sampling and laboratory testing programs. The goal of the overall research program was: first to develop an understanding of the response and strength of peat foundations subjected to heavy axle loads through *in situ* measurements and laboratory testing; and secondly to evaluate differing remediation methods.

This focus of this thesis is the first part of the research program. This work was undertaken in three parts; i) instrumentation of sites to measure the response of the peat foundations to heavy axle loads, including the development of new instrumentation for this purpose; ii) laboratory evaluation of the constitutive behaviour of peat using peat samples collected from these sites;

and iii) an evaluation of reaction and strength of the peat foundations under heavy axle loads based on finite element modelling, and the measured response of the peat interpreted with the developed constitutive model.

1.1 Description of the Sites

This study includes the results from three instrumented railway embankments over peat, two located in Alberta and one in Quebec (Figure 1.1).The sites selected for investigation were provided by CN and were selected based on either a history of maintenance issues, as a result of new traffic loads, or new construction. The sites included in this study all have approximately 3 m of intact soft peat foundations supporting the railway embankments. The sites vary in the method of embankment construction and the consistency and degree of humification of the peat.

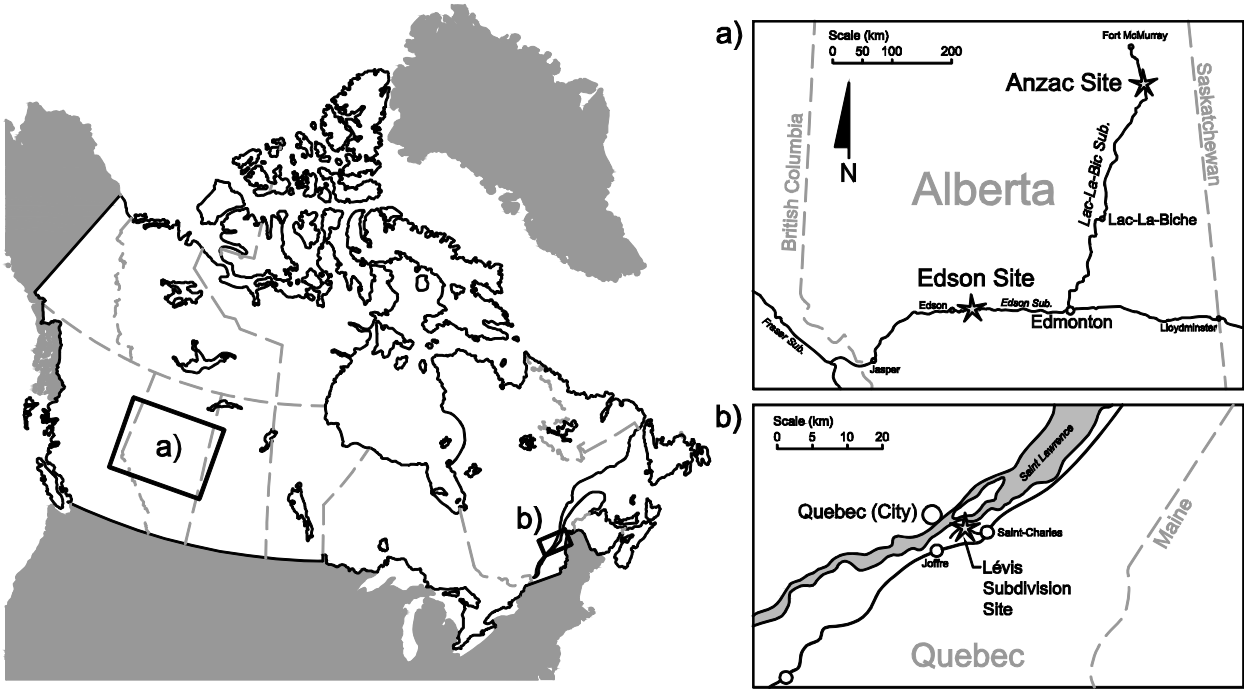

Figure 1.1 : Location of CN sites included in this study in a) Alberta, and b) Quebec.

1.1.1 Edson subdivision mile 102.0

This site is referred to throughout this document as the Edson site. The Edson site is located at mile 102.0 of the Edson subdivision near the town of Niton Junction, Alberta, on CN's mainline. The aerial photograph in Figure 1.2 shows the railway embankment crossing the peat bog from mile 101.3 to 102.6. The boundaries of the peat bog are delineated by changes in vegetation with

the peat area appearing to have a smoother texture. South of the railway line is a circular lake. This lake is indicative of a peat bog formation process referred to as terrestrialization in which shallow lakes are filled from their periphery towards the center leaving a circular lake of open water (Section 2.1).

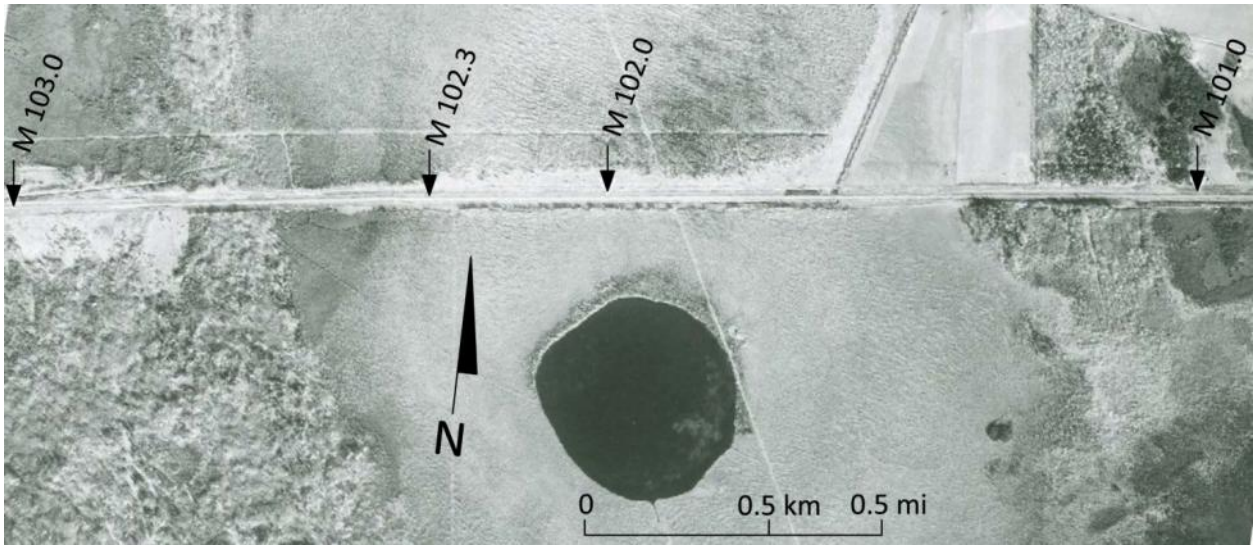

Figure 1.2 : Arial photograph of the Edson Subdivision peat bog crossing. Instrumentation installed at Mile 102.0.

This embankment was constructed as part of the Grand Trunk Railway between 1909 and 1912 (Lester 2005). The embankment was constructed on the original peat surface using a timber raft (corduroy) construction. This timber raft construction method was common for railway embankments over peat, and served to reinforce the base of the embankment and spread the load over the peat foundation (MacFarlane 1969). Figure 1.3 shows a picture of the construction of a similar embankment over soft peat foundations, with logs lying perpendicular to the embankment placed upon stringers.

The Edson site has required significant amounts of maintenance over its operating life with sections of the embankment remediated in 1998. This remediation included the addition of gravel berms on both sides of the embankment[1], and the driving of timber piles[2] under the track

[1] The results from the modelling of the effect of the addition of berms on the stress state of the peat beneath the embankment is presented in Appendix D: Section D.3.

between miles[3] 102.2 and 102.6. From toe to toe the embankment and berms are now 23 m in width.

Figure 1.3 : Use of timber raft (corduroy) construction for an embankment over peat subgrade (MacFarlane 1969).

1.1.2 Lac La Biche subdivision mile 263.9

This site is referred to as the Anzac site throughout this document. This site is located at mile 263.9 of the Lac-la-Biche (formerly Waterways) subdivision, near the town of Anzac, Alberta. This line was originally constructed between 1916 and 1918 (Lester 2005). This subdivision runs from the mainline, near Edmonton, to Fort McMurray, Alberta (Figure 1.1). CN has recently reacquired the Fort McMurray to Lac-La-Biche section of the Lac-La-Biche subdivision from the

---

[2] The effect of the installation of the timber piles beneath the embankment was measured and presented in the conference paper titled "Assessing the Condition of Peat Subrades Subjected to Heavy Axle Loads: Effectiveness of the use of Piles to Strengthen Embankments." Presented in Appendix E.

[3] Locations along Canadian railway track are described using milepost markers and the units of 'miles'. Though not in SI units this is the standard for the industry and is accepted and used by the governmental regulators such as the Transportation Safety Board and Transport Canada. This standard was used within this thesis to describe the locations of the study sites to ensure that these sites can readily be found.

short-haul operator, Athabasca Northern Railway and Lakeland & Waterways Railway. An aerial photograph of the site is presented in Figure 1.4. The site is located in a large area of wetlands and peat. A bridge required to cross a very soft section of peat south of the site at mile 263.5 is also visible in Figure 1.4.

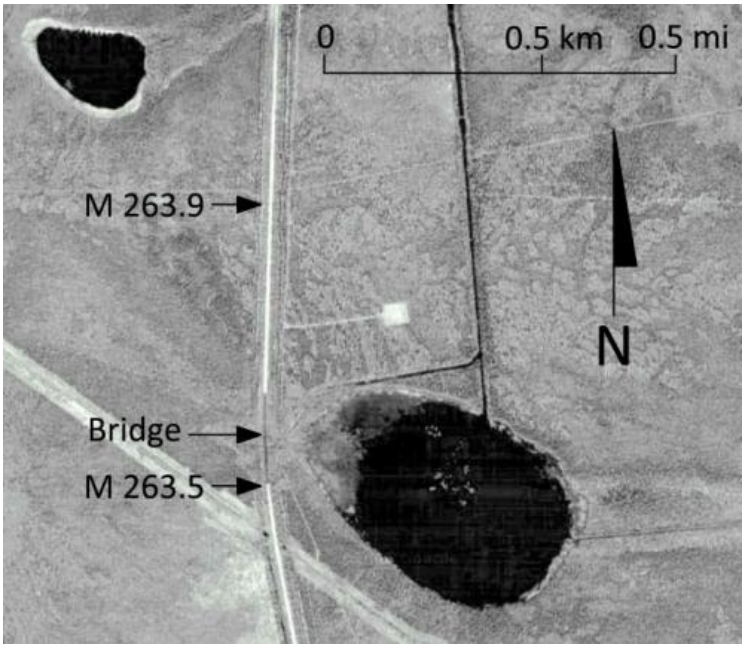

Figure 1.4 : Arial photograph of the Anzac Subdivision peat bog crossing. Instrumentation installed at Mile 263.9

The line was in an inoperable condition in 2007 and the previous operators were set to abandon the line. Since reacquiring the line CN has invested approximately $135 million in improvements to to allow heavy trains to safely average 40 km/h between Fort McMurray and Edmonton (Figure 1.5). The long-term objective is to increase traffic from the current rate of two to three trains per week, up to ten trains per day. The goal of this investment is “the pipeline on rails” concept which would allow trains of 100 or more tank cars to deliver oil to Gulf of Mexico refineries in eight to 10 days (Alberta Oil 2009). The subdivision is estimated to have more than 75 miles of embankments over peat; consequently understanding the impact heavy axle loads on peat is critical to CN’s upgrade of this line for increased traffic.

1.1.3 Lévis subdivision mile 3.9

This site is referred to throughout this document as the Lévis site. The Lévis subdivision is located near the south shore of the St. Lawrence River, across from Quebec City (Figure 1.1).

The embankment was originally constructed in between 1879 and 1884. The wetland associated with this peat area is considered to be an environmentally sensitive area, and there is significant public pressure to preserve it. Two derailments have occurred at this site, the first in 1999 and the second in 2004. The first derailment was attributed to rail movement due to the soft (peat) subgrade that resulted in high lateral forces and the failure of track components (TSB 1999). The second derailment was caused by an embankment and subgrade failure which resulted in the spilling of 200,000 L of fuel into the wetland area. Following the derailment in 1999 and before the embankment failure in 2004 significant rehabilitation work was done to reinforce the roadbed between Mile 3 and Mile 5.9 including an increase in the ballast depth and the addition of a berm and new ditch north-east side of the track (TSB 2008). The 2004 embankment failure is described in more detail in Section 2.7.4. This investigation included the study presented in Konrad et al. (2007) and in a detailed TSB report (TSB 2008). The data gathered during the course of this study (Konrad et al. 2006; Konrad et al. 2007; TSB 2008) is utilized in this thesis and compared to the data gathered from the other two study sites.

Figure 1.5 : Before and after photos showing the rehabilitation and upgrades conducted on the Lac-La-Biche subdivision (after Alberta Oil, 2009).

1.2 Description of Problem

The major railways have experienced problems with embankments built over peat foundations since their construction. The performance of railway embankments over peat has become a more critical concern to CN following their acquisition of the Athabasca Northern Railway from Lac-La-Biche to Fort McMurray (now part of the Lac-La-Biche Subdivision), Alberta and the Mackenzie Northern Railway to Hay River, North West Territories. Both of these lines are northern railways with large stretches of peat crossings.

The recent investigation of the catastrophic failure at the Lévis subdivision (Section 1.1.3) suggested that the increase in axle loads and traffic lead a progressive settlement of the embankment which resulted in reorientation of peat fibres and the loss of the strength associated with the fibres (Konrad et al. 2007, TSB 2008). The study also highlighted that the response of peat to heavy axle loads is as yet poorly understood and further study is required.

Traffic and axle loads are increasing on most railway lines in Canada, as CN and CP continue to build and expand sidings[4] on mainlines to allow for increased train lengths and train traffic. The failure at the Lévis subdivision as well as increasing maintenance costs have highlighted the need to develop a more fundamental understanding of the response of peat to heavy axle loads.

1.3 Research Objectives

The global objectives of this research are: first, to develop an understanding of the mechanisms that govern the spatial and temporal distribution of stress, strain and pore pressure within the cyclically loaded peat foundation of a railway embankment; and second, to determine the implications of these mechanisms on the strength and stability of these structures. This understanding is to be applied to future modelling and the assessment of the effectiveness of remediation methods. The specific objectives of this thesis are:

1. To develop and install an instrumentation system to observe and evaluate the spatial and temporal distribution of pore pressure generation and strain within the peat foundation material.

2. To conduct laboratory testing of samples collected from these sites to determine the undrained elastic response and strength of peat, inclusive of the effect of the fibrous nature and *in situ* structure.

[4] Most railway lines in Canada consist of single track; a 'siding' is a short length of track constructed beside the main track which allows trains travelling in opposite directions to pass. The lengths of trains which can be placed in the siding are limited by the length of the siding.

3. To develop a theoretical and analytical interpretation of the observed deformations and pore-pressure responses with a particular focus on the elastic (reversible) deformation of the embankments and foundations.

4. To conduct an analysis of the strength of the peat foundations at all three sites based on results of the conceptual model developed, the undrained elastic response peat and the interpretation of the observed deformations and pore-pressure responses.

1.4 Overview of Thesis

The thesis consists of eight chapters including this first introductory chapter. Chapter Two presents the necessary literature review for this study. Chapter Three (Manuscript #1) presents the development of the instrumentation required for *in situ* field measurements of the response of peat foundations to heavy axle loading. Chapter Four (Manuscript #2) presents the laboratory testing conducted on peat to characterise the anisotropic elastic response and strength of the peat. Chapter Five (Manuscript #3) presents a comparison of the undrained response and strength of the peat from all three sites, an analysis on the net effect of the fibrous nature of peat on these properties, and the development of a conceptual model the behaviour of peat. Chapter Six (Manuscript #4) presents the measured *in situ* response of the peat foundations, develops a conceptual model for the behaviour of peat foundation subjected to moving heavy axle loads, and evaluates the strength of these foundations with finite element modelling and an analysis of the measured data. Chapters Seven provides a summary of the results and recommendations.

Chapter Two: Literature Review

This chapter provides background information and a review of the literature published on topics related to this project. The literature review is divided into several parts:

- The morphology and classification of peat.
- The (geotechnical) engineering properties of peat.
- The (geotechnical) engineering properties of fibre reinforced soils.
- A description of a typical rail track structure and modes of deterioration.
- A description of the response of soils to train loading.
- A review of previous studies of embankments over peat foundations.
- A review of elastic and elastic anisotropic soil models.
- Instrumentation used for field measurements of soil response to loading.

2.1 Morphology and Classification of Peat

Canada has more peat lands than any other country in the world, covering 18 % of the land area, primarily in northern areas of the country (Hobbs 1986) (Figure 2.1). As resource and infrastructure development continues to expand, particularly in northern Canada, it is anticipated that the number of engineering projects involving peat will only increase.

The common view of peat in geotechnical engineering is that it should be avoided as a foundation material whenever possible. However, avoidance is not always an option, particularly for linear, continuous structures such as those required for railways, pipelines and roads. Peat foundations pose unique problems for construction and maintenance of railway infrastructure. A strong understanding of the complexities of material behaviour and genesis of the peat is required.

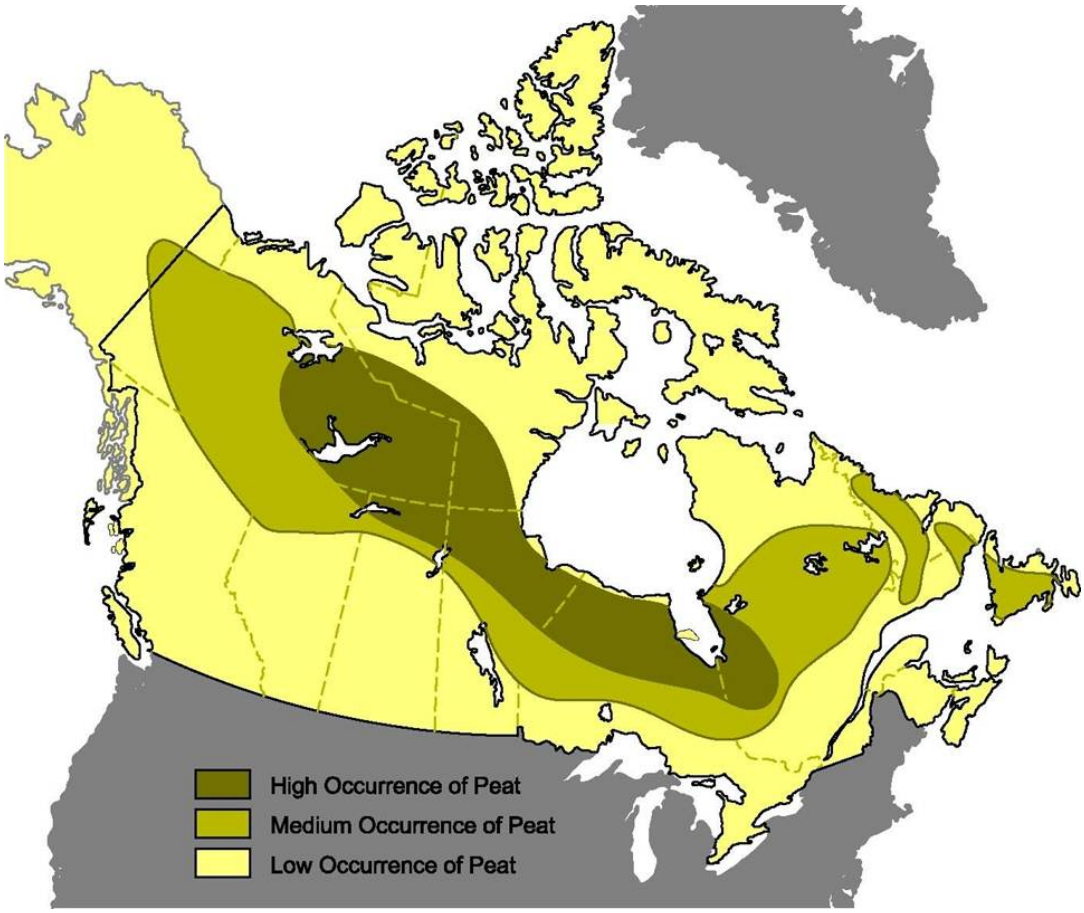

Figure 2.1 : Map showing distribution of peat lands within Canada, with high concentrations in northern areas (after MacFarlane 1969).

The composition and morphology of peat are integral to an understanding of its engineering properties. Peat forms on both raised and depressed terrain. With sufficient precipitation, peat can form as raised bogs on elevated terrain such as hillsides, as found in the British Isles and on the west coast of Canada. The formation of peat bogs in poorly drained depressions, small lakes, or the periphery of larger lakes is more common within the interior of Canada. The formation of peat bogs occurs by the process of terrestrialization. This process starts at the margins of a shallow body of water, and due to the acidity, anoxic conditions, and temperature of the water, the decay of the plant material is slowed to a pace at which it begins to accumulate and fill in the lake (Hobbs 1986). This results in a range of peat formations depending on the type of accumulated plant material, the state of decay and the access to oxygen. As the depth of the peat formation increases the vertical stresses on the peat increase, resulting in compression of the peat. These large vertical strains cause the plant fibres which compose a large component of the peat to align in the horizontal direction (Landva and Pheeney 1980).

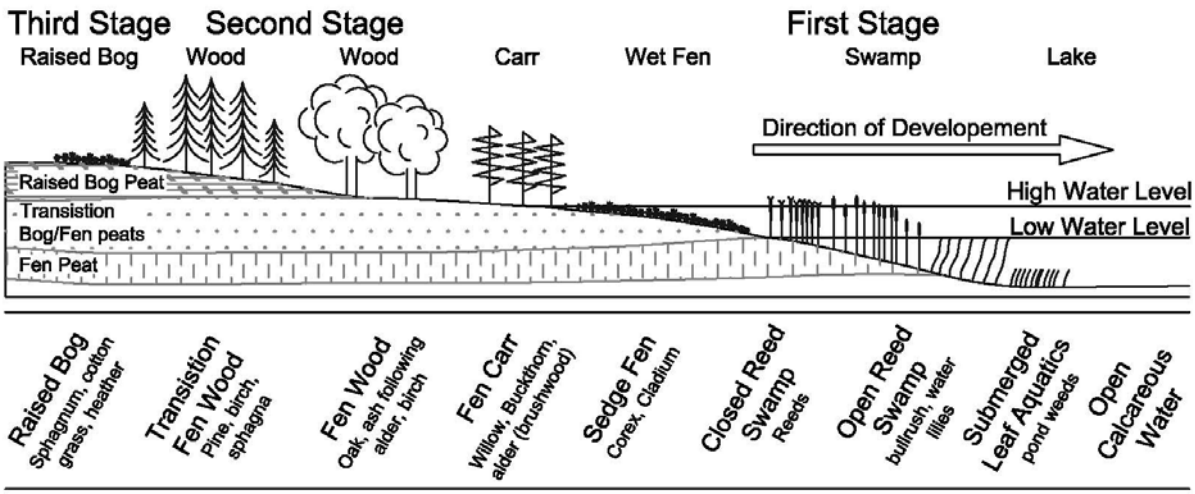

Figure 2.2 : Vegetation and peat succession in the filling of a lake (after Hobbs 1986) Note: raised bog starts in centre of a lake after it is filled but is shown in the figure at the lake margin for convenience.

The form of the peat in any deposit will vary with depth. The acrotelm is the upper 10-60 cm of a peat formation, defined as the aerobic zone, and typically consists of plant or forest litter. Below the acrotelm is the catotelm that extends to the base of the peat mire and is often of most concern in geotechnical engineering, as it forms the majority of the peat. The catotelm has a much lower hydraulic conductivity, higher compressibility and lower strength than the acrotelm.

Historically, there have been two methods used to classify peat in Canada; the Radforth classification and the von Post classification. The Radforth system is based on visible structure with the engineering properties estimated from this structure. The Radforth system is derived from a wealth of experience with Canadian peat, and has only been adopted in Canada (Hobbs 1986). The peat for which the Radforth classification system was developed is referred to as Radforth Peat; peats with very high organic contents (Landva and La Rochelle 1983). The von Post system is a more extensive classification method and forms the basis for the American Society for Testing and Materials (ASTM) standards for the classification and testing of peat and peaty organic soils (ASTM D4427). The von Post system is a testable classification of the physical peat properties, some of which have shown strong correlations to the engineering properties. These physical properties include: the extent of humification (decay of plant mater) (ASTM D5715), the predominant plant, the content of fibres (ASTM D1997), and the presence of wood and shrub remains. Other ASTM standards used in the classification include bulk unit

weight/density (ASTM D4531), water content (ASTM D2974), specific gravity (ASTM D854), pH (ASTM D2976), and Atterberg limits (ASTM D4318). It should be noted that the Atterberg limits are not applicable to all types of peat as liquid and plastic limits cannot be determined for the more fibrous peats (Hobbs 1986).

2.2 Engineering properties of peat

Hobbs (1986) describes peat as an "ordinary extraordinary material". This phrases highlights the fact that peat exhibits similar traits and correlations between engineering properties and classification properties as mineral (particulate) soils (and thus ordinary); but with values for these properties that are greatly different from mineral soils (thus extraordinary). One example of this is the strength of peat, which is remarkably high given its exceptionally high water content and liquid limit. Peat also demonstrates a high degree of variability spatially as well as between different formations within a single peatland (Hobbs 1986; Elsayed 2003).

2.2.1 Water Content

Gravimetric water content is defined as the ratio of the mass of water to the mass of solids. The water content of peat can often range from 200 to as high as 2,000 % (Hobbs 1986). This measure of water content is highly variable, and magnifies the difference in the water content between two specimens with increasing water content. Alternatively, the water content can be expressed as a ratio of the mass of water to the total mass of the peat. With this definition of water content the computed values become less sensitive to the small variations in the measured dry mass, and the values typically ranges from to 67 to 95%.

2.2.2 Hydraulic Conductivity

The hydraulic conductivity of peat is highly dependent on the depth and the degree of humification. The acrotelm is typically highly permeable while the catotelm has a much lower hydraulic conductivity. Hogan et al. (2006) undertook field-based measurements of the hydraulic properties of a Boreal Fen consisting of non-Sphagnum mosses and found values of hydraulic conductivity as high as 9.0×10^{-3} m/s near the surface, decreasing to 10^{-6} to 10^{-5} m/s below a depth of 2 m.

The structure of peat is such that when fibrous peat is consolidated, the channels through which water flows collapse as the water is forced out. Once consolidated, peat will undergo very large decreases in hydraulic conductivity commensurate with a large decrease in void ratio (or water content). The hydraulic conductivity of fibrous peat has been shown in testing to decline by three orders of magnitude with the reduction of the void ratio by one half. (Ingram 1983; Hobbs 1986)

2.2.3 Consolidation and Compression

The high water content of peat makes the deposit susceptible to large volume changes. The structure of the peat causes water to be held in three distinct phases: inter-particle water, intercellular water (macropores) and adsorbed or bound water (held in micropores). The distribution of the water within these phases determines the manner in which pore water is held and expelled during 'primary' consolidation and 'secondary' compression. The proportion of water stored in each phase depends on the structure and degree of humification of the peat. Volume changes within the micropores and macropores dominate consolidation in more fibrous, less humified peat. In highly humified (decomposed) amorphous peat with very few micropores or macropores the inter-particle water dominates consolidation (Hobbs 1986; Mesri 2007).

The initial phase in the consolidation of peat includes the expulsion of water and the simultaneous rearrangement of the particles and structure of the peat. This continues until there is a dissipation of the pore pressure. Following this initial consolidation, volume change continues in a creep like process as the peat structure continues to undergo rearrangement and water is expelled almost exclusively from the micropores in the organic structures. The consolidation of peat does not conform to Terzaghi's theory of consolidation, as there is a simultaneous expulsion of water, restructuring, and a rapid reduction in hydraulic conductivity during consolidation. The terminology used for the consolidation of mineral soils such as primary consolidation for the initial phase and secondary compression for the creep like behaviour, are used with caution for peat. The boundary between these two phases is often only distinguishable from pore-pressure measurements to determine when the pore water pressure generated due to the applied load has fully dissipated (Hobbs 1986; Mesri 2007). The primary consolidation of peat occurs rapidly due to its initial high hydraulic conductivity and can be measured in weeks and months. The duration of the secondary compression of peat is measured in years, much longer than primary consolidation. Weber (1969) reported significant linear

secondary settlement under embankments constructed over peat deposits in San Francisco Bay for 25 years. The magnitude and the rates of secondary compression are high, and may in the end account for more than 60% of the total settlement (MacFarlane 1965; Elsayed 2003). Secondary compression is often the dominant consolidation process.

2.2.4 Strength and Stiffness

The strength and stiffness of a peat are a function of factors such as: the presence of organic fibre layers and fibre properties as controlled by the source plant species and the degree of humification. These plant fibres act to reinforce the structure of the peat.

The measured strength of peat is dependent on the test method. Triaxial testing of fibrous peat results in high values of effective angles of friction (ϕ') as high as 48˚ to 68˚ (Landva and Rochelle 1983; Farrell and Hebib 1998; Hebib 2001; Long 2005). Direct shear testing and ring shear testing of peats result in lower values which have been found to range between 20˚ and 38˚ (Farrell and Hebib 1998; Hebib 2001). The differing values of the strength have been attributed to the reinforcing effect of the peat fibres, with the triaxial testing providing a measurement of the strength inclusive of this reinforcing effect. The ring and direct shear testing results provide a frictional strength that is indicative of the frictional resistance generated between the particulate and fibrous materials (Landva and Rochelle 1983; Farrell and Hebib 1998; Hebib 2001). The magnitude of the reinforcing effect of the fibres at yielding can be determined from a comparison of the yield surface defined by testing which includes the reinforcing effect (triaxial testing) to the yield surface defined by testing which measures the strength derived from friction between the particles and fibres (ring or direct shear testing) (Landva and Rochelle 1983). The reinforcing effect is represented by an internal reinforcing stress (σ_{FR}) that acts to reduce the shear stress applied to the peat, thus increasing the shear stress which the peat can bear (Figure 2.3).

The predominantly horizontal directionality to the fibres also results in strength anisotropy. Within the study presented in Yamaguchi et al. (1985) values of ϕ' of 51° to 55° were measured for vertically orientated specimens when the specimen axis was perpendicular to the horizontal plane of the fibres. This decreased to 35° for specimens with the axis of the sample aligned in the horizontal plane. This reinforcing effect is thought to be a result of tension generated in the fibres of peat (Den Haan 1997; Yamaguchi et al. 1985). The reinforcing effect of fibres within a

soil is further explored in section 2.3 with a review of fibre reinforced soils. Yamaguchi et al. (1985) showed that strength increases with increasing organic content.

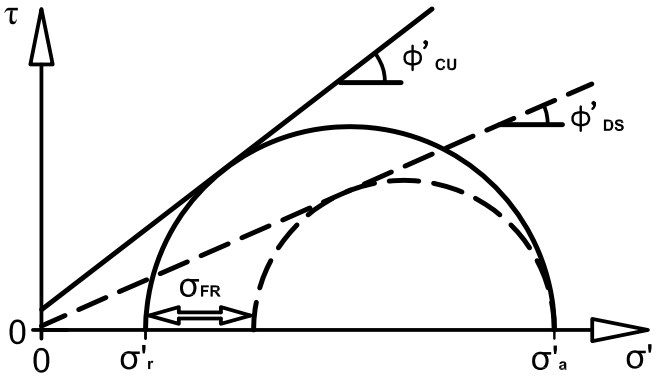

Figure 2.3 : Model for the calculation of the reinforcing effect of the fibres in peat on the strength of peat as an internal reinforcing stress (σ_{FR}).

Both the volumetric and shear deformation of peat can influence the observed strength. The dependency of peat on the interlocking of fibres for its strength results in the requirement for large strains to mobilize the full strength of the peat (Mesri 2007). Consolidation is a common tool for increasing the strength of peat as the large reduction in water content often leads to large increases in strength (Den Haan 1997). Alternatively, shearing of peat in the plane of the predominant fibre orientation (horizontal plane) can lead to a reduction of frictional resistance resulting in a post-peak or residual shear strength. Middleton peat sheared in a drained direct shear test (in plane of fibre orientation) resulted in a peak effective friction angle of 54° and a post peak angle of 37° (Ajlouni 2000 and Mesri 2007).

The stiffness of peat, represented as an elastic Young's modulus, is typically low and highly variable. Values reported in the literature range from 400 to 7000 kPa (Hallem et al. 1978; Dhowian and Edil 1978; Elsayed 2003). Horizontal fibre orientation results in a cross-anisotropy in stiffness and in strength (Yamaguchi et al. 1985). Elsayed (2003) also reported that the horizontal (secant) modulus of peat was 50% higher than the vertical secant modulus. Similar to shear strength, the stiffness of the peat can also be increased with a large reduction of water content through consolidation (Den Haan 1997).

The distribution of shear strength within an unconsolidated peat formation results from the presence and condition of fibres as expressed by the degree of humification (Den Haan 1997). This relationship is shown in vane shear tests in peat (muskeg formations) in Northern Ontario

where the shear strength typically increases to a depth of approximately 2 m and then begins to decrease. This strength profile was correlated to an increase of water content to an approximate depth of 2.6 m followed by a decrease in water content with depth. The higher water content of the upper 2.6 m suggests that the material is less humified; corresponding to the higher shear strength (MacFarlane and Rutka 1960).

In summary, it is clear that peat fibres produce a reinforcing effect within the peat. The potential for reinforcement, and thus increases in strength, is correlated to the prevalence and quality of the fibres. The orientation of the fibres is in a predominantly horizontal direction which results in peat behaving in an anisotropic manner with respect to both the strength and stiffness of the peat (more on this in section Figure 2.20).

2.2.5 Pore Pressure Response to Loading

Very little data is available on the pore pressure response of peat during undrained shearing, most of the studies within the literature focus on strength and not the effective stress path. Elsayed (2003) reported values of the Skempton *A* pore-pressure parameter ranging from 0.13 to 0.88 for vertically oriented specimens and 0.24 to 2.13 for horizontally oriented specimens. Yamaguchi et al. (1986) presented *A* parameter values which varied over a smaller range of 0.71 to 0.93 for vertically oriented specimens and 0.54 to 0.56 for horizontally oriented specimens with greater pore pressure response in the vertically orientated specimens. The results presented by Yamaguchi et al. (1986) also showed increasing organic content, and associated increasing fibre content, resulted in increased pore pressure responses.

2.2.6 Cyclic Properties of Peat

Very little research has been performed on the dynamic / cyclic response of peat and peaty organic materials (Kramer 2000). The majority of the available research comes from research into the failure of levies built upon peat formations in areas in California prone to earthquakes (Boulanger et al. 1998; Wheling et al. 2003). These investigations focus on the dynamic, small strain (shear strains of 0.1 to 0.3 %), response of peat in terms of its shear modulus, the reduction of the shear modulus with strain, dampening properties and the variation of the shear modulus under strain. large strain cyclic behaviour of peat has been the study of even less research, with Yasuhara et al (1994) providing insight into reductions in post-cyclic undrained shear strength.

Peat has been shown to exhibit a viscous component of resistance that causes the measured shear modulus and damping ratio to change with increasing frequency of strain. The shear modulus was shown to increase by 10% with an increase of frequency of tenfold (Stokoe et al 1994; Kramer 2000). Kramer (2000) concluded (from data presented in Stokoe et al. 1994) that at frequencies less than 0.1 Hz the damping increases with increasing frequency; and from results presented in Boulanger et al (1998) Kramer (2000) concluded that at frequencies greater than 0.1 Hz the damping decreases with increasing frequency.

Small-strain cyclically loaded soils typically exhibit a decrease in strength analogous to 'fatigue' in metals. This degradation is proportional to the number of cycles of loading applied to the material. The effect of cyclic decrease in strength is expressed by a degradation index (δ) in which the shear modulus decreases with the number of cycles (N):

$$\delta = \frac{G_N}{G_1} = N^{-t} \qquad [2.1]$$

where G_1 is the shear modulus for the first cycle of deformation, G_N is the shear modulus during the Nth cycle, and t is the degradation parameter which is representative of the cyclic degradation properties quasi-independent of the number of cycles (Idriss et al. 1978; Wehling et al. 2003). Wehling et al. (2003) suggested, based on laboratory test results, the degradation parameter to be typically very low for peat relative to mineral soils. Thus, cyclic degradation is less of a concern in peat than for mineral soils.

The results from cyclic triaxial testing presented in Yasuhara et al (1994) show that peat subjected to large cyclic strains due to undrained loading results in the partial destruction of the peat fabric. This destruction of the peat fabric results in a loss of post-cyclic undrained shear strength, which is defined as the undrained shear strength after the dissipation of cyclically induced pore pressures. This reduction in undrained shear strength was markedly increased at a higher frequency of loading (1 Hz) compared to a lower frequency of loading (0.5 Hz). Unfortunately Yasuhara et al (1994) does not define the magnitude of strains which are referred to as large cyclic strains.

2.3 Fibre Reinforced soils

The stiffness and strength of peat has been shown to be strongly related to the reinforcing effect of the fibres within the peat. There is a significant body of research which has been conducted into the use of polymer fibres to reinforce mineral soils. This research provides important insights into the role of the fibres in increasing strength and stiffness of soil. The testing of fibre reinforced mineral soils can be undertaken with greater control over the properties, orientation and amount of fibres within specimens and can produce more definitive conclusions as to the affect of each of these variables. The focus of this research has been on the drained response of the reinforced soil with no testing conducted to determine the resulting undrained effective stress paths.

From the fibre reinforced literature the primary response of the fibres to shear deformation is the generation of tensile stress within the fibres resulting in increased stiffness and strength. The orientation of the fibres with respect to the principal stresses is critical to the increase in stiffness and strength. Only fibres acting in tension, thus aligned in a direction with expansive strains, contribute to increased stiffness and strength. Fibres aligned in the direction of compressive strains have been shown in some cases to have an adverse effect on the engineering properties (Michalowski and Čermák 2001). A predominant orientation of the fibres within a soil would result in anisotropic stiffness and strength. This anisotropy was demonstrated by Michalowski and Čermák (2002) for fibre reinforced specimens tested with fibres oriented randomly, horizontally or vertically (Figure 2.4). Randomly oriented fibres resulted in an increase in stiffness and a modest increase in strength. Horizontally oriented fibres (perpendicular to axial applied load) resulted in an increase in stiffness and a significant increase in strength. Vertically oriented fibres were detrimental to the stiffness, with a modest increase in strength, similar in magnitude to the randomly oriented fibre specimens but achieved at higher strains.

The fibre content of reinforced soils is measured as a ratio (ρ) of the volume of fibres to the volume of soil. The maximum volumetric ratio in the reported studies was 2%. Increasing the fibre content results in increasing soil strength and stiffness (Michalowski and Čermák 2001; Kumar et al 2006) and cyclic stiffness (Li and Ding 2002). Increasing the length or aspect ratio (η) (length/diameter) of the fibres has also been shown to increase the strength of the soil (Kumar et al 2006; Michalowski and Čermák 2003).

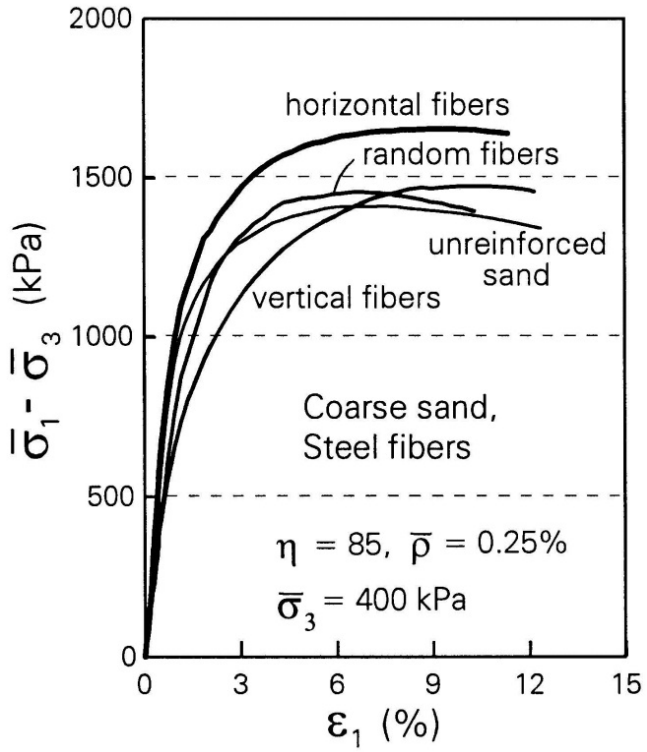

Figure 2.4 : Effect of fibre orientation on the strength and stiffness of a fibre reinforced coarse sand (Michalowski and Čermák 2002).

Yielding of fibre reinforced soil occurs as a result of stretching, breaking and slipping of the fibres (Maher and Gray 1990; Kumar et al. 2006). In some cases reinforced soils have shown a strain hardening effect upon yielding (Figure 2.5) (Michalowski and Čermák 2001; (Michalowski and Čermák 2003; Sadek et al. 2010). From the data presented in Sadek et al. (2010) (Figure 2.6) the presence of this strain hardening effect is a result of high fibre content and high aspect ratio of the fibres. The data presented in Michalowski and Čermák 2003 (Figure 2.5) clearly shows that the rate of strain hardening is strongly dependant of the effective confining pressure applied to the reinforced soil. This effect was hypothesised to be the result of the reorientation of the fibres during deformation so that they align with the principal strains (Michalowski and Čermák 2001).

The interaction between the fibres and the surrounding mineral soil should be purely frictional in nature. The friction developed between the soil and the fibre is dependent on the mean stress normal (σ_N) to the fibre surface and an angle of interface friction (Michalowski and Čermák 2001). For a small fibre segment oriented in the horizontal direction (Figure 2.7) the resulting

mean effective normal stress is calculated as per Equation 2.2, where σ'_V and σ'_H are the vertical and the horizontal effective stresses acting upon the fibre.

$$\sigma'_N = \frac{(\sigma'_V + \sigma'_H)}{2} \qquad [2.2]$$

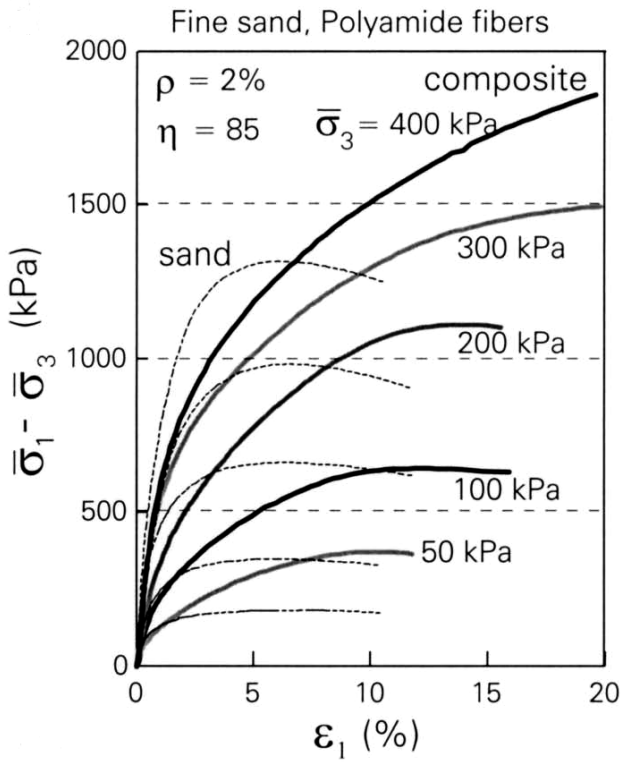

Figure 2.5 : Strain hardening due to fibres in a fibre reinforced fine sand (Michalowski and Čermák 2003).

Strong parallels can be drawn between the response of fibre reinforced soil and peat. Both benefit from the development of tension within fibres in the form of increased stiffness and strength. A predominant alignment of fibres within a plane or direction results in the effectiveness of the fibre reinforcement being determined by the orientation of the principal stresses as the fibres only generate tension with expansive strains. The reinforcing effect of the fibres is maximized if the orientation of the major (compressive) principal stress is perpendicular to the axis or plane of predominant fibre orientation. This was shown for fibre reinforced soil in Michalowski and Čermák (2002). These are mirrored in the anisotropic properties of peat described above in Section 2.2.4, and most clearly demonstrated in the laboratory testing results presented in Yamaguchi et al. (1985). Increasing the volumetric content and aspect ratio of the

fibres increases the reinforcing effect, this results in increased stiffness and strength (Michalowski and Čermák 2001; Kumar et al 2006). Corresponding correlations are found in the peat literature showing increasing strength and stiffness with increasing fibre content, organic content and humification, all of which are directly related to the quality and quantity of fibres that compose the peat (Section 2.2.4). Further examination presented later within this thesis will also show commonalities between the strain hardening response during the yielding of fibre reinforce soils and that observed in the laboratory testing conducted as part of this study.

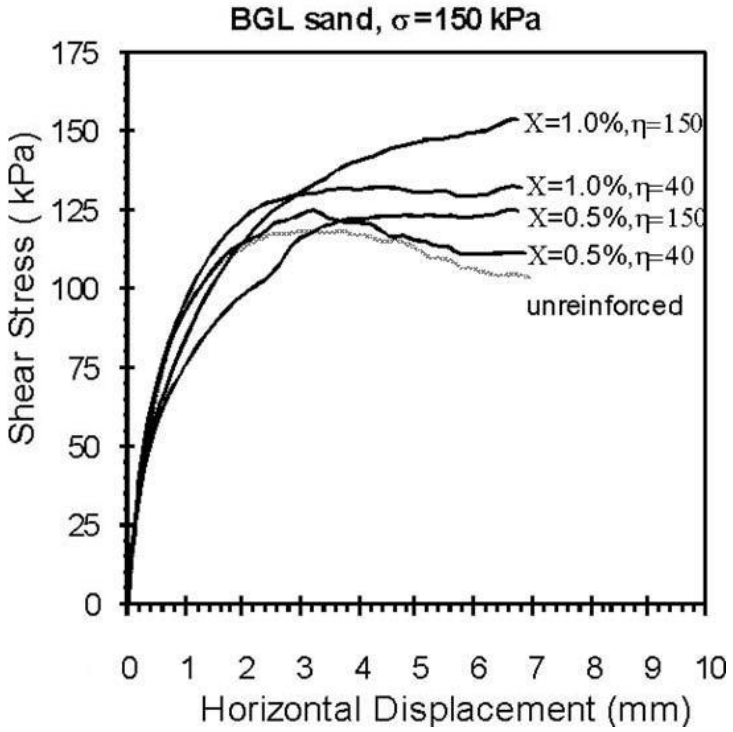

Figure 2.6 : The effect of high fibre volumetric content and aspect ratio on generating a strain hardening response during the yielding of fibre reinforced sand (Sadek et al. 2010). Note: volumetric fibre content is denoted by symbol X in this figure.

2.4 Rail-Track and Embankment Structure

Rail-track structure is a term used to refer to the rails, ties, ballast and sub-ballast, all of which transfer the train load to the foundation soils. The rail-track structure provides an interface between the train loading and the foundation soils and acts to distribute the load. Poor embankment and foundation conditions can increase the rate of deterioration of the rail-track structure. Excessive tie and track wear is often a good indicator of embankment and foundation performance (Brawner and Tessier 1969; Edwards 2007).

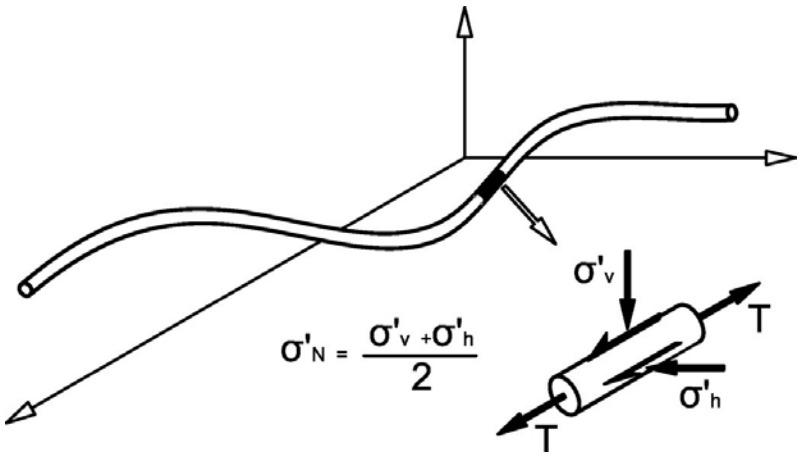

Figure 2.7 : Normal stresses acting on the surface of a segment of horizontal fibre.

2.4.1 Train Loading of Soils

Train loading of soils is unique in both the magnitude of axle loads and the consistent cyclic nature of the loading. Trainloads have been increasing steadily since the original construction of the Canadian railway network and maximum loads are currently 195 tonnes for a locomotive and 131.5 tonnes for a freight car. Table 2.1 presents historically authorized axle loads for CN. Train lengths have also steadily increased and this has created increasingly longer periods of cyclic loading. This section presents an overview of soil response to the train loading of soils.

Table 2.1: Authorized loads for locomotives and cars (in tonnes) (after TSB 2007)

Period	Locomotives	Cars (Passenger)	Cars (Freight)
1879 - 1920	75 (8 - 10 axles)	50 (4 axles)	40 (4 axles)
1920 - 1950	140 (14 axles)	90 (6 axles)	75 (4 axles)
1950 - 1960	135 (4 axles)	70 (4 axles)	100 (4 axles)
1960 - 1990	175 (6 axles)	70 (4 axles)	131.5 (4 axles)
1990 - Present	195 (6 axles)	70 (4 axles)	131.5 (4 axles)

The axle loads act as moving point loads along the rail, with the rail-track structure spreading the load over the sub-grade materials (Hendry et al. 2010). In this load configuration, the vertical, horizontal and shear stresses on a given soil element will change with the relative location of the moving load with respect to the soil element. The loading from a train results in the repeated loading and unloading of the soil with the passage of each axle and changes in the magnitude and orientation of the principle stresses (Figure 2.8) (Lekarp et al. 2002a). This distribution of stresses and strains is commonly reduced to a simplified two-dimensional problem, however, it is fundamentally a three dimensional problem with variations of stress and strain perpendicular to

the track in the same order of magnitude as those along the length of the track (Figure 2.9) (Hall 2000; Hall 2003).

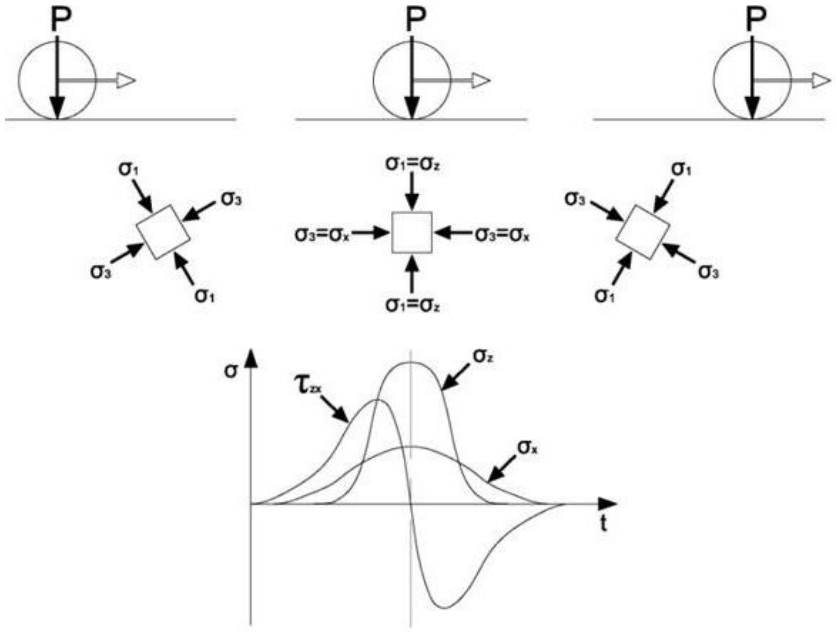

Figure 2.8 : Two dimensional principal stresses induced from a moving (rolling) axle load on a static soil and a graph showing the change in vertical, horizontal and shear stresses on the element (after Lekarp et al. 2000a).

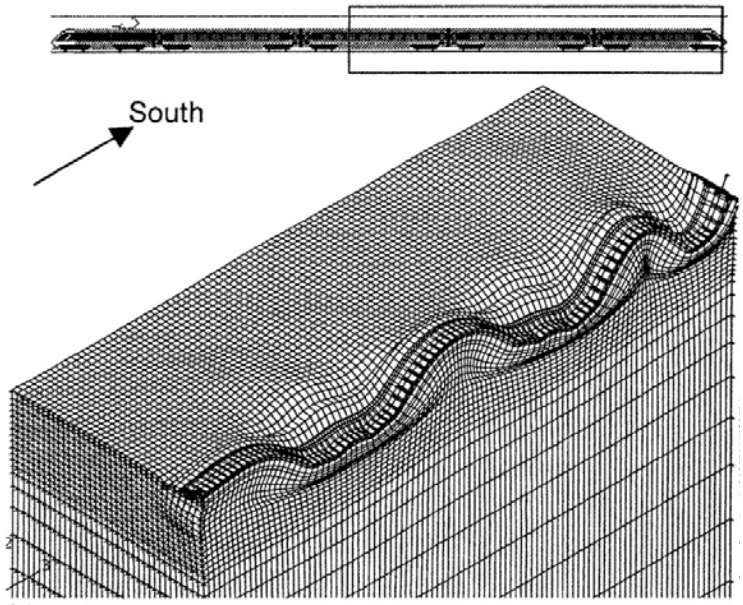

Figure 2.9 : Deformed mesh (magnified) from the three dimensional modelling of the passage of a high speed train from Hall (2002).

2.5 Dynamic versus Cyclic Response

The nature of the train loading of soils is that of repeated loading and unloading of the soil at frequencies ranging from 0.5 Hz to 7 or 8 Hz at operational train speeds. The rate of loading is dependent on the speed of the train and the spacing of the axles. Figure 2.10 presents the resulting frequency domain plot of the load applied to the surface of the embankment from a passenger train travelling 105.5 km/h (65.6 mph). The applied loading and the response of the embankment occurs at a frequency of between 0 and 4 Hz. For Canadian freight trains applied loading was measured to occur at rates of 1.3 to 1.4 Hz for a train traveling 50 km/h (Wong et al. 2006).

The strain response of soils subjected to applied loads is different when the load is cyclic rather than a single load event. These differences in the response can include increases in pore water pressure in excess of those generated during single load applications (as presented in section 2.6). With higher frequency loading, inertial and damping forces contribute significantly to the force balance and result in dynamic excitation and free wave propagation, which lead to increased deformations and the response of the soil to waves at different phases. (Frýba 1999; Hall 2000; Hendry 2007)

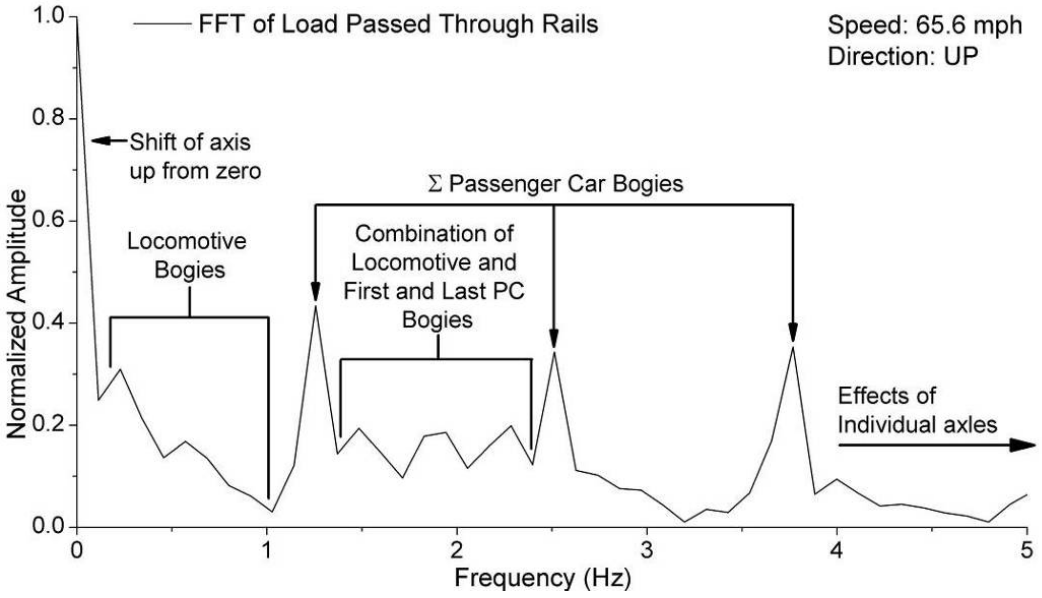

Figure 2.10 : Causes of characteristic peaks in train loading frequency domain plot (Hendry 2007).

For this study, the term dynamic, whether in conjunction with loading or response, refers to repeated loading at frequencies sufficient to cause dynamically induced forces (inertia and damping forces) to contribute to the force balance, as defined in Hendry (2007). Dynamic loading and response is typical of high-speed trains. Cyclic loading or response refers to the repeated loading without the dynamically induced forces contributing significantly to the deformation of the embankment, and may include the generation of excess pore water pressure.

2.6 Pore Pressure Response

The short duration of the axle loads causes the foundation soil to behave in an undrained (constant volume) manner. This requires the pore water to bear a large component of the load (Bishop 1954; Skempton 1954). The pore-pressure response to the loading can reduce the shear strength of the soil increasing the potential for failure (cyclic failure).

Under higher frequency loading, it has been observed that pore pressure increases are in excess of the pore pressures generated solely due to the applied load; and continue to increase with the number of cycles of applied loading (Clifton and Associates 1988). Much of the research into the generation of excess pore-pressures has been undertaken for dynamic loading (e.g. earthquake engineering). The threshold shear strain (γ_t) for the generation of excess pore water pressure has been identified as a fundamental property of saturated soils undergoing cyclic loading (Hsu and Vucetic 2006; Kramer 1996), though it has not been shown in peat. The basis of this property is that below this threshold value the soil acts as per Skempton's equation where the change on pore pressure is directly proportional to the change in total stresses. Upon exceeding this threshold value, excess pore water pressure is generated with each cycle, the quantity of which is dependent on the extent by which the threshold shear strain is exceeded. Thus, higher cyclic shear strains (Figure 2.11a) results in the generation of higher levels of excess pore water pressure (Figure 2.11b), and an increased rate of accumulation of excess pore pressure (based on the number of cycles) (Figure 2.11c).

Three instances of the measured pore pressure generation in peat foundations under train loading from the literature have been found. The first, conducted by Clifton and Associates in 1988 measured the pore water pressure in a CP railway embankment. The measurements showed a distinct generation and growth in pore pressures with cyclic loading followed by a decrease in

pore pressures as the train continued to pass (Figure 2.12). The second, conducted for CP, shows a very similar pattern of generation and growth in pore pressures with cyclic loading followed by decreasing pore pressures as the train continued to pass. In the final case, Konrad et al. (2007) observed increases in pore pressure under train loading as shown in Figure 2.14.

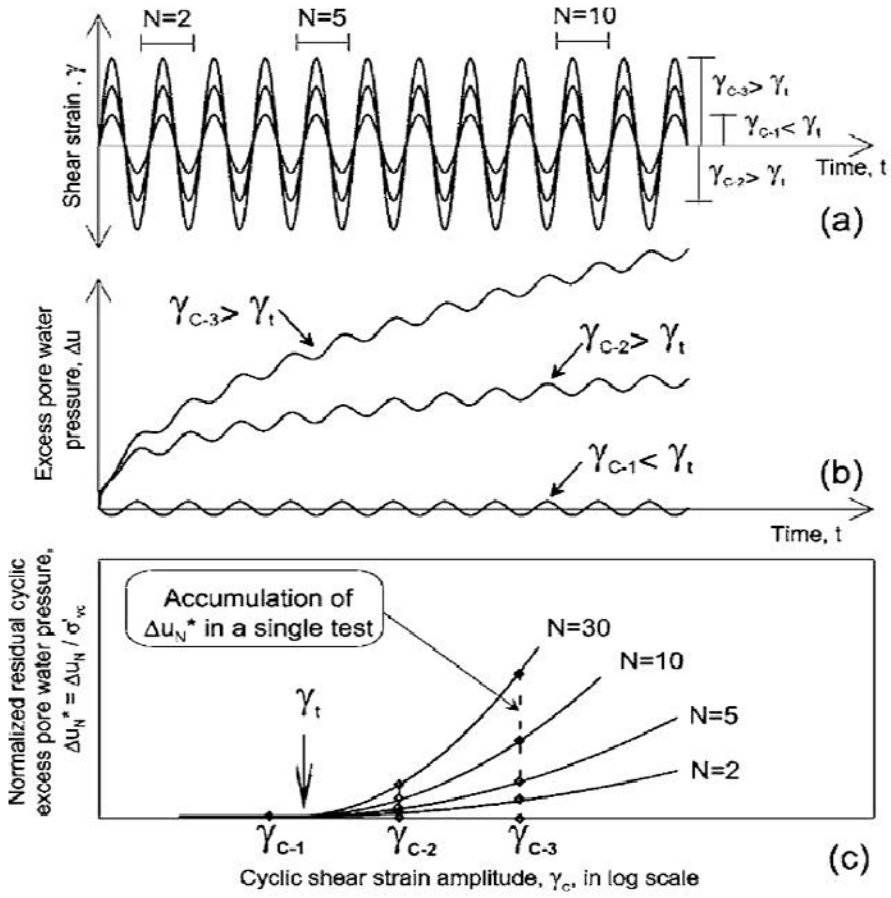

Figure 2.11 : Generation of excess pore pressure due to loading exceeding the threshold shear strain (γ_t) (Hsu and Vucetic 2006)

The data from both Clifton and Associates (1988) and Wong et al (2006) show a dissipation of the pore pressure during the passage of the train. Both sites were under investigation because of reported occurrences of subgrade pumping (Section 2.7.1). Wong et al. (2006) suggested this dissipation of pore pressure was due to the pore pressure reaching a threshold value which forced open drainage paths leading to the dissipation of the pore pressure. The pore pressure data from Konrad et al. (2007) does not show the dissipation of pore pressure during the passage of the train, and there are no notes in TSB (1999), Konrad et al. (2007) or TSB (2008) of pumping

features. Konrad et al. (2007) did note that there was an apparent increase in pore pressure generated in the peat under train loading with increasing train speed.

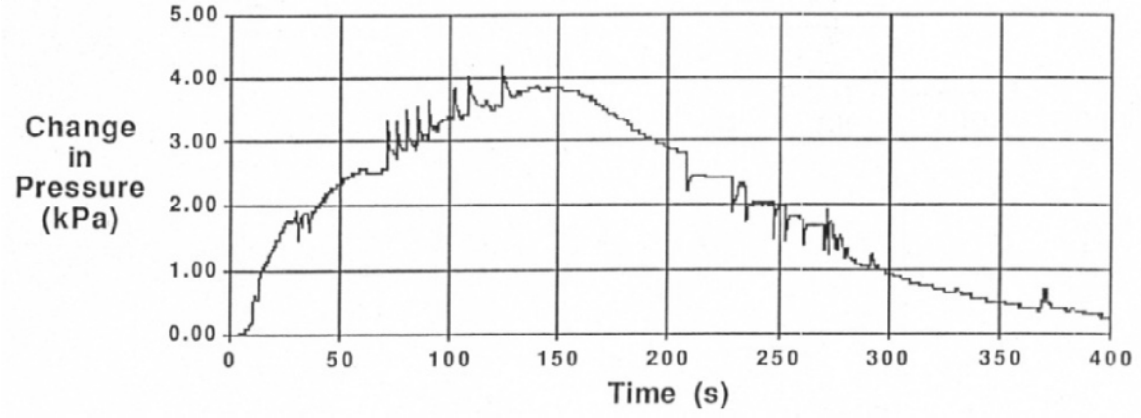

Figure 2.12 : Change in pore water pressures measured under passing trains (Clifton and Associates 1988)

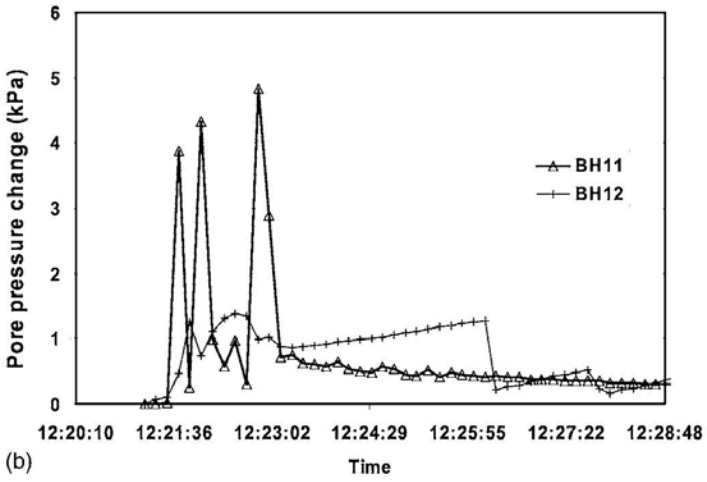

Figure 2.13 : Change in pore water pressures measured under passing trains (Wong et al. 2006)

The data collected by Clifton and Associates (1988) and Wong et al (2006) were taken at 0.2 Hz and 0.1 Hz respectively. This data collection rate was limited by the measurement frequency of the vibrating wire piezometers. This low rate of data acquisition likely resulted in the missing of peak pore pressures under axle loads which occurred at frequencies of approximately 1.3 to 1.4

Hz (Section 2.5) (Wong et al. 2006). The pore pressure data from Konrad et al. (2007) was recorded at a much higher frequency (> 100 Hz) and shows the effect of individual axle loads.

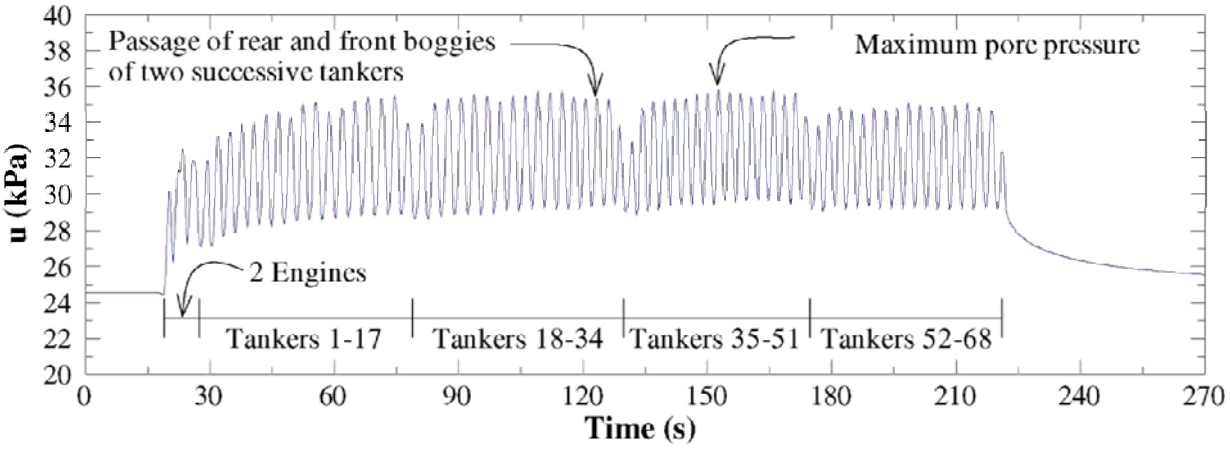

Figure 2.14 : Pore water pressure measurements in peat under railway embankment during the passage of a train. The data is from CN's Lévis Subdivision (Konrad et al. 2007).

2.7 Embankments over Peat

Several studies have been conducted within the transportation industry to understand the response of peat subgrades to railway loading. These studies have often been initiated in response to problems with a specific embankment. A review of the literature and site reports has yielded several common themes in the problems associated with embankments over peat. These include the generation of pore water pressure and the resulting pumping of material to the surface, excessive cyclic deformation, excessive settlement of the embankment and rapid shear failure of embankments and peat foundations.

2.7.1 Pumping features

The pumping of materials to the surface is a concern with railway embankments on soft soils. It is particularly common in embankments over peats where it often occurs as peat "boils" or "volcanoes". These boils consist of peat material expelled to the surface of the embankment during the passage of trains. The shape of the peat boils has been compared to volcanoes and their size can approach 1 m across with a sinkhole extending nearly as deep (Figure 2.15) (Choi 1998; Wong et al. 2006; Clifton 1988 , Maki 2002). The formation of these features beneath the track or in the embankment presents a hazard to the stability of these structures. From the available case studies, it appears these are most common for embankments over thinner peat

formations (less than 2 m), and occurs at sites were the track alignment has been noted to be ‘wavy’; referring to the poor alignment of the rails and the undulating surface of the embankment (DST Consulting Engineers 2002). Investigations into these boils have identified the generation of excess pore water pressure as the cause (Clifton and Associates 1988; Wong et al. 2006) and suggest that it is the ‘waves’ of pore water pressure from moving axle loads that is driving this behaviour (DST Consulting Engineers 2002). These ‘waves’ of pore water pressure from the moving axles were modelled by Wong et al. (2006) as the result of increasing stresses due to increasing proximity of the heavy axle loads as described in Section 2.4.1.

Figure 2.15 : Examples of large pumping features common in embankments over peat foundations (Moyie Subdivision Courtesy of CP).

2.7.2 Cyclic Deformations

The large movements associated with rail-track structures over soft peat result in excess wear on the rail-track structure and the need for increased maintenance. The motion of the rail structure can be a concern unto itself, as in the case of Northern Ireland Railways, where reduced speeds were required on a section of track over peat bogs, due to concerns over magnitude of the vertical motion of the track (Hendry 2007).

The cumulative effect of the plastic components of the cyclic strains can also lead to permanent settlements. Figure 2.16 shows the measured vertical deformation of the embankment and sub

grade during the passage of a train at the Levis site (Konrad et al. 2007). The residual displacement following passage of each train is in the range of 1 to 2 mm. Konrad et al. (2007) suggested that this deformation accumulates with each passing train. The accumulation of settlement measured at the Lévis site is presented in Figure 2.17 (Konrad 2007; TSB 2008).

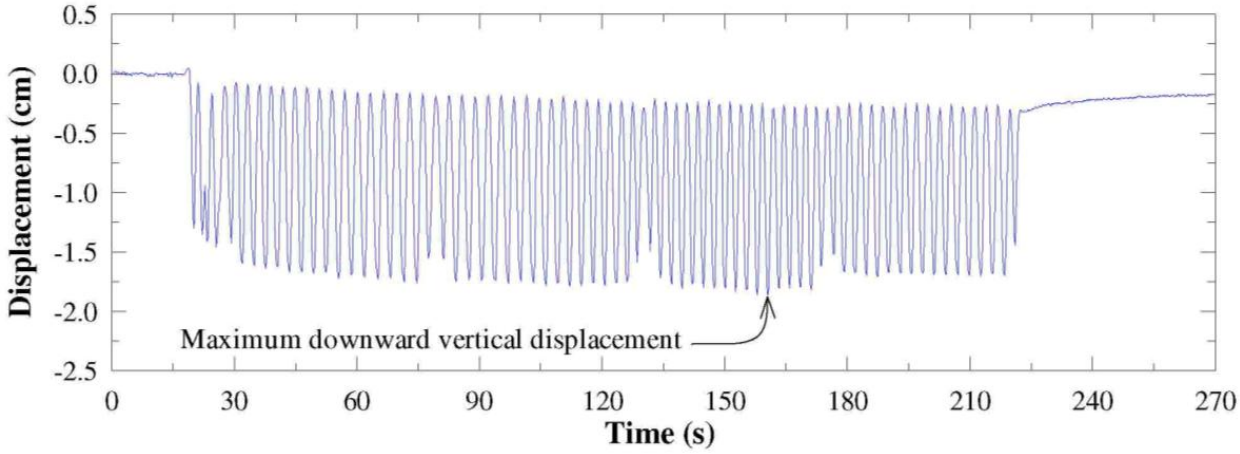

Figure 2.16 : Displacement data measured with potentiometers anchored in the bedrock under the peat and a sleeper during the passage of a train. The data is from CN's Lévis Subdivision (Konrad et al. 2007).

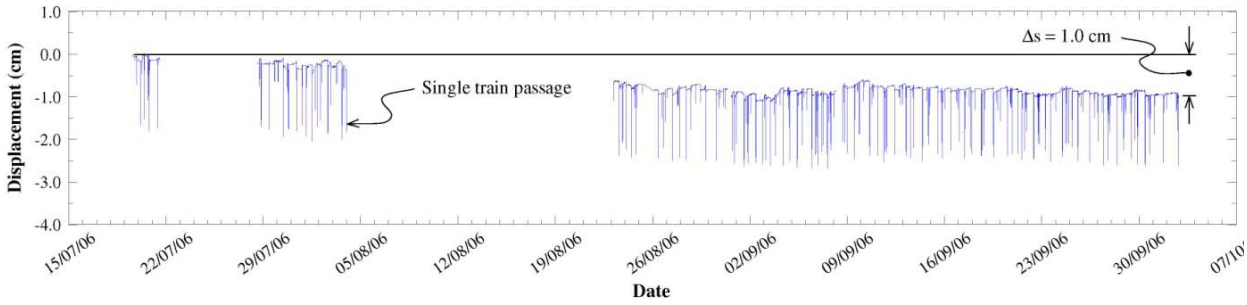

Figure 2.17 : Long-term displacement measured with potentiometers anchored in the bedrock under the peat and a sleeper during the passage of a train. The data is from CN's Lévis Subdivision. Note the individual 'spikes' in displacement represent the passages of individual trains, and the resulting accumulated vertical displacement (Konrad et al. 2007).

DeNie (1948) is the oldest study found which makes note of the 'undulations' of the embankments and soft peat subgrades during the passage of trains. This study suggested that the factors that affect the magnitude of these deformations were train velocity, embankment thickness, the pressure distribution on the subgrade, and the spacing of axles and trucks (bogies). The thickness of the embankment and the pressure distribution on the subgrade follow closely together as the former influences the latter. Hendry (2007) showed that the magnitude of the

embankment deformation was not sensitive to train velocity at speeds of below 145 km/h (90 mph) for embankments over peat foundations in Northern Ireland. Thus, the response of the peat is similarly insensitive to frequencies of loading generated from the trains at these speeds (less than 6 Hz). This insensitivity suggests that its behaviour can be described with static properties as opposed to cyclic and dynamic properties. Hendry (2007) also found that the height of the embankment did play a significant role on deformation, with the highest embankment (Adavoyle bog site) found to deform significantly less than a shallower embankment (Brackagh bog site) under similar loading and peat foundation conditions.

2.7.3 Settlement

The settlement of embankments built on peat is not just a concern during and immediately following construction but also over the long term (MacFarlane and Rutka 1960). The accumulated plastic deformation from passing trains and post-cyclic recompression can lead to long-term settlement (Yasuhara et al. 1994; Konrad 2007, TSB 2008). It stands to reason that increases in the magnitude of axle loads and train traffic can lead to increased magnitudes of settlement. Settlement can be divided into settlement resulting from volume change (i.e. consolidation) of the underlying peat subgrade, and settlement without volume change (deformation), though these are rarely considered exclusively (Hanrahan 1964).

Settlement under embankments due to volume change can be very large for peats due to their high water content (Hanrahan 1954). Peat gains strength with consolidation and this would suggest that this process has a limited life cycle under continued loading. (Hanrahan 1964; Adams 1965; Hobbs 1986; Farrell and Hebib 1998; Elsayed 2003; Mesri 2007).

Settlement under embankments not associated with volume change is the result of related forms of lateral ‘creep’, spreading or flow, all of which are the result of ongoing shearing. Hanrahan (1954) describes this settlement due to non-volume change deformation as ‘wasteful’ in that it requires excess maintenance and material with little or no beneficial strengthening of peat (as is found with settlement due to consolidation). Peat sub grades under embankments are especially subject to the shearing type of creep due to the low submerged density of the peat (Hanrahan 1954). Testing of the Sherman Island peat and the associated performance of a levee constructed over the same peat was studied by Wehling et al. (2003). They suggested that shearing of the

peat during the construction of the levee may have resulted in the development of residual shear strengths which led to continual lateral spreading and strength reduction in the peat.

The long-term settlement of railway embankments after decades of service proved to be significant in the case of the Lévis Subdivision site, the accumulated settlement is estimated as being as high as 240 to 320 mm between 1996 and 2004 (Konrad et al. 2007). There is settlement attributed to the net effect of residual deformation from the passages of individual trains (previously presented in section 2.7.2), and the time frame for this settlement corresponds to the introduction of new rail traffic, which increased from 850,000 tons to up to 6 million tons per year. Much of this increase in traffic was due to the introduction of unit trains, comprised solely of tanker cars, carrying hydrocarbons from the Saint-Romuald refinery. Thus, this settlement is most likely due to the increased tonnage (annual tons of rail traffic) on the line and the resulting increase in accumulated residual cyclic deformation. Measurements taken at the site (following the derailment) indicated that over a four month period there was an accumulation of 10 mm of settlement (Konrad 2007; TSB 2008). No measurements were available to determine whether this settlement was due to volume change or lateral deformation of peat.

2.7.4 Rapid Shear Failures

The failure of embankments over peat is often similar to failures of embankments over soft mineral soils and is often analyzed assuming peat behaves as a soil with a single value of shear strength as obtained from a laboratory or *in situ* test. These failures are conceptualized as slope stability or simple bearing capacity problems. The analyses to determine the stability of the embankments for these modes of failure have been the same for peat sites as for site with just mineral soils.

Konrad et al. (2007) suggested a failure mode specific to peat and made in the light of field observations associated with the catastrophic embankment failure and derailment at the Lévis subdivision (Konrad et al 2007; TSB 2008). This failure was characterized by a significant, sudden and localized settlement as shown in Figure 2.18. The proposed mode of failure at Lévis subdivision was significant continuous settlement leading to the development of shear planes rather than general plastic deformation. It was postulated that the peat fibres were realigned in the direction of the shear planes (Figure 2.19) which resulted in a shear failure with the ballast

and sub ballast punching through the underlying peat foundation (Figure 2.20) (Konrad et al 2007; TSB 2008). No measurements have been taken which verify the existence of these shear planes.

Figure 2.18 : Settlement feature which led to derailment of train at the Lévis subdivision site in 2004 (Konrad et al. 2007)

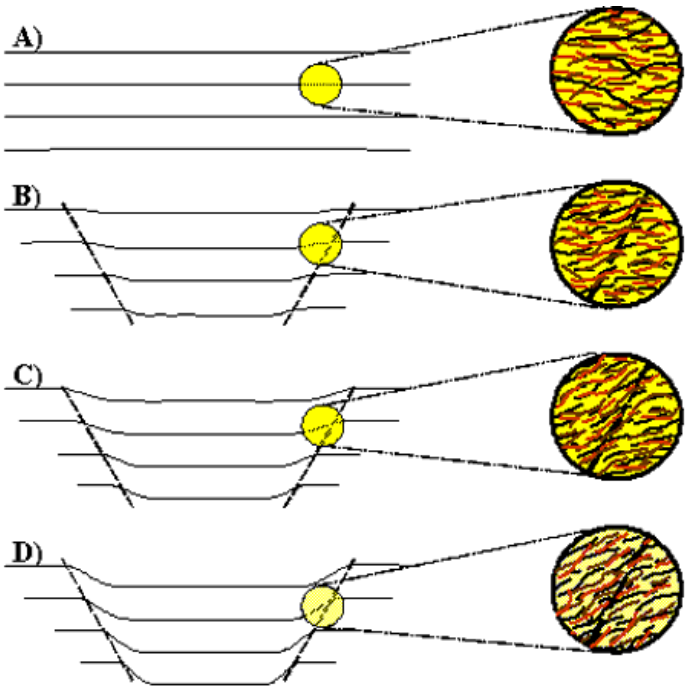

Figure 2.19 : Evolution of settlement and distortion of peat fibers (TSB 2008)

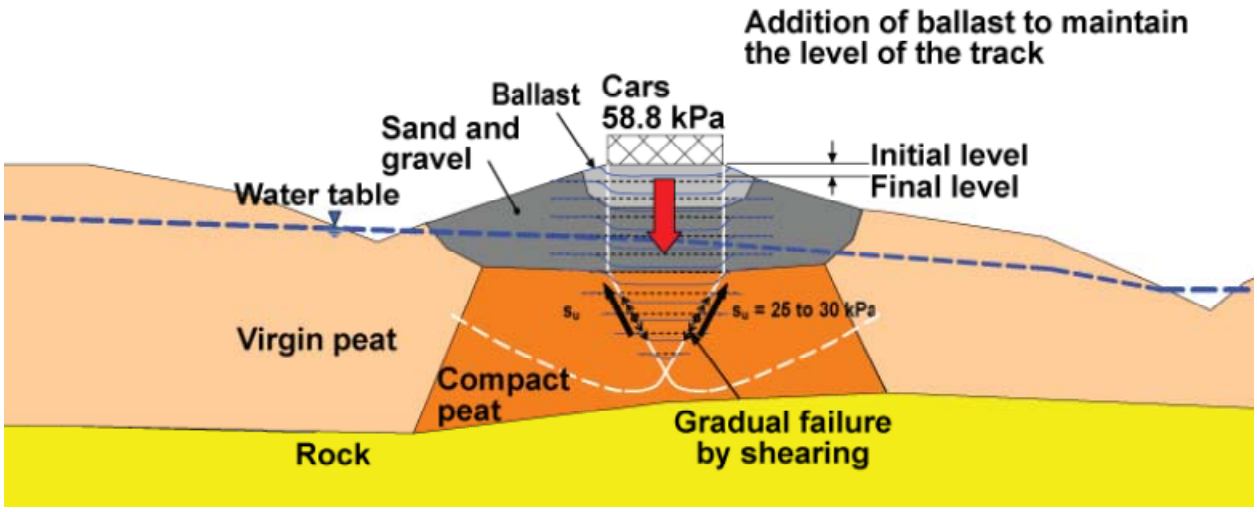

Figure 2.20 : Shearing failure by punching at mile 3.87 of the Lévis subdivision (TSB 2008)

There is also evidence that the material underlying the peat may have had a significant effect on the mode of failure. Observations from a study on the quality of roads built on embankments over peat (muskeg) formations in Northern Ontario found an empirical correlation between the presence of clay underlying the peat and the occurrence of rotational slip failures. Rotational slip failures were found where deep soft clay was found underneath the peat. No investigation was undertaken to determine the depth of the shear planes. Both the peat and the clay had low shear strength and the failure would have been as likely to occur in the peat as in the clay. Further, formations with a combined depth of 7.6 m (25') or more of soft material (peat plus clay) were much more likely to fail than sites with less than 7.6 m of soft material (MacFarlane and Rutka 1960).

2.8 Isotropic and Anisotropic Elastic soil models

As described in section 2.2.4, peat is anisotropic with greater stiffness when the principal loading axis in a triaxial texted oriented vertically, perpendicular to the *in situ* horizontal axis of the specimen. The purpose of this section is to summarize the models used to describe elastic behaviour of anisotropic soils under undrained loading.

2.8.1 Isotropic elasticity

The simplest formulation of elastic behaviour in soils is for the isotropic case. For an isotropic elastic soil the properties are uniform in all directions and the response can be described as a

function of effective stress with the compliance matrices below in Equation 2.3, for the axial and radial directions of a triaxial specimen; and in Equation 2.4 in terms of the mean effective (p') and deviatoric stress (q); with the effective bulk modulus (K') and the effective shear modulus (G') defined in Equations 2.5 and 2.6 respectively. The purpose of the mean effective and deviatoric stress formulation is to decouple the volumetric and deviatoric responses of the soil. This is apparent in Equation 2.4 where the change in volumetric strain is represented only as a function of the mean effective stress and the deviatoric strain is represented solely as a function of deviatoric stress (Wood 1990).

$$\begin{bmatrix}\delta\varepsilon_a\\ \delta\varepsilon_r\end{bmatrix} = \frac{1}{E'}\begin{bmatrix}1 & -2\nu'\\ -\nu' & (1-\nu')\end{bmatrix}\begin{bmatrix}\delta\sigma'_a\\ \delta\sigma'_r\end{bmatrix} \quad [2.3]$$

$$\begin{bmatrix}\delta\varepsilon_v\\ \delta\varepsilon_q\end{bmatrix} = \begin{bmatrix}1/K' & 0\\ 0 & 1/3G'\end{bmatrix}\begin{bmatrix}\delta p'\\ \delta q\end{bmatrix} \quad [2.4]$$

$$K' = \frac{E'}{3(1-2\nu)} \quad [2.5]$$

$$G' = \frac{E'}{2(1+\nu)} \quad [2.6]$$

For the case of an undrained (constant volume: $\delta\varepsilon_v=0$) soil the application of load results in the generation of pore pressure. Equation 2.4 and the constant volume constraint results in Equation 2.7. Equation 2.7 also indicates that change in mean effective stress must be equal zero for a finite value of K'. The result of a zero change in mean effective stress is that the change in pore pressure must equal the change in mean total stress (Equation 2.8). When plotted in p'-q space the stress path for an isotropic elastic soil would be vertical, with a constant p' value.

$$\delta\varepsilon_v = 0 = \frac{\delta p'}{K'} \quad [2.7]$$

$$\delta u = \delta p \quad [2.8]$$

2.8.2 Anisotropic Elasticity

The anisotropic elastic behaviour of peat (or mineral soils) can be viewed as cross anisotropy (also, transverse isotropy). Cross anisotropy has uniform stiffness properties within the horizontal plane, and differing properties in the vertical axis. This results in a much more

complex relationship between the stress and strain response, than for an isotropic soil, as this relationship is dependent on direction. The resulting relationship between the stress and strain increments for a cross anisotropic soil is shown in Equation 2.9. This relationship requires five elastic constants to describe the behaviour of the soil.

$$\begin{bmatrix} \delta\varepsilon_{xx} \\ \delta\varepsilon_{yy} \\ \delta\varepsilon_{zz} \\ \delta\gamma_{yz} \\ \delta\gamma_{zx} \\ \delta\gamma_{xy} \end{bmatrix} = \begin{bmatrix} 1/E_h & -\nu_{hh}/E_h & -\nu_{vh}/E_v & 0 & 0 & 0 \\ -\nu_{hh}/E_h & 1/E_h & -\nu_{vh}/E_v & 0 & 0 & 0 \\ -\nu_{vh}/E_v & -\nu_{vh}/E_v & 1/E_v & 0 & 0 & 0 \\ 0 & 0 & 0 & 1/2G_{vh} & 0 & 0 \\ 0 & 0 & 0 & 0 & 1/2G_{vh} & 0 \\ 0 & 0 & 0 & 0 & 0 & 2(1+\nu_{hh})/E_h \end{bmatrix} \begin{bmatrix} \delta\sigma'_{xx} \\ \delta\sigma'_{yy} \\ \delta\sigma'_{zz} \\ \delta\tau_{yz} \\ \delta\tau_{zx} \\ \delta\tau_{xy} \end{bmatrix}$$

[2.9]

A simplification of this cross anisotropic relationship was developed by Graham and Houlsby (1983) to reduce the number of elastic constants to three. This simplification was to allow for the description of the response of anisotropic soils in triaxial compression tests when the vertical axis of the soil is aligned with the axis of the testing apparatus. The simplified Graham and Houlsby (1983) compliance matrix is presented in Equation 2.10. Equation 2.10 introduces three new parameters E*, α and ν*. The parameter E* is equivalent to the vertical stiffness E_V; α is the ratio of the horizontal stiffness to the vertical stiffness (E_H/E_V); and ν* is similar to the Poisson's ratio. Of these parameters ν* is the least well defined, and the values used by Graham and Houlsby (1983) are not determined from the results of the triaxial test being interpreted, but back calculated from more comprehensive testing conducted on similar material. Numerically possible values for ν* are from 0 to 0.5, with a ν* of 0 resulting in maximum value for α, and a ν* of 0.5 resulting in an α value of 1, representing an isotropic soil. Equation 2.10 can be simplified with the use of the mean effective and deviatoric stress parameters as per Equation 2.11 or 2.12, where, K*, G* and J* are functions of E*, α and ν* as per Equations 2.13, 2.14 and 2.15 respectively.

$$\begin{bmatrix}\delta\varepsilon_{xx}\\ \delta\varepsilon_{yy}\\ \delta\varepsilon_{zz}\\ \delta\gamma_{yz}\\ \delta\gamma_{zx}\\ \delta\gamma_{xy}\end{bmatrix} = \frac{1}{E^*}\begin{bmatrix} 1/\alpha^2 & -\nu^*/\alpha^2 & -\nu^*/\alpha & 0 & 0 & 0\\ -\nu^*/\alpha^2 & 1/\alpha^2 & -\nu^*/\alpha & 0 & 0 & 0\\ -\nu^*/\alpha & -\nu^*/\alpha & 1 & 0 & 0 & 0\\ 0 & 0 & 0 & 2(1+\nu^*)/\alpha & 0 & 0\\ 0 & 0 & 0 & 0 & 2(1+\nu^*)/\alpha & 0\\ 0 & 0 & 0 & 0 & 0 & 2(1+\nu^*)/\alpha^2 \end{bmatrix}\begin{bmatrix}\delta\sigma'_{xx}\\ \delta\sigma'_{xx}\\ \delta\sigma'_{xx}\\ \delta\tau_{yz}\\ \delta\tau_{zx}\\ \delta\tau_{xy}\end{bmatrix} \quad [2.10]$$

$$\begin{bmatrix}\delta\varepsilon_p\\ \delta\varepsilon_q\end{bmatrix} = (3K^*G^* - J^2)^{-1}\begin{bmatrix}3G^* & -J\\ -J & K^*\end{bmatrix}\begin{bmatrix}\delta p'\\ \delta q\end{bmatrix} \quad [2.11]$$

$$\begin{bmatrix}\delta p'\\ \delta q\end{bmatrix} = \begin{bmatrix}K^* & J\\ J & 3G^*\end{bmatrix}\begin{bmatrix}\delta\varepsilon_p\\ \delta\varepsilon_q\end{bmatrix} \quad [2.12]$$

$$K^* = \frac{E^*(1-\nu^*+4\alpha\nu^*+2\alpha^2)}{9(1+\nu^*)(1-2\nu^*)} \quad [2.13]$$

$$G^* = \frac{E^*(2-2\nu^*-4\alpha\nu^*+\alpha^2)}{6(1+\nu^*)(1-2\nu^*)} \quad [2.14]$$

$$J = \frac{E^*(1-\nu^*+\alpha\nu^*-\alpha^2)}{3(1+\nu^*)(1-2\nu^*)} \quad [2.15]$$

The loading of an elastic anisotropic soil will also result in the generation of pore pressures, much in the same manner as that for isotropic soils. Equation 2.12 and the application of the constant volume constraint results in Equation 2.16. From Equation 2.16 it is apparent that the change in pore pressure is not simply equal to the change in mean total stress. The effect of the coupling between shear and volumetric effects results in pore pressure generation that is a function of both changes in the mean total and deviatoric stress such that the elastic stress path no longer follows a path of constant mean effective stress (Wood 1990). The stress path and the pore pressure generation can be determined from the ratio of the change in deviatoric stress to the change in mean effective stress (Equation 3.16) (Graham and Houlsby 1983). The slope of the elastic stress path for an anisotropic soil is a function of ν^* and α (Figure 2.21). The pore

pressure parameter, a, can be determined from Equation 2.17 and the slope of the anisotropic elastic stress path. The pore pressure parameter a is used as per Equation 2.18.

$$\delta\varepsilon_p = 0 = \frac{3G^*\delta p\prime - J^*\delta q}{3K^*G^* - J^2} \quad [2.16]$$

$$\frac{\delta q}{\delta p\prime} = \frac{3G^*}{J} = \frac{3\left(2-2\nu^*-4\alpha\nu^*+\alpha^2\right)}{2(1-\nu^*+\alpha\nu^*-\alpha^2)} = -\frac{1}{a} \quad [2.17]$$

$$\delta u = a\delta q + \delta p \quad [2.18]$$

2.9 Instrumentation and Measurement

In order to identify the response of the embankment and underlying foundation to train loading, it is necessary to measure deformation (strain) and pore pressure responses. This section presents an overview of the commercially available instrumentation for the measurement of cyclic vertical and horizontal deformations and pore water pressure.

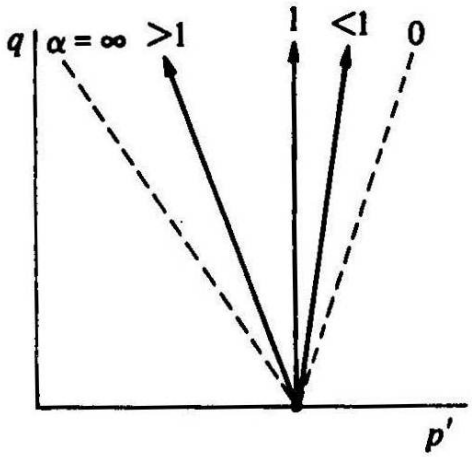

Figure 2.21 : Effective stress paths for constant volume (undrained) deformation of cross-anisotropic elastic soil (Wood 1990).

2.9.1 Measurement of Motion

Instruments such as geophones and accelerometers are commonly used to measure the cyclical deformation and propagation of waves in geotechnical structures, including railway embankments and foundations (Hall 2000; Madshus and Kaynia 2000). To measure the magnitude of displacements with geophones and accelerometers, the measured acceleration is

numerically integrated twice to obtain displacements versus time. The measurement of cyclic displacements is sensitive and requires a large amount of analysis to filter 'noise' and to apply baseline corrections (Hall 2000; Hendry 2007).

Extensometers installed in boreholes measure relative displacement between a 'reference head' at an anchor installed at the bottom of the borehole. The measurements are taken within the reference head using a variety of methods; however the most common are piezoelectric sensors or linear variable differential transformers (LVDT). These provide an analogue signal which can be interpreted by data loggers. Extensometers are more prone to mechanical failure than accelerometers and geophones since they have more mechanical parts. The resulting data from extensometers is much more accurate, free from noise and simpler to interpret, than that from accelerometers (Slope Inclinometer 2004).

2.9.2 Pore-pressure response

The three most common type of piezometers used to measure pore-pressure are pneumatic, vibrating wire and strain gauge piezometers. Pneumatic piezometers require manual reading with a pneumatic indicator and are thus impractical for high frequency measurements. The vibrating wire piezometer measures changes in pressure by measuring the strain of a diaphragm on which the water pressure is acting. The strain of the diaphragm is calculated from the measured tension in a wire attached to the diaphragm. The tension in the wire is measured by measuring the natural vibration frequency of the wire after it is excited by an electromagnetic coil. Vibrating wire piezometers provide good long-term accuracy, stability of readings and reliability, and have become the industry standard. The use of vibrating wires does; however, limit the frequency of readings (i.e. several seconds per reading). This low rate of measurement can result in peak pore pressures being missed during cyclic axial loading (Wong et al.2006).

A strain gauge piezometer operates on a similar principle as the vibrating wire piezometer; however in place of a vibrating wire a strain gauge is attached to the diaphragm. The strain-gauge increases in electrical resistance with increasing strain, allowing the pressure to be read by a change in resistance. (RST instruments, communications with RST instruments). Strain gauge piezometers are the only option for measuring cyclic pore-pressures under rapid train loading.

2.9.3 Micro-Electro-Mechanical Systems based Instrumentation

Micro-Electro-Mechanical Systems (MEMS) are simple electro-mechanical systems such as sensors, actuators and electronics, reduced to fit on microchips. The MEMS used in geotechnical instrumentation are accelerometers and are often used to replace traditional accelerometers in tilt-meters, such as those found in inclinometers (Sellers and Taylor 2008). Measurand Inc. developed a product called the ShapeAccelArray (SAA), which consists of 305 mm (1 foot) rigid segments connected by a two degrees of freedom joint which allows the joint to bend but not twist (Figure 2.22 and Figure 2.23). The three dimensional coordinates of each joint (or node), and thus the 3D shape of the SAA, are calculated from the orientation and fixed length of each SAA section and the assumption that one of the ends is fixed in space (Abdoun et al. 2007). The SAA is not axially compressible and is often installed within a PVC access tube; consequently, the array should not be used to measure vertical movement of the soil (Mikkelsen and Dunnicliff 2008). Interpretation of the data from a (near) vertically installed SAA can be used to measure the horizontal (2D) movement of each joint along the length of the array in a similar manner to an inclinometer but in near-real-time.

The SAA was initially developed to measure long-term deformation and is often installed vertically to act as an in-place inclinometer or horizontally to measure settlement (Abdoun et al. 2005, Abdoun et al. 2007). The slow rate of movement in these applications allows many readings to be averaged to obtain an accurate measurement of displacement. The SAA has been the subject of several studies to ensure the accuracy of the measurements under near static and slow rates of deformation (Abdoun et al. 2005, Abdoun et al. 2007). These studies compared the displacement measured with the SAA at a single node compared to the same motion measured with a linear variable differential transformer (LVDT). The results from Abdoun et al. (2005) (Figure 2.24) showed good agreement between the SAA and LVDT measurements for cyclic motions for frequencies ranging between 0.05 Hz to 0.2 Hz. The results from Abdoun et al. (2007) (Figure 2.25) also show a strong correlation between the data obtained from the SAA and the LVDT. The motion shows two different contributing frequencies. The first frequency is a very low frequency (estimated at 0.006 Hz) which contributes to the large overall motion. The error in the SAA in comparison to the LVDT as a percentage of overall displacement is estimated to be less than 2 %. The accuracy of the SAA at higher frequencies (0.5 Hz) and

smaller oscillations cannot be established the data as presented, though it appears to be comparable to the LVDT.

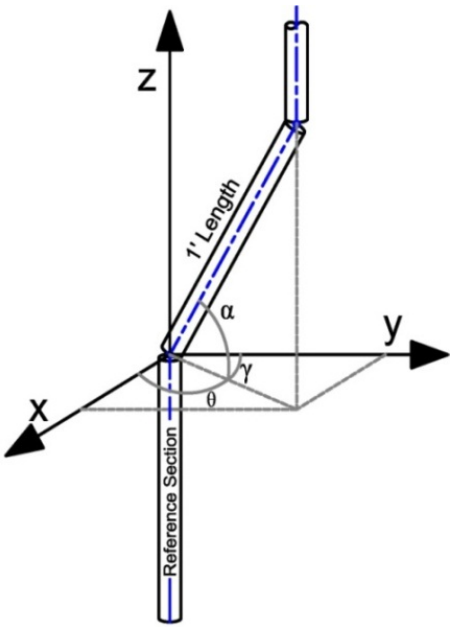

Figure 2.22 : Calculation of orientation of a single SAA section.

Figure 2.23 : Picture of SAA (104' in length) wrapped around reel.

The ability of the SAA to measure displacements at higher frequencies has not yet been evaluated. Based on above studies, the SAA does provide accurate measurements of displacement at frequencies less than 0.5 Hz. Typical frequencies associated with embankment deformations during the passage of trains can be much higher than this. For example, for a train

travelling at 110 km/h, the measurement frequency would be approximately 7 Hz (Hendry 2007). Abdoun et al. did (2007) did show conclusively that the acceleration measured by the MEMs within the SAA system provided a very close match to high quality traditional accelerometers simultaneously undergoing the same cyclic motion.

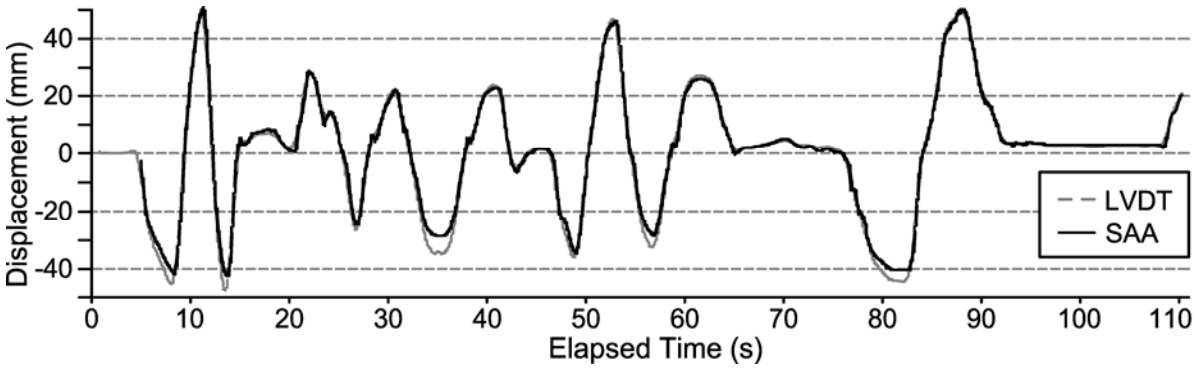

Figure 2.24 : Comparison between lateral displacements (mm) measured using traditional displacement sensors (LVDT) and a ShapeAccelArray sensor (after Abdoun et al. 2005).

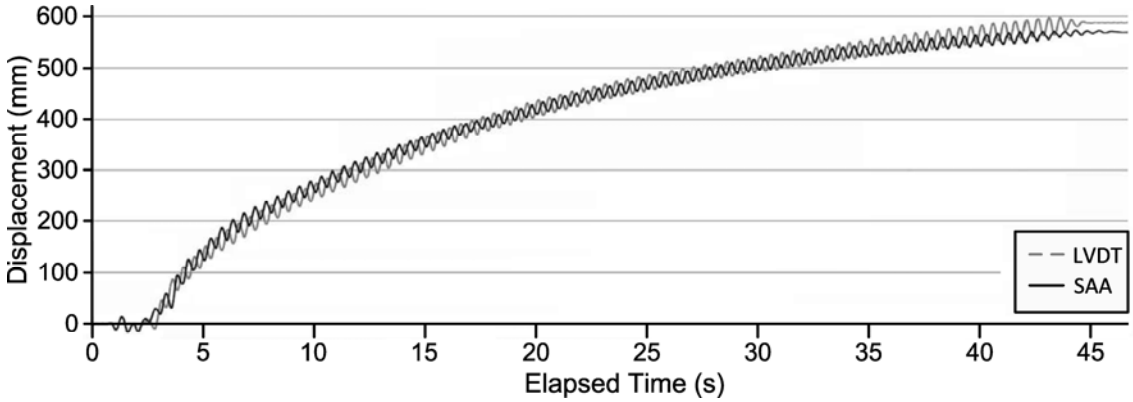

Figure 2.25 : A comparison of the displacements measured by the WSAA (SAA) and a reference LVDT (after Abdoun et al. 2007)

Chapter Three: An evaluation of real-time deformation monitoring using motion capture instrumentation and its application in monitoring railway foundations.

Contribution of the Ph.D. candidate

All work reported in this chapter, including field installation, design of the experimental program, implementation of the experiments, review of the literature, development of the theoretical framework, analysis and discussion of the results and writing of the text, has been carried out by the Ph.D. candidate.

As supervisors, Dr. S. L. Barbour and Dr. C.D. Martin have reviewed all parts of the work. This chapter has been published with the following citation:

Hendry, M.T., Barbour, S. and Martin, C.D. (2011). An evaluation of real-time deformation monitoring using motion capture instrumentation and its application in monitoring railway foundations, Geotechnical Testing Journal, **34**(6), 1-11.

Contribution of this chapter to the overall study

The instrumentation developed for installation at the study sites was designed to be comprehensive, in that it was to allow for the determination of the distribution of the change in effective stress (pore-pressure) and strain throughout the peat foundation during cyclic axle loading. This instrumentation design was based on the Lévis subdivision instrumentation, as well as experience gained from the study presented in Hendry (2007). The instrumentation packages included piezometers to measure the pore water pressure response of the soil. Extensometers were installed to measure the relative vertical motion at various depths within and below the embankment. The ShapeAccelArray (SAA) was to provide high resolution (many points with depth) and high accuracy measurements of the horizontal deformation of the foundation material during the passage of a train. These horizontal displacement measurements were to provide a clear picture of the distribution of horizontal strain with depth and consequently a clear picture of the deviatoric stress with depth.

The initial field SAA measurements provided data sets which were difficult to reconcile with expected soil behaviour. This manuscript presents the result a comprehensive laboratory testing program to test the accuracy of the array and the development of a method of interpreting the SAA measurements recorded in the field. This manuscript is unique as it presents the first application of MEMS based instrumentation to map both elastic and plastic horizontal deformations of a railway embankment and foundations and the first to provide a correction for MEMS readings under rapid cyclic deformation. The findings of this manuscript address the global objectives of this research as the spatial and temporal resolution of measurement taken with the SAA system clearly show the distribution and magnitude of the horizontal cyclic displacement within the embankment and the soft peat foundation due to the cyclical heavy axle loads.

Abstract

The purpose of this study was to evaluate the use of motion capture instrumentation to monitor the response of a railway embankment and the underlying soft peat mire foundation soils to freight train loading. Initial datasets were obtained from the motion capture system, called the ShapeAccelArray^{TM} (SAA), installed in a railway embankment. Review of the datasets from the site installation raised questions as to the ability of the SAA to provide accurate displacement measurements. Testing of the SAA in the laboratory confirmed that the output from the SAA system (inclusive of software) would not provide a true measurement of horizontal deformations during large cyclic motions. This inaccuracy was due to the magnitude of acceleration associated with the cyclical motion on the MicroElectroMechanical Systems (MEMS) accelerometers and the effect of this on the ability of the system to determine its shape.

A method for determining the magnitude of cyclic displacement from the output of the MEMS accelerometers was developed from the laboratory testing data. This involved the double integration of the change in acceleration measured by the accelerometers to obtain a change in displacement. This method was applied to the datasets obtained from the field installation to obtain a profile of cyclic displacement with depth.

3.1 Introduction

Railway embankments over peat foundations are difficult to build and maintain. Many of the existing embankments in Canada were constructed over 100 years ago, for shorter, slower and lighter trains. Large cyclic strains are produced within the peat foundation as a result of train loading. The large concentrated loads associated with trains are particularly destructive to rail-track structures due to the wear produced by large cyclic movements of the embankment and foundation.

A motion capture instrumentation system produced by Measurand Inc., called the ShapeAccelArray (SAA), was selected to obtain near continuous measurements of lateral deformation along vertical profiles within the embankment and underlying peat during cyclic train loading. This instrumentation was supplemented with more conventional geotechnical instrumentation (piezometers and extensometers). Since this was the first time the SAA had been used for such an application its performance under these conditions required evaluation. In order to evaluate the performance of the SAA for the types of motion experienced in the field it was essential that it be calibrated under controlled conditions in the laboratory, as this was the first time the SAA had been used for such an application. This paper presents the results of a laboratory calibration and interpretation of real-time SAA measurements and demonstrates how these interpretation methods can be applied to monitored horizontal deformations of a railway embankment and underlying foundation at a field site.

3.2 Background

The measurement of displacement within an earth structure during cyclic loading has traditionally relied upon the use of accelerometers, geophones and extensometers. Extensometers accurately measure the displacement of the surface of the embankment relative to a fixed anchor installed at the base of a borehole. Accelerometers and geophones measure acceleration and double integrate acceleration to obtain displacement. This approach has met with varying degrees of success (Hall 2000; Heelis et al. 2000; Kaynia et al. 2000; Madshus and Kaynia 2000; Konrad 2007). The resulting data from accelerometers and geophones is limited as they are installed at discrete depths and are restricted to a single axis (direction) of measurement.

The SAA is a MEMS (MicroElectroMechanical Systems)-based deformation monitoring system. The SAA consists of 305 mm (1 foot) rigid segments connected by a two degrees of freedom joint which allows the joint to bend but not twist (Fig. 3.1 and Fig. 3.2). The three dimensional coordinates of each joint (or node), and thus the 3D shape of the SAA, are calculated from the orientation and fixed length of each SAA section and the assumption that one of the ends is fixed in space (Abdoun et al. 2007). The SAA is not axially compressible and is often installed within a PVC access tube. Consequently, the array should not be used to measure vertical movement of the soil (Mikkelsen and Dunnicliff 2008). Interpretation of the data from a (near) vertically installed SAA can be used to measure the horizontal (2D) movement of each joint along the length of the array in a similar manner to inclinometer but in near-real-time as the earth structure deforms.

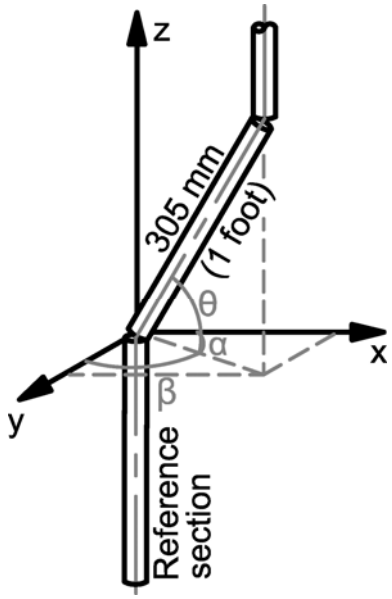

Figure 3.1 : Calculation of 3D shape of array from orientation of sections.

A Measurand Inc. research-grade SAA system along with a desktop computer for data processing was used in this study. This system allowed rates of data acquisition of up to 120 Hz. The system was modified for field use by installing the PCI card for data acquisition in a MAGMA external PCI to PCMI adaptor (MAGMA 2008). This alteration allowed the system to be run with a laptop computer. The use of the PCI to PCMI adapter resulted in slightly lower maximum data acquisition rates of up to 100 Hz. This reduced rate of data collection still provides sufficient resolution for the measurement of motion that occurs at frequencies less than 10 Hz.

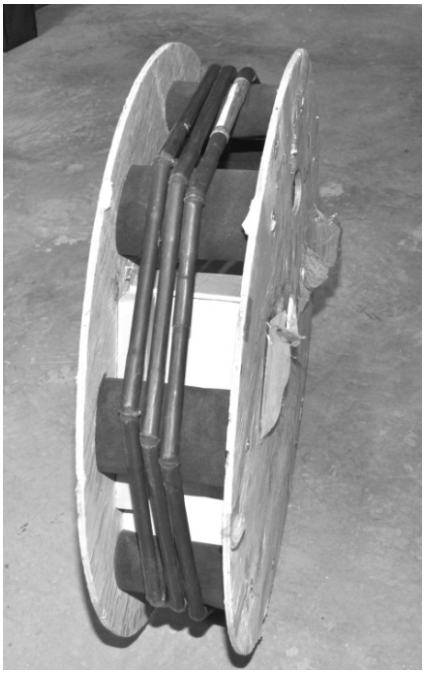

Figure 3.2 : Figure 2. SAA on spool (7.2 m (24 foot) array shown).

The SAA was initially developed to measure long-term deformation and is often installed vertically to act as an in-place inclinometer or horizontally to measure settlement (Abdoun et al. 2005, Abdoun et al. 2007). The slow rate of movement in these applications allows many readings to be averaged to obtain an accurate measurement of displacement. The SAA has been the subject of several studies to ensure the accuracy of the measurements under near static and slow rates of deformation (Abdoun et al. 2005, Abdoun et al. 2007). These studies compared the displacement measured with the SAA at a single node compared to the same motion measured with a linear variable differential transformer (LVDT). The results from Abdoun et al. (2005) (Fig. 3.3) showed good agreement between the SAA and LVDT measurements for motions occurring at estimated frequencies ranging between 0.05 Hz to 0.2 Hz. The results from Abdoun et al. (2007) (Fig. 3.4) also show a strong correlation between the data obtained from the SAA and the LVDT. The motion shows two different contributing frequencies. The first frequency is a very low frequency (estimated at 0.006 Hz) which contributes to the large overall motion. The error in the SAA in comparison to the LVDT as a percentage of overall displacement is estimated to be less than 2 %. A determination of the accuracy of the SAA measurement at the higher frequency (0.5 Hz), which produces the smaller oscillations, cannot be made from the data as it is presented, though it is comparable to the LVDT. The MEMS accelerometers contained within the SAA to measure the orientation of the SAA segments have been shown to

provide measurements of acceleration with accuracy comparable to high quality piezoelectric accelerometers (Abdoun et al. 2005).

The response at higher frequencies has not yet been thoroughly tested. Based on the studies mentioned above the SAA does provide an accurate measurement of *cyclic* displacement at frequencies less than 0.5. Typical frequencies associated with embankment deformations during the passage of trains can be much higher than those at which the SAA had been previously tested. For example, for a train travelling at 110 km/h, the measurement frequency would be approximately 7 Hz (Hendry 2007).

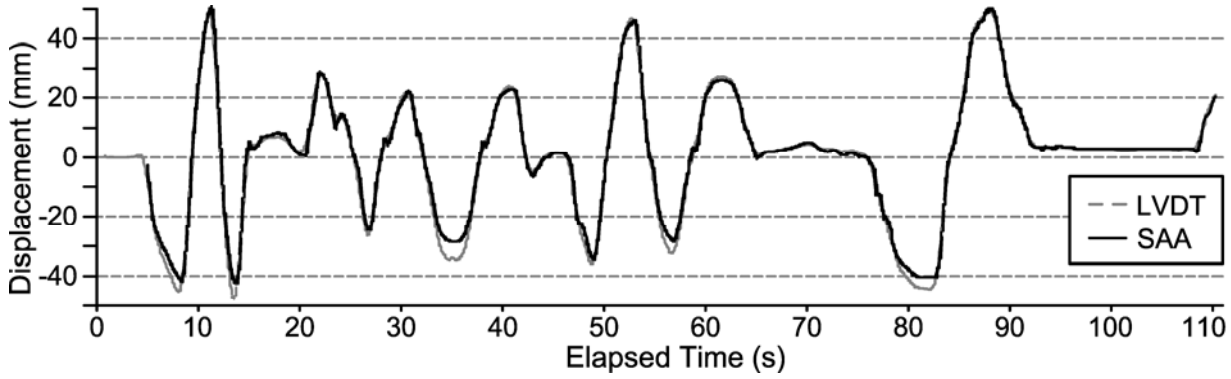

Figure 3.3 : Comparison between lateral displacements (mm) measured using traditional displacement sensors (LVDT) and a ShapeAccelArray sensor (after Abdoun et al. 2005).

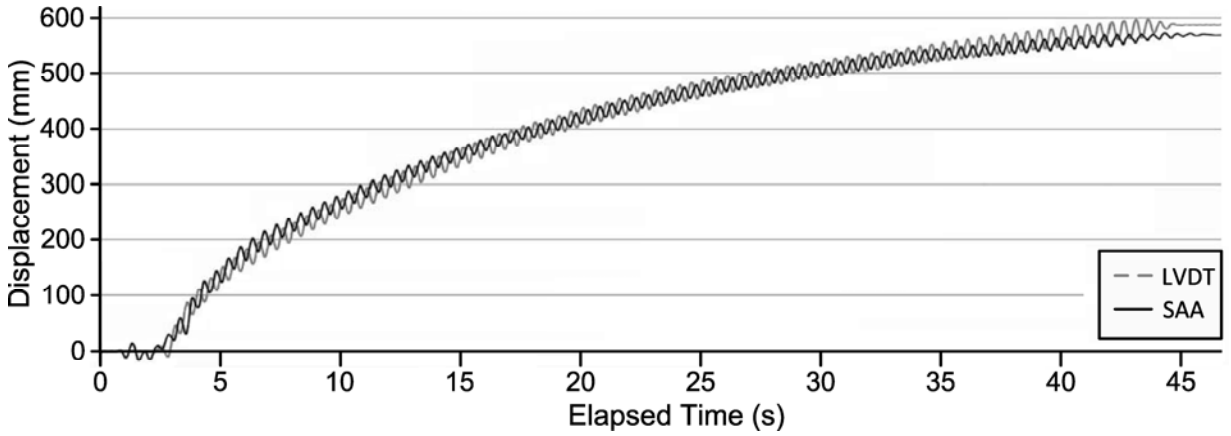

Figure 3.4 : A comparison of the displacements measured by the WSAA (SAA) and a reference LVDT (after Abdoun et al. 2007)

3.3 Study site

The CN mainline railway track runs east-west through Alberta, passing through Edmonton and Edson. The study site is located on a peat mire formation east of Edson between miles 101.4 and

102.6 (Fig. 3.5) of the Edson subdivision. The embankment was initially constructed in the 1920s, using a timber raft construction. The local terrain is flat (Fig. 3.6) and the embankment ranges from 1.6 to 2.0 m in height.

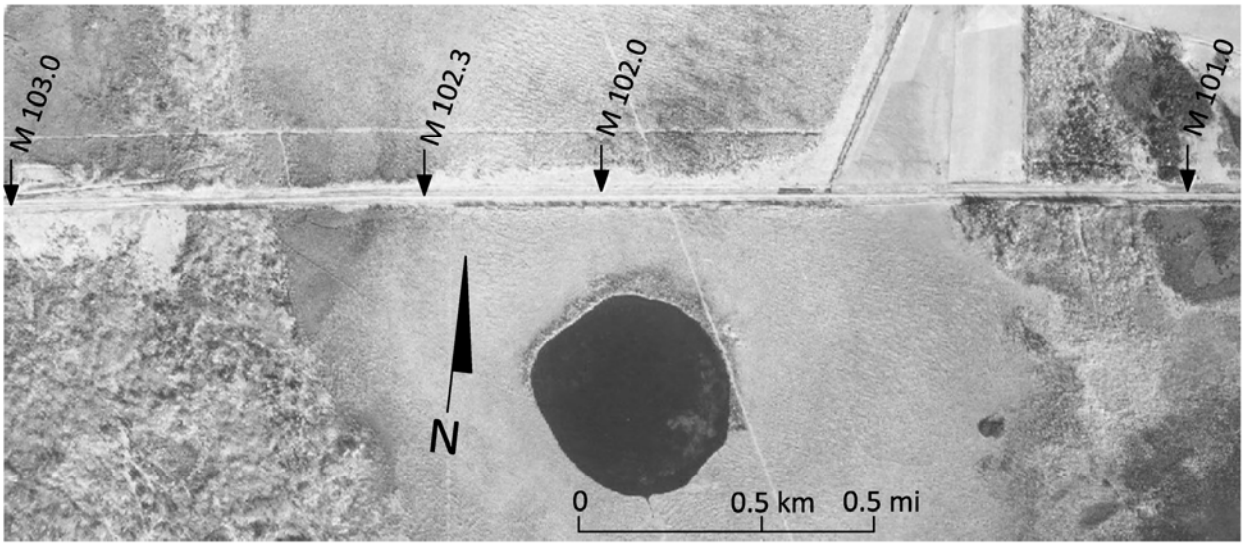

Figure 3.5 : Arial photograph of the Edson Subdivision peat bog crossing. Instrumentation installed at Mile 102.0.

Figure 3.6 : Surface conditions at Mile 102.0 during installation of instrumentation.

A ground investigation was conducted to determine the construction and composition of the embankment, and to provide information for the design and installation of a monitoring system. The embankment consists of ballast and sub-ballast to a depth of 1.2 m, underlain by

approximately 1.0 m layer of peaty organic fill material, a timber corduroy log raft, and then approximately 3 m of intact peat overlying silty-clay (Fig. 3.7). The timber corduroy was found to be in very good condition as was evident by the difficulty in drilling through it and the well preserved condition of samples obtained during drilling.

The 'conventional' instrumentation installed at the site consisted of strain-gauge piezometers and extensometers (constructed by RST instruments). Both types of instruments are capable of reading at a rate of up to 90 Hz, though most measurements were taken at 50 Hz. Three piezometers were installed under the centreline of the track, at depths of 5.8 m, 4.7 m and 3.1 m, to measure the generation of pore water pressure under train loading (Fig. 3.7). Three extensometers were installed approximately 0.6 m off the north end of the railway ties. The anchors of the extensometers were installed at depths of 7.46 m, 5.46 m and 3.46 m (Fig. 3.7). The data from this instrumentation is not presented in the paper, with the exception of extensometer data which is compared to the results from the SAA. The SAA was installed vertically in a PVC access tube 0.6 m off the north end of a railway tie (Fig. 3.7). A more detailed examination of the monitoring data from this instrumentation is presented in Hendry et al. (2008).

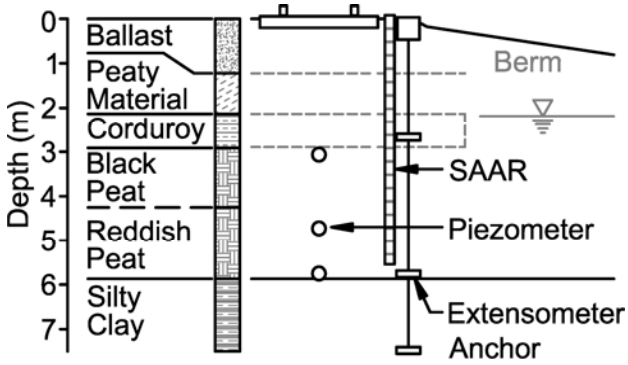

Figure 3.7 : Cross-section of embankment and foundation at Mile 102.0. Location and depths of the instrumentation are shown.

3.4 Preliminary field measurements

The horizontal motion of the embankment and peat measured by the SAA at the Edson subdivision site was resolved in two directions perpendicular and parallel to the rail (Fig. 3.8). Motion perpendicular to the rail is positive with deflections away from the rail, which indicates a

horizontal expansion of the embankment. Motion parallel to the rail is positive in the direction of train travel.

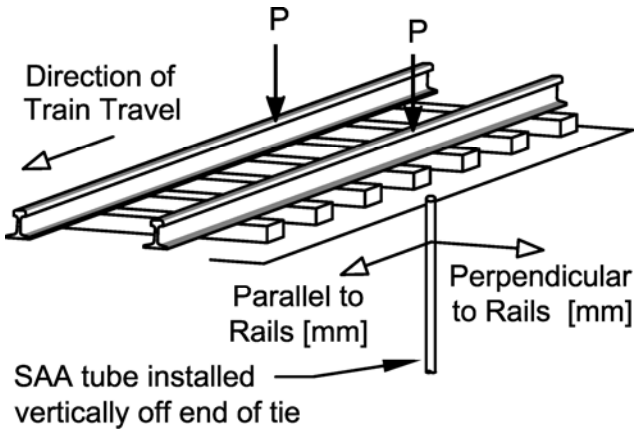

Figure 3.8 : Directions of SAA measured displacements in the railway embankment and foundation.

Given that the wheel loads are applied and removed quickly it is reasonable to assume that the peat behaves in a nearly undrained manner during the passing of individual axles or grouping of axles. Due to the undrained behaviour of the soil the vertical displacement should be strongly correlated to the horizontal displacements measured by the SAA. The SAA measurements of horizontal deflection and the extensometer measurements of vertical deformation are shown in Fig. 3.9. The dataset in Fig. 3.9 shows the overall patterns of movement obtained using a 30 point moving average. The 30 point averaging was required as the raw data showed very large peaks in calculated displacement which resulted in the data being unreadable. The 30 pt average was the minimum number of averaged points which revealed a correlation between the SAA displacements and the applied axle loads. A direct correlation between the extensometer and SAA data is apparent for node 1 but not for node 14 in Fig. 3.9. The perpendicular displacement measured at node 14 (Fig. 3.9) shows negative horizontal displacements, representing contraction of the embankment during train loading. The weights of locomotives and cars are routinely weighed by CN for billing purposes. The weights of the cars which comprise this train were used to determine the average axle loads shown in Fig. 3.9.

When plotted within the frequency domain (Fig. 3.10(a)) the frequency versus normalized magnitude plots of the extensometer data and the *parallel* SAA data (for node 14) show a strong correlation. The major frequencies contributing to these data sets range from 0.4 and 0.7 Hz (Fig. 3.10(b)). From examination of the extensometer data and the train geometry this

corresponds to the frequency of the passage of groupings of four axles at the coupling point of two railcars. The extensometer data and the *perpendicular* SAA data show a similar strong correlation between 0.4 and 0.7 Hz (Fig. 3.10(c) and Fig. 3.10(d)) but also with higher contributing frequencies, ranging from 0.8 to 1.4 Hz, which have relatively large magnitudes. The application of a low pass filter at 0.7 Hz to the SAA data output data results in displacement versus time plots very similar to those shown in Fig. 3.9. These higher frequency deformations are unlikely to be due to 'noise' in the measurements, as the distribution of the magnitude over the frequencies (or the shape of the graph) is very similar to that found between 0.4 and 0.7 Hz. It is most likely that these higher frequency responses are due to the higher frequency load applications of the loads from pairs of axles, which were not measured by the extensometer. The presence of this band of higher frequency (and magnitude of deformation) suggests that there may be exaggeration of the magnitude of deformation under higher frequency motion.

3.5 Laboratory testing of SAA

The laboratory component of this study compared the controlled, cyclic, deformations of a PVC tube used to house the SAA to those measured using the SAA under a range of frequencies. The laboratory apparatus consisted of a schedule 40 PVC conduit (the same as was used in the field installation) with the locations of the SAA nodes marked on the outside of the conduit. The SAA was inserted into the tube with webbing to ensure a tight fit. The tube was clamped in a vertical orientation to the side of an I-beam (Fig. 3.11). The clamps were custom made from U-Bolts with rubber backs and were clamped to the PVC tube at the marked locations of nodes to provide known stationary points at which comparisons could be made. A linear hydraulic actuator was used to create the deformation of the PVC tube along with a LVDT to measure the motion. The linear hydraulic actuator was clamped to the PVC tube at a location corresponding to node 8. The LVDT measurements were collected to allow for a comparison between the resulting SAA data and a known displacement. The LVDT measurements were made at a rate of 120 Hz. The tests were carried out with sinusoidal functions of varying frequency and magnitude. The frequencies were varied between 0.1 and 4.0 Hz and the amplitude of the motion ranged from 1 to 41 mm.

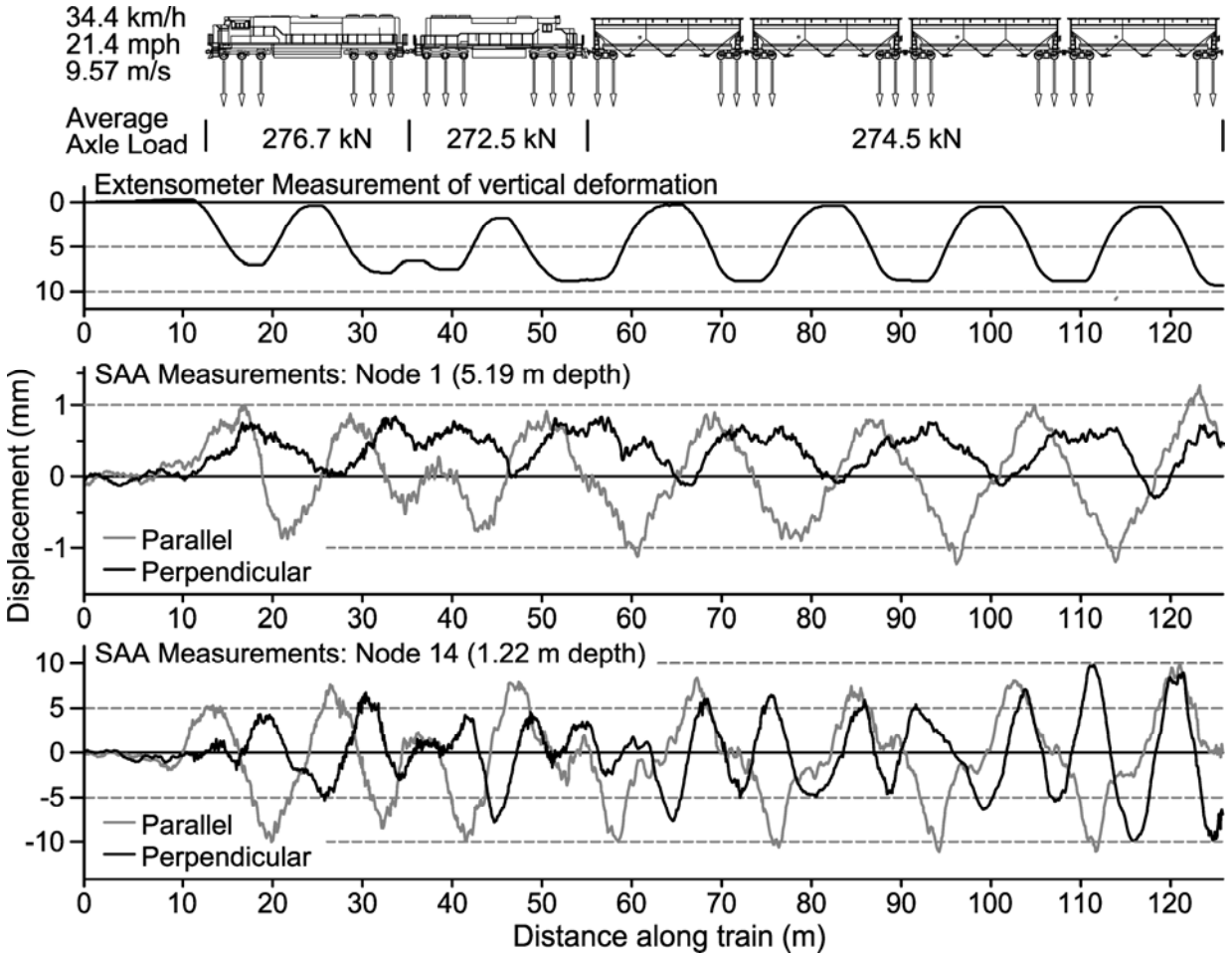

Figure 3.9 : Vertical displacement of the embankment and foundation (extensometer data) and the horizontal displacement observed from the *raw* SAA data for both the perpendicular and parallel directions at two different depths. Note: data was smoothed using a 30 pt average.

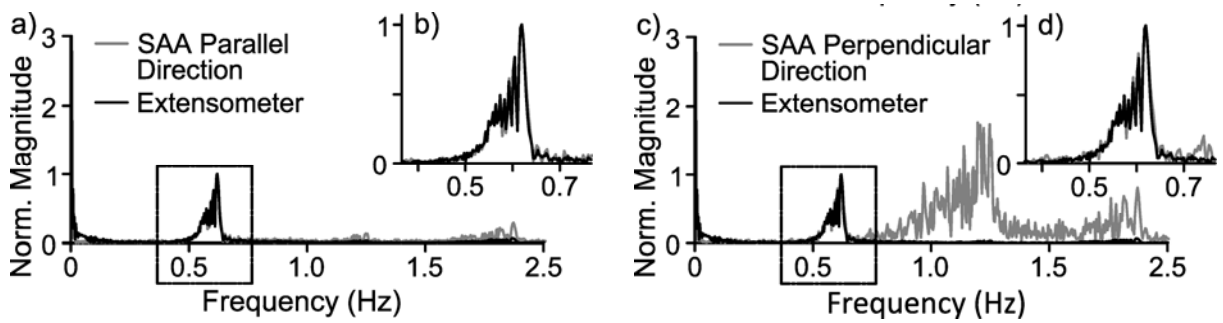

Figure 3.10: Comparison of the vertical displacement of the embankment and foundation (extensometer data) and the horizontal displacement from the *raw* SAA data in the frequency domain in the parallel (a) and perpendicular (b) directions. Note: Magnitudes of plots normalized to maximum value between 0.4 Hz and 0.7 Hz for each data set.

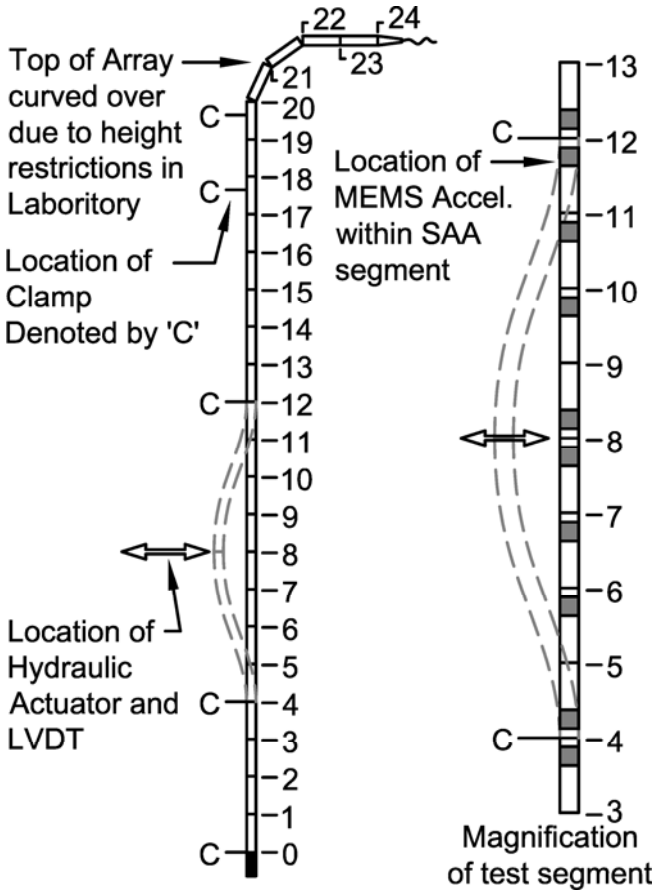

Figure 3.11 : Schematic of testing of SAA in laboratory. Node (joint) numbers and locations of MEMS accelerometers are shown. MEMS accelerometers are located one quarter of the length of the SAA segments (0.076 m) from nearest node or joint.

This preliminary evaluation of the SAA data sets highlighted concerns regarding the validity of the SAA measurements at higher frequencies. First, based on the literature review it was apparent that the SAA had not been tested at the frequencies and magnitudes of motions that were being measured within the embankments and peat sub grade at the Edson site. Second, the SAA measured negative horizontal displacements perpendicular to the track, representing a contraction of the embankment during train loading (Fig. 3.9). Finally, there were discrepancies between the nature of the measured vertical and horizontal (perpendicular) deformations within the peat. These discrepancies appear to increase with increasing frequency. Due to these inconsistencies between expected and measured behaviour of the soils, controlled testing of the SAA in the laboratory was undertaken to determine the accuracy and precision of the array.

3.5.1 Laboratory testing results

The difference between the displacements measured using the SAA and the LVDT during sinusoidal motion at a given frequency was expressed as a cyclic error factor (CE) defined as follows:

$$CE = \frac{M_{SAA}}{M_{LVDT}} \qquad [3.1]$$

where, M_{SAA} is the amplitude of the cyclical displacements as measured by the SAA and M_{LVDT} is the amplitude of the cyclical displacements as measured by the LVDT. A plot of CE versus frequency is presented in Fig. 3.12. These results clearly show increasing exaggeration of the magnitude of the motion with increasing frequency, diverging from a CE value of (near) 1 at very low frequencies to CE values and greater than 40 at a frequency of 4 Hz.

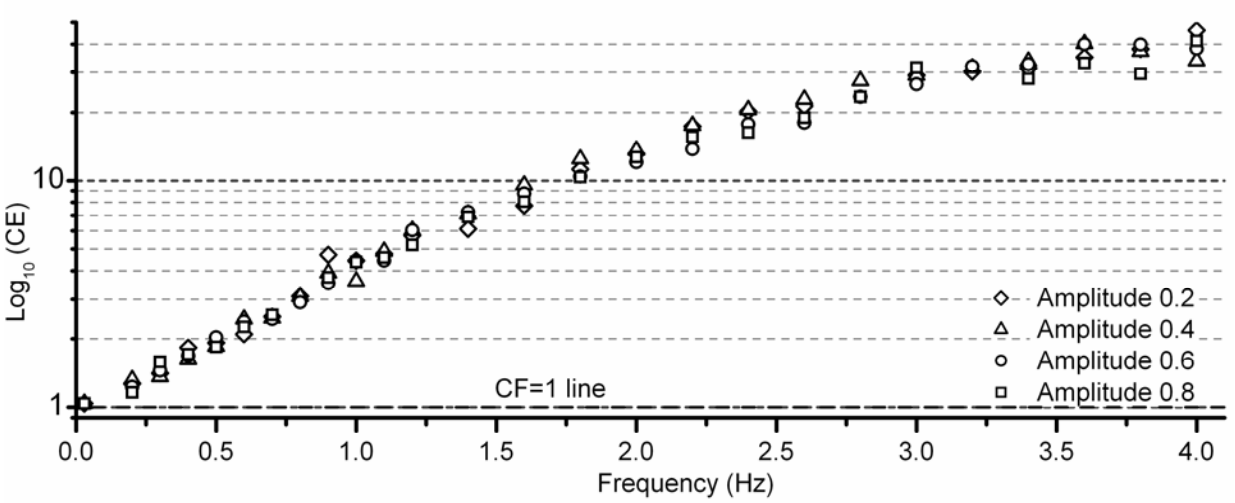

Figure 3.12: Resulting plot of error factor required for data sets (SAA/LVDT) versus frequency from laboratory testing data.

The observed discrepancy between the SAA and LVDT readings was hypothesised to be the result of the method by which the SAA software determines the direction of gravity and thus its vertical orientation from the MEMS accelerometer measurements and the acceleration due to the cyclical motion of the array.

The displacement and acceleration due to cyclical motion is described by equations 2 and 3 respectively.

$$d(t)_{cyclic} = D\cos(2\pi ft - \phi) \quad [3.2]$$

$$a(t)_{cyclic} = -(2\pi f)^2 D\cos(2\pi ft - \phi) \quad [3.3]$$

where, $d(t)_{cyclic}$ and $a(t)_{cyclic}$ are the displacement (mm) and the acceleration (mm/s^2), respectively, as functions of time, *D* is the amplitude of the cyclic displacement (mm), f is the frequency of motion (Hz) and ϕ is a phase shift (Radians).

The effect of the acceleration produced by the cyclic motion on the measured orientation of the SAA segment as determined by the SAA system (inclusive of the software) can be large. The orientation of the SAA segments is calculated by assuming that the direction of gravity is in the direction of the resultant of the accelerations measured by the three orthogonal MEMS accelerometers. This assumption works well under slowly changing or static conditions but not for cyclic motion as is evident in both the field and laboratory data. As shown in Fig. 3.14, the effect of the acceleration due to motion (**a**) on the orientation of the resultant acceleration (**R**) is a function of the magnitude of **a** and the orientation of the SAA segments (Fig. 3.13). The acceleration due to cyclic motion can thus result in an amplification (Fig. 3.13a), reduction (Fig. 3.13b) or event reversal (Fig. 3.13c) of the horizontal displacement.

The horizontal displacement at node 8 was known from the LVDT measurements during each test. The *actual* shape and horizontal displacements of all of the remaining nodes was interpolated for differing frequencies from measurements taken at a frequency of 0.03 Hz. From the interpolated shape of the array it was possible to calculate the horizontal acceleration, and thus model the SAA output. Fig. 3.14 presents a comparison of the interpolated (actual) shape of the SAA, the shape obtained directly from the SAA output and the modelled shape, for differing frequencies of motion. The modelled and measured SAA output show very close agreement. This suggests that the acceleration due to the cyclical motion is the cause of the erroneous SAA output.

It is apparent from the controlled testing in the laboratory that the SAA system cannot be used directly to provide accurate displacement measurements for cyclic displacements above 0.03 Hz. Several different approaches were of modifying the SAA output to directly provide accurate measurements; however these proved unsuccessful. Since the error is a function of the magnitude and frequency of the motion, any attempt to modify the SAA software outputted displacement

dataset within the frequency domain does not take into account the effect of the orientation of the array segments (Fig. 3.13) and is consequently ineffective. An attempt to overcome the statically indeterminate nature of the forces on the accelerometers was attempted by assuming that the cyclical acceleration due to motion is occurring strictly in the horizontal plane (the same assumption used in the modelling of the laboratory data above) However, the variations in the magnitude of the output from one accelerometer to another were large enough to limit the ability to fully distinguish the acceleration due to gravity from the measured acceleration (due to both gravity and horizontal motion) without extensive calibration of each individual segment.

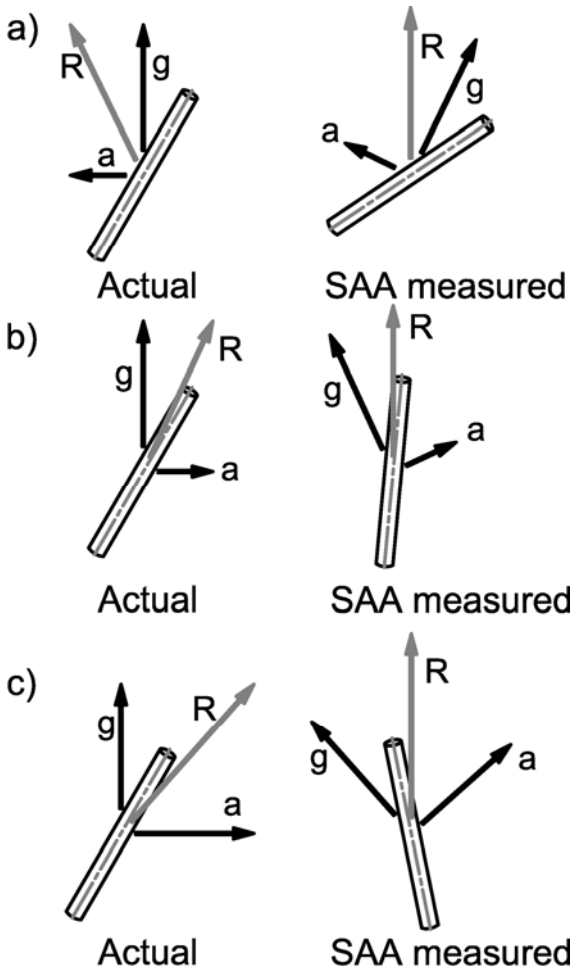

Figure 3.13 : An illustration of a) amplification errors b) reduction errors and c) reversal of direction errors in the measured orientation of the SAA section and the horizontal location due to the SAA software's interpretation of the horizontal acceleration (**a** is the acceleration due to motion, **g** is the acceleration due to gravity and **R** is the resultant of **a** and **g** the direction of which the SAA software interprets as the direction of **g**)

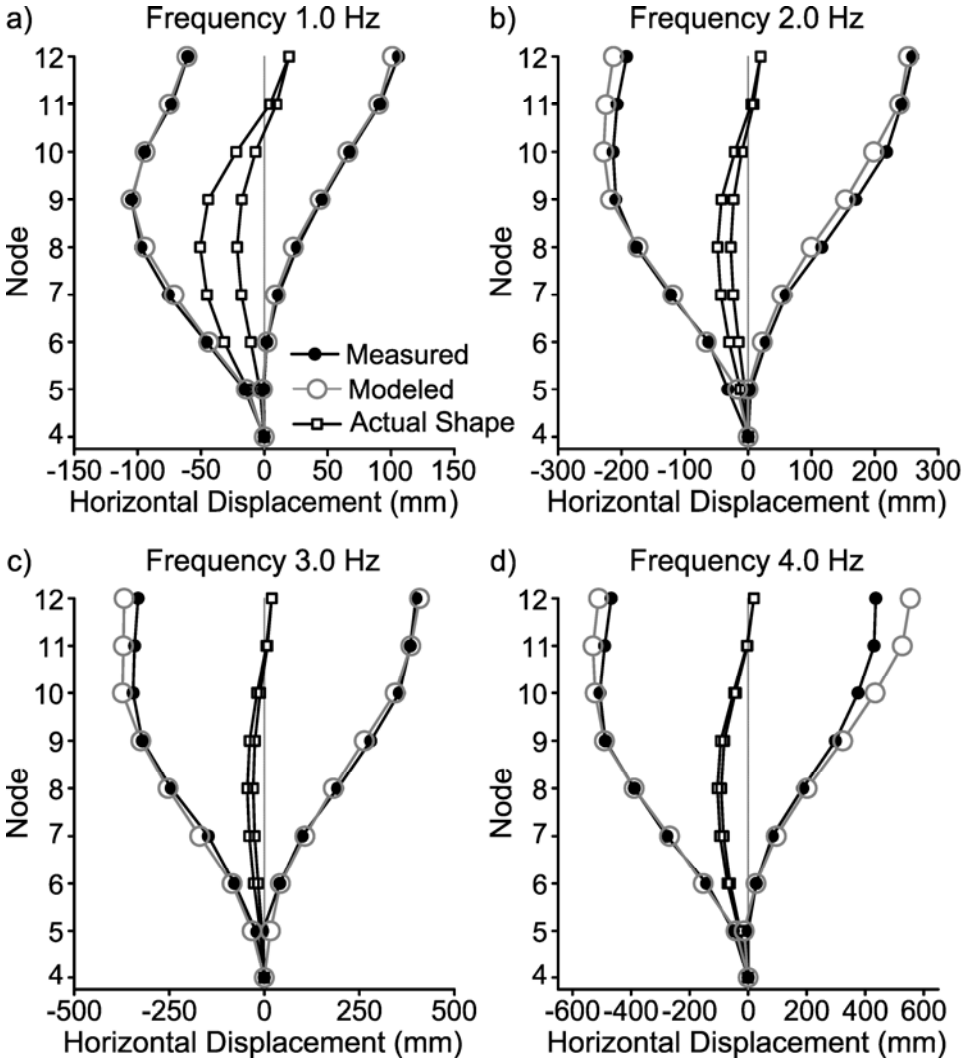

Figure 3.14: Comparison of the measured SAA motion as provided by the SAA software, the actual SAA shape and motion determined from the LVDT data, and the SAA output modelled from the actual SAA shape and motion and the orientation of the array with respect to gravity. Shown for cyclic frequencies of a) 1.0 Hz, b) 2.0 Hz, c) 3.0 Hz and d) 4.0 Hz.

The method which proved most successful was using the MEMS accelerometers to directly measure the changes in acceleration due to motion. The accelerations can then be integrated with time to obtain velocity versus time and then again to obtain displacement versus time. This integrated displacement is calculated for the accelerometer within the SAA segment - not the nodes/joints of the array. This calculation is done with the assumption that the measured change in acceleration is due to translational motion, and thus the change in acceleration due to gravity as the section undergoes slight rotation with the horizontal motion is insignificant. The basis for the double integration method and the required baseline correction was drawn from Hall (2000).

The double integration is conducted for various times resulting in a measurement of the change in displacement. The calculated displacement at any time is the sum of all changes in displacement which have proceeded that time. The resulting error in the displacement at any time is consequently the sum of the error which has proceeded that time.

In the case of sections that are not near vertical, the initial (static) output from the SAA provides the orientation of the sections and thus the orientation of the MEMS accelerometers with respect to vertical. This initial orientation measurement taken along with the three dimensional displacements from the double integration, allows for the rotation of the Cartesian axis of the integrated displacements into the horizontal plane, rather than relative to the orientation of the SAA section. The two resulting horizontal directions allows for rotation of the data about the vertical axis in post processing in the event that the X and Y axis as defined by the SAA are not in the ideal directions for the interpretation of the displacements. This would be the case when the X and Y directions of the SAA are not aligned with the perpendicular and parallel directions relative to the railway track.

Fig. 3.15 shows the results of this interpretation of the SAA measurements as compared to the LVDT data. It is apparent from the start of each data set (before cyclic motion) that the hydraulic actuator generates a high frequency oscillation. The accuracy of the SAA measured datasets are thus affected by this high frequency oscillation and this results in some deviations of the SAA values from the measured LVDT values at any individual peak (standard deviation of ±2 mm). These deviations do appear to increase with increasing frequency of cyclic motion. However, the overall pattern of movement taken over multiple peaks provides an accurate measurement of the LVDT motion with error between the median LVDT cyclic displacement and the corresponding SAA measured cyclic displacements ranging between 0.04 and 0.33 mm. This error expressed as CE values ranges from 0.92 to 0.97. This suggests that a statistical analysis of the *cyclic* displacements should provide reasonably accurate measurements of ground motion.

3.6 Field application

The proposed method for processing the SAA readings developed from the laboratory study was applied to the datasets collected at the Edson Subdivision site. Fig. 3.16 shows the same data set as shown in Fig. 3.9, but with displacements obtained directly from double integration of the

measured accelerations. The integrated displacements did not require filtering or smoothing unlike the original SAA output. As the double integration calculation is cumulative it is insensitive to these very high frequency and magnitude accelerations measured by the MEMS accelerometers which constituted the 'noise'. The correlation between the extensometer data and the SAA data in Fig. 3.16 is now evident. The maximum and minimum deformations from the extensometer data and the perpendicular SAA data show a strong correlation with the applied axle loads. This data set is displayed as cyclic displacement versus depth in Fig. 3.17 for all accelerometers. Fig. 3.17 shows the measured cyclic displacement of the embankment and foundation during the passage of grain cars from the last 30 cars of the dataset. It is for the measurement of the cyclic displacement that the accuracy of the SAA has been determined.

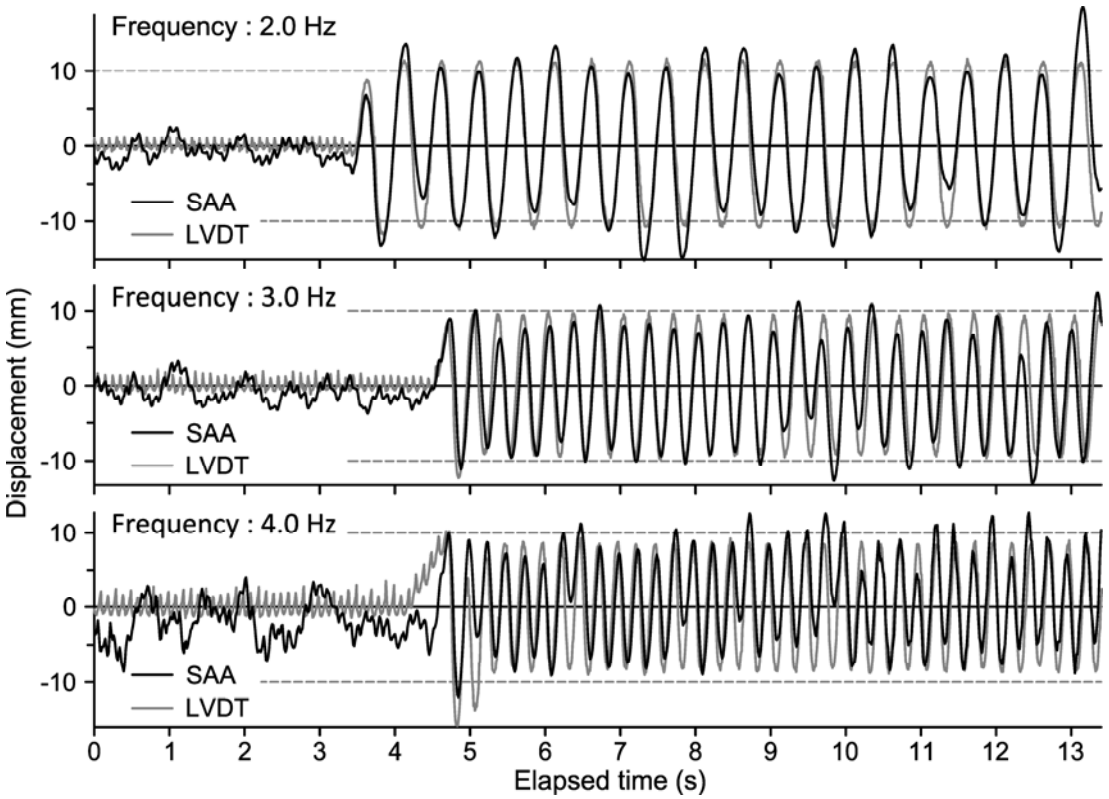

Figure 3.15: Comparison of measured (LVDT) displacements and displacements calculated from double integration of the SAA accelerometer output from the laboratory study. The graphs present a comparison of the motion of node 8 to the integrated displacement for accelerometer 8 which is located 76.2 mm (3") above the node.

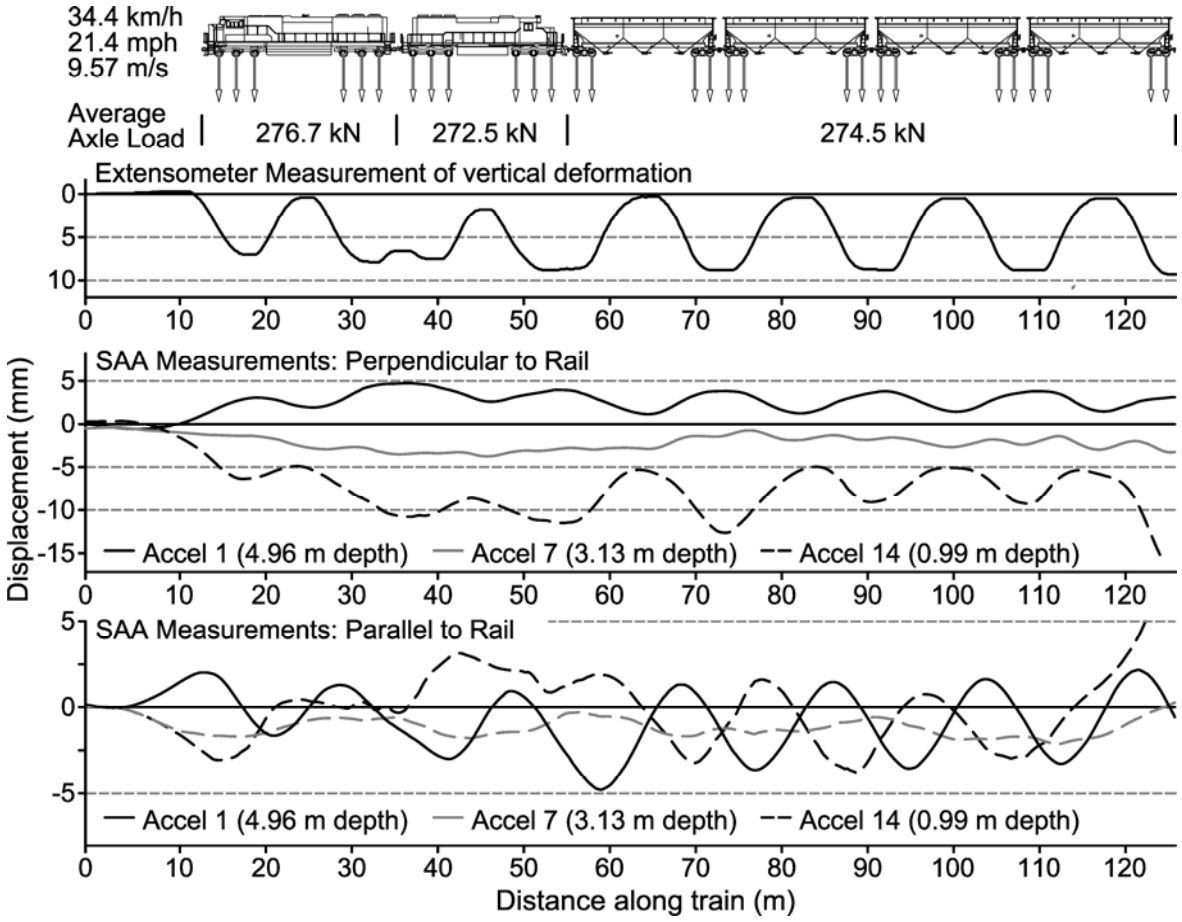

Figure 3.16: Vertical displacement of the embankment and foundation (extensometer data) and the horizontal displacement from the double *integrated* SAA data for both perpendicular and parallel directions at three different depths.

The pattern of *cyclic* displacement shown in Fig. 3.17 is consistent with results from finite element modelling of the embankment and foundation as a simple linear elastic soil, though the magnitudes and distribution of the displacement are currently under investigation[5]. The lower peat foundation material was found to spread laterally during the undrained (fast) loading, consistent with an undrained soil acting as an elastic solid. The embankment materials were measured and modelled to be rotating inwards with the formation of a deflection bowl on the surface. The measured peat responses in both perpendicular and parallel directions are very similar both in shape and magnitude. Considering the stiffness and negligible vertical strain (as measured with the extensometers) of the silty-clay base, the cyclic displacement of the deepest

[5] Further explanation of this modelling is presented in Appendix D; Section D.2.

MEMS accelerometer suggests that there is a zone of significant shear at or near the interface between the peat layer and the underlying silty-clay. The differences in magnitude of the response of the embankment materials in the perpendicular and parallel directions are likely to be a result of the differences in geometry of the embankment in those directions. The rigidity of the PVC tube and SAA are assumed to smooth large gradients of displacement found in shear zones likely resulting from the contrasting stiffness of the fill and peat materials and the presence of the corduroy.

An alternative method to the double integration procedure is the use of a Fast Fourier Transform (FFT) to determine the major contributing acceleration frequencies and their magnitudes. The benefit of the FFT method is that the major contributing frequencies can be obtained from a sampling rate of only twice the frequency being measured. In the case of this train passage this would have required a sampling rate of only 1.24 Hz as opposed to the 100 Hz at which these measurements were taken. Equation 3.4 is derived from Equations 3.2 and 3.3 and shows the correlation between the magnitude of cyclic displacements and cyclic accelerations.

$$d(t)_{cyclic} = \frac{\mathrm{a}(t)_{cyclic}}{-(2\pi f)^2} \qquad [3.4]$$

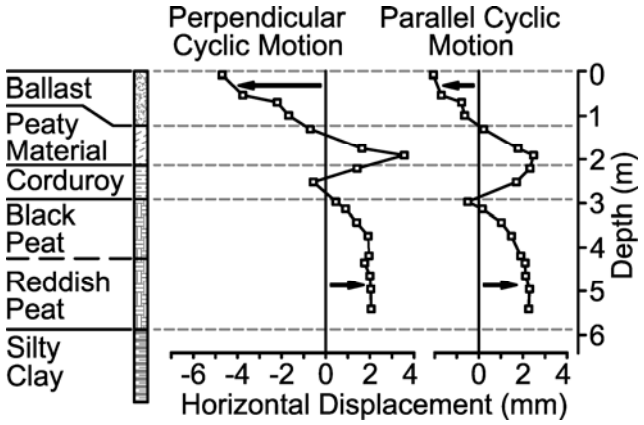

Figure 3.17: The magnitude and direction of the cyclic deformation measured by the SAA during train loading by the heavy grain train in both the perpendicular and parallel directions. Note: the cyclical displacement in parallel direction is calculated as one half of the cyclic displacement as the displacement cycles between in front and behind the moving train loads.

A FFT was applied to a small segment of the dataset in which there is consistent loading so that the frequency (*f*) and the magnitude of the cyclic acceleration can be determined. Fig. 3.19 shows

a comparison of the cyclic displacements determined using the magnitude of acceleration at the major contributing frequency (0.62 Hz) and the displacements determined from the double integration of the acceleration measured by all MEMS accelerometers. From Fig. 3.19 it is apparent that the FFT method overestimates the motion, likely due to the actual displacement pattern deviating from a sinusoidal shape, as is shown in the extensometer data in Fig. 3.16.

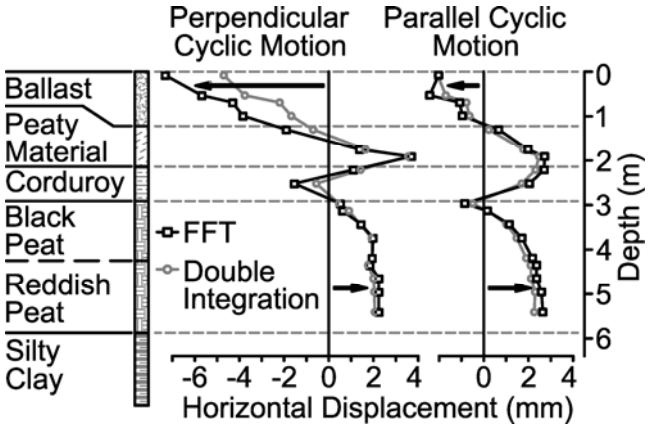

Figure 3.18: A comparison between the magnitude and direction of the cyclic deformation versus depth profiles determined by use of the Fast Fourier Transform (FFT) and by Double Integration.

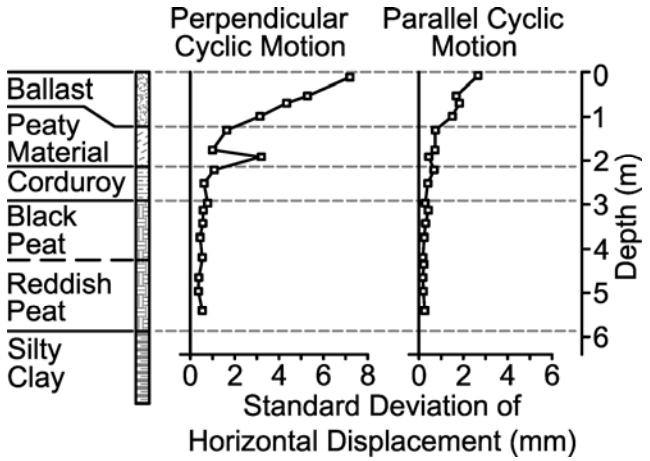

Figure 3.19: Standard deviation of the cyclic horizontal displacement as determined by double integration versus depth plots of for the cyclic horizontal displacements measured by the SAA during train loading by the heavy grain train.

Since the deformation of the soil is cyclic, with a consistent magnitude and frequency, a measurement can be made of the accuracy and consistency of the measurements *in situ*, in the form of a standard deviation of the horizontal displacements with depth. The results of this analysis are presented in Fig. 3.20. It is interesting to note that there is an increasing reliability

in the readings with increasing depth as the standard deviation reduces from a range of 2 to 6 mm near the surface down to 0.3 mm within the peat. This is also apparent in Fig. 3.16 when comparing the consistency of the measured cyclic displacement from accelerometer 1 to that of accelerometer 14. As with the laboratory data, the upper section of the SAA is subject to higher frequency motion due to the dynamics of the train. The effect of this higher frequency motion is decreased with depth resulting in increased reliability of individual measurements with increasing depth.

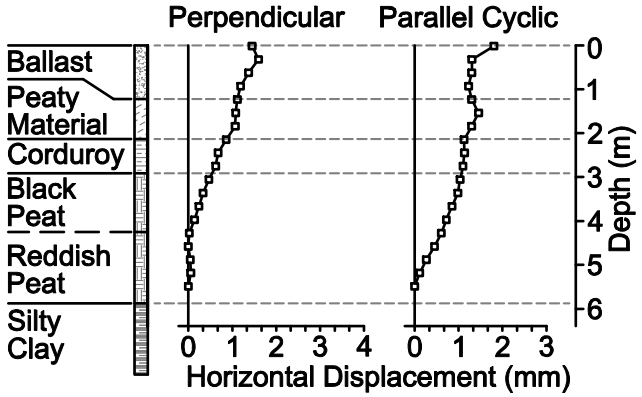

Figure 3.20: Horizontal deformations not recovered (relative to the lowest SAA section) as measured by the SAA before and after train loading by the heavy grain train.

The linear baseline correction of the data during processing forces the final shape of the SAA to be the same as it was at the beginning of the dataset. This baseline correction was done as only the calculation of the cyclic displacement from the SAA measured accelerations was determined to be accurate, and consequently does not allow for the measurement of non recoverable horizontal deformation. However, since the array is not undergoing cyclic motion at the beginning (before the train) and at the end (after the train) of the data set the SAA can still function accurately as an in-place inclinometer, the original purpose of the instrument. The resulting change in shape of the array provides a measure of the distribution and magnitude of permanent deformation within the embankment. Unlike the displacements integrated from the accelerometers, the SAA change in shape is taken relative to the base of the instrument, thus the lower node is assumed static, similar to the assumption for interpreting slope inclinometer data. In the installation at the Edson site this is obviously not the case as the lowest section is known to move considerably (Fig. 3.17). For this data set the permanent horizontal displacement of the embankment and underlying peat relative to the deepest SAA section is shown in Fig. 3.20. This plastic deformation did not recover before the passage of the next train 14 minutes later.

3.7 Conclusion

SAA output when used as an in-place inclinometer provides accurate measurements of displacement at very low frequencies of motion. However, results from the laboratory testing presented in this paper show that this accuracy is lost with cyclic motion at frequencies greater than 0.02 Hz. This loss of accuracy was shown to be due to the SAA software interpreting the acceleration due to the cyclical motion as a component of gravity, resulting in an incorrect determination of the orientation of the SAA segments and of the shape calculated from these orientations. The use of the SAA outputs for the displacement of the instrument at higher frequencies results in significant errors due to the large cyclical accelerations measured by the MEMS accelerometers in the SAA segments. When used as an array of accelerometers to directly measuring the magnitude of cyclic motion, the SAA becomes a useful and accurate instrument. The SAA was shown to have less than 0.33 mm of error for the measurement cyclic motion with consistent amplitude.

The spatial and temporal resolution of measurement and ease of installation of the SAA system made it possible to obtain measurements at the Edson site which are unique, and clearly show the distribution and magnitude of the horizontal cyclic displacement within the embankment and the soft peat foundation due to the cyclical heavy axle loads. Other available methods of measurement could not have produced this quality of data set. This technology is now being used to assess the foundation performance at various soft soil sites in Western Canada.

3.8 Acknowledgements

The writers would like to acknowledge the contribution of Canadian National Railways for providing both the research site and funding, and in particular Tom Edwards for his support of this project. This research was made possible through the Railway Ground Hazard Research Program, funded by the Natural Sciences and Engineering Research Council of Canada (NSERC), Canadian Pacific Railway, Canadian National Railway, and Transport Canada. The writers would also like to acknowledge Measurand Inc. for providing assistance in installation and development of a SAA system to meet the needs of this study.

3.9 References

Abdoun, T., Danisch, L., and Bennett, V. 2005, "Wireless Remote Monitoring of Geotechnical Systems," Geotechnical Engineering for Disaster Mitigation and Rehabilitation, Proceedings of the 1st International Conference., Singapore. pp. 515-520

Abdoun, T., Abe, A., Bennett, V., Danisch, L., Sato, M., Tokimatsu, K., and Ubillia, J. 2007, "Wireless Real Time Monitoring of Soil and Soil-Structure Systems," GeoDenver 2007: New Peaks in Geotechnics, ASCE Conf. Proc. Vol. 224, No. 5 pp. 1-10.

Hall, L. 2000, "Simulations and Analyses of Train-Induced Ground Vibrations," Doctoral Thesis, Royal Institute of Technology, Stockholm, Sweden.

Heelis, M.E., Collop, A.C., Dawson, A.R., Chapman, D.N., and Krylov, V. 2000, "The 'Bow-Wave' Effect in Soft Subgrade Beneath High Speed Rail Lines," Performance Verification of Constructed Geotechnical Facilities, Geotechnical Engineering Special Publication Vol. 94, pp. 338-349.

Hendry, M. 2007, "Measurement and Analysis of the Train-induced Dynamic Response of Railway Track and Embankments Constructed over Soft Peaty Foundations," MSc. Thesis, University of Saskatchewan, Saskatoon.

Hendry, M., Martin, C.D., Barbour, S.L., and Edwards, T. 2008, "Monitoring cyclic strain below a railway embankment overlying a peaty foundation using novel instrumentation," In 61st Canadian Geotechnical Conference, Edmonton, Alberta, Canada, pp. 1034-1041.

Kaynia, A.M., Madshus, C., and Zackrisson, P. 2000, "Ground Vibrations from High-Speed Trains: Prediction and Countermeasure," Journal of Geotechnical and Geoenviromental Engineering, Vol. 126, No. 6, pp. 531-537.

Konrad, J.-M., Grenier, S., and Garnier, P. 2007, "Influence of Repeated Heavy Axle Loading on Peat Bearing Capacity," In 60th Canadian Geotechnical Conference. Ottawa, pp. 1551-1558.

Madshus, C., and Kaynia, A.M. 2000, "High-Speed Railway Lines on soft Ground: Dynamic Behaviour at Critical Train Speeds," Journal of Sound and Vibration, Vol. 231, No. 3, pp. 689-701.

MAGMA 2008. 1 Slot PCI Expansion System, http://www.magma.com/products/pci/1PCI/index.html, San Diego, CA.

Mikkelsen, E., and Dunnicliff, J. 2008, “Some Views on a Recent Addition to our Instrumentation Tool Box-the ShapeAccelArray (SAA),” In Geotechnical News. pp. 28-30.

Chapter Four: Effect of fibre content and structure on anisotropic elastic stiffness and shear strength of peat.

Contribution of the Ph.D. candidate

All work reported in this chapter, including sample collection, design of the experimental program, implementation of the experiments, review of the literature, development of the theoretical framework, analysis and discussion of the results and writing of the text, has been carried out by the Ph.D. candidate.

As supervisors, Dr. S. L. Barbour and Dr. C.D. Martin have reviewed all parts of the work. This chapter will be published with the following citation:

Hendry, M.T., Sharma, J., Martin, D. and Barbour, S., 2011. Effect of fibre content and structure on anisotropic elastic stiffness and shear strength of peat. *Canadian Geotechnical Journal*, in press.

Contribution of this chapter to the overall study

The unique strength and stiffness characteristics of peat are due to the presence and properties of the organic fibre which form the bulk of the peat structure. The measured strength of peat has been shown to be dependent on the test method employed, with higher values of strength determined from triaxial testing of fibrous peat and lower values from the direct shear testing and ring shear testing (Section 2.2). These differing values of the strength have been attributed to the reinforcing effect of the peat fibres. The following manuscript endeavours to understand and characterize the effects of fibre content and the *in situ* structure on the undrained elastic response and strength of the peat. This study is a unique and comprehensive investigation into the effect that peat fibres and *in situ* structure have on the anisotropic elastic response of peat based on analysis of the resulting effective stress paths. Further, the manuscript quantifies the effect of the

fibre reinforcement on strength and develops this understanding within a conceptual framework developed from the literature on fibre reinforced soils and critical state soil mechanics. The findings directly address the global objective of this research as the undrained cross-anisotropic pore pressure generations, stiffness, and strength define the response and stability of the peat foundations while subjected to cyclic axle loads.

Abstract

This paper presents the results of a laboratory testing program involving consolidated undrained triaxial tests and direct shear tests on remoulded peat, remoulded peat fibre and Shelby specimens of peat obtained from a field site located on the Edson Subdivision of the Canadian National railway in Alberta, Canada. These results were analyzed within the frameworks of elastic behaviour of cross-anisotropic materials and shear strength of fibre-reinforced soil. Shelby specimens were found to be inherently cross-anisotropic whereas the remoulded peat and peat fibre specimens showed a transition from isotropic to cross-anisotropy with increasing vertical strain and effective confining pressure. The horizontal stiffness of Shelby specimens was found to be 2.6 to 2.9 times their vertical stiffness. The shear strength of intact peat is made up of inter-particle friction as well as tension in the peat fibres. A novel procedure for estimating the critical state inter-particulate frictional strength of fibrous peat from CU triaxial test results is proposed. It involves extrapolating the linear strain hardening portion of the stress-strain curve to obtain deviatoric stress at zero axial strain and plotting the deviatoric stress values thus obtained against initial mean effective confining pressure to obtain the critical state frictional strength. Using this procedure, a value of 31° was obtained for the inter-particle friction, which compares favourably with a value of 31° obtained from direct shear tests. It is recommended that the further studies be undertaken to assess if inter-particle frictional strength is the most appropriate strength parameter to evaluate the stability of structures founded on fibrous peat.

4.1 Introduction

Allowable axle loads have tripled on Canadian railways, since the construction of a majority of the railway infrastructure. The volume of traffic on the main lines of the Canadian National (CN) and Canadian Pacific (CP) railways are close to their maximum capacities with trains now reaching over 3.6 km (12,000 feet) in length (Van Hattem 2011). These two factors have had

detrimental effects on the infrastructure, particularly those that are built on poor foundations, such as railroad embankments built over peat. Both CN and CP railways are experiencing continuing problems with large stretches of embankments built over peat. These problems, which range from excessive settlements requiring increased amounts of maintenance to sudden catastrophic failures, have highlighted the need to develop a better understanding of the load-deformation response of peat foundations subjected to heavy axle loads (Konrad et al. 2007).

Peat specimens for the laboratory testing program presented in the paper were obtained from a study site located on mile 102.0 on CN railway's Edson subdivision in Alberta, Canada. The laboratory testing program comprised consolidated undrained triaxial tests and direct shear tests on remoulded peat specimens and consolidated undrained triaxial tests on Shelby specimens trimmed from Shelby tube samples. The results of these tests were analyzed within the frameworks of elastic behaviour of cross-anisotropic materials and shear strength of fibre-reinforced soil.

4.2 Background

The shear strength of peat is dependent on the means by which it is tested. Triaxial testing of fibrous peat gives values of the effective angle of friction (ϕ') as high as 48° to 68° (Landva and Rochelle 1983; Farrell and Hebib 1998; Hebib 2001; Long 2005; Mesri and Ajlouni 2007). Direct shear testing and ring shear testing of peat results in lower values of ϕ', ranging between 20° and 38° (Farrell and Hebib 1998; Hebib 2001). Higher values of ϕ' obtained from triaxial tests can be attributed to the reinforcing effect of peat fibres. Lower values of ϕ' obtained from direct shear and ring shear tests represent the inter-particle frictional resistance (Landva and La Rochelle 1983; Farrell and Hebib 1998; Hebib 2001).

Fibre orientation in peat is predominantly horizontal because of fibre deposition and the large vertical strains experienced during the one-dimensional consolidation following fibre deposition (Landva and Pheeney 1980). This predominantly horizontal orientation of the fibres provides additional shearing resistance and an elastic stiffness that is cross-anisotropic (Yamaguchi et al. 1985). Peat fibres have negligible compressive strength. As such, the reinforcing effect of these fibres is due to tension generated in the fibres during expansive (tensile) strains in the horizontal plane. Thus, normal compression of peat in the vertical direction results in fibres' mobilizing

tension and providing reinforcing. No such mobilization of tension occurs during compression of peat in the horizontal direction. Consequently, the load-deformation response of peat is a function of the orientation of the principal stresses with respect to the predominant (horizontal) orientation of fibres, with the stiffest response observed for the case in which the major principal stress is perpendicular to the predominant orientation of fibres. The results of laboratory testing of peat presented by Yamaguchi et al. (1985) confirm such anisotropic load-deformation behaviour. For vertically-oriented peat specimens (that is, horizontal orientation of fibres), Yamaguchi et al. (1985) report a value of ϕ' between 51° and 55° whereas a significantly lower value of 35° is reported for horizontally-oriented specimens.

This anisotropic load-deformation response in peat is similar to that of fibre-reinforced soils which is also dependent upon the orientation and the amount of fibre present (e.g. Michalowski and Čermák 2002; Li and Ding 2002; Michalowski and Čermák 2003; Kumar et al. 2006). The strain hardening response of fibre-reinforced soil at large strains (Michalowski and Čermák 2002) is also observed in peat. These similarities in behaviour are discussed in more detail in the subsequent sections describing the results of the laboratory testing program.

4.3 Study Material

The study site is located on CN's main line between miles 101.0 and 103.0 on the Edson Subdivision near the town of Niton Junction, Alberta (Figure 4.1) where the railroad crosses a large expanse of peat bog (Figure 4.2). The railroad embankment was constructed between 1909 and 1912 as part of the Grand Trunk Railway (Lester 2005). Extensive repairs were needed in 1998 for several sections of railroad embankment and the site has continued to require extensive maintenance to present day.

A ground investigation was conducted to determine the construction and composition of the embankment, and to provide information for the design and installation of a monitoring system (Hendry et al. 2008). The embankment consists of ballast and sub-ballast to a depth of 1.2 m, underlain by approximately 1.0 m layer of peaty organic fill material, a timber corduroy log raft, and then approximately 3 m of intact peat overlying unoxidized silty clay. The upper half of the intact peat layer is dark brown whereas the lower half of the peat layer is reddish brown. The peat has a fine fibrous texture as observed in scanning electron micrographs (Figure 4.3). Figure

4.4 presents the distribution of water content, organic content and fibre content of intact peat with depth. These properties were found to be fairly uniform with depth with an average water content of 450%, average organic content of 82% and average fibre content of 62%, all expressed as a percentage of total dry mass. As per the extension of the Von Post peat classification system proposed by Hobbs (1986), the peat is classified as $H_2B_2F_2R_1W_1N_2$.

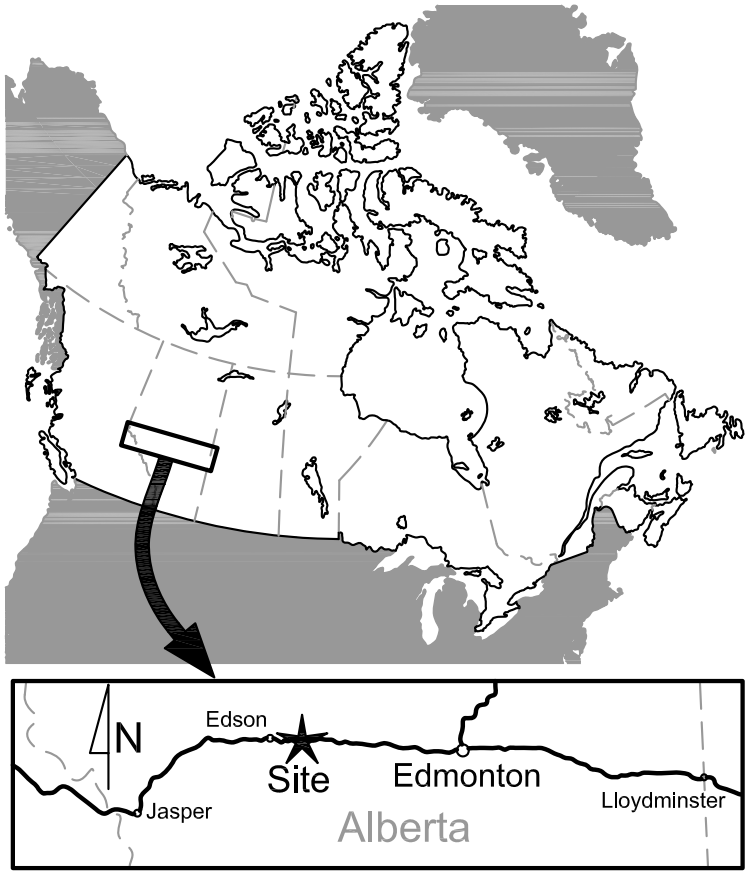

Figure 4.1 : Map showing location of Edson subdivision site (Hendry et al. 2008).

4.4 Laboratory Testing Methodology

4.4.1 Specimen Preparation

Remoulded peat specimens were prepared from auger cuttings obtained during soil sampling. Large inclusions of roots and stones were removed before placing the cuttings inside a 38-mm-diameter steel tube up to a height of 130±3 mm. The trimmings were then subjected to vertical compression under a normal stress of 90 kPa until the settlement versus time curve flattened; usually after 16 hours. The vertical strain at the end of compression was 27±3%. The compressed

sample was pushed out of the tube and trimmed to a length of 76±4 mm for consolidated undrained (CU) triaxial testing.

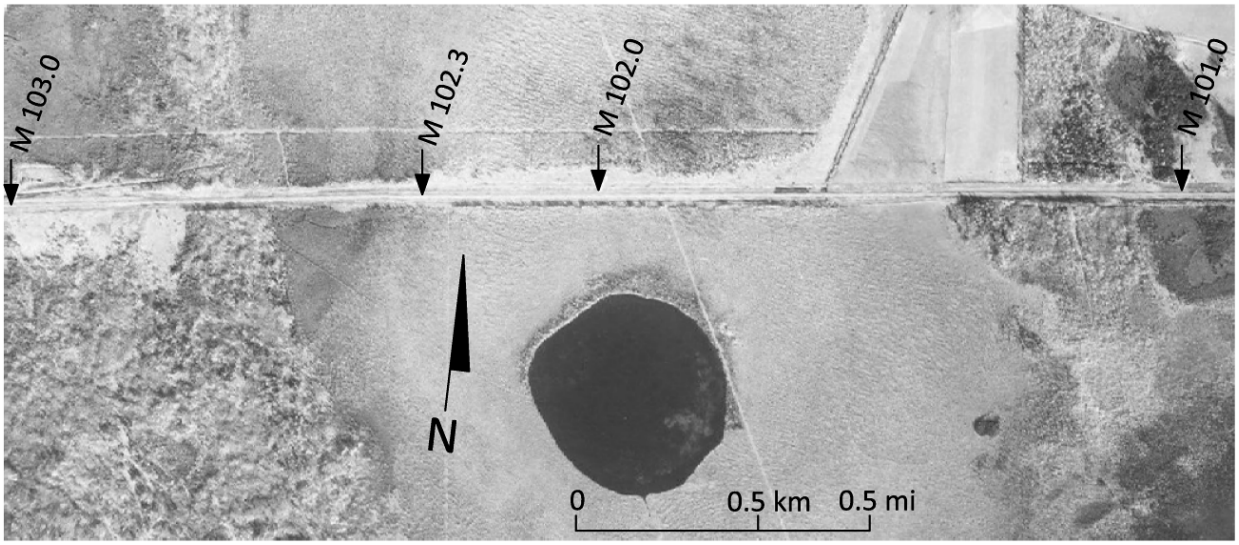

Figure 4.2 : Arial photograph of the Edson Subdivision peat bog crossing. Instrumentation installed at Mile 102.0.

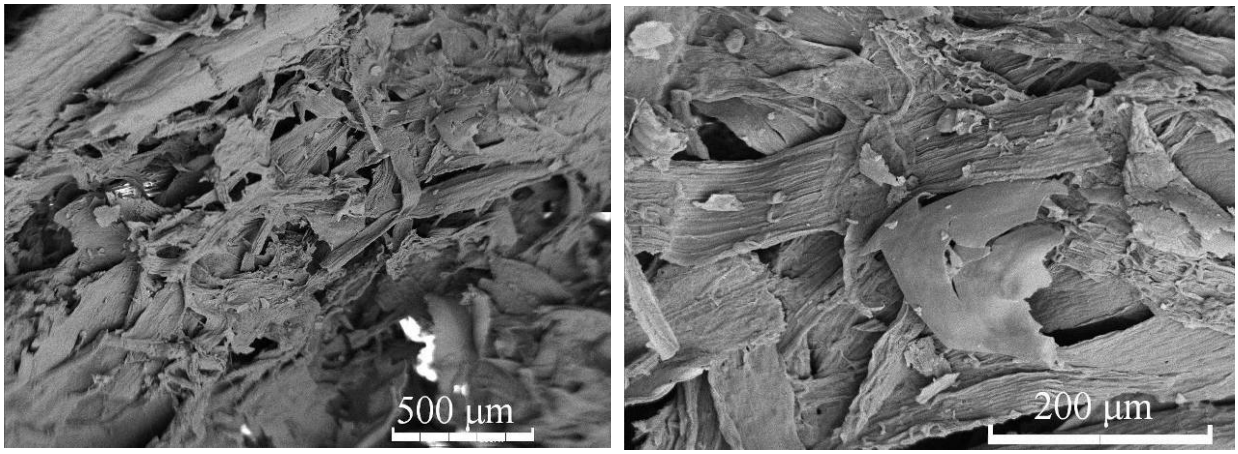

Figure 4.3 : Scanning electron micrographs showing peat fibres from the Edson site peat samples.

Fibre-only remoulded samples of peat were prepared to isolate the effect of fibres and fibre content on strength and stiffness. Peat fibres were separated from the particulate components of the peat by washing the peat samples over an ASTM #100 sieve (opening size 150 μm) (ASTM D1997). Nearly all of the particulate material could be removed using this procedure. Fibres retained on the sieve were placed inside a 38-mm-diameter steel tube up to a height of 130±3 mm and subjected to vertical compression under a normal stress of 90 kPa until the settlement

versus time curve flattened, generally in less than 4 hours. The vertical strain at the end of compression was 43±5%. The compressed samples were pushed out of the tube and trimmed to a length of 73±6 mm for consolidated undrained triaxial testing.

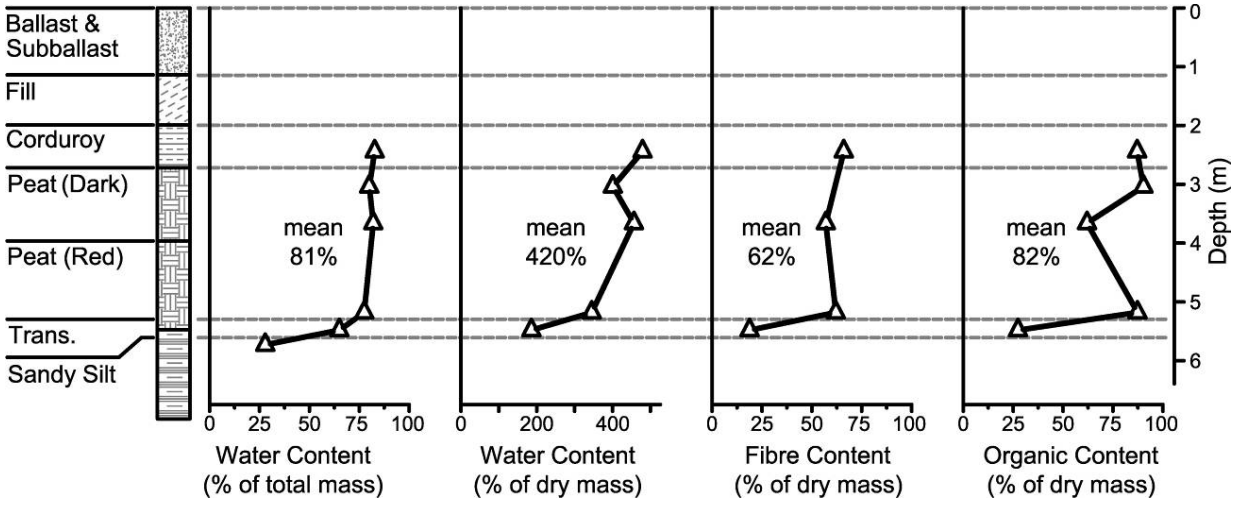

Figure 4.4 : Vertical profiles of water content, organic content and fibre content of peat for the Edson Subdivision site.

Remoulded peat specimens for direct shear (DS) testing were prepared using the same peat and peat fibre samples as used for the preparation of remoulded specimens for CU triaxial testing. Peat and peat fibre material was placed inside a 64-mm-diameter cylindrical mould and subjected to vertical compression under a normal stress of 50 kPa until settlement versus time curve flattened. The compressed specimens were pushed out of the mould and trimmed into 25-mm-thick specimens for DS testing.

Four Shelby specimens, 72±2 mm in diameter and 150±15 mm length, were trimmed from two 76-mm-diameter Shelby tube samples of peat taken from a depth of 1.8 m and 4.6 m below the top of the embankment. These four Shelby specimens were subjected to CU triaxial test at different effective confining stresses.

4.4.2 Consolidated Undrained (CU) Triaxial Tests

The CU test specimens underwent back pressure saturation using a back pressure of 200 kPa and a cell pressure of slightly greater than 200 kPa. Full saturation was confirmed by checking the B value, which was found to be greater than 0.97 for all tests. The specimen was then consolidated

to the desired value of effective confining pressure. It was then subjected to displacement-controlled undrained triaxial shear test at a rate of 0.150 mm/min. Excess pore-water pressure inside the specimen was measured using a pressure transducer connected to a de-aired pressure line. Axial load was measured using a load cell and the axial displacement was measured using a linear variable differential transformer (LVDT). A total of five remoulded peat specimens and five remoulded peat fibre specimens were tested at effective confining stresses (p_0') ranging from 11 kPa to 101 kPa.

4.4.3 Direct Shear Tests

Drained direct shear tests were conducted on remoulded peat and peat fibre specimens. Each specimen was initially subjected to vertical compression under a desired normal stress until consolidation was complete, which typically took less than 4 hours. For vertical compression at higher normal stresses, extra porous disks were inserted to compensate for the reduction in the thickness of the specimen. The rate of shearing was 0.127 mm/min. Shear force was measured using a load cell and the shear and vertical displacements were measured using LVDTs. The specimen was kept submerged in a water bath during testing to prevent drying.

In the first few direct shear tests the specimens sheared without forming a well-defined failure plane. Subsequently, it was decided to pre-cut a failure plane by running a thin wire through the gap between the top and bottom shear boxes. A total of four remoulded peat specimens and five remoulded peat fibre specimens were tested at effective normal stresses ranging from 10 kPa to 100 kPa.

4.5 Results

4.5.1 Consolidated Undrained (CU) Tests

Figures 4.5, 4.6 and 4.7 summarize the results of CU triaxial tests on remoulded peat specimens, remoulded peat fibre specimens, and Shelby specimens, respectively. The results are presented in terms of stress paths in deviatoric stress (q): mean effective stress (p') space; q vs. axial strain (ε_a) plots; and, (c) excess pore-water pressure (Δu) vs. ε_a plots.

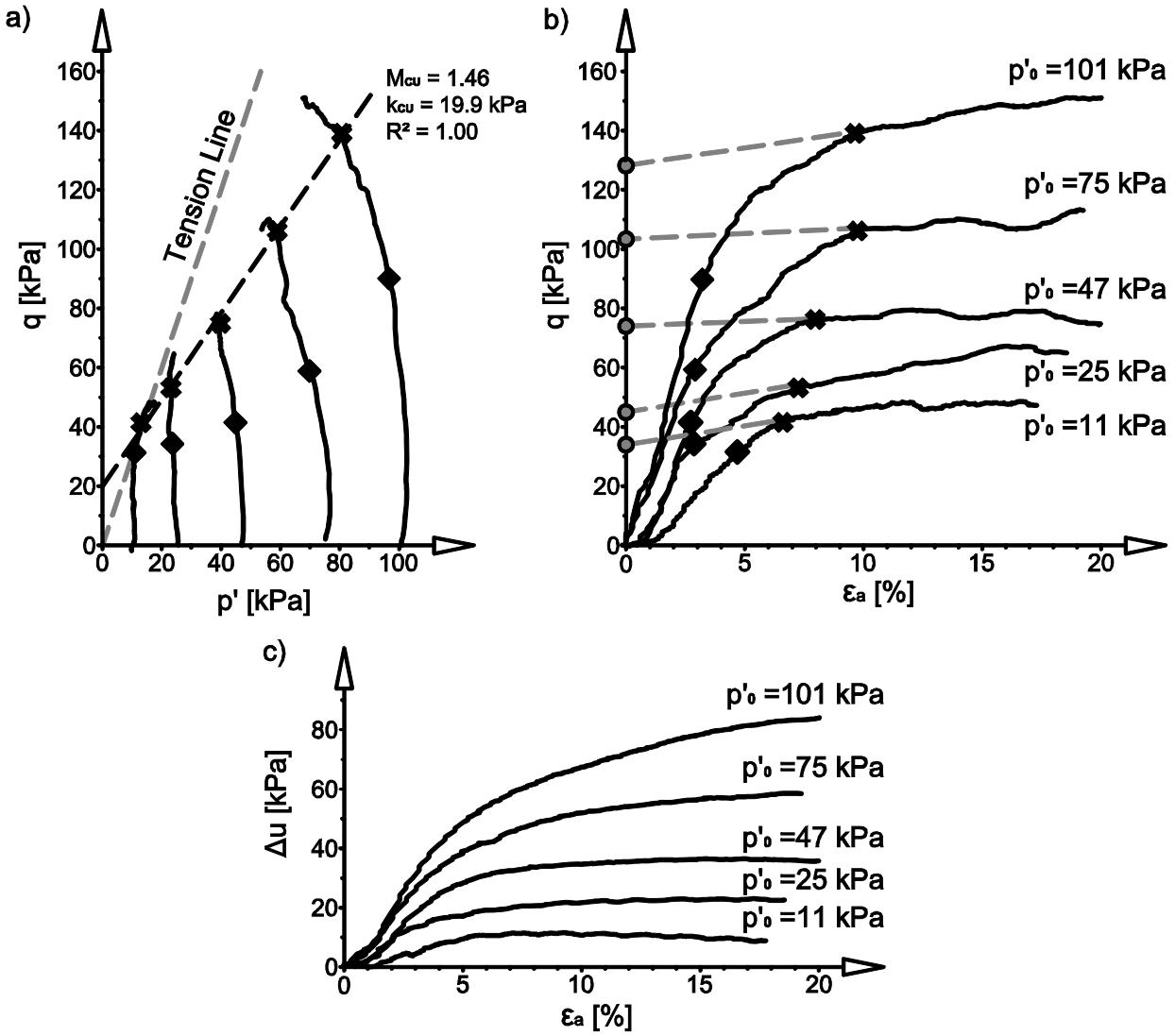

Figure 4.5 : Results from consolidated undrained (CU) triaxial testing of remoulded peat specimens: a) deviatoric stress q vs. effective mean stress p'; b) deviatoric stress q vs. axial strain ε_a; and c) excess pore-water pressure Δu vs. axial strain ε_a.

Plots of q vs. ε_a for the remoulded peat and remoulded peat fibre specimens indicate a linear elastic response up to about 5% ε_a (Figure 4.5(b) and 4.6(b)). Shelby specimens exhibit linear elastic response only up to about 2% ε_a (Figure 4.7(b)). Following the initial elastic behaviour, all samples show a gradual transition from a linear elastic to a linear strain hardening stress-strain response (Figure 4.5(b) and 4.6(b) and 4.7(b)). The specimens showed no signs of approaching failure and the tests had to be stopped because of excessive axial compression of the specimens. The Shelby specimen tested with a p'_0 of 73 kPa shows a reduction in strength but

this was due to geometrical eccentricity developing in the specimen rather than the development of a shear plane. Michalowski and Čermák (2002) have observed similar responses in triaxial tests of fibre-reinforced sands. They attributed this behaviour to increased reinforcement produced by reorientation of the fibres perpendicular to the major principal stress direction.

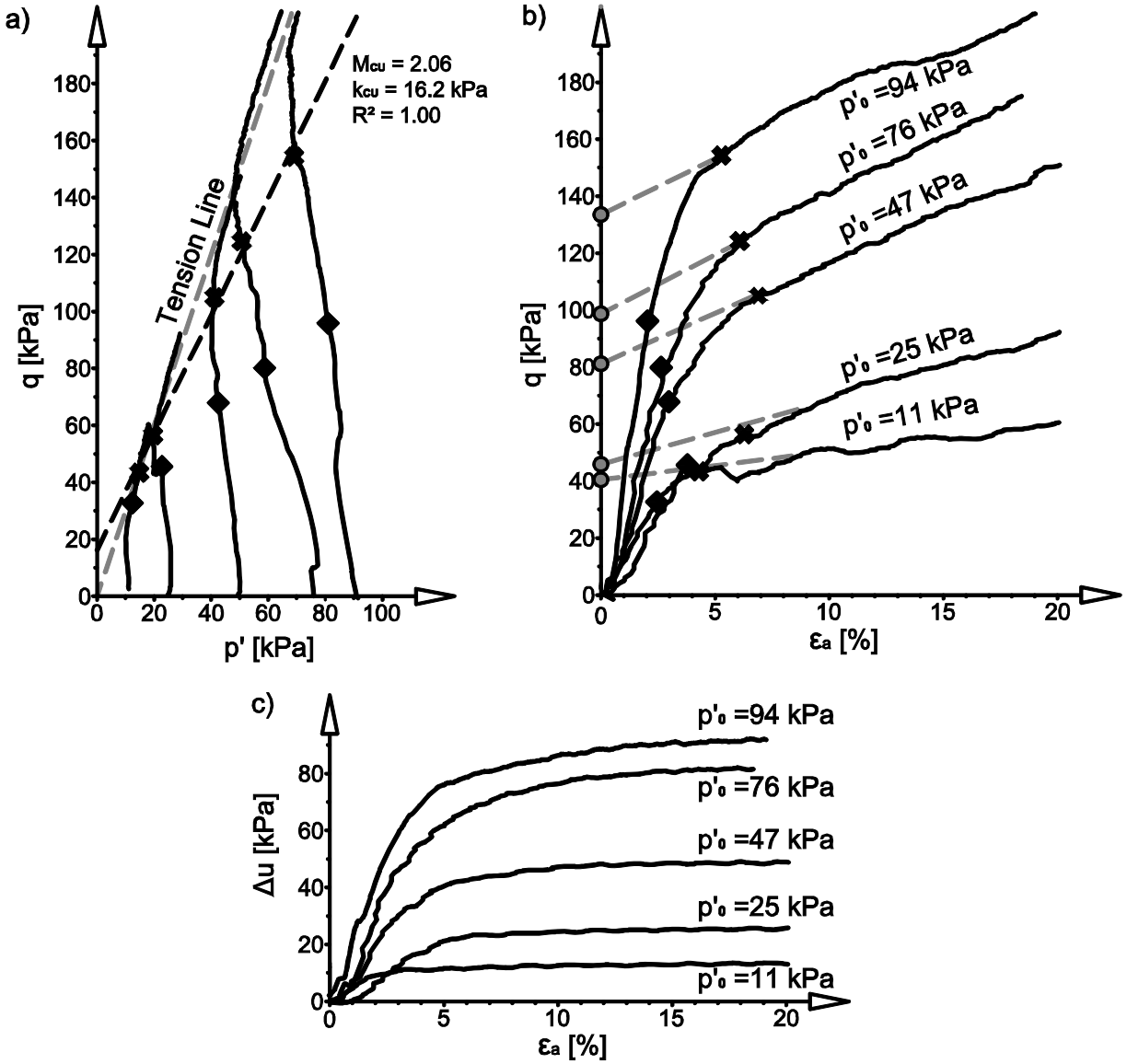

Figure 4.6 : Results from consolidated undrained (CU) triaxial testing of remoulded peat fibre specimens: a) deviatoric stress q vs. effective mean stress p'; b) deviatoric stress q vs. axial strain ε_a; and c) excess pore-water pressure Δu vs. axial strain ε_a.

The increase in q during linear strain hardening response is accompanied by an increase in p' in the q- p' stress space for all of the remoulded peat and remoulded peat fibre specimens (Figure 4.5(a) and 4.6(a)) and for the Shelby specimens (Figure 4.7(a)). The Shelby specimens taken

from the deeper 4.5 to 5.7 m Shelby tube show a lower rate of strain hardening. The portion of stress path in q- p' space corresponding to the linear strain hardening portion traverses the tension cut-off line, which has a slope of 3:1. A similar behaviour can be seen in the CU triaxial test results presented by Konrad et al. (2007) for Shelby specimens obtained from CN railway's Levis Subdivision site, located near the south shore of the St. Lawrence River, across from Quebec City, Canada. The test results presented by Konrad et al. (2007) have been replotted and presented in Figure 4.8 to facilitate their direct comparison with the results from the present study. It can be seen from Figure 4.8 that the specimens show an initial linear elastic response followed by a gradual transition to linear strain hardening at high axial strains, similar to that exhibited by the Shelby specimens from the present study.

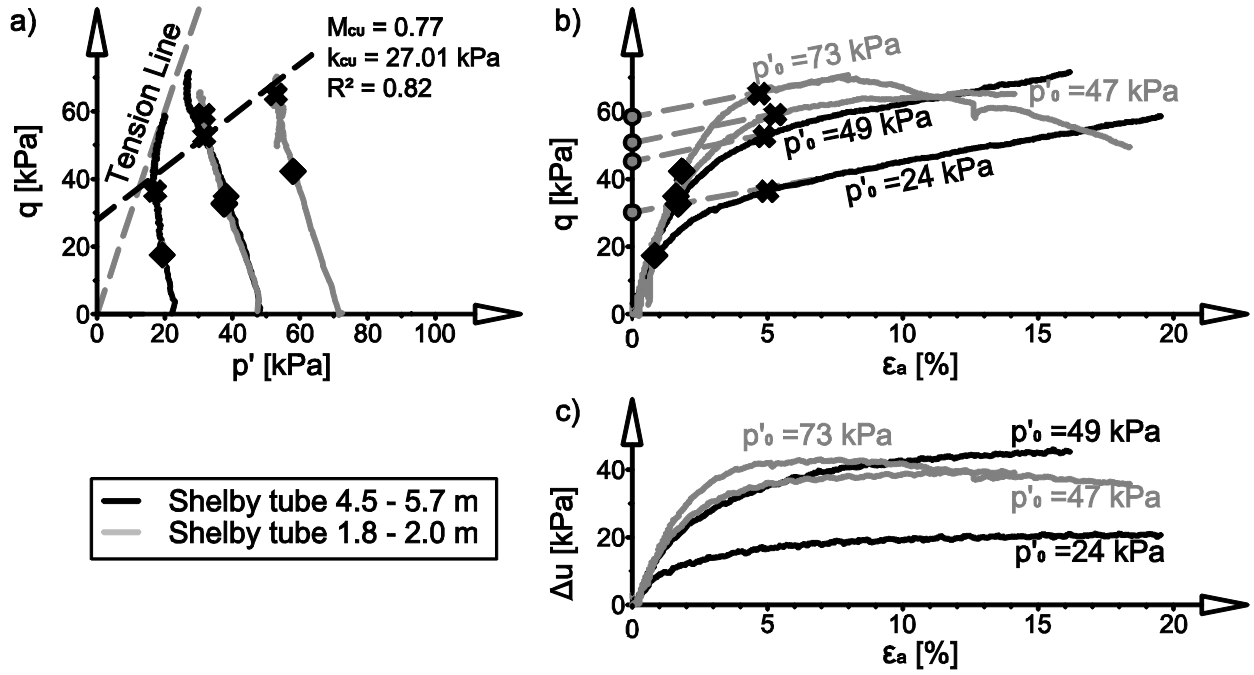

Figure 4.7 : Results from consolidated undrained (CU) triaxial testing of intact peat specimens from Edson Subdivision: a) deviatoric stress q vs. effective mean stress p'; b) deviatoric stress q vs. axial strain ε_a; and c) excess pore-water pressure Δu vs. axial strain ε_a.

The excess pore-water pressure (Δu) vs. ε_a is shown in Figures 4.5(c), 4.6(c) and 4.7(c). Remoulded peat fibre and Shelby specimens exhibit a greater rate of increase of Δu with ε_a compared with that for the remoulded peat specimen. The values of Δu at the end of the tests are very nearly equal to the applied cell pressure, which implies that the specimens have nearly zero effective confining stresses. Yet, the specimens do not show any signs of failure, indicating that

the increase in q is solely due to the increase in tension mobilized by the fibres. The values of Δu remain virtually unchanged for those specimens that end up traversing the tension cut-off line in q - p' space. As such, the specimens can be considered to be undergoing drained shear along the tension cut-off line.

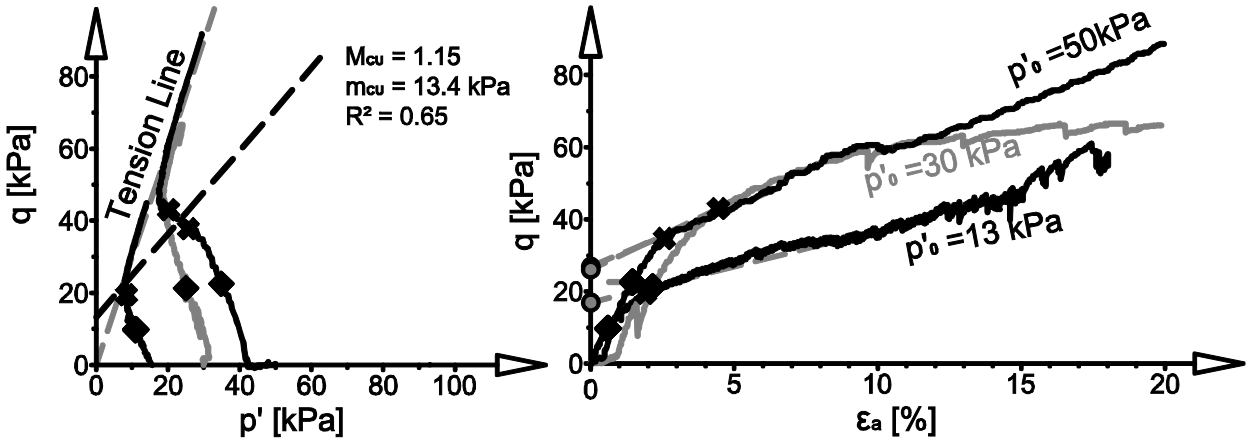

Figure 4.8 : Results from consolidated undrained (CU) triaxial testing of intact peat specimens from Edson Subdivision: a) deviatoric stress q vs. effective mean stress p'; b) deviatoric stress q vs. axial strain ε_a; [Results extracted from Konrad et al. 2007 and replotted in terms of q and p'.]

4.5.2 Direct Shear (DS) Tests

The results from the DS testing of remoulded peat and remoulded peat fibre specimens are shown in Figure 4.9. It can be seen that the remoulded peat specimens (Figure 4.9 (a)) show a greater rate of increase of shear stress with shear displacement compared with remoulded peat fibre specimens (Figure 4.9 (b)). Figure 4.10 shows ultimate shear stress values plotted against normal effective stress for both the remoulded peat and remoulded peat fibre specimens. The fitted Mohr-Coulomb failure envelope passing through origin gives angle of friction ϕ' of 31°, which represents shear strength of the peat without the contribution of the reinforcing effect of the fibres.

4.6 Discussion

4.6.1 Anisotropic Elastic Stiffness of Fibrous Peat

The undrained Young's modulus in the vertical direction (E_V) for each specimen is approximated as the slope of the linear portion of the q vs. ε_a plot (Graham and Houlsby 1983).

Figure 4.11 shows the values of E_V in MPa for remoulded peat and peat fibre specimens plotted against initial mean effective stress normalized using atmospheric pressure (p_{atm} = 101.325 kPa). Figure 4.11 also shows power law curves fitted to the experimental data, with a theoretical intercept at the origin (E_V=0 at p'_0=0).The E_V values for remoulded peat and peat fibre specimens increase with increasing p'_0. The E_V values for remoulded peat fibre specimens appear to increase more with increasing p'_0 than the E_V values for remoulded peat specimens; this is expected because peat fibres are able to mobilize greater amount of tension at higher effective confining pressures and offer greater contribution towards the elastic stiffness of the specimen. Figure 4.11 shows the values of E_V for the Shelby specimens plotted, the values are similar in magnitude to the remoulded peat and remoulded peat fibre specimens with similar p'_0 values.

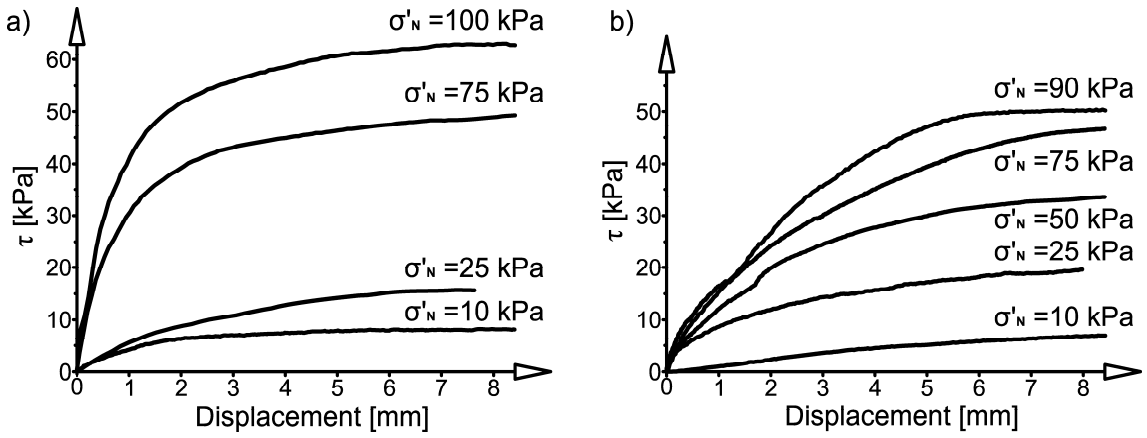

Figure 4.9 : Results from the direct shear (DS) testing: a) remoulded peat specimens; b) remoulded peat fibre specimens.

Excess pore-water pressure (Δu) in a saturated linear elastic porous material is the sum of the pore-water pressure generated by increases in total mean stress (Δp) and increases in deviatoric stress (Δq) as expressed by equation [4.1] (Wood 2004).

$$\Delta u = \Delta p + a\Delta q \qquad [4.1]$$

where a is a pore-water pressure parameter that accounts for the stiffness anisotropy of the material. Equation [4.1] represents the difference between the effective and total stress paths in

$q - p'$ space experienced by the material during an undrained triaxial test (Figure 4.12). The slope of the undrained effective stress path is equal to $-1/a$ (Figure 4.12).

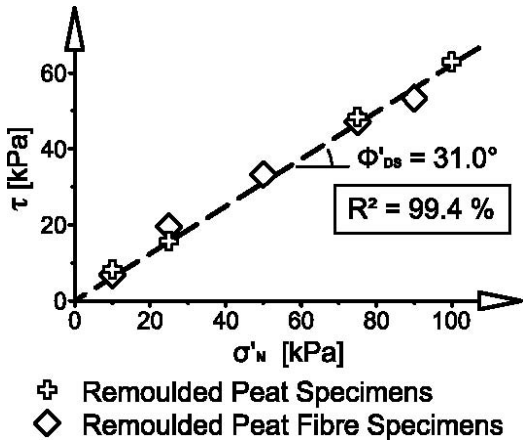

Figure 4.10 : Mohr-Coulomb failure envelope for remoulded peat and peat fibre specimens obtained using the results of direct shear (DS) testing.

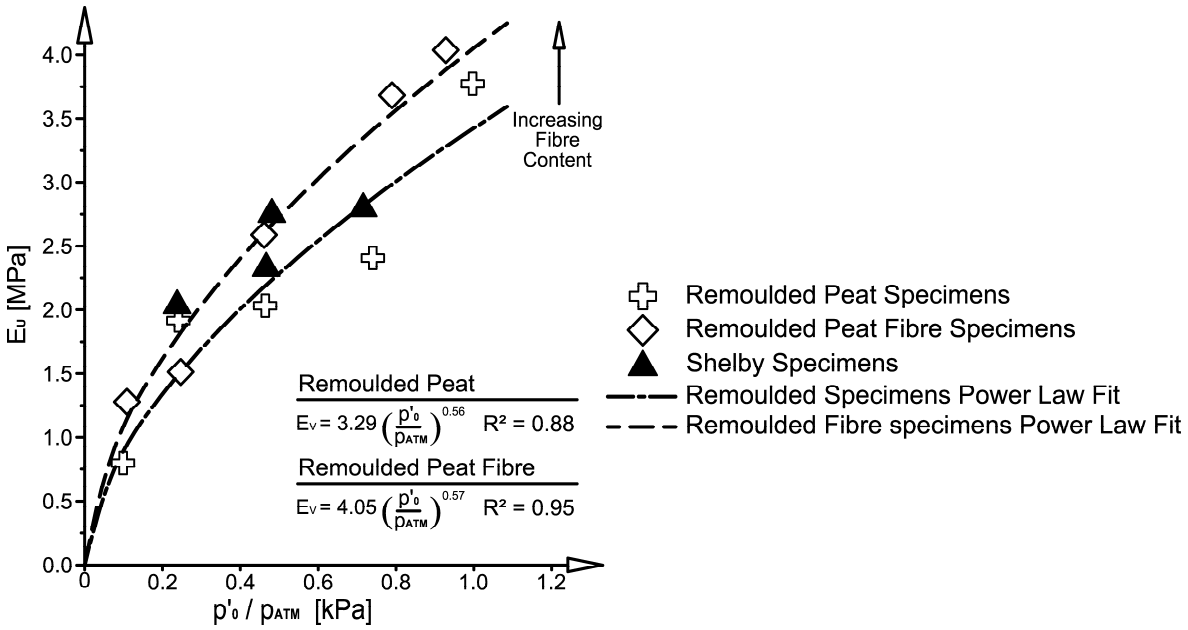

Figure 4.11 : Plots of the initial Young's modulus in vertical direction (E_V) vs. normalized initial effective preconsolidation pressure (p_0'/p_{atm}) for all remoulded peat, remoulded peat fibre and intact peat specimens obtained from the results of CU triaxial testing.

The undrained effective stress path of an isotropic, linear elastic material in $q - p'$ space is vertical because the condition of zero volumetric strain requires that there be no change in p' (Wood 2004). In other words, there is no coupling between the volumetric and shear behaviour of an isotropic linear elastic material. As such, Δu induced in the material is entirely due to

change in total mean stress (Δp) and the a is equal to zero. For a cross-anisotropic elastic material the undrained effective stress path is not vertical. The slope of the undrained effective stress path is positive with a negative a value if the Young's modulus of the material in the vertical direction (E_V) is greater than its Young's modulus in the horizontal direction (E_H). The slope is negative with a positive a value if E_V is smaller than E_H (Graham and Houslby 1983; Wood 2004). The limits for a are a = -1/3 for $E_V >> E_H$ and a = 2/3 for $E_V << E_H$ (Graham and Houlsby 1983).

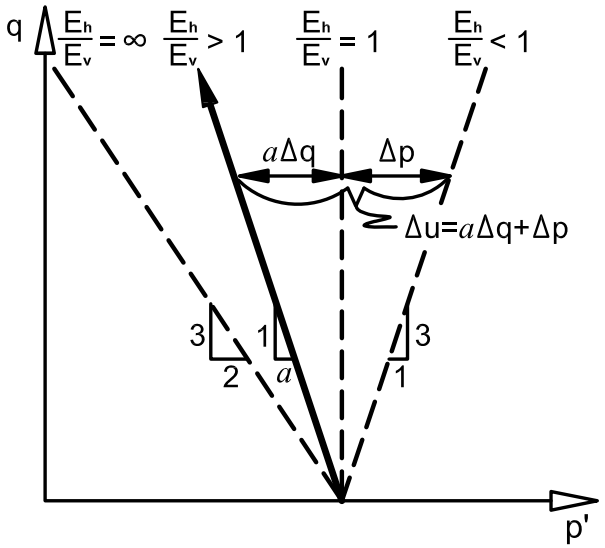

Figure 4.12: Conceptual representation and theoretical limits of shear-induced excess pore-water pressures as a consequence of cross-anisotropic elastic behaviour of peat.

Deviation of the undrained effective stress path from the vertical can be considered as an indication of anisotropic elastic response. If the modified Poisson's ratio ν^* (Graham and Houlsby 1983) of the anisotropic elastic material is known, it is possible to estimate the extent of cross-anisotropy from the measured value of a using equation [4.2] (Wood 2004).

$$a = -\frac{\Delta p'}{\Delta q} = -\frac{2(1-\nu^* + \alpha\nu^* - \alpha^2)}{3(2-2\nu^* - 4\alpha\nu^* + \alpha^2)} \qquad [4.2]$$

where $\alpha^2 = E_H / E_V$ is the cross-anisotropy parameter (Graham and Houlsby 1983). Figure 4.13 shows the influence of the a and ν^* on the value of E_H/E_V as described by equation [4.2]. A positive value of a corresponds to E_H/E_V > 1, a negative value of a corresponds to E_H/E_V < 1

and a = 0 for $E_H = E_V$ (Figure 4.13). It is evident from Figure 13 that as ν^* increases, the magnitude of the stiffness anisotropy of the material reduces.

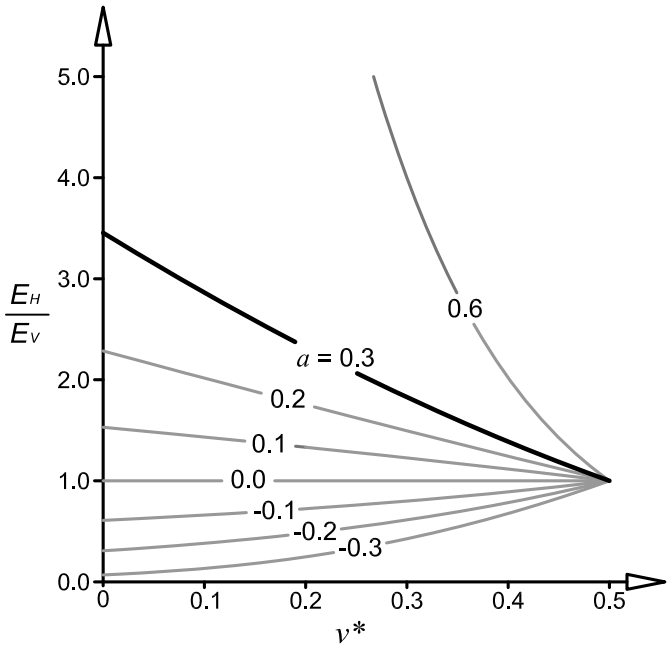

Figure 4.13 : Effect of pore-water pressure parameter a and Poisson's ratio ν^* on anisotropic stiffness ratio $\alpha^2 = E_H / E_V$.

The undrained effective stress paths in q - p' for the remoulded peat, the remoulded peat fibre and the Shelby specimens (Figure 4.5(a), 4.6(a) and 4.7(a)) can now be examined in the light of cross-anisotropic elastic behaviour in terms of the pore-water pressure parameter a. The undrained effective stress paths for the remoulded peat and peat fibre specimens are nearly vertical in the beginning (Figure 4.5(a), 4.6(a)) indicating isotropic stiffness and a = 0. For the specimens tested at low effective confining stresses, there is very little deviation from the vertical as the specimens undergo further axial compression, indicating that there is virtually no evolution of cross-anisotropy. For the specimens tested at higher effective confining stresses, the slope of stress paths gradually become negative as the specimens undergo further axial compression, indicating the development of anisotropic stiffness (E_H / E_V > 1) and a corresponding increase in the value of a. As the stress paths approach the tension cut-off line, the value of a approaches 0.30 (Figure 4.14). This transition in the value of a shows that the remoulded peat and peat fibre specimens tested at higher effective confining stresses gradually become stiffer in the horizontal direction. This development of cross-anisotropic behaviour can

be attributed to the realignment of peat fibres in the direction of expansive strain (perpendicular to the axis of the specimen) and an accompanied increase in the mobilization of tension by the fibres.

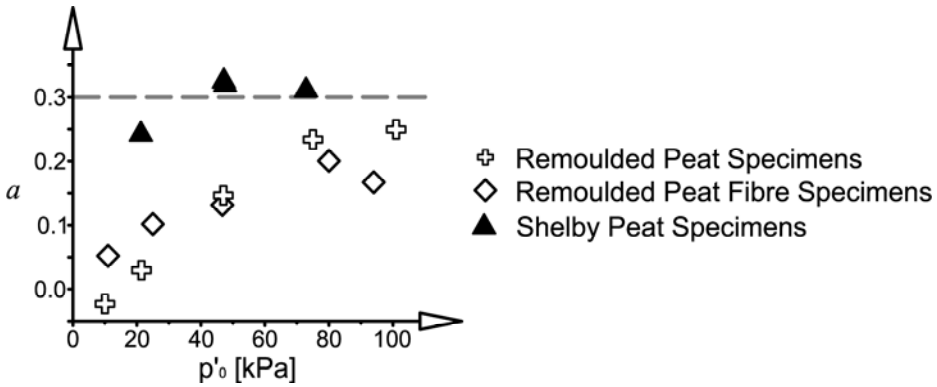

Figure 4.14: Variation of pore-water pressure parameter a with initial mean effective stress p_0' for remoulded peat, remoulded peat fibre and intact peat specimens.

The undrained effective stress paths for the Shelby specimens (Figure 4.7(a)) show a negative slope of around 3:1 from the onset of shearing until they approach the tension cut-off line (a values ranging from 0.24 to 0.33; average a = 0.30), irrespective of the magnitude of effective confining stress (Figure 4.14). This indicates the presence of *in situ* cross-anisotropic structure in Shelby specimens with in situ E_H values greater than the in situ E_V values. Such cross-anisotropic structure in Shelby specimens is due to the tension mobilized in the fibres, likely due to interlocking of fibres without reliance on increasing frictional resistance.

Because radial strains were not measured independently, it is not possible to estimate the Poisson's ratio of the specimens. Consequently, it is not possible to assign a value to the E_H/E_V ratio. It is possible to establish a range of values for the E_H/E_V ratio using Figure 4.13. For a = 0.30, E_H/E_V ranges from E_H/E_V = 3.5 at ν^* = 0.00 to E_H/E_V = 1.0 for ν^* = 0.50. The value of ν^* was not measured in the present study. Effective Poisson's ratio values for fibrous peat of 0.10 (Zwanenberg 2005), 0.11 (Rowe et al. 1984) and 0.15 (Rowe and Mylleville 1996; Yong 2008) have been quoted in the published literature. For a = 0.30 and a range of ν^* values from 0.10 to 0.15, E_H/E_V varies from 2.9 to 2.6.

4.6.2 Shear Strength of Fibrous Peat

It has been noted previously that beyond the initial elastic response, all specimens show a gradual transition from linear elastic to linear strain hardening stress-strain (Figures 4.5(b), 4.6(b) and 4.7(b)). It is hypothesized that this transition to linear strain hardening stress-strain response is indicative of the critical state shear strength associated with frictional interactions; and that the linear increase in q during strain hardening is the result of additional shear resistance due to fibre tension. As the fibre content of peat increases, the slope of the linear strain hardening portion of the stress-strain curve increases. If it is assumed that the contribution of fibre tension is linear for the entire duration of shearing, that is, there is no slipping or breaking of fibres, the linear portion of the strain hardening response can be extrapolated to a ε_a= 0%. The q-intercept thus obtained represents the critical state deviatoric stress (q_{cs}) associated only with interphase friction. This concept is illustrated in Figure 4.15 using idealized stress-strain behaviour of peat specimens. A horizontal line drawn through q_{cs} marks the transition from the interphase frictional strength to interphase frictional strength plus fibre reinforcement (Figure 4.15). Figure 4.15 also depicts two key points X and Y on the stress-strain curve. Point X represents the upper limit of the linear elastic behaviour and Point Y represents the full mobilization of the frictional critical state shear strength (Figure 4.15).

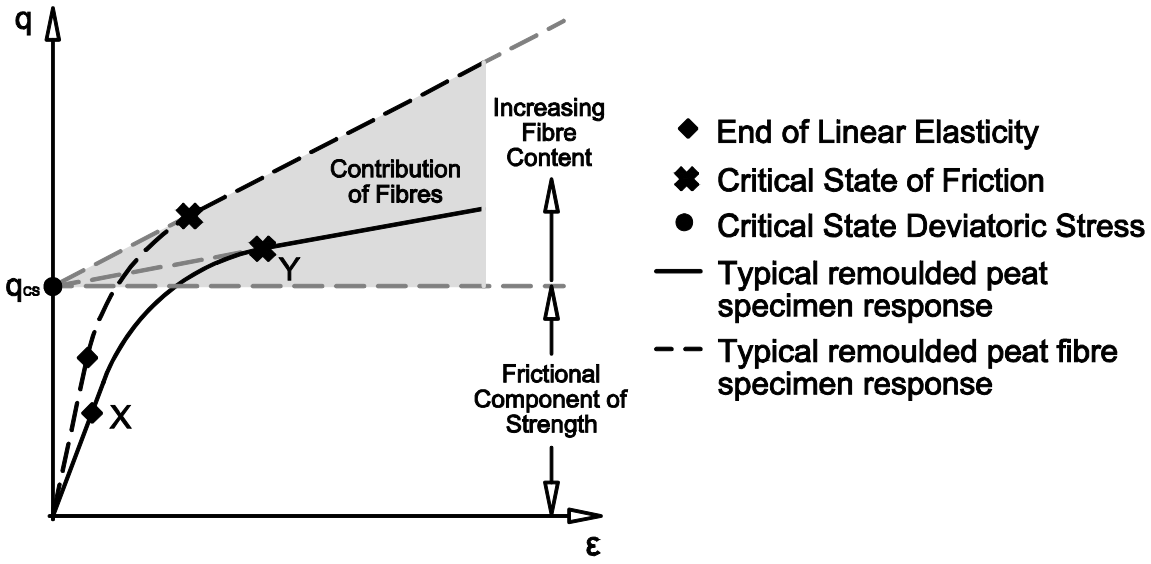

Figure 4.15 : Conceptual representation of frictional critical state deviatoric stress q_{cs} of fibrous peat.

Figure 4.16 shows the values of q_{cs} for remoulded peat, remoulded peat fibre and Shelby specimens plotted against values of p'_0. Shown in Figure 4.16(a) is a fitted critical state line (CSL) passing through the origin (cohesive intercept k = 0) for the remoulded peat and remoulded peat fibre specimens, a value of 1.25 is obtained for the slope of the CSL (M), which corresponds to a value of 31° for the critical state angle of friction (ϕ'_{cs}) of frictional strength of peat. The value of ϕ'_{cs} obtained from this approach is equal to ϕ'_{ds} of 31° obtained from direct shear testing of remoulded peat and remoulded peat fibre specimens (Figure 4.10). This confirms the validity of this approach in obtaining the frictional shear strength of the peat. A value of 1.01 is obtained for the slope of the CSL (M) for the Shelby specimens (Figure 4.16(b)), this corresponds to a ϕ'_{cs} value of 26°. From a comparison of the CSL fit to the test results for the remoulded peat, remoulded peat fibre and the CSL fit to the Shelby specimens (Figure 4.16), the Shelby specimens have lower frictional critical state shear strength.

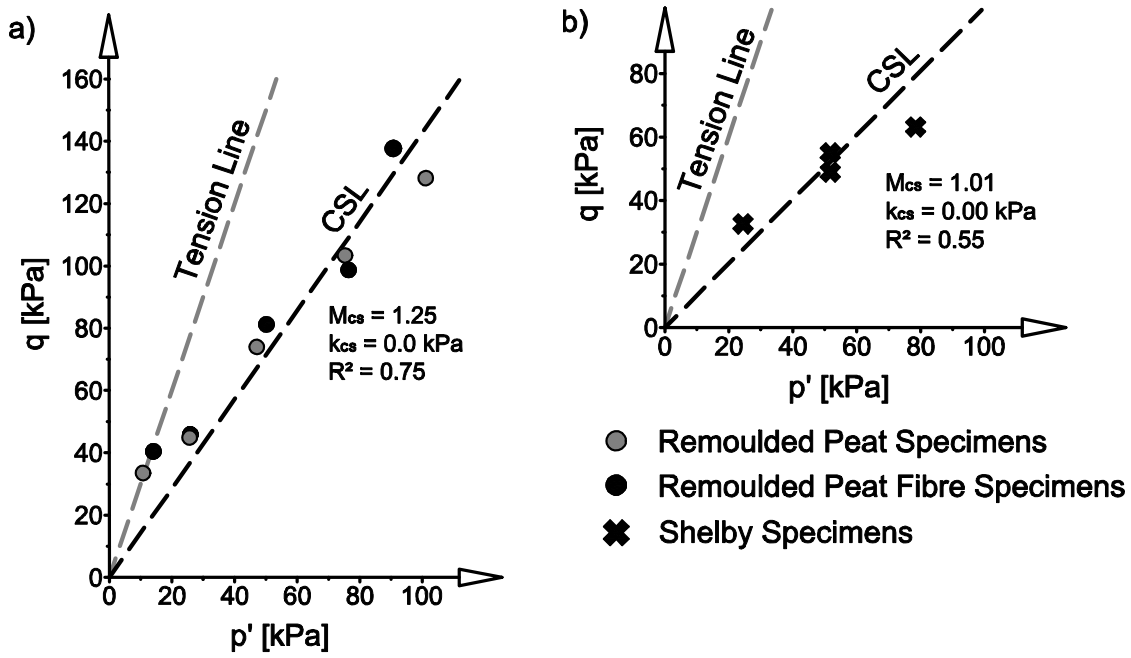

Figure 4.16: Frictional critical state lines (CSL) for (a) the remoulded peat and peat fibre specimens and (b) for the Shelby tube specimens; experimental data points correspond to q_{cs} extracted from Figures 5(a), 6(a), 7(a).

The reinforcing effect of peat fibres results in the mobilization of shear strength in excess of the frictional shear strength of peat (Landva and La Rochelle 1983; Farrell and Hebib 1998; Hebib 2001). Landva and La Rochelle (1983) quantified the reinforcing effect of peat fibres in terms of

an additional horizontal reinforcement stress (σ_{FR}) beyond the effective confining stress (σ'_r) to ensure that at a given axial effective stress (σ'_a) the stress state of the specimen represented by Mohr's stress circle satisfies the Mohr-Coulomb failure criterion corresponding to the frictional shear strength (Figure 4.17). In Figure 4.17, the yield criterion for fibrous peat is defined using the angle of friction ϕ'_{cu} and cohesion intercept c'_{cu}, which can be estimated, respectively, from the slope (M_{cu}) and y-intercept (k_{cu}) of the yield line in q - p' space obtained from CU triaxial tests (Figures 4.5(a), 4.6(a) and 4.7(a)) using equations [3] and [4].

$$\phi'_{cu} = \sin^{-1}\left(\frac{3M_{cu}}{6 + M_{cu}}\right) \qquad [3]$$

$$c'_{cu} = k_{cu}\left(\frac{3 - \sin\phi'_{cu}}{6\cos\phi'_{cu}}\right) \qquad [4]$$

The Mohr-Coulomb failure criterion is defined using ϕ'_{ds} obtained from direct shear tests. Using simple trigonometry, σ_{FR} can be written in terms of σ'_a, ϕ'_{cu}, c'_{cu}, and ϕ'_{ds} as:

$$\sigma_{FR} = (K_{ds} - K_{cu})\sigma'_a + K_{cu}\frac{2c'_{cu}\cos\phi'_{cu}}{1-\sin\phi'_{cu}} \qquad [4.5]$$

where $K_{ds} = (1-\sin\phi'_{ds})/(1+\sin\phi'_{ds})$ and $K_{cu} = (1-\sin\phi'_{cu})/(1+\sin\phi'_{cu})$.

Equation [4.5] represents a linear relationship between σ_{FR} and σ'_a of the form

$$\sigma_{FR} = A\sigma'_a + Bc'_{cu} \qquad [4.6]$$

where $A = (K_{ds} - K_{cu})$ and $B = 2K_{cu}\cos\phi'_{cu}/(1-\sin\phi'_{cu})$ are dimensionless parameters that are functions of ϕ'_{cu} and ϕ'_{ds}. For a given ϕ'_{ds} value, A increases from a value of $(K_{ds} - 1)$ at ϕ'_{cu} = 0° to a value of K_{ds} at ϕ'_{cu} = 90° (tension cut-off) as shown in Figure 4.18(a). It can also be observed from Figure 18(a) that the A = 0 for $\phi'_{cu} = \phi'_{ds}$ and A < 0 for $\phi'_{cu} < \phi'_{ds}$. The value of B decreases from a value of 2 at ϕ'_{cu} = 0° to a value of 0 at ϕ'_{cu} = 90° as shown in Figure 4.18(b). The values of A and B for remoulded peat, remoulded peat fibres and Shelby

specimens can be obtained from the results of CU triaxial test; these values are presented in Table 4.1.

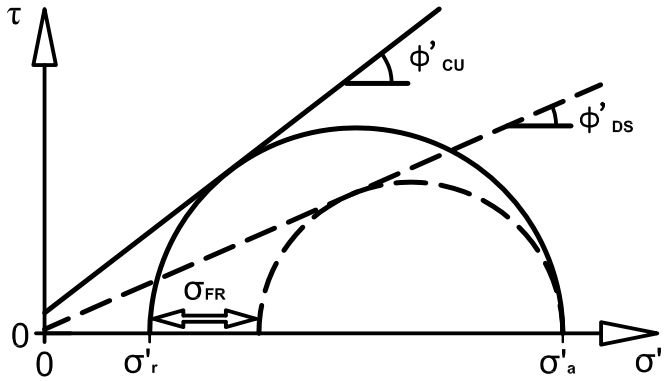

Figure 4.17: Conceptual representation of increase in effective confining stress as a consequence of tension mobilized by peat fibres.

Table 4.1: Dimensionless Parameters A and B for the estimation of σ_{FR}

Specimen	M_{cu}	k_{cu} (kPa)	ϕ'_{cu} (°)	c'_{cu} (kPa)	A	B
Remoulded Peat	1.46	19.9	36.0	9.89	0.06	1.02
Remoulded Peat Fibres	2.06	16.2	50.1	9.39	0.19	0.73
Intact Peat – Edson	0.77	27.0	20.0	12.73	-0.17	1.40
Intact Peat – Lévis[1]	1.15	13.4	28.8	6.42	-0.03	1.18

[Note: M_{cu} and k_{cu} are the slope and y-intercept, respectively, of the yield line in q- p' space; ϕ'_{cu} and c'_{cu} are the slope and y-intercept, respectively of the yield line in Mohr-Coulomb stress space; [1] – Results extracted from Konrad et al. (2007).]

The values of A for remoulded peat and remoulded peat fibres are positive, indicating a greater contribution from fibre reinforcement at higher axial effective stresses. The value of A for remoulded peat fibre is more than 3 times that of the remoulded peat, which is to be expected given its significantly higher fibre content. The Shelby specimens show negative A values, with the A value for the Edson Subdivision specimens more negative than that for Lévis Division specimens. This indicates that the reinforced strength of intact peat is less than the frictional shear strength of the remoulded peat. The most probable explanation for this is that the remoulded specimens were created from consistent material, whereas the Shelby specimens were

found to contain segments of roots and twigs along with rounded stones which may have interfered with the mobilization of tension in the fibres and created weak planes along which the specimens most likely failed.

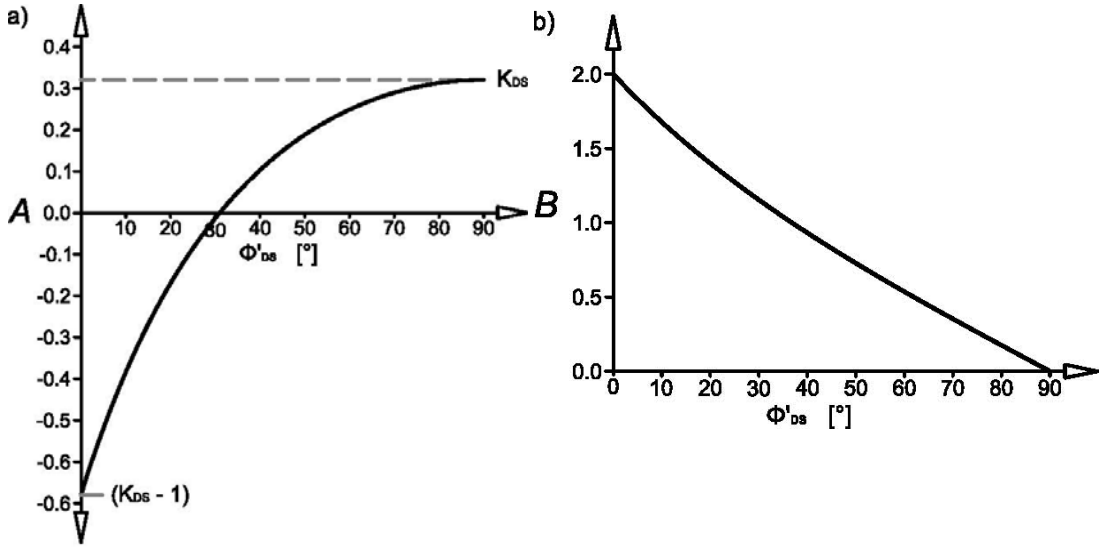

Figure 4.18: Variation of dimensionless parameters A and B (equation [6]) with ϕ'_{cu}: (a) Parameter A; (b) Parameter B.

4.7 Conclusions

This paper has presented the results from a laboratory testing program involving consolidated undrained (CU) triaxial tests and direct shear (DS) tests on remoulded peat, remoulded peat fibre and Shelby specimens obtained from a test site located in the Edson Subdivision of Canadian National Railway. The results have been presented in terms of effective stress paths in the deviatoric stress-mean effective stress space and analyzed using the framework of cross-anisotropic elasticity and fibre-reinforced soil.

The results of the CU triaxial tests have confirmed that fibrous peat specimens are cross-anisotropic when fibres are aligned normal to the direction of the axial compressive stress. The extent of cross-anisotropy was found to increase with an increase in fibre content. Remoulded peat specimens showed cross-anisotropy only after undergoing considerable vertical straining whereas cross-anisotropy was evident from the beginning of the test for Shelby specimens. The degree of cross-anisotropy could not be fully characterized from the results of CU triaxial tests. The horizontal stiffness of the Shelby specimens was estimated to be 2.6 to 2.9 larger than the

vertical stiffness based on values of effective Poisson's ratio for fibrous peat obtained from literature.

The existence of cross-anisotropy results in shear-induced excess pore-water pressures in peat specimens. The magnitude of shear-induced excess pore-water pressure is controlled by the pore pressure parameter a. The value of parameter a for remoulded peat and peat fibre specimens was found to increase gradually from a value of 0 at the beginning of the test to around 0.3 at the end of the test, which and is indicative of increasing cross-anisotropy with increasing vertical strain because of greater mobilization of tension in the fibres. The parameter a was also found to increase with an increase in initial effective confining pressure p'_0 for the remoulded peat and peat fibre specimens. This was attributed to increasing frictional resistance leading to greater mobilization of fibre tension. The near-constant value of parameter a for the Shelby specimens suggests a cross-anisotropic structure. Greater horizontal stiffness in Shelby specimens is due to the tension mobilized in the fibres, likely due to the interlocking of fibres rather than increasing frictional resistance alone.

A novel procedure was proposed for estimating the critical state frictional strength of fibrous peat from CU triaxial test results. This procedure involves extrapolating the linear strain hardening portion of the stress-strain curve to obtain its intercept with the q-axis. The values of q, when plotted against the values of initial mean effective stress p'_0, gave a critical state angle of friction ϕ'_{cs} of 31°. This value compared favourably with the value ϕ'_{ds}(31°) obtained from direct shear tests in which fibres were aligned parallel to the direction of shear and were unable to mobilize tension.

The shear resistance of fibrous peat over and above the frictional component of the shear strength was assessed in terms of the increase in the effective confining stress σ_{FR} provided by the tension mobilized by the fibres. The increase in the effective confining stress was found to be a function of the angle of friction ϕ'_{cu} and cohesion intercept c'_{cu} representing the yield strength of peat specimens obtained from CU triaxial tests and the angle of friction ϕ'_{ds} obtained from the DS tests. It was found that the increase in the effective confining stress is a linear function of the effective axial stress. In case of the remoulded peat and peat fibre specimens it was found that

increases in fibre content resulted in an increased reinforcing effect and thus increases in strength.

The yield strength of Shelby specimens obtained from CU triaxial tests was found to be lower than the frictional strength for the remoulded specimens obtained from DS test, which gave a negative value of peat fibre reinforcing stress (σ_{FR}). It is suggested that this negative value of σ_{FR} does not represent an inherent weakness in intact peat, but is indicative of specimen heterogeneity caused by the presence of roots, twigs and river pebbles in the Shelby specimens. The critical state frictional strength of the Shelby specimens was 26°, lower than the 31° determined for the remoulded specimens. It is recommended that further studies be undertaken to assess if inter-particle frictional strength is the most appropriate strength parameter to evaluate the stability of structures founded on fibrous peat.

4.8 Acknowledgements

The authors acknowledge the contribution of Canadian National Railways in terms of providing both the research site and funding. The authors also thank Tom Edwards for his support of this project. This research was made possible through the Railway Ground Hazard Research Program, funded by the Natural Sciences and Engineering Research Council of Canada (NSERC), Canadian Pacific Railway, Canadian National Railway, and Transport Canada.

4.9 References

ASTM D1997 Standard Test Method for Laboratory Determination of the Fiber Content of Peat Samples by Dry Mass.

Farrell, E.R. and Hebib, S. 1998. The determination of the geotechnical parameters of organic soils. Proceedings of the International Symposium on Problematic Soils, IS-TOHOKU 98, pp 33-36.

Graham, J. and Houlsby, G.T. 1983. Anisotropic elasticity of a natural clay. Géotechnique, **33**(2):165-180.

Hebib, S. 2001. Experimental investigation on the stabilisation of Irish peat. Ph.D. thesis, University of Dublin, Trinity College, Dublin, Ireland.

Hendry, M., Martin, C.D., Barbour, S.L., and Edwards, T. 2008. Monitoring cyclic strain below a railway embankment overlying a peaty foundation using novel instrumentation. Proceedings of the 61st Canadian Geotechnical Conference, Edmonton, Alberta, Canada, pp 1034-1041.

Hobbs, N.B. 1986. Mire Morphology and the Properties and Behaviour of some British and Foreign Peats. Quarterly Journal of Engineering Geology, **19**: 7-80.

Konrad, J.M., Grenier, S. and Garnier, P. 2007. Influence of repeated heavy axle loading on peat bearing capacity. Proceedings of the 60th Canadian Geotechnical Conference, Ottawa, Ontario, Canada, pp 1551-1558.

Kumar, A., Wailia, B.S. and Mohan, J. 2006. Compressive strength of fiber reinforced highly compressible clay. Construction and Building Materials, **20**: 1063-1068.

Landva, A.O., and La Rochelle, P. 1983. Compressibility and Shear Characteristics of Radforth Peats. In Testing of Peats and Organic Soils. ASTM Special Technical Publication, **820**: 157-191.

Landva, A.O. and Pheeney, P.E. 1980. Peat fabric and structure. Canadian Geotechnical Journal, **17**: 416-435.

Lester, G. 2005. *Atlas of Alberta Railways*. University of Alberta Press, Edmonton, Canada. Available on-line at http://railways.library.ualberta.ca/ [Accessed January 27, 2011]

Li, J. and Ding, D.W. 2002, Nonlinear elastic behaviour of fiber-reinforced soil under cyclic loading. Soil dynamics and earthquake engineering, **22**: 977-983.

Long, M. 2005. Review of peat strength, peat characterization and constitutive modelling of peat with reference to landslides. Studia Geotechnica et Mechanica, **27**(3-4): 67-90.

MacFarlane, I.C. 1969. *Muskeg Engineering Handbook*. University of Toronto Press, Toronto.

Mesri, G. and Ajlouni, M. 2007. Engineering properties of fibrous peats. ASCE Journal of Geotechnical and Geoenvironmental Engineering, **133**(7): 850-866.

Michalowski, R. L., and Čermák, J., 2002. Strength anisotropy of fiber-reinforced sand. Computers and Geotechnics, **29**: 279-299

Michalowski, R. L., and Čermák, J., 2003. Triaxial compression of sand reinforced with fibers. ASCE Journal of Geotechnical and Geoenvironmental Engineering, **129**(2): 125-136

Rowe, R.K., MacLean, M.D. and Soderman, K.L. 1984. Analysis of a geotextile reinforced embankment constructed on peat. Canadian Geotechnical Journal, **21**(3): 563-576.

Rowe, R.K. and Mylleville, B.L.J. 1996. A geogrid reinforced embankment on peat over organic silt: a case history. Canadian Geotechnical Journal, **33**(1): 106-122.

Tan, Y. 2008. Finite element analysis of highway construction in peat bog. Canadian Geotechnical Journal, **45**(2): 147–160.

Wood, D.M. 2004. Soil Behaviour and Critical State Soil Mechanics. Cambridge University Press

Yamaguchi, H., Ohira, Y., Kogure, K. and Shigeru, M. 1985. Undrained shear characteristics of normally consolidated peat under triaxial compression and extension conditions. Soil and Foundations, **25**(3):1-18.

Zwanenberg, C. 2005. The influence of anisotropy on the consolidation behaviour of peat. Ph.D. thesis, TU Delft, Delft, The Netherlands.

Chapter Five: The variability and net effect of the stiffness and strength derived from the fibrous nature of peat.

Contribution of the Ph.D. candidate

All work reported in this chapter, including sample collection, design of the experimental program, implementation of the experiments, review of the literature, development of the theoretical framework, analysis and discussion of the results and writing of the text, has been carried out by the Ph.D. candidate.

As supervisors, Dr. S. L. Barbour and Dr. C.D. Martin have reviewed all parts of the work. This chapter will be submitted with the following citation:

Hendry, M.T., Barbour, S., and Martin, D., 2011. The variability and net effect of the stiffness and strength derived from the fibrous nature of peat. *To be submitted to the Journal of Geotechnical and Geoenviromental Engineering.*

Contribution of this chapter to the overall study

The effect of fibre content and *in situ* peat structure on the undrained elastic response and strength of the peat was described in the last chapter (Manuscript #2). This chapter further develops our understanding of peat behaviour by comparing the properties of the peat at the three study sites. The defined frictional and fibre reinforced properties resulting from tension generated in the peat fibres are then used to develop a conceptual model for fibrous peat. Further analysis conducted within this manuscript explores combined effects of the reinforcement of the effective strength and the counteracting shear induced pore pressure response. From modelling of the *in situ* stress states at the field sites, the net effect of fibres beneath the embankments at the field sites is beneficial. This study is unique as it provides a direct comparison of the fibre reinforced strengths anisotropic elastic responses from three distinct sites in Canada with

differing degrees of humification and fibre content. The findings directly address the global objectives of this research as they characterize the undrained response and strength characteristics of peat at all of the study sites.

Abstract

This paper presents the results of an investigation into the role of peat fibres in the development of anisotropic stiffness and strength within peat samples taken from below three railway embankments across Canada. These sites include two from Northern Alberta on Canadian National Railway's Edson and Lac-La-Biche subdivisions, and one from the Lévis subdivision in southern Quebec. The peat samples were collected in Shelby tubes and were subjected to a program of consolidated undrained testing. These samples represented a wide variation in fibre content and degree of humification. The laboratory testing demonstrated an anisotropic elastic response to undrained loading evident in the shear induced pore pressure response. This pore pressure response was similar in the peat from all three sites and with a pore pressure parameter, *a* of approximately 0.3. The stiffness and strength of the different peats was also similar with initial elastic moduli of approximately 1.7 to 2.3 MPa and an effective shear strength of 38°. Observations of the yielding of the laboratory specimens suggest that the plastic yielding of peat occurs in a general shearing without the developed of failure planes. Accompanying the yielding of peat is the potential for strain hardening. Further analysis conducted within this manuscript explores combined effects of the reinforcement of the effective strength and the counteracting shear induced pore pressure response. This analysis showed that the net effect is dependent on the initial stress state of the peat; and for high mean effective and low deviatoric initial stress states the net effect of the fibres on the strength may be detrimental. From modelling of the *in situ* stress states at the field sites, the net effect of fibres in the field is beneficial.

5.1 Introduction

Allowable axle loads have tripled on Canadian railways, since the construction of a majority of the railway infrastructure. The volume of traffic on the main lines of the Canadian National (CN) and Canadian Pacific (CP) railways are close to their maximum capacities with trains now reaching over 3.6 km (12,000 feet) in length. These two factors have had a detrimental effects on the railway infrastructure built on soft foundations such as over peat. Both CN and CP railways

are experiencing continuing problems with large stretches of embankments built over peat. These problems, which range from excessive settlements requiring increased amounts of maintenance to a recent catastrophic failure, have highlighted the need to develop a better understanding of the load-deformation response of peat foundations subjected to heavy axle loads (Konrad et al. 2007).

Three sites have been included within this study; these sites were investigated to characterize the undrained response and strength of these peat foundations. A comparison of the results of the consolidated undrained testing of peat specimens retrieved from the three sites is made to examine the variation in anisotropic response and fibre reinforced yield strength between the sites. A conceptual model of peat behaviour is developed based on the test results and the understanding of the behaviour of fibre reinforced soils. This model is used to evaluate whether the presence of peat fibres has a net stabilizing effect in peat foundations during loading.

5.2 Background

An earlier investigation into the undrained behaviour of peat by Hendry et al. (2011) resulted in two major findings. First, the elastic behaviour of peat is highly anisotropic with considerably greater stiffness in the horizontal direction. This is attributed to the reinforcing effect of fibres which are predominantly horizontal because of fibre deposition and the large vertical strains experienced during the one-dimensional consolidation following fibre deposition (Landva and Pheeney 1980, Farrell and Hebib 1998; Hebib 2001). The second major finding was that the magnitude of the strength is dependent on the fibre content of the peat and the strength and the stiffness arise as a result of the orientation of the principal stresses with respect to the predominant horizontally aligned fibres within the peat. The effect of the fibre quantity and orientation are common themes within the peat literature and has been extensively studied (MacFarlane 1969; Yamaguchi et al. 1985; Hobbs 1986; Mesri and Ajlouni 2007).

The use of fibre reinforcement within soils has been extensively studied (Michalowski and Čermák 2002; Li and Ding 2002; Kumar et al 2006). These artificial soils allow for a high degree of control on elements of specimen composition such as fibre content, fibre aspect ratio (length to diameter), orientation of fibres and the effective confining pressures. The findings from these studies are generally consistent with the results reported for peat in regard to the effect of the

fibres on strength and stiffness of soil. In fibre reinforced soils the frictional strength of the soil is augmented by the development of tension within the fibres. Increasing the volumetric fibre content or orienting the fibres perpendicular to the major principal stress direction results in a corresponding increase in stiffness and strength (Michalowski and Čermák 2001; Michalowski and Čermák 2003; Kumar et al 2006). The reinforcing effect of the fibres is maximized if the orientation of the major (compressive) principal stress is perpendicular to the axis or plane of predominant fibre orientation. This anisotropy due to fibre orientation was demonstrated by Michalowski and Čermák (2002) for fibre reinforced specimens with three orientations (random, horizontal and vertical) tested under drained conditions in a triaxial cell. Randomly oriented fibres resulted in an increase in stiffness and a modest increase in strength. Horizontally oriented fibres (perpendicular to axial applied load) resulted in an increase in stiffness and a significant increase in strength. Vertically oriented fibres were detrimental to the stiffness, with a modest increase in strength, similar in magnitude to the randomly oriented fibre specimens but achieved at higher strains.

The fibrous nature of the peat changes both the strength and the nature of the yielding. Hendry et al. (2011) notes a linear strain hardening stress-strain response after yielding. A similar strain hardening response has been demonstrated in fibre reinforced soils (Michalowski and Čermák 2001; Michalowski and Čermák 2003; Sadek et al. 2010). The presence of this strain hardening effect in fibre reinforced soils is a result of high fibre content, high fibre aspect ratio (Sadek et al. 2010) and the slope of the strain hardening response is strongly dependant of the effective confining pressure applied to the reinforced soil (Michalowski and Čermák 2003). The effect of this strain hardening is that yielding does not result in the formation of distinct failure planes. CU tested specimens continue to deform plastically even with very high (>20%) axial strains (Hendry et al. 2011). Similarly, in direct shear testing a well-defined failure plane did not develop and instead the peat experienced tearing. Pre-cutting of a failure plane was required to obtain a measurement of the frictional strength (Hendry et al. 2011).

5.3 Site descriptions

All of the study sites are located on Canadian National (CN) railway lines. The Edson and Anzac sites were selected by CN based on a maintenance history, new traffic loading, and new construction. The Lévis site was included due to the amount of data available, and the

importance of the site to CN. All of the sites have approximately 3 m of intact peat supporting the railway embankment. The construction of the embankments and the consistency and degree of humification of the peat foundations varies between the sites.

The Edson site is located on the CN mainline between miles 101.0 and 103.0 on the Edson subdivision, near the town of Niton Junction, Alberta (Figure 5.1a). The embankment consists of ballast and sub-ballast to a depth of 1.2 m, underlain by approximately 1.0 m layer of peaty organic fill material, a timber corduroy log raft, underlain by 3m of peat. The underlying mineral soil is an unoxidized silty clay (Figure 5.2a). This site required ongoing maintenance and sections of the embankment were remediated in 1998 by placing gravel berms on both sides of the embankment. With the addition of the berms the toe to toe width of the embankment is now 23 m. The upper half of the peat layer is dark in colour while the lower half has a red colour. Both layers have a fine fibrous texture. The distribution of gravimetric water content, organic content and fibre content of the peat are presented in Figure 5.3. The water content of the peat was found to decrease slightly with depth, with a mean value of 450%. Both the organic content and fibre content of the peat appeared to be consistent with depth with mean values of 82% and a fibre content of 62%. The specific gravity of the specimens retrieved from the site varied from 1.25 to 1.30. The peat was determined to be only slightly hummified and the Hobbs (1986) and Von Post peat classification of the peat was $H_3B_3F_2R_1W_0N_4$.

The Anzac site is located at mile 263.5 of the Lac-la-Biche (formerly Waterways) subdivision, near the town of Anzac, Alberta (Figure 5.1a). The Anzac embankment consists of ballast, added in 2008, placed over sand for a combined thickness of 1.1 m. The embankment is built upon an intact peat layer that is 2.6 to 3 m thick (Figure 5.2b). The peat has a course fibrous texture, and is yellow-brown in colour. The base of the peat is an unoxidized silty clay. The water content, organic content and fibre content of the peat were found to decrease with depth (Figure 5.4), with mean values of 450%, 87% and 88% respectively. The degree of humification was determined to be insignificant, with the plant structures within the peat appearing to be intact. The classification of the peat as per Hobbs (1986) and the Von Post peat classification (Landva and Pheeney 1980) system is $H_2B_3F_2R_2W_1N_4$.

The Lévis site is located near mile 3.9 of the CN Lévis subdivision in southern Quebec (Figure 5.1c). The composition of the embankment and foundation consist of a ballast layer, which

varies in thickness between 0.3 and 0.9 m, underlain by a layer of brown to grey coarse sand containing some silt which is between 0.6 and 1.2 m thick. The intact peat layer below the embankment had a relatively constant thickness of 3 m (Figure 5.2c). The peat was described in Konrad et al. (2007) as black in colour, fibrous and highly compressible. The water content of the peat under the embankment was found to be approximately 500 %. The specific gravity of the peat was reported as approximately 1.0 (Konrad et al. 2007). The organic and fibre contents were not available for this site.

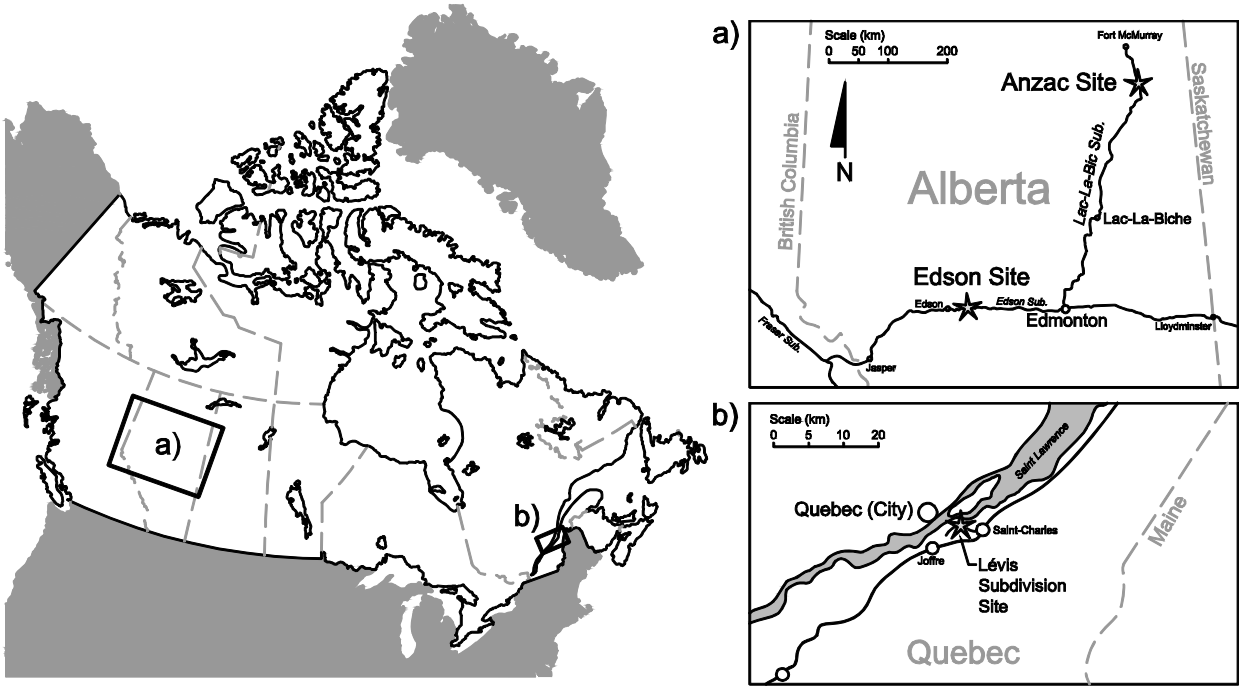

Figure 5.1 : Location of CN sites included in this study in a) Alberta, and b) Quebec.

5.4 Laboratory Testing Methodology

Consolidated undrained (CU) triaxial testing was conducted on Shelby tube samples retrieved from the all three sites. The Shelby tube samples from the Edson and Anzac sites were 72±2 mm in diameter and were trimmed to a length of 150±15 mm long specimens after extrusion. These CU test specimens underwent back pressure saturation using a back pressure of 200 kPa and a cell pressure of slightly greater than 200 kPa. Full saturation was confirmed by checking the B value, which was found to be greater than 0.97 for all tests. The specimen was then consolidated to the desired value of effective confining pressure. It was then subjected to displacement-controlled undrained triaxial shear test at a rate of 0.150 mm/min. Excess pore-water pressure

inside the specimen was measured using a pressure transducer connected to a de-aired pressure line. Axial load was measured using a load cell and the axial displacement was measured using a linear variable differential transformer (LVDT). The results from the CU testing of the specimens from the Edson site have been previously presented in Hendry et al. (2011) and are shown in Figure 5.5. The results from the CU testing of the peat from the Anzac site are presented in Figure 5.6. The CU testing results for specimens from the Lévis sites were re-plotted from Konrad et al. (2007) using the deviatoric and mean effective definition of stresses (Figure 5.7).

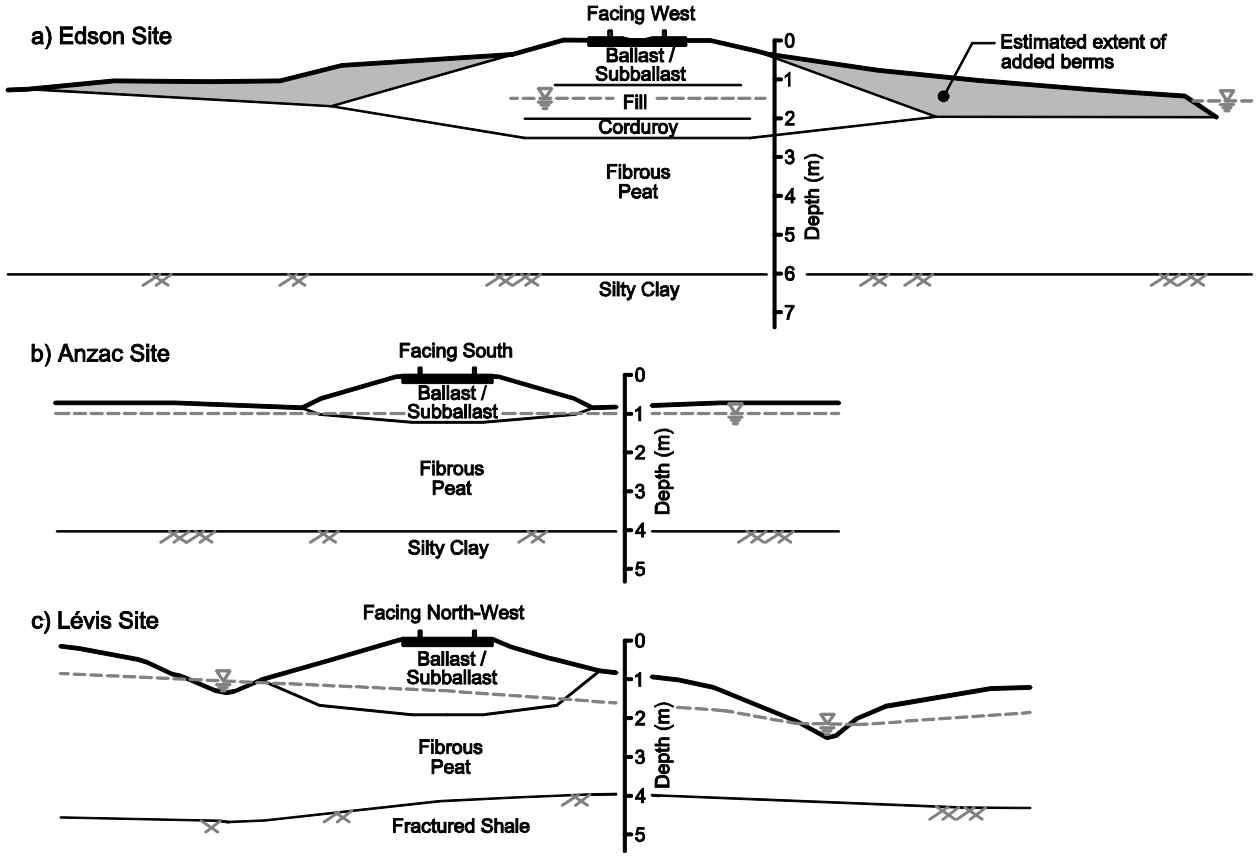

Figure 5.2 : Summary of stratigraphy and embankment geometry at (a) the Edson site, (b) the Anzac site and (c) the Lévis site.

5.5 Strength of properties of peat

The yield surfaces for the peat specimens from each site as determined from the CU triaxial testing are presented in Table 5.1. These yield surfaces were fit to the fibre reinforced critical state (Hendry et al. 2011). The Anzac site showed the highest yield strength parameters (ϕ' of

40°); followed by the Edson site (ϕ' of 34°) and Lévis site (ϕ' of 29°). Further analysis shows that these differences in the estimated yield surface are likely due to the limited number of tests rather than differences in the strength of the peat. Plotting the yield points from all sites and samples together produces a common yield line as shown in Figure 5.8a. This yield line does not take into account a yield point, labelled "Outlier" from a Shelby specimen from the Edson site. That specimen developed geometrical eccentricity during testing which led to the development of a shear plane rather than the continual yielding observed in other specimens (Hendry et al. 2011).

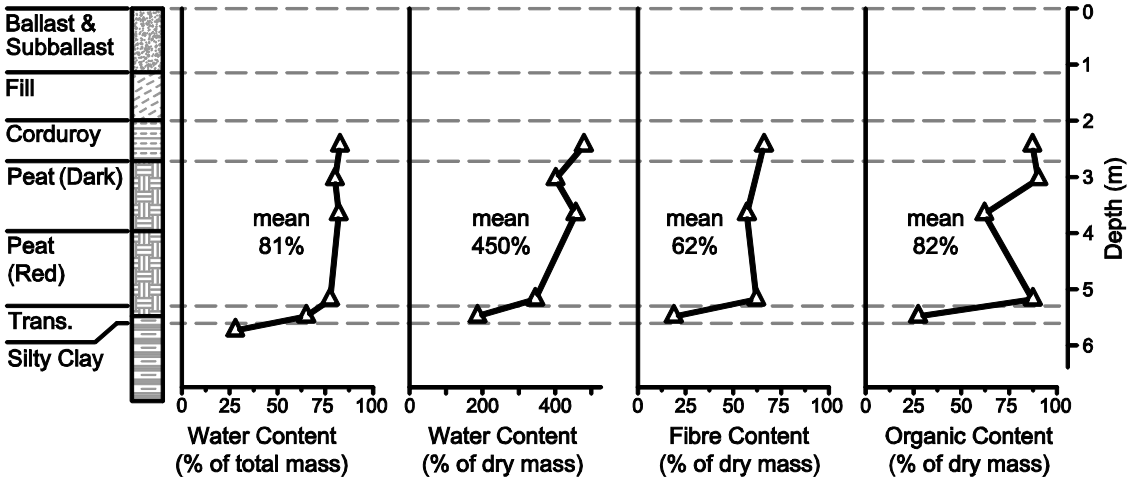

Figure 5.3 : Vertical profiles of water content, organic content and fibre content of peat for the Edson subdivision site (Hendry et al. 2011)

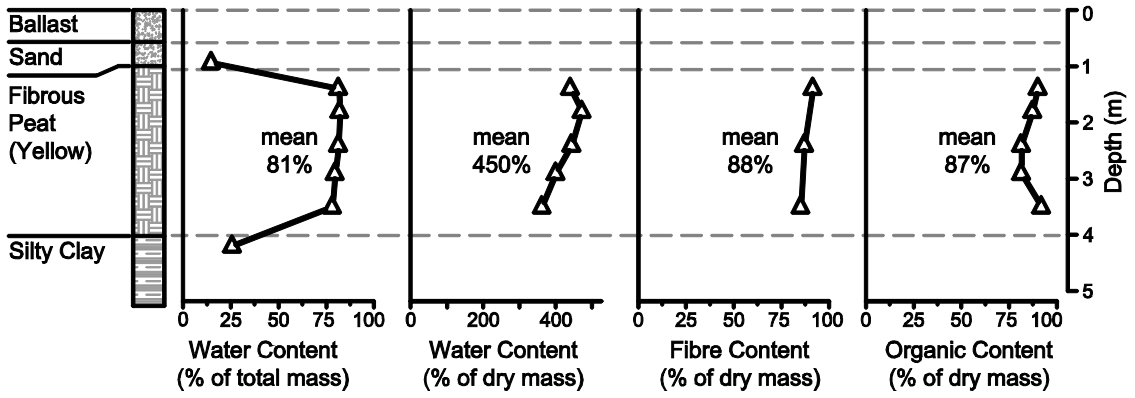

Figure 5.4 : Vertical profiles of water content, organic content and fibre content of peat for the Anzac site.

Support for the common yield surface is provided by plotting the yield surface determined from the Shelby specimens (Figure 5.8a) with the yield points determined from the CU testing of remoulded Edson peat from Hendry et al. (2011) (Figure 5.8b). This comparison of shows that

the yield surface from the Shelby specimens also describes the yield strength of the remoulded Edson peat specimens. At lower confining pressures the remoulded Edson peat specimen have higher yield strength. This is similar to behaviour that might be observed for dilatant sand and may be the result of over consolidation of the remoulded peat specimens by the one dimensional vertical stresses used to prepare the remoulded specimens. Figure 5.8b not only supports the idea of a common yield surface but it also demonstrates that there is a low effective cohesion value suggesting that intact peat does not exhibit substantial cohesion.

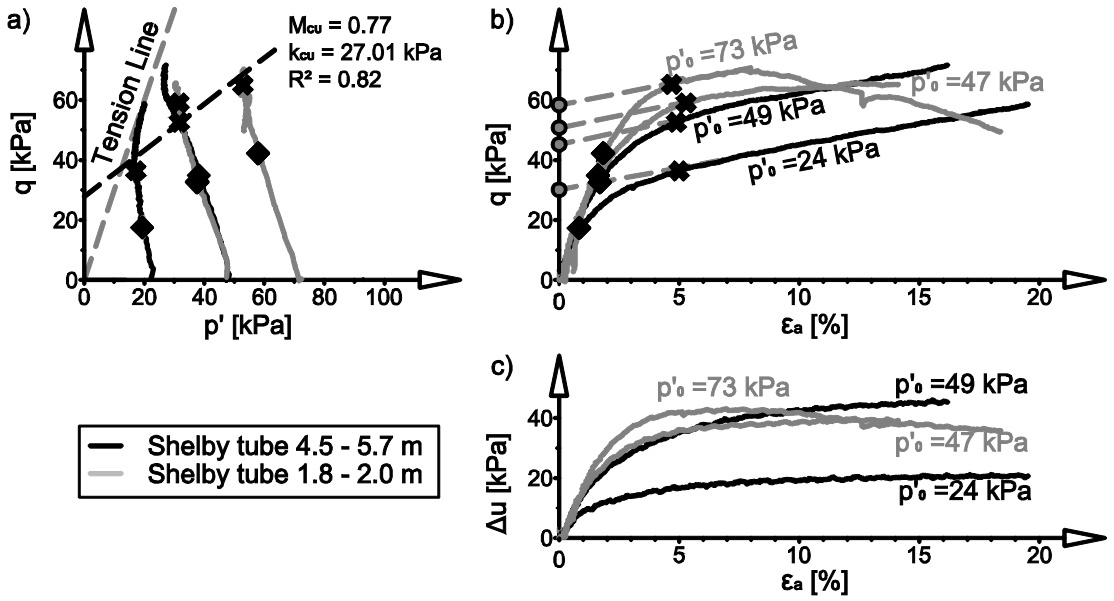

Figure 5.5 : Testing results from consolidated undrained triaxial testing of Shelby tube samples from the Edson subdivision site showing (a) the stress paths (p'q space), (b) the stress strain response and (c) the pore pressure response (Hendry et al. 2011).

The similar yield strength for the Anzac and Edson Shelby peat specimens is surprising as these properties are strongly correlated to the organic and fibre content of peat and the Anzac site has significantly greater organic and fibre content than the Edson site (Yamaguchi et al. 1985; Hobbs 1986; Hendry et al. 2011).

The test to measure fibre content (ASTM D 1997) was modified so that the peat was passed through a #10 sieve (2 mm mesh) prior to passing through the #100 sieve (150 μm mesh). The test showed that almost all of the fibres from the Edson site passed through the #10 sieve with the exception of a few small twigs and root segments. The total dry mass retained on the #10 sieve for the Anzac site was 56% of the total dry mass on the #100 sieve. Thus, the fibres which

compose the Anzac peat are much coarser than the fibres which compose the Edson peat but with no resulting increase in reinforced strength.

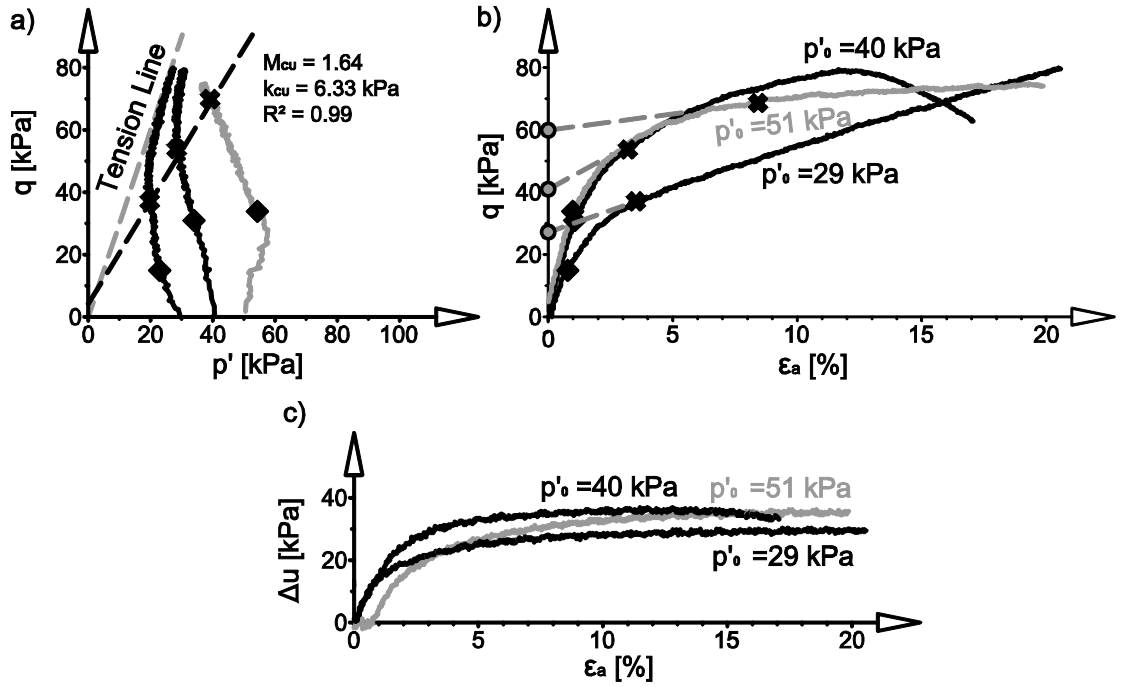

Figure 5.6 : Testing results from consolidated undrained triaxial testing of Shelby tube samples from the Anzac site showing (a) the stress paths (p'q space), (b) the stress strain response and (c) the pore pressure response.

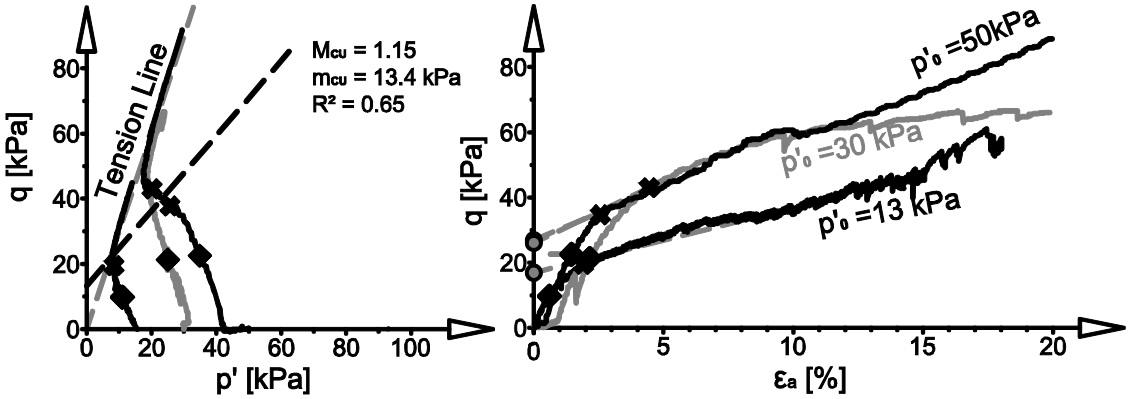

Figure 5.7 : Testing results from consolidated undrained triaxial testing of Shelby tube samples from the Levis subdivision site showing (a) the stress paths (p'q space) and (b) the stress strain response (after Konrad et al. 2007; Hendry et al. 2011).

Hendry et al. (2011) noted that yielding in the laboratory specimens did not result in the development of a failure plane during CU testing of remoulded and Shelby specimens of peat

from the Edson site. The specimens continued to deform plastically even with very high (>20%) axial strains and the specimens from all sites show a gradual transition from linear elastic to linear strain hardening after yielding (Figure 5.5b, Figure 5.6b and Figure 5.7b). The strain hardening and the pore pressure generation were shown to be due to the generation of fibre tension even after yielding.

Table 5.1: Yield strength properties for the peat from the three study sites.

Site	M	m (kPa)	Φ'	c' (kPa)
Edson	1.39	12.2	34°	6.0
Anzac	1.64	6.33	40°	3.3
Lévis	1.15	13.4	29°	6.4
Common	1.55	7.3	38°	3.7

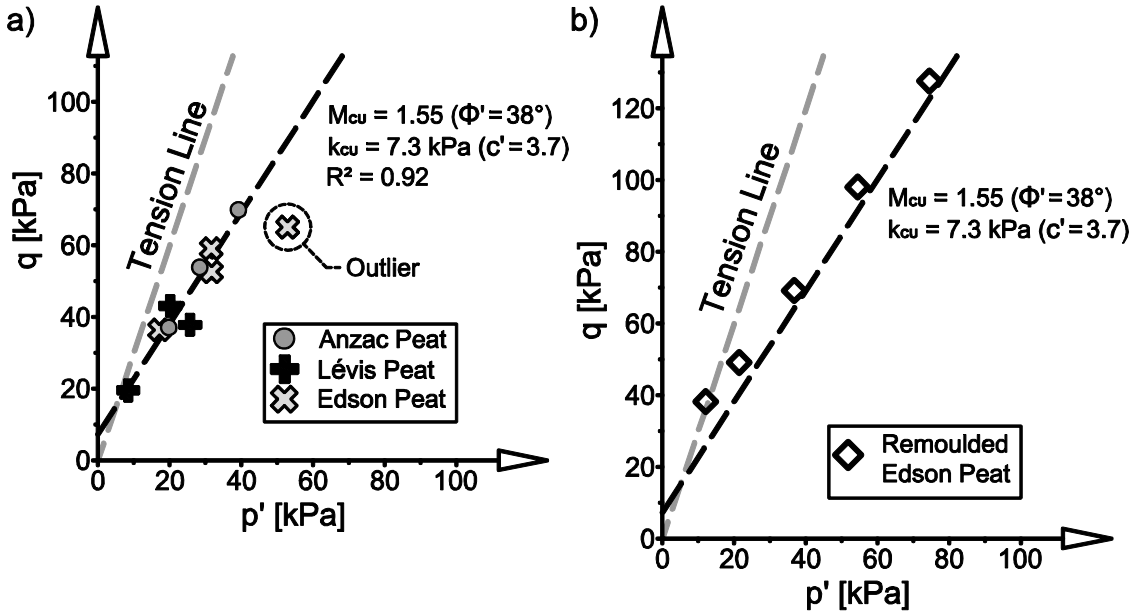

Figure 5.8 : A comparison of the yield points derived from consolidated undrained triaxial testing of (a) Shelby tube samples from all three sites and (b) the remoulded Edson peat specimens from Hendry et al. (2011).

5.6 Undrained Anisotropic response of peats

The elastic undrained anisotropic response of peat is characterized by both the stress strain response in terms of moduli and the pore pressure response resulting from the stiffness anisotropy. The stiffness of the peat, as defined by an initial Young's modulus (E_V), is plotted versus the initial sample preconsolidation pressure (p'_0) in Figure 5.9. These moduli were for

tests in which the major principal stress is perpendicular to the plane (horizontal) of the fibres. There is a strong correlation between p'_0 and E_V for the peat from the Edson site (Hendry et al. 2011) as well as the Anzac site but was not apparent for the Lévis site. Overall, there is little variation in the stiffness of the different peats with all peats having low E_V values ranging from 1.7 to 2.2 MPa at *in situ* preconsolidation pressures estimated to be between 15 to 32 kPa.

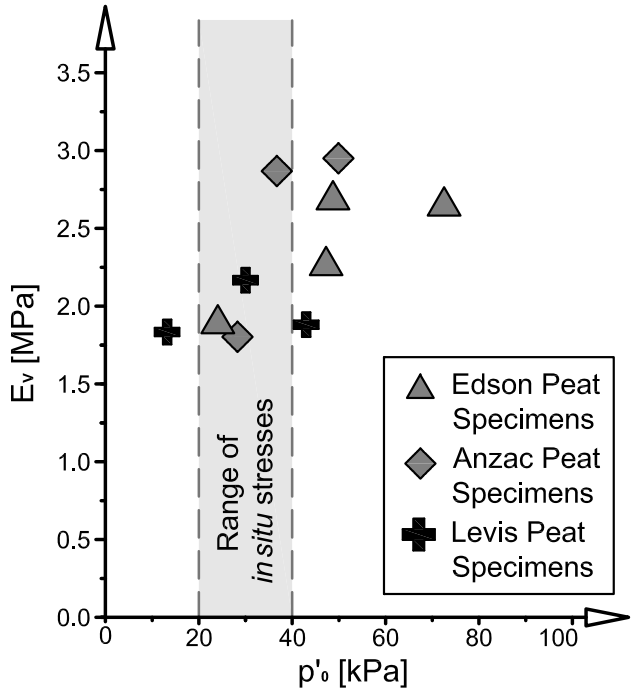

Figure 5.9 : Resulting initial modulus of the peat specimens from the CU triaxial testing for all three instrumented sites.

The pore-pressure generation within the peat samples was evaluated using a variation of Skempton's equation (equation 5.1) in which the change in pore pressure (Δu) is in terms of the change of mean total stress (Δp), change in deviatoric stress (Δq) and the shear induced pore pressure parameter (*a*).

$$\Delta u = \Delta p + a\Delta q \qquad (5.1)$$

The cross-anisotropic stiffness of the peat results in shear-induced excess pore-water pressures. The shear stress is related to the excess pore pressure by the pore pressure parameter, *a*. The average pore pressure parameter is 0.30 for the Edson site, 0.29 for the Anzac site, and 0.31 for the Lévis site. The variation between specimens from each site was greater than the variation in the mean *a* value between sites (Figure 5.10). The *a* pore pressure parameter determined for the

remoulded specimens was found in Hendry et al. (2011) to be a function of the preconsolidation pressure, this was not the case for the Shelby specimens (Figure 5.10). As the *a* pore pressure parameter was similar at all sites it was estimated that the ratio of horizontal modulus to vertical modulus were also similar in magnitude and range between 2.6 and 3.4 (Hendry et al. 2011).

Hendry et al. (2011) used the slope of the linear strain hardening response to estimate the contribution of the fibres to the fibre reinforced strength. This was done by assuming that the contribution of fibre tension is linear for the entire duration of shearing the linear portion of the strain hardening response can be extrapolated to zero axial strain (ε_a = 0%) with the q-intercept obtained from this extrapolation representing the critical state deviatoric stress (q_{CS}) associated only with friction. The resulting q_{CS} determined from remoulded specimens were plotted with respect to the mean effective preconsolidation pressure (p'_0) (Figure 5.11a). The resulting yield line from the q_{CS} p'_0 plot was very similar to that obtained from direct shear testing of specimens of the same material (Figure 5.11a). Thus, this yield surface represents the frictional strength (ϕ' =31°) and the linear strain hardening is indicative of the rate of tension generation with strain.

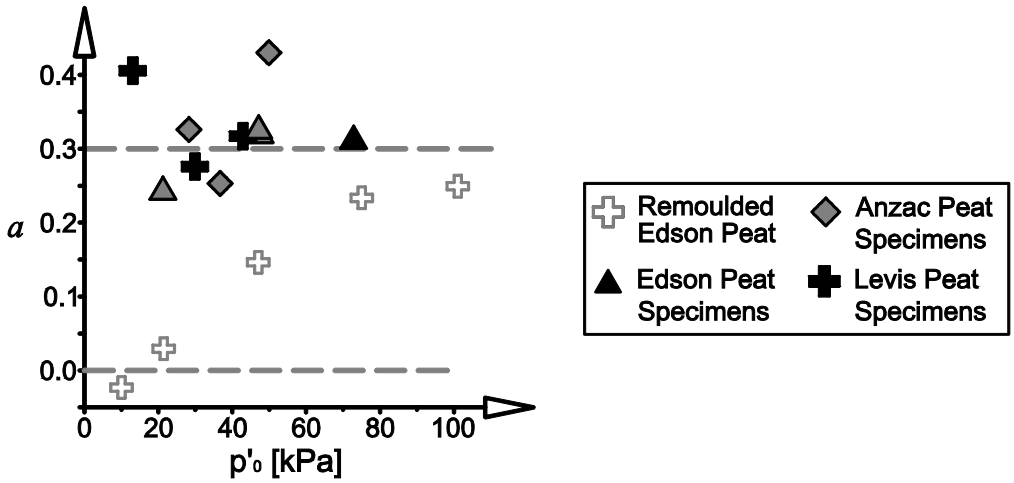

Figure 5.10: Resulting pore pressure parameter *a* for CU triaxial testing for all three instrumented sites.

The Estimation of the frictional strength of the Edson Shelby tube specimens from CU testing by Hendry et al. (2011) resulted in a much lower effective strength (ϕ'=26°) than that attained from the remoulded specimens (ϕ'=31°). Since the material within the remoulded and Shelby specimens was the same this difference was ascribed to the *in situ* structure of the Shelby specimens. The frictional strength is underestimated when this analysis is applied to specimens

with intact structures. This is hypothesised to be the result of a greater generation of fibre tension within the Shelby tube specimens than for the remoulded specimens. This difference in the development of tension within the peat fibres is visible from a comparison of the in the pore pressure parameter *a* plotted for the Shelby tube and remoulded specimens in Figure 5.10. The remoulded specimens have lower pore values for *a* due to a lower horizontal stiffness.

This analysis was conducted on the results from the CU testing conducted on Shelby specimens from all three sites. The resulting plot of critical state deviatoric stress versus the initial preconsolidation pressures as defined by Hendry et al. (2011c) is shown in Figure 5.11b. Figure 5.11b shows a common critical state line, defined by ϕ'=24°, fit to these points. Despite the inaccuracies in determining the frictional strength this allows for another avenue of comparison. The similarity of the critical state line suggests similarities in the tension generated within the Edson, Anzac and Lévis specimens. The frictional strength remains the lower limit of strength for the peat specimens. This strength was measured to be ϕ'=31° for the Edson peat. As the reinforced strength and the development of tension within fibres (apparent in the common pore pressure parameter) is similar for all three peats, the frictional strength of ϕ'=31° is assumed to be a good estimate for the frictional strength of the Anzac and Lévis peats.

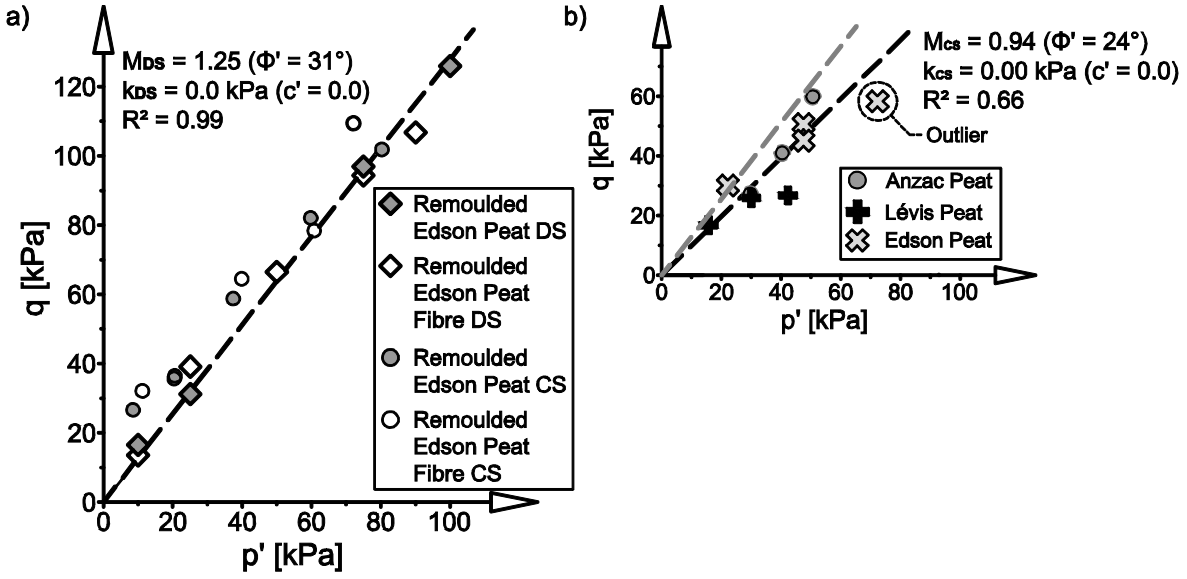

Figure 5.11: A comparison of the critical state yield points derived from (a) the CU triaxial testing of Shelby tube samples from all three sites and (b) the CU triaxial and direct shear (DS) testing of remoulded Edson peat and peat fibres specimens to determine the frictional strength of peat (Hendry et al. 2011).

5.7 Conceptual model for undrained peat behaviour

A conceptual model of peat behaviour was developed based on the peat and fibre reinforced soil literature and the laboratory testing conducted as part of this study. The basis of the model is that undrained behaviour of peat is defined by its cross-anisotropic and stiffness resulting from the development of tension within the peat fibres.

The strength can be divided into two components: the first component is the interphase friction between the solid phases of the fibres and particles which compose peat; and the second is the tension in the fibres and the resulting reinforcement of the peat. The sum of these components is the effective fibre reinforced strength. The frictional strength is a fundamental property of the surfaces of the fibres and particles; whereas the fibre reinforcement component is dependent on the fibre content, fibre length and fibre orientation with respect to the principal stresses. Thus, the cross-anisotropic nature of the strength properties is derived from the fibre reinforcement component.

The cross-anisotropic stiffness of the peat occurs as a result of the tensile stresses generated within the horizontally oriented fibres. This causes the peat to behave several times stiffer in the horizontal direction than in the vertical direction. This stiffness cross-anisotropy is only apparent when the fibres are in tension and thus does not occur during compression. The impact of this stiffness cross-anisotropy is a shear induced component of pore pressure generation. As this shear induced pore pressure is a result of the tension developed within the fibres it is also a function of the orientation of the fibres with respect to the principal stresses.

The limits of these cross-anisotropic properties are defined by response of the peat to the two extremes in the orientation of the principal stresses with respect to the horizontal plane of the peat fibres. If the major principal stress is perpendicular to the horizontal plane the result is the largest expansive strains in the horizontal directions, for the magnitude of stresses, with a corresponding maximum generation of tension within the peat fibres. This fibre tension results in the upper limit of the effective fibre reinforced strength ($\phi' = 38°$) and the greatest generation of shear induced pore pressures ($a = 0.3$). Rotation of the major principal stress away from this orientation will result in a reduction of tension in the fibres and a tendency *towards* an isotropic pore pressure response ($a \rightarrow 0$) and a lower frictional strength ($\phi' \rightarrow 31°$). The test results

presented by Yamaguchi et al. (1985) suggest that even in the extreme case in which the principal stress coincides with the horizontal plane, the pore pressure response will still show evidence of reduced cross-anisotropy as a result of some lower level of fibre reinforcement.

5.8 Net effect of fibre reinforcement

The presence of the fibres within the peat results in an increased effective fibre reinforced strength and an increased pore pressure response. The increased effective strength shows and increased ability to withstand higher deviatoric stresses at a given mean effective stress. Conversely, the shear induced pore pressure response leads to a reduction of the mean effective stress and an associated reduction of the change in deviatoric stress which will results in yielding. These two effects have competing results on the shear stresses applied during undrained loading conditions which results in the plastic yielding of peat.

To determine the net effect of the fibre reinforcement a comparison is made between a fibre reinforced peat with effective strength (38°) and pore pressure parameter *a* determined from the CU testing (0.3), and a hypothetical peat without fibre reinforcement with a strength defined by the frictional strength and an isotropic pore pressure response ($a = 0$). For this comparison the net effect of the properties on the undrained effective stress paths for the two materials are considered based on a common initial stress state and change in shear stress until yielding along their respective effective stress paths. A division between the initial stress states which result in these two outcomes was found by considering the cases which would result in a detrimental effect arising from anisotropic pore pressure generation which was equal to the beneficial effect of the fibre reinforcement on the strength (Figure 5.12). Figure 5.12 shows a division line (zero net effect) between initial stress states that result in a net beneficial effect of fibre reinforcement (above); and those that result in detrimental effects of the anisotropic pore pressure response exceed the benefits from the reinforcing effect of the fibres on the strength (below).

The net effect can be quantified as the ratio (η) of the increase in shear stress which can be withstood by the peat with the presence of the fibres ($\Delta q_{Reinforced}$) to the shear stress due to the frictional alone ($\Delta q_{Frictional}$) (Equation 5.2). Two regions are defined by the zero net effect line and bounded by the frictional strength and the mean effective stress axis. The region of initial stress states which results in a beneficial net effect of the fibrous nature of peat is further divided

into contours showing the change in the net effect of the fibre reinforcement based on the initial effective stress state (Figure 5.13). The effect of the shear induced pore pressure response is that the full benefit of the reinforcing effect of the peat fibres on the strength cannot be realized for undrained loading.

$$\eta = {}^{\Delta q_{\text{Reinforced}}}\!/_{\Delta q_{Frictional}} \tag{5.2}$$

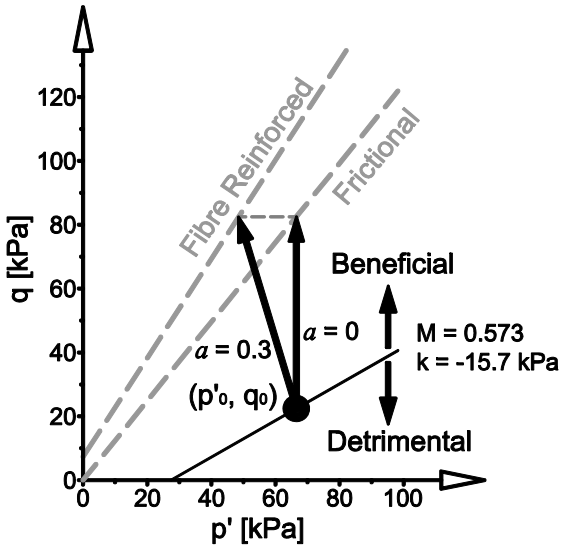

Figure 5.12 : Graphical representation of the initial stress states which determine if the net effect of the fibre reinforcement is beneficial or detrimental to the strength of the peat.

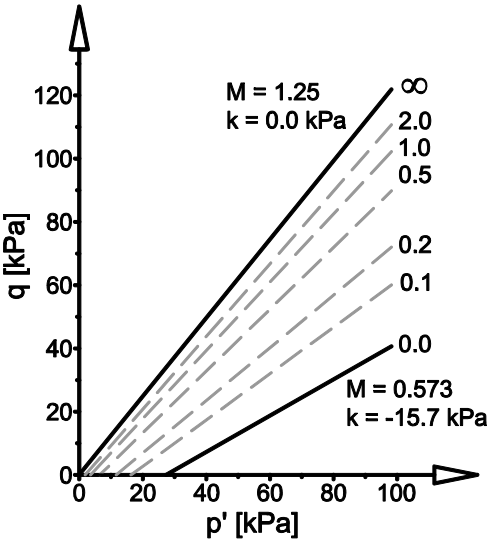

Figure 5.13 : Graphical representation of the initial stress states which determine if the net effect of the fibre reinforcement is beneficial or detrimental to the strength of the peat. The contours represent different values of η representing the net effect of the fibrous nature of the peat base on initial stress state.

5.9 Application of undrained response to embankment foundations.

The *in situ* stress states of the peat (p'_0, q_0) at the study sites was simulated using the finite element software SIGMA/w (GeoSlope 2007) based on the geometry of the sites and the density of the materials (13 kN/m^3 for peat and 26 kN/m^3 for ballast and subballast)[6]. The initial stress states within the peat foundation at the Edson, Anzac and Lévis sites are plotted along with the fibre reinforced strength and the frictional strength in Figure 5.14. Based on this initial *in situ* stress state the effect of the fibre is expected to be beneficial during undrained loading.

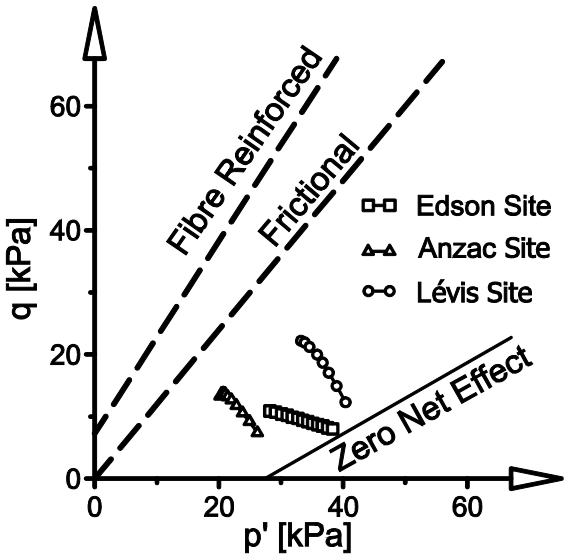

Figure 5.14 : Plot of the modelled *in situ* stress states beneath the centerline of the embankments.

5.10 Conclusions

This paper has presented the results from a laboratory testing program involving consolidated undrained (CU) triaxial tests Shelby specimens obtained from peat beneath railway embankments at three sites. The results have been presented in terms of effective stress paths in the deviatoric stress-mean effective stress space and analyzed using the framework of cross-anisotropic elasticity and fibre-reinforced soil.

There is little variation in the anisotropic elastic response of the peat from all three sites to undrained loading during CU testing. All three peats had similar pore pressure parameters (a ~

[6] The modelling for the *in situ* stresses beneath the center line of the embankments is presented in more detail in Appendix D.

0.3) and moduli (approximately 1.7 to 2.2 MPa). The specimens from all sites appear to share a common yield line defined by the effective shear strength of 38° and an apparent cohesion of 3.7 kPa. This similarity in reinforced strength was surprising due to the variation in the organic content and the fibre content between the sites.

The nature of yielding within the peat specimens was not consistent with typical mineral soils since distinct failure planes did not form in peat. Specimens used for the CU testing continued to deform plastically even under high (>20%) axial strains. In a similar manner, the direct shear tested specimens did not develop well-defined failure planes but only underwent tearing. Measurement of frictional strength within the direct shear tests required a pre-cut failure plane (Hendry et al. 2011). In addition to the lack of failure plane the CU test results also showed strain hardening after the identified yield condition.

The calculation of the frictional strength from the results of CU testing conducted on Shelby peat specimens and extrapolation of resulting strain hardening characteristics leads to an underestimation of this strength. This is hypothesised to be due to the increased generation of tension at lower strains. This increase in tension within the fibres is attributed to the *in situ* structure in the form of interwoven and interconnected fibres.

From the response of peat and fibre reinforced soils a conceptual model was presented which combines the cross-anisotropic stiffness and strength developed from the tension in the fibres and the orientation of the principal stresses to the predominant fibre orientation. From this concept of fibre reinforcement the net effect, the increased strength and anisotropic pore pressure response was evaluated. This analysis showed that the net effect is dependent on the initial stress state of the peat; and for high mean effective and low deviatoric initial stress states the net effect of the fibres on the shear strength may be detrimental. Simulation of the *in situ* stress states within the peat foundation suggests that the peat below the Edson and Anzac embankments the initial deviatoric stress and preconsolidation pressure as such that the net effect of the peat fibres is beneficial to withstand additional undrained loading.

5.11 Acknowledgements

The writers would like to acknowledge the contribution of Canadian National Railways for providing both the project and funding. The authors also thank Tom Edwards for his support of

this project. This research was made possible through the Railway Ground Hazard Research Program, funded by the Natural Sciences and Engineering Research Council of Canada (NSERC), CN, CP Rail, and Transport Canada.

5.12 References

Farrell, E.R. and Hebib, S. 1998. The determination of the geotechnical parameters of organic soils. Proceedings of the International Symposium on Problematic Soils, IS-TOHOKU 98, pp 33-36.

GeoSlope International, Ltd. (GeoSlope) (2007). GeoStudio 2007: SIGMA/w (Version 7.17) [Computer software]. Calgary, Alberta, Canada. Available from http://www.geo-slope.com/

Graham, J. and Houlsby, G.T. (1983) "Elastic Anisotropy of a Natural Clay", Géotechnique, 33, No. 2: 165-180

Hendry, M., Sharma, J., Martin, D., Barbour, L., 2011 Laboratory investigation of the fibre content and in situ structure on the anisotropic strength and stiffness of fibrous peats. Submitted to Canadian Geotechnical Journal.

Hobbs, N.B. 1986. Mire Morphology and the Properties and Behaviour of some British and Foreign Peats. Quarterly Journal of Engineering Geology, **19**: 7-80.

Konrad, J.-M., Grenier, S., and Garnier, P. 2007. Influence of Repeated Heavy Axle Loading on Peat Bearing Capacity. In 60th Canadian Geotechnical Conference. Ottawa, pp. 1551-1558.

Konrad, J-M. ., Grenier, S., and Garnier, P.2006. Heavy Axle Load over Muskeg Déraillement de l'Ultratrain a St-Henri-de-Lévis. Presentation at the Railway Ground Hazard Research Program annual workshop, Kingston, Ontario.

Kumar, A., Wailia, B.S. and Mohan, J. 2006. Compressive strength of fiber reinforced highly compressible clay. Construction and Building Materials, 20: 1063-1068.

Landva, A.O., and La Rochelle, P. 1983. Compressibility and Shear Characteristics of Radforth Peats. In Testing of Peats and Organic Soils. ASTM Special Technical Publication, **820**: 157-191.

Landva, A.O. and Pheeney, P.E. 1980. Peat fabric and structure. Canadian Geotechnical Journal, **17**: 416-435.

Lester, G. 2005. *Atlas of Alberta Railways*. University of Alberta Press, Edmonton, Canada. Available on-line at http://railways.library.ualberta.ca/ [Accessed January 27, 2011]

Li, J. and Ding, D.W. 2002, Nonlinear elastic behaviour of fiber-reinforced soil under cyclic loading. Soil dynamics and earthquake engineering, 22: 977-983.

Long, M. 2005. Review of peat strength, peat characterization and constitutive modelling of peat with reference to landslides. Studia Geotechnica et Mechanica, **27**(3-4): 67-90.

MacFarlane, I.C. 1969. Muskeg Engineering Handbook. University of Toronto Press, Toronto.

Mesri, G. and Ajlouni, M. 2007. Engineering properties of fibrous peats. ASCE Journal of Geotechnical and Geoenvironmental Engineering, 133(7): 850-866.

Michalowski, R. L., and Čermák, J., 2002. Strength anisotropy of fiber-reinforced sand. Computers and Geotechnics, 29: 279-299

Michalowski, R. L., and Čermák, J., 2003. Triaxial compression of sand reinforced with fibers. ASCE Journal of Geotechnical and Geoenvironmental Engineering, **129**(2): 125-136

Sadek, S., Najjar, S., and Freiha, F. 2010. Shear Strength of Fiber-Reinforced Sands. ASCE Journal of Geotechnical and Geoenvironmental Engineering, **136**(3): 490-499

Tan, Y. 2008. Finite element analysis of highway construction in peat bog. Canadian Geotechnical Journal, **45**(2): 147–160.

The Transportation Safety Board of Canada (TSB). 2008. Railway Investigation Report R04Q0040. Cat. No. TU3-6/04-2E, ISBN 978-0-662-47573-6

Wood, D.M. 1990. Soil Behaviour and Critical State Soil Mechanics. Cambridge University Press

Yamaguchi, H., Ohira, Y., Kogure, K. and Shigeru, M. 1985. Undrained shear characteristics of normally consolidated peat under triaxial compression and extension conditions. Soil and Foundations, 25(3):1-18.

Zwanenberg, C. 2005. The influence of anisotropy on the consolidation behaviour of peat. Ph.D. thesis, TU Delft, Delft, The Netherlands.

Chapter Six: The measurement and analysis of the cyclic response of railway embankments and underlying soft peat foundations to heavy axle loads.

Contribution of the Ph.D. candidate

All work reported in this chapter, including instrumentation design and installation, review of the literature, development of the theoretical framework, analysis and discussion of the results and writing of the text, has been carried out by the Ph.D. candidate.

As supervisors, Dr. S. L. Barbour and Dr. C.D. Martin have reviewed all parts of the work. This chapter will be submitted with the following citation:

Hendry, M.T., Martin, D. and Barbour, S., (2011). The measurement of the cyclic response of railway embankments and underlying soft peat foundations to heavy axle loads. *To be submitted to Geotechnique.*

Contribution of this chapter to the overall study

Previous field studies of the response of peat foundations to railway loading have focussed on specific problems at a single site. These problems have included the generation of pore water pressure and the resulting pumping of material to the surface, excessive cyclic deformations, excessive settlement of the embankment or rapid shear failure of embankments and peat foundations. A more comprehensive evaluation of the performance of railway embankments over soft peat foundations must include multiple sites with different conditions to be generally applicable. The following manuscript endeavours to provide a general explanation of the undrained response and performance of peat foundations through the investigation of three distinct field sites. This was accomplished by comparing the measured responses and soil properties and then simulating the loading conditions at each site to demonstrate the proximity of the loaded stress state to failure. A further comparison of the zones of potential plastic deformation and the stress mobilized within the peat relative to the yield condition. This comparison provided insight into how indicative the most recent failure at the Lévis site is of the

increasing potential for similar incidents of foundation failure at a larger number of sites as traffic and axle loads increase throughout the railway network. This study is unique as it is the first side by side comparison of the performance of multiple railway embankments over peat foundations based on *in situ* measurements; laboratory defined elastic responses, and the development and application of a conceptual model for the behaviour of the peat foundation under heavy axle loads. The findings from this paper directly address the global objectives of this research as it presents the direct measurement of the spatial and temporal distribution of strain, pore pressure within the cyclically loaded peat foundation beneath a railway embankment. Further, it develops a model for the distribution of the stresses and strength of the peat within the peat from the existing literature on the undrained response of peat, fibre reinforce soils, and stresses under moving axle loads

Abstract

This paper presents the results of research conducted at three sites to understand the response of peat foundations under railway embankments to the cyclic application of heavy axle loads. The three field sites include two in Northern Alberta on Canadian National Railway's Edson and Lac-La-Biche (Anzac) subdivisions, and one on the Lévis subdivision in southern Quebec. This research included the installation of instrumentation in the field to measure the distribution of strain and pore pressure generation under cyclic loading and the laboratory testing of peat specimens retrieved from these sites. A ShapeAccelArray (SAA) was used to measure the distribution of horizontal cyclic displacement with depth. This paper presents the measured response of the peat foundations at the three sites. The discussion of the data sets provides an analysis of the spatial distribution of strain, pore pressure generation and stress and the effect of these on the strength of the structures. Further analysis was conducted with finite element modelling to determine the spatial distribution of increase potential for yielding and to determine how close the peat is to yielding based on the effective stress paths calculated from the measured responses.

6.1 Introduction

Allowable axle loads have tripled on Canadian railways, since the original construction of the railway infrastructure. The volume of traffic on the main lines of the Canadian National (CN)

and Canadian Pacific (CP) railways are close to their maximum capacities with trains now reaching over 3.6 km (12,000 feet) in length. This increase in axle loads and traffic volume have had detrimental effects on the infrastructure, particularly those that are built on soft foundations, such as railroad embankments built over peat. Both CN and CP railways are experiencing continuing problems with large stretches of embankments built over peat. These problems range from excessive settlements requiring increased amounts of maintenance to sudden catastrophic failures.

This research program was prompted by two derailments of trains on the CN Lévis subdivision, both attributed to soft subgrade issues. Both incidents were investigated by the Transportation Safety Board (TSB) investigation. The first derailment was a result of a failure of a track component from increased stresses due to the soft foundation (TSB 1999). The second derailment was due to the failure of the embankment and peat foundation (TSB 2008). The results of the TSB investigation suggested that the second failure was a result of an increase in axle loads and traffic volume led to progressive settlement of the embankment which cause reorientation of reinforcing peat fibres and a loss of the strength that they provided (Konrad et al. 2007, TSB 2008). This study has highlighted the need to develop a better understanding of the load-deformation response of peat foundations subjected to heavy axle loads.

In addition to the Lévis site, two other sites were investigated. Instrumentation to measure displacements and pore pressure response within the peat foundations were installed at both sites. The design and development of the instrumentation installed at the study sites was described previously by Hendry et al. (2008) and Hendry et al. (2011a). Laboratory testing of peat specimens from these sites has also been undertaken to determine the elastic behaviour and shear strength of the peat and to develop a conceptual model of the undrained response of the peat to loading (Hendry et al. 2011b; Hendry et al. 2011c). In this paper the field observations and laboratory determined properties of the peat from these sites are brought together to evaluate the strength of the structures and their foundations with respect to their current loading conditions. The site conditions, monitoring data for the Lévis site are presented and reanalysed for comparison.

6.2 Background

The pore pressure and deformation response of peat under heavy axle loads has been extensively investigated to explain the formation of large 'peat boils' or pumping features on the surface of railway embankments over peat foundations (Wong et al. 2006), the effect of train speed on deformation (Hendry et al. 2006; Hendry et al. 2010), and to investigate the stability of the peat foundations under train loading (Konrad et al. 2007; TSB 2008). From these studies the following characteristics of the response of peat foundations to heavy axle loads have been described:

- Cyclically loaded peat foundations behave in an undrained manner, unless piping or pumping features are present which limit the maximum induced pore pressure by rapid dissipation of excess pore water pressure through cracks or openings in the subgrade/ballast (Wong et al. 2006).
- The magnitude of excess pore pressure measured below railway embankments was greater than what could be explained using an idealized isotropic elastic soil model (Wong et al. 2006). Similarly, Konrad et al. (2007) showed a concentration of pore pressures mid-depth in the peat layer and suggested there was an accumulation of excess pore pressure.
- The deformation within peat foundations have been measured and found to be predominantly elastic and recoverable (Hendry et al. 2006; Konrad et al. 2007; Hendry et al. 2010). This has been confirmed by the low magnitude of the residual pore pressure following the passage of trains (Wong et al. 2006; Konrad et al. 2007). Extrapolation of data collected over three months at the Lévis site suggested a significant long-term settlement issues resulting from the accumulation of small plastic strains created by each passing train (Konrad et al. 2007).
- The results of increased train speed have little effect on the magnitude of the measured deformations (Hendry et al. 2006; Konrad et al. 2007; Hendry et al. 2010). Modelling has demonstrated that at normal operating speeds the magnitudes of deformations were correlated to the magnitude of the axle loads and were not affected by dynamic effects

associated with train speed. However, the extrapolated magnitude of pore pressure has been shown to increase with increasing train speed (Konrad et al. 2007).

- The peat fibres have two contradictory consequences on the undrained shear strength of peat: first, an increased effective strength; and second, a shear induced pore pressure response. The net effect of the peat fibres is dependent on the initial stress state of the peat; for high mean effective and low deviatoric initial stress states the net effect of the fibres on the strength may be detrimental. The results of the modelling of the initial (no axle loads) stress state of the peat foundation indicated that the net effect of the fibrous nature of peat is beneficial in that the additional strength derived from the fibres exceeds the effect of the generation of shear induced excess pore pressure (Hendry et al. 2011c).

A detailed examination of undrained peat behaviour in the laboratory by Hendry et al. (2011b) and Hendry et al. (2011c) resulted in three major findings. First, the elastic behaviour of peat is highly anisotropic with considerably greater stiffness in the horizontal direction. These testing results are in agreement with the results presented by Yamaguchi et al. (1985). This stiffness anisotropy results in a component of pore pressure generation generated by shear stress. This is consistent with the conclusion of Wong et al. (2006) that the measured pore pressure response within peat could not be explained with an isotropic elastic soil model. The second major finding was that the magnitude of the strength, stiffness, and cross-anisotropic pore pressure response arises as a result of the orientation of the principal stresses with respect to the predominant horizontally aligned fibres which constitute the peat. The effect of the quantity and orientation of the peat fibres are common themes within the peat literature and have been extensively studied (MacFarlane 1969; Yamaguchi et al. 1985; Hobbs 1986; Mesri and Ajlouni 2007). Finally, the properties of the peat from the different sites were found to have very similar anisotropic elastic responses to loading and similar shear strengths as a result of fibre reinforcement (Hendry et al. 2011c).

Hendry et al. 2011c developed a conceptual model for the response of peat to undrained loading based on the peat and fibre reinforced soil literature (Michalowski and Čermák 2002; Li and Ding 2002; Kumar et al 2006), and the laboratory testing conducted as part of this study (Hendry et al. 2011b; Hendry et al. 2011c). The basis of the material model is that undrained behaviour of peat is defined by its cross-anisotropic stiffness and strength, which occurs as a result of the

development of tension within the peat fibres. The ability to generate tension within these fibres, leads to an increase in stiffness and strength and reduces pore-pressure generation. These effects are dependent on the orientation and magnitude of the principal stresses with respect to the predominantly horizontal fibres. If the major principal stress is perpendicular to the horizontal plane this will result in expansive horizontal strains and maximize tension in the fibres, the pore pressure response (a = 0.3), stiffness and strength (ϕ'=38°). Rotation of the major principal stress away from this orientation will result in a reduction of tension in the fibres and a tendency *towards* an isotropic pore pressure response ($a \rightarrow 0$) and a frictional strength (ϕ'=31°). In the exceptional case in which the principal stress coincides with the horizontal plane, the major principal stress will still result in expansive strains the horizontal direction perpendicular to the stress; this will result in a minimum reinforced strength and shear induced pore pressure response (Hendry et al. 2011c).

6.3 Site descriptions

All of the study sites are located on CN railway lines. The Edson and Anzac sites were selected by CN based on a maintenance history, new traffic loading, and new construction. The Lévis site was included due to the amount of data available for the site and the importance of the failure. All of the sites have approximately 3 m of intact peat supporting the railway embankments; the peats vary in consistency and degree of humification. The construction of the embankments also varies between the sites.

The Edson site is located on the CN mainline is at mile 102.0 on the Edson subdivision, near the town of Niton Junction, Alberta (Figure 6.1a). An aerial photograph of the site is presented in Figure 6.2. The extent of the peat deposit is clearly visible as smoother textured vegetation (mile 101.4 to 102.5). The circular lake south of the embankment is indicative of the morphology of the site and represents the terrestrialization, the infilling of a shallow lake.

The Edson embankment (Figure 6.8a) was constructed as part of the Grand Trunk Railway between 1909 and 1912 (Lester 2005). The embankment consists of ballast and sub-ballast to a depth of 1.2 m, underlain by approximately 1.0 m layer of peaty organic fill material. A timber corduroy log raft was placed directly over the original peat (Figure 6.3). This type of construction was typical for railway embankments over peat at that time (MacFarlane 1969). The

timber corduroy was found to be in good condition as was evident by the difficulty in drilling through it and the well preserved condition of samples of the timber obtained during drilling. This site required significant amounts of maintenance and sections of the embankment had undergone remediation in 1998 by placing gravel berms on both sides of the embankment. With the addition of the berms the toe to toe width of the embankment is now 23 m. Beneath the Edson embankment is 3m of peat overlying an unoxidized silty clay.

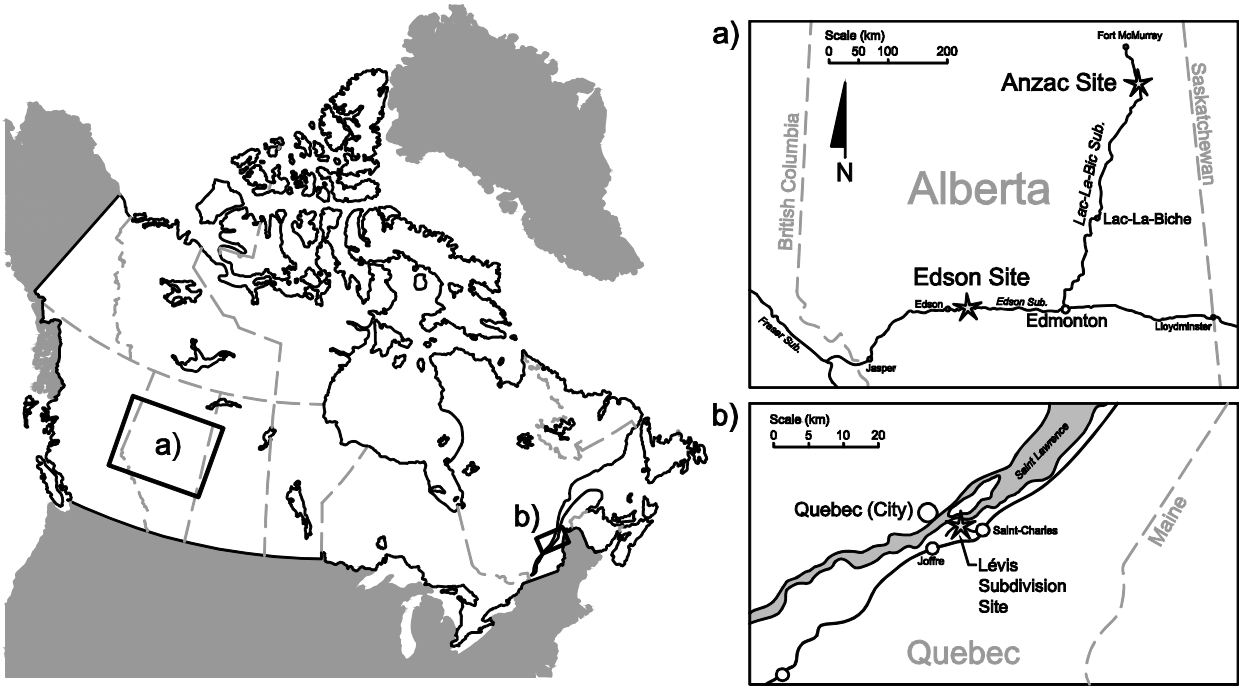

Figure 6.1 : Location of CN sites included in this study in a) Alberta, and b) Quebec.

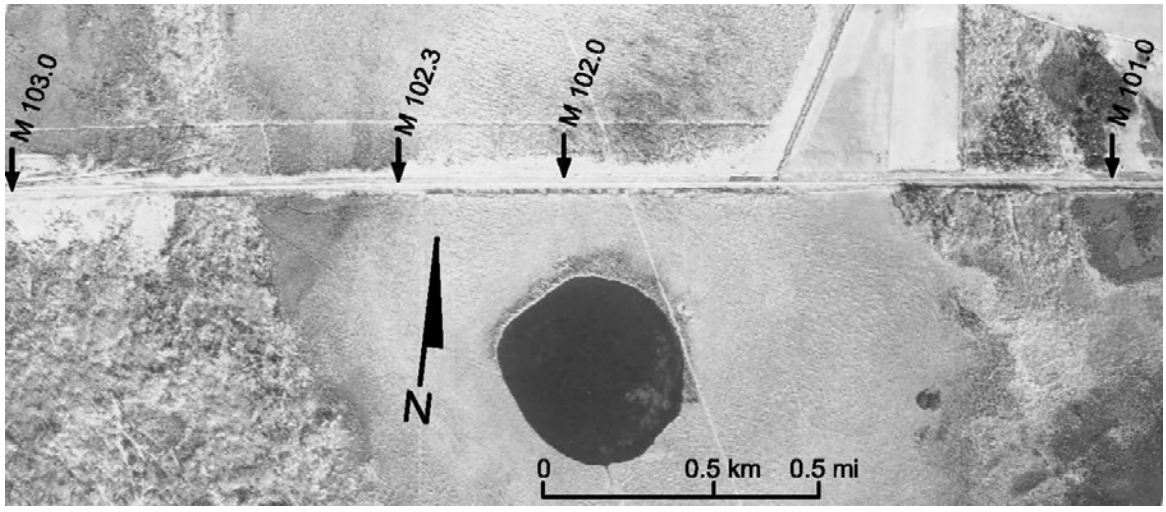

Figure 6.2 : Arial photograph of the Edson Subdivision peat bog crossing. Instrumentation installed at Mile 102.0 (Hendry et al. 2011a)

Figure 6.3 : Photograph of the construction of a railway embankment over peat using corduroy raft construction (MacFarlane 1969).

The peat has a fine fibrous texture. The upper half of the peat is dark in colour while the lower half of the peat layer has a red colour. The distribution of gravimetric water content, organic content and fibre content of the peat are presented in Figure 6.4. The water content of the peat was found to decrease slightly with depth, with a mean value of 450%. Both the organic content and fibre content of the peat appeared to be consistent with depth with mean values of 82% and 62%, respectively. The specific gravity of the specimens retrieved from the site varied from 1.25 to 1.30. The peat was determined to be only slightly hummified and the Hobbs (1986) and Von Post peat classification of the peat was $H_3B_3F_2R_1W_0N_4$.

The Anzac site is located at mile 263.5 of the Lac-la-Biche (formerly Waterways) subdivision, near the town of Anzac, Alberta (Figure 6.1a). This recently re-acquired subdivision runs from the mainline, near Edmonton, to Fort McMurray, Alberta, and contains 120 km of embankments over peat. An aerial photograph of the site (Figure 6.5) shows that the terrain consists of many large peat formations. The Anzac embankment consists of ballast, added in 2008, placed over sand for a combined thickness of 1.1 m. The embankment is built upon an intact peat layer that is 2.6 to 3 m thick. The peat has a course fibrous texture, and is yellow-brown in colour. Below the base of the peat is unoxidized silty clay. The water content, organic content and fibre content

of the peat were found to decrease with depth (Figure 6.6), with mean values of 450%, 87% and 88% respectively. The degree of humification was determined to be insignificant, with the plant structures within the peat appearing to be intact. The classification of the peat as per Hobbs (1986) and the Von Post peat classification (Landva and Pheeney 1980) system is $H_2B_3F_2R_2W_1N_4$.

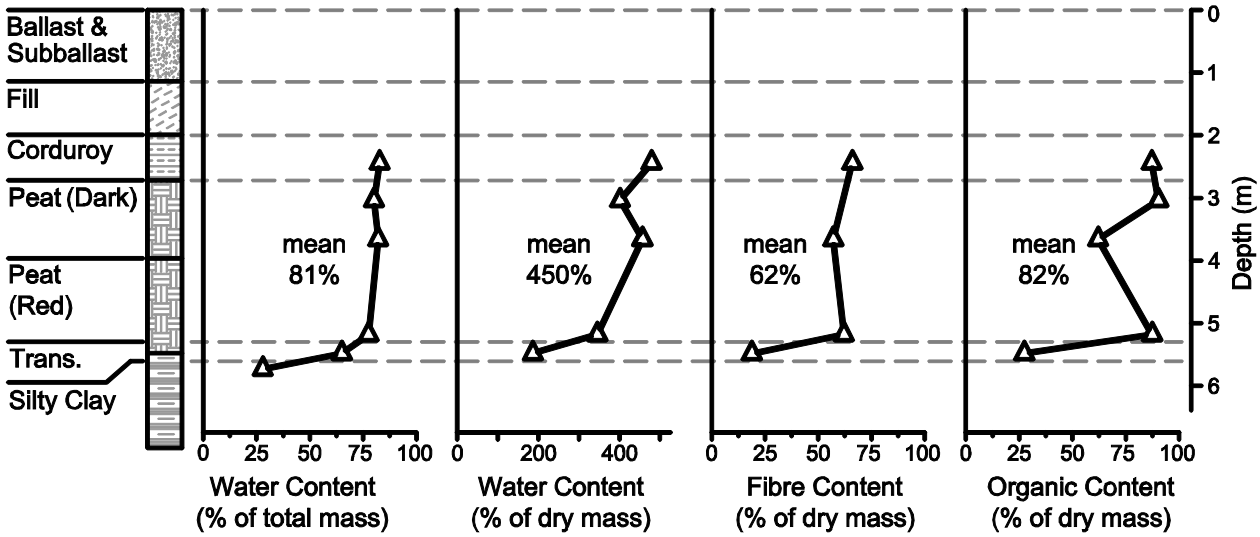

Figure 6.4 : Vertical profiles of water content, organic content and fibre content of peat for the Edson site (Hendry et al. 2011b)

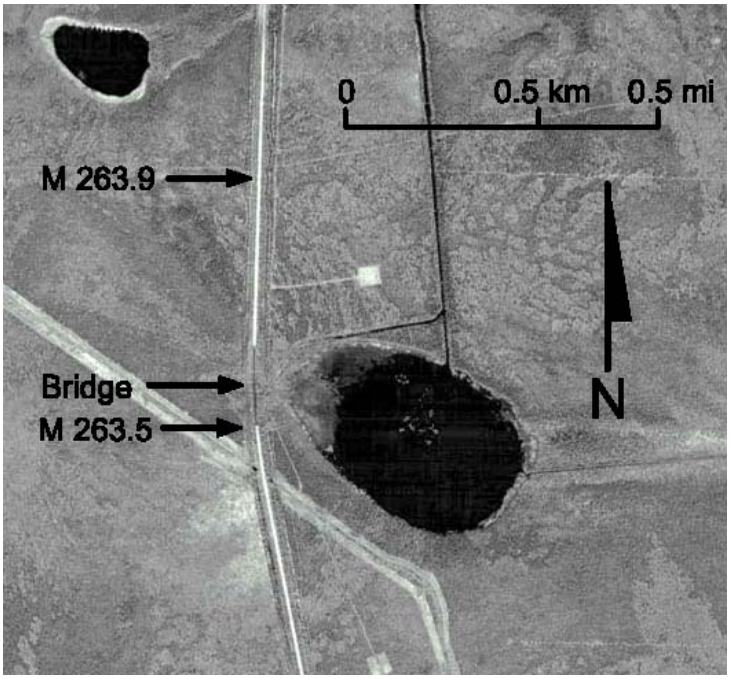

Figure 6.5 : Arial photograph of the Anzac Subdivision peat bog crossing. Instrumentation installed at Mile 263.9

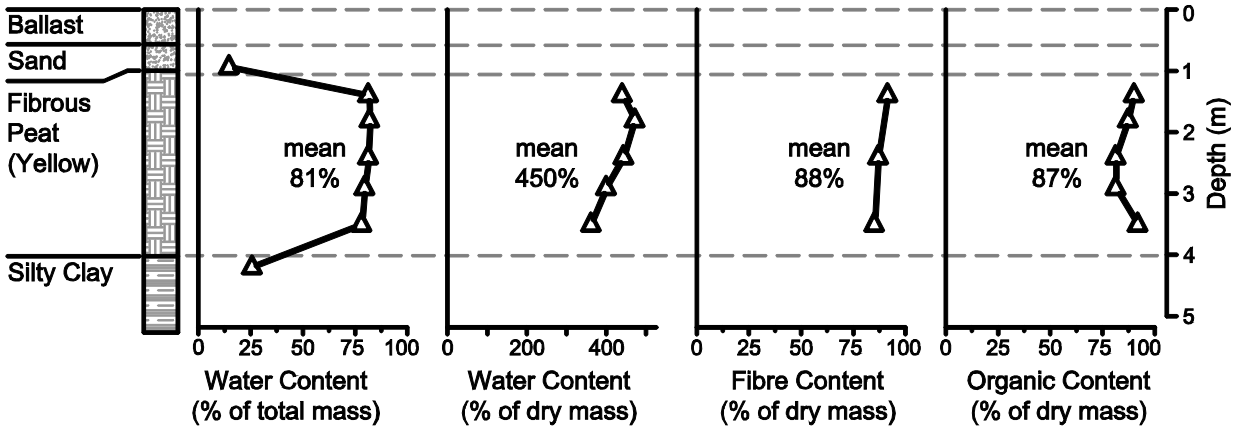

Figure 6.6 : Vertical profiles of water content, organic content and fibre content of peat for the Anzac site (Hendry et al. 2011c).

The Lévis site is located near mile 4.0 of the CN Lévis subdivision in southern Quebec (Figure 6.1). This embankment was originally constructed in between 1879 and 1884. The composition of the embankment and foundation consists of a ballast layer, which varies in thickness between 0.3 and 0.9 m, underlain by a layer of brown to grey coarse sand containing some silt which is between 0.6 and 1.2 m thick. The intact peat layer below the embankment had a relatively constant thickness of 3 m (Figure 6.8c). The peat was described by Konrad et al. (2007) as black in colour, fibrous and highly compressible. The water content of the peat under the embankment was found to be approximately 500 %. The specific gravity of the peat was reported as approximately 1.0 (Konrad et al. 2007). The organic and fibre contents were not available for this site.

A derailment occurred at this site in 1999 due to the degradation and failure of track components due to the soft nature of the foundation (TSB 1999). Significant rehabilitation work was done following the derailment in 1999, and before the embankment failure in 2004, to reinforce the roadbed between Mile 3 and Mile 5.9. This included an increase in the ballast depth and the addition of a berm and new ditch north-east side of the track (TSB 2008) (Figure 6.8c).

There appears to be little variation in the anisotropic elastic response of the peat from the various study sites to undrained loading. The pore pressure parameters (a ~ 0.3) and moduli (approximately 1.7 to 2.2 MPa) measured in consolidated undrained triaxial testing on specimens from all three sites were similar within the range of *in situ* stresses (Hendry et al. 2011c). Only a small number of specimens were available for each type of peat; the fibre reinforced yield

strength of the peats evaluated from these specimens appeared to vary significantly between the sites. However, when all of the yield points from all of the specimens were plotted together it is apparent the peat from all of the sites has a common yield surface defined by the ϕ'=38° and an apparent cohesion of 3.7 kPa (Figure 6.7a). This was surprising due to the variation in the organic content and the fibre content between the sites (Hendry et al. 2011c).

Direct shear testing of remoulded Edson peat resulted in a lower yield strength representative of the shear strength of the peat without the contribution of the reinforcing effect of the fibres (Hendry et al. 2011b). This strength is referred to as the frictional strength and is hypothesised to be the interface angle of friction between the solid phases of the peat. The fitted failure envelope passing through origin show a ϕ'=31° (Figure 6.7b). From the conceptual model for the undrained behaviour of peat this represents a minimum value of strength for the peat. As the reinforced strength and the development of tension within fibres (apparent in the common pore pressure parameter) is similar for all three peats, the frictional strength of ϕ'=31° is assumed to be a good estimate for the frictional strength of the Anzac and Lévis peats (Hendry et al. 2011c).

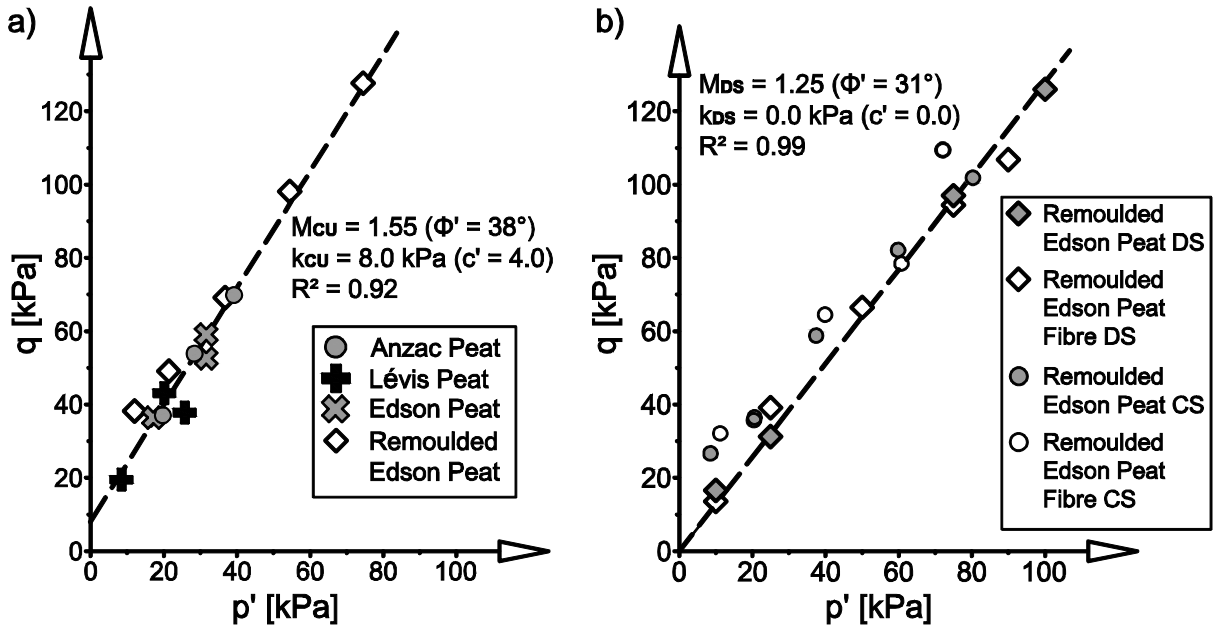

Figure 6.7 : Laboratory testing results for the (a) reinforced strength and (b) the frictional strength of the peat specimens from the study sites. (after Hendry et al. 2011b and Hendry et al. 2011c)

6.4 Instrumentation

The instrumentation installed at the Lévis site extended over a 200 m of the embankment as part of the investigation into the cause of the 2004 failure (Konrad et al. 2007; TSB 2008). At the Alberta sites, the instrumentation was installed a specific track locations to focus on the measurement of the response of the peat to heavy axle loads.

The instrumentation at the Edson site consisted of three strain-gauge piezometers installed under the centreline of the track (depths of 5.8 m, 4.7 m and 3.1 m); three extensometers installed approximately 0.4 m off the north end of the railway ties site with anchors installed at depths of 7.46 m, 5.46 m and 3.46 m; and the SAA installed approximately 0.4 m off the north end of the railway ties to a depth of 5.64 (Figure 6.8a) (Hendry et al. 2011a). The different depths of extensometer anchors allows for the isolation of the vertical deformations within the embankment, peat and underlying clayey silt. The head (top) of the extensometers were anchored within the ballast layer not to the ties as these been observed to move upwards between the axle loads independently of the surface of the embankment. The ShapeAccelArray (SAA) (Measurand Inc.) allowed for the measurement of the distribution of horizontal cyclic displacement with high accuracy and resolution with depth.

The instrumentation at the Anzac site consisted of four piezometers installed under the centreline of the track, at depths of 2.1 m, 3.1 m, 3.5 m and 4.5 m; an extensometer and a SAA installed 1.9 m from the centreline, both anchored well into the silty clay (depths of 7 m and 7.32 m respectively). Instrumentation was also added at the toe of the embankment to measure the distribution of strain and pore pressure generation away from the centreline of the track. This included two piezometers at depths of 4.2 m and 4.6 m at a distance of 3.9 m from the centreline and an extensometer and a SAA both 3.7 m from the centerline (Figure 6.8b).

The instrumentation at the Lévis site was distributed over a large area; however the data presented within this paper is from one cluster of instruments that has a similar configuration as the Alberta sites. This cluster of instruments consisted of four piezometers and a single potentiometer. The piezometers were installed under the centreline of the track at depths of 1.7, 3.0 and 3.5 m (Pz-1a, Pz-1 and Pz-1b) with a fourth piezometer installed 2 m from the centreline of the track at a depth of 3.0 m (Figure 6.8c). The response of the peat foundation during the passages of trains was measured at a rate of 100 Hz (Konrad et al. 2007).

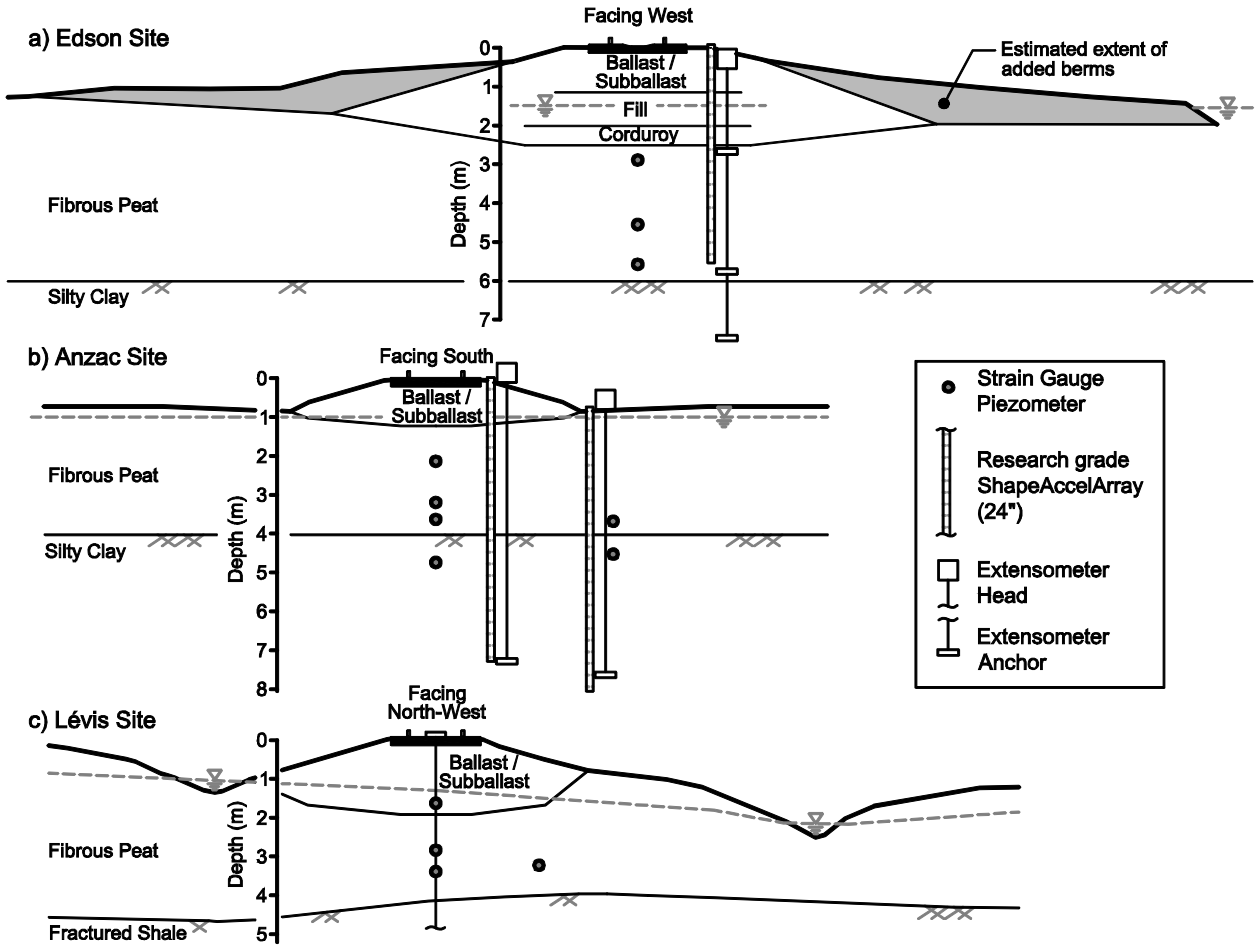

Figure 6.8 : Summary of stratigraphy embankment geometry and instrumentation installed at (a) the Edson site, (b) the Anzac site and (c) the Lévis site

6.5 Measured response of peat foundations

The following is a presentation of typical data sets collected during the passage of freight trains over the three instrumented sites. The data sets from the sites show similar measured responses to train load, with some difference in the distribution of strain and pore pressure response with depth.

6.5.1 Presentation of data

The mainline carries a range of weights and train configurations and consequently a range of measured responses were measured at the Edson site. The heaviest loads were carried in hopper cars full of grain in which axle loads are typically 283 kN (63,800 lbs). These measurements associated with these trains were selected for analyses due to the magnitude and consistency of their axle loads. Figure 6.9 shows an example set of extensometer and piezometer data for the

passage of a fully loaded grain car (92 rail cars) travelling at an average speed of 34.5 km/h (21.4 mph) on October 10, 2007. Horizontal cyclic displacements were measured by the SAA in directions defined relative to the track (Figure 6.10). Figure 6.11 presents the maximum cyclic horizontal displacement with depth as measured by the SAA and the maximum and minimum pore pressures with depth as measured by the piezometers.

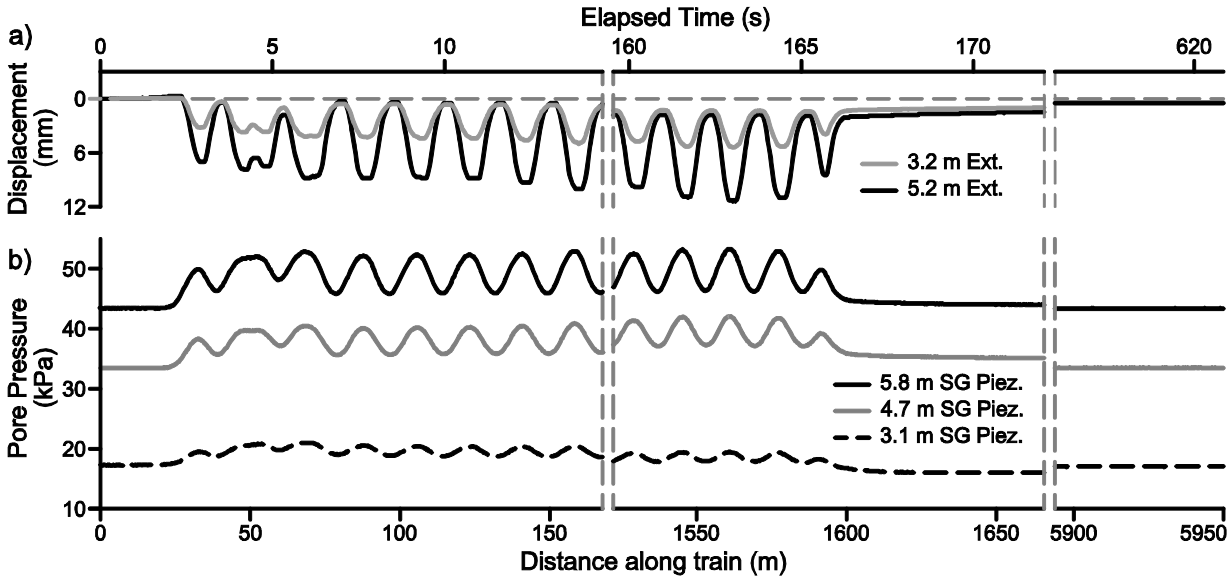

Figure 6.9 : Plot of (a) vertical displacement (extensometer) and (b) pore pressure (piezometer) data from the Edson site.

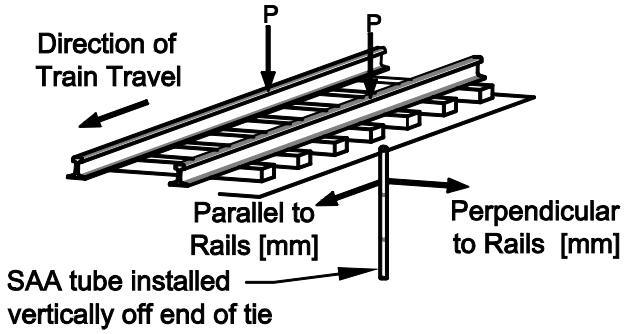

Figure 6.10: Directions of SAA measured displacements (Hendry et al. 2011a).

The data collected at the Anzac site is for a limited range of train types and configurations with most trains containing a mixture of car types and loads. Figure 6.12 shows extensometer and piezometer data sets for the passage of a mixed train of 57 cars containing two different car and axle loads travelling at an average speed of 10.1 km/h (6.28 mph) (October 22, 2010). The first type of car is a longer hopper car while the second type is a shorter tanker car. The mean axle load for both types of rail cars was approximately 260 kN. Figure 6.13 shows the cyclic

horizontal displacement with depth measured by the SAA near the end of the railway tie, and the maximum and minimum cyclic pore pressures with depth as measured by the piezometers below the centre line of the track. Figure 6.14 shows the cyclic horizontal displacement with depth measured by the SAA at the toe of the embankments, 3.25 m from the centreline of the track. The pore pressure generation at the toe of the embankment is not presented with depth as the change in the pore pressure is minimal at this location (Figure 6.14).

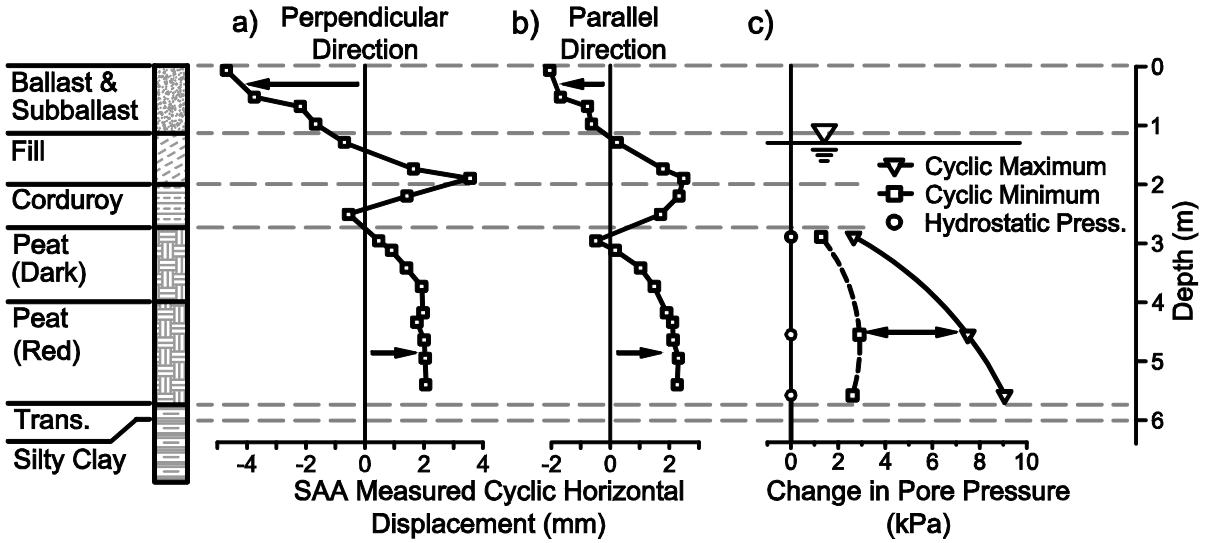

Figure 6.11: Plot of profiles of horizontal displacement (SAA data) (a) perpendicular to the track (b) parallel to the track and (c) cyclic pore-water pressure change with depth for the Edson site.

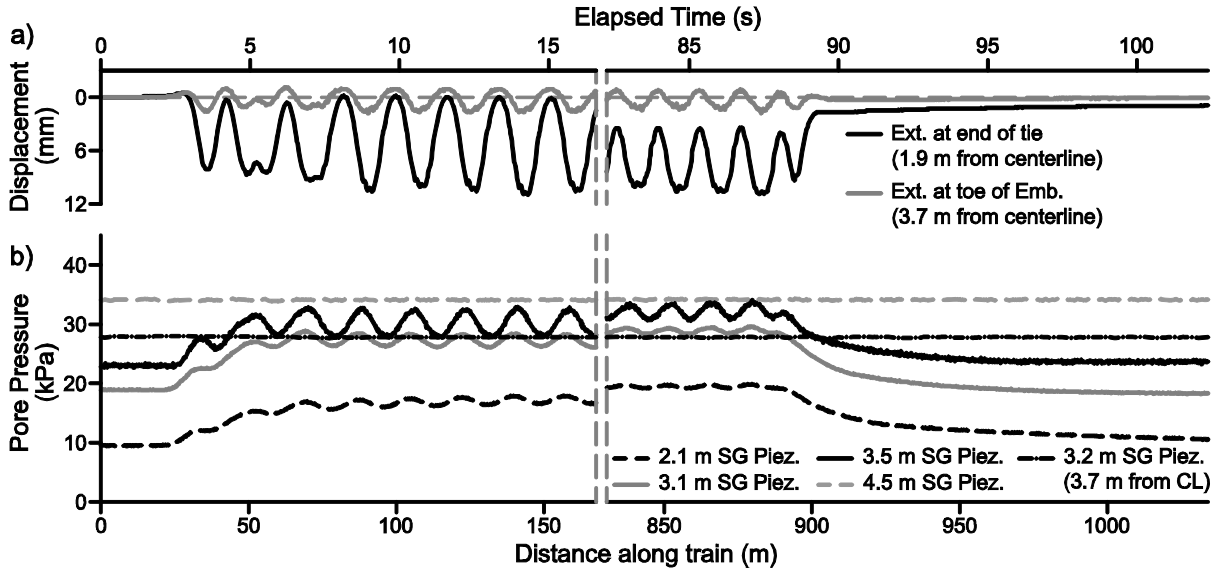

Figure 6.12: Plot of (a) vertical displacement (extensometer) and (b) pore pressure (piezometer) data from the Anzac site.

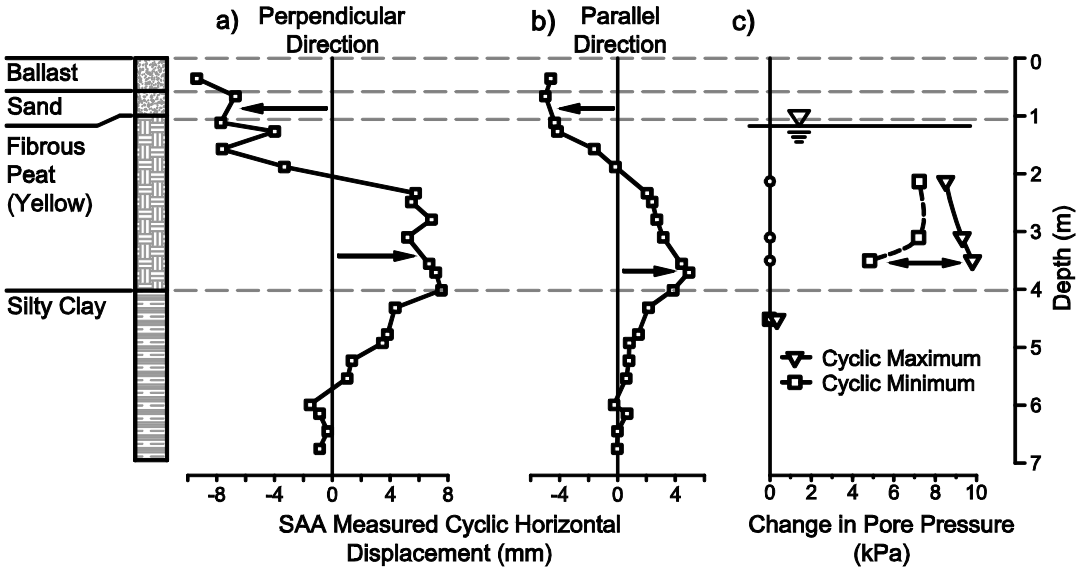

Figure 6.13: Plot of profiles of (a) perpendicular horizontal displacement (SAA data) (b) parallel horizontal displacement and (c) the pore-water pressure generation with depth from the Anzac site.

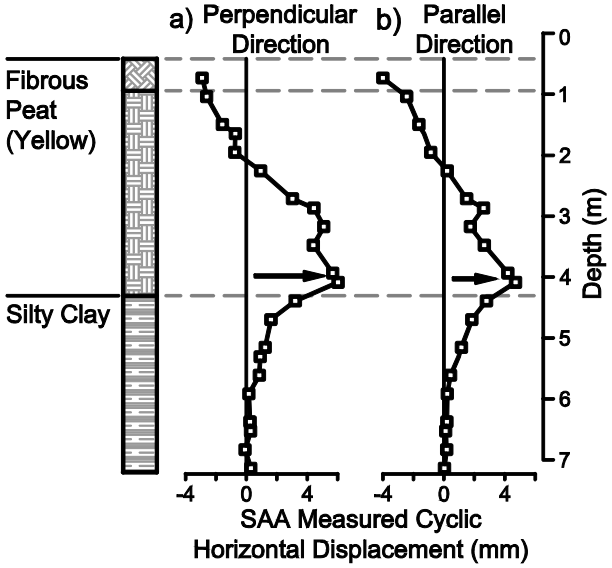

Figure 6.14: Plot of profiles from toe of embankment (3.6 m from the centreline of the track); (a) perpendicular horizontal displacement (SAA data) (b) parallel horizontal displacement and (c) the pore-water pressure generation with depth from the Anzac site.

The train cars passing over the Lévis site are only tanker cars as the rail line services a refinery. The tanker cars are all the same length and have consistent axle loads of approximately 318 kN (Konrad et al. 2007). The displacement and pore pressure response data set presented in Figure 6.15 is based on a composite of two data sets presented by Konrad et al. 2006 and Konrad et al.

2007. Figure 6.16 shows the measured maximum and minimum cyclic pore pressures plotted with depth for a train travelling 16 km/h (9.9 mph).

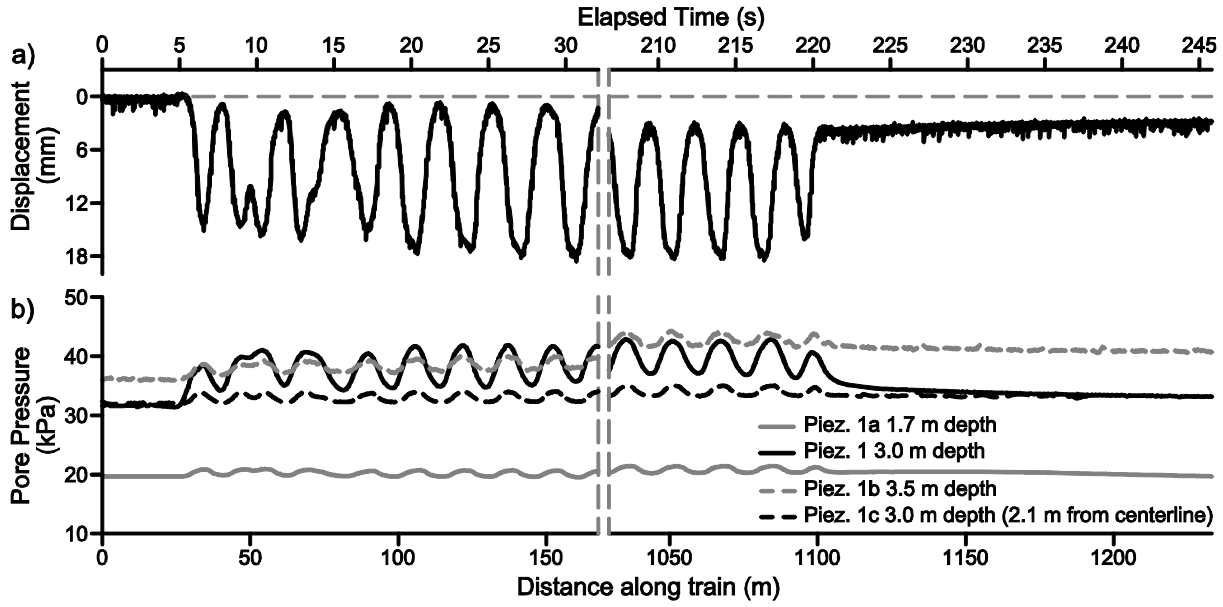

Figure 6.15: Plot of (a) vertical displacement (extensometer) and (b) pore pressure (piezometer) data from the Lévis site (after Konrad et al. 2007, Konrad 2007).

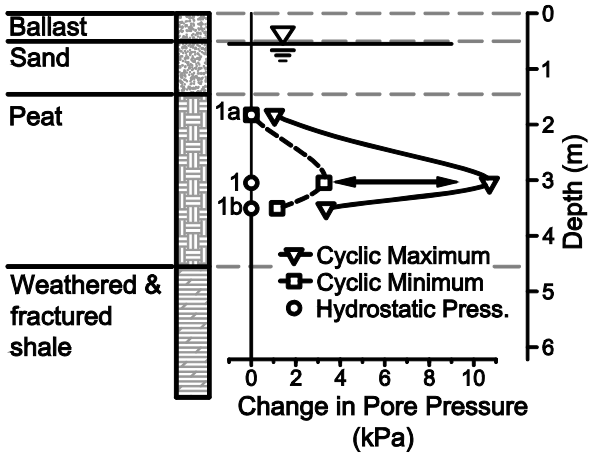

Figure 6.16: Profile of the change in pore pressure generation with depth from the Lévis site (after Konrad et al. 2007, Konrad 2007).

6.5.2 Measured vertical elastic displacement

The maximum vertical deformations at the Edson site were 11.3 mm, equivalent to an overall average vertical strain of 0.25%. A comparison between the deformations measured with the 5.2 m and 3.2 m deep extensometers show that up to 48% (5.4 mm) of the vertical deformation occurs within the soft embankment fill material. The magnitude of vertical deformation within

the soft embankment fill (48%) is likely contributing to the increased wear of track components and associated maintenance requirements. The deepest extensometer (7.46 m) ceased to work shortly after installation; however initial data sets showed that there the difference in the deformation measured by the 5.2 m and 7.46 m deep extensometers was negligible suggesting that vertical deformation within the silty clay was minimal. Thus, 52 % (5.9 mm) of the overall vertical deformation occurred within the peat, this corresponds to an average vertical strain of 0.19%.

The vertical deformations measured at the Anzac and Lévis sites reached maximums of 10.9 mm and 20 mm respectively. Assuming that this deformation occurred within the peat layer at both sites, the average vertical strain within the peat is approximately 0.36 % at the Anzac site and 0.67 % at the Lévis site. The vertical strain measured at the Lévis site is twice the magnitude measured at the Anzac site and almost three times the magnitude measured at the Edson site.

6.5.3 Measured cyclic pore pressure response

The peak pore pressure responses measured at all of the sites were coincident with the maximum displacement. The maximum change in pore pressure at the Edson and Anzac sites were 9.39 kPa and 9.8 kPa respectively and occurred near the base of the peat foundations. The magnitude of the generated excess pore pressure increased with depth at both sites (Figure 6.11 and Figure 6.13). At the Lévis site the maximum excess pore pressure was 10.7 kPa at was in the middle of the peat layer (Figure 6.16). These maximum values of excess pore pressure vary little between sites and are proportional to the applied axle loads.

The shallowest piezometer at the Edson site (3.1m in Figure 6.9b) shows a small decrease in pore pressure during passage of the train until the mean pore pressure during cyclic loading is equal to the preloading hydrostatic pore pressure. This is interpreted as an indication of drainage near the surface which enables pore pressure dissipation. This rate of drainage is slow relative to the duration of the axle loading cycle, suggesting that the cyclic response of the peat near the surface may still be considered undrained. The pore pressure measurements at the two other sites show no evidence of drainage.

The minimum cyclic pore pressures at all of the sites (Figures 6.9, 6.12, 6.15) are always greater than zero even though the vertical displacement measurements are nearly fully recovered

following passage of the wheel loads. This is due to the overlap in the volume of soil influenced by the axle loads at either end of the car which produces an increase in the change of mean total stress and a corresponding change in pore pressure generation. The variation of the rail car types at the Anzac site highlight the effect of axle spacing and car lengths on pore pressure response. The shorter tanker cars have closer trucks which result in greater minimum cyclic pore pressures (Figure 6.12).

6.5.4 Cyclic Horizontal Displacement

Both the Anzac and Edson site had SAAs installed to measure the horizontal cyclic deformation with depth. These are unique data sets which provide high resolution and high accuracy profiles of horizontal displacement with depth during train loading. These measurements show that the peat foundations spread laterally as well as deforming vertically, indicative of an undrained cyclic response. The embankment materials appear to be rotating inwards with the formation of a deflection bowl on the surface of the peat as described by Hendry et al. (2011a). At the Edson site the maximum cyclic horizontal displacement was measured to be 2 mm (a horizontal strain of approximately 0.12 %) near the base of the peat. The effect of the corduroy is evident as there is very little horizontal deformation at the depth at which the SAA passes through the corduroy. There is a similar pattern of displacement at the Anzac site but without the influence of the corduroy. At the Anzac site the maximum measured horizontal displacement near the base of the peat layer was 6.68 mm (a horizontal strain of approximately 0.35%).

A comparison of the cyclic horizontal displacements in the perpendicular direction to that in the parallel direction provides insight into the effect of the embankment structure and geometry in the distribution of the stress and strain. For a simple embankment configuration, as found at the Anzac site, the rail acts to spread the load along the length of the embankment. The effects of this are evident at in the cyclic horizontal displacements measured at the Anzac site as the displacements in the perpendicular direction are almost twice the magnitude of those in the parallel direction. The effect of the corduroy in the Edson embankment is evident as the measured horizontal cyclic displacements in the perpendicular and parallel are very similar in shape and magnitude. This shows that the corduroy has a similar effect as the rail in spreading the load, but perpendicular to the embankment.

A comparison of the variation of the horizontal cyclic displacements measured near the track and at the toe of the Anzac embankment provides an indication of the spatial distribution of strain. The shape and magnitude of the horizontal cyclic displacements measured near the track and the toe were similar within the peat. Based on the difference in the displacement measured by the two SAAs and the distance between them, the average horizontal strain is estimated at approximately 0.09% near the base of the peat. The shear strain with depth was calculated from the cyclic displacements from the two SAAs data by dividing the magnitude of the cyclic displacement by the distance between the MEMS accelerometers. A comparison of the two SAAs at the Anzac site shows that the shear strain profile with depth is constant over the 2.1 m between the edge of the track and toe of the embankment.

At both the sites there is evidence of a zone of high shear at the interface between the peat and the stiffer underlying silty clay. This was not measured directly at the Edson site; however, the large cyclic displacement of the deepest SAA segment (Figure 6.11) combined with the extensometer measurements showing negligible vertical strain within the silty clay suggests that there is a zone of significant shear at or near the interface between the peat and the underlying silty clay (Hendry et al. 2011a). The change in the cyclic horizontal displacement measured at the base of the peat at the Anzac site shows a zone of higher shear at the interface between the peat and the underlying silty clay, though this may be smoothed by the rigidity of the PVC tube in which the SAA is installed. Visual inspection of Shelby tube samples taken across the interface between the peat and silty clay were undertaken at the two sites. The two Shelby tube samples from the Edson site broke and crumbled at the location of a 10 to 15 cm thick layer of soft and weak transition material (Figure 6.17). This layer contained small smooth shells identified as bivalves and gastropods commonly found in fresh water streams and in standing water in Alberta. Triaxial testing of remoulded specimens of this transitional material measured frictional angles (ϕ') of 23° and a very low elastic modulus (approximately 1.0 MPa). The inspection of a single Shelby tube sample taken across the peat and silty clay interface at the Anzac site showed a clean interface with coarse peat directly on the silty clay surface.

6.5.5 Recovery of Embankment and Structure

The measured vertical displacements at the Edson and Anzac sites showed a similar trend of increasing in the displacement during the passage of the train. After the passage of each train a

residual deformation is apparent. This deformation was 1.2 mm at the Edson site of which 66 % occurred with the embankment. At the Anzac site the residual deformation was 1.4 mm while at the Lévis site it was greater than 1 mm. Continuous measurements at the Edson site show that after 10 minutes the vertical deformation of the embankment and peat foundation had fully recovered and the excess pore pressure had dissipated. The Anzac site also showed an almost complete recovery of the residual deformation and dissipation of the pore pressure 15 seconds after the passage of the train with full recovery by the time the next set of readings were taken three hours later.

Figure 6.17: Pictures of the peat and silty clay interface and possible shear zone from Shelby tube sample taken at the under the centreline of the rail embankment at the Edson site.

6.5.6 Effect of train speed

The effect of train speed on the magnitude of strains and excess pore pressure has been studied at the Lévis site for speeds of up to 25 km/h. Over this range there was very little change in vertical displacement though there was an increase of excess pore pressure generated with increasing speed (Konrad et al. 2007). An extrapolation of this pore pressure showed the potential for a large increase in pore pressure at higher speeds. The results of increased train speed have been shown to have little effect on the magnitude of measured deformations (Hendry et al. 2006; Konrad et al. 2007; Hendry et al. 2010). This was confirmed at the Edson site with a comparison of twelve unit trains of grain cars with consistent axle loads and varying train speeds.

6.6 Analysis of stresses and strength under train loading

Interpretation of the measured responses at the three study sites in the context of the conceptual model of undrained peat response developed by Hendry et al. (2011c) will be undertaken in two ways. Numerical modelling of the stress field within the embankment and foundation is utilized to identify the orientation of the principal stresses within the peat and zones in which plastic strains are likely to develop. Applying the complex conceptual model for the behaviour of peat within finite element code requires further development; however it is assumed that modelling the soil as isotropic and elastic perfectly plastic will provide sufficient insight for the purposes of this interpretation. The stresses generated beneath the embankment are also calculated from the modelled (unloaded) *in situ* stresses and the effective stress path as determined from the measured response. A comparison between the resulting stress state and the yield surface provides a good measure how close the peat foundation is to failure at the locations at which the measurements were taken.

6.6.1 Application of Conceptual Model of Peat

Applying the conceptual model for the undrained behaviour of peat developed by Hendry et al. (2011c) material model to the peat which comprises the embankment foundation material requires an understanding of the orientation of the principal stresses and strains beneath moving axle loads. This has been presented in Lekarp et al. (1998) and Wong et al. (2006) and is summarized in Figure 6.18. Figure 6.18 shows the resulting orientation and magnitude of the principal stresses resulting from the applied axle loads spatially both along the length of the embankment and perpendicular to the embankment. The major principal stress directly under the axle loads is vertical and coincides with the maximum value of stress carried by the soil. With increasing distance from the applied load the principal stresses rotate to the extreme case where the major principal stress lies within the horizontal plane.

6.6.2 Finite Element Modelling

The finite element modelling software SIGMA/w (GeoSlope 2007) was used to determine locations within the peat foundations that may experience plastic deformations. The initial *in situ* stresses were calculated using the total density of the soils and an assumed pore pressure distribution. The geometry was determined from surveys and the stratigraphy developed from the

site investigation. A linear elastic modulus of 2.0 MPa was used for the peat. The boundary conditions at the base of the peat layers were fixed to reflect the presence of stiffer underlying material. Structures such as the ties and the corduroy at the Edson site were modelled with beam elements. A Winkler model of the displacements from the measured axle loads was used to estimate the maximum load distributed to the surface of the embankment from the rail track structure (Hendry 2007; Hendry et al. 2010). This distributed surface stress to the surface of the embankment was 43 kPa. The strength parameters used for the peat foundation were varied, ranging from a low value representative of the peat frictional strength to a high value which reflects the effect of peat fibre reinforcement. It is important to note that although the model is useful in simulating the stress distribution it was unable to replicate the measured pore pressure response.

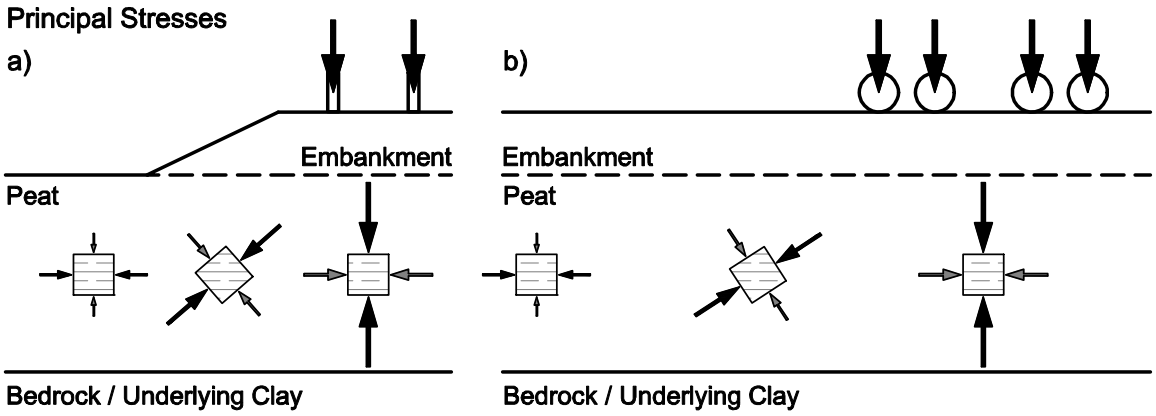

Figure 6.18: Spatial distribution of the principal stresses in (a) the cross sectional plane of the embankment and (b) in a plane parallel to the embankment with respect to the predominant fibre orientation.

For the nearly symmetrical Edson and Anzac embankments, the highest deviatoric stresses simulated with the model are concentrated beneath the embankment where the major principal stress is near vertical, corresponding to the maximum effective fibre reinforced strength (ϕ' =38°). From the application of the different ϕ' the area directly beneath these embankments is most susceptible to plastic deformation. Figure 6.19a shows the locations of the simulated plastic yielding for the Anzac embankment at different ϕ' values. The model for the Edson site showed very similar distributions of stress beneath the embankment, however yielding of the peat did not occur beneath the Edson embankment for the assumed range of strength parameters.

Figure 6.19a illustrates the potential for plastic deformation to occur at the interface between the peat and the stiffer underlying silty clay. The SAA measurements from Edson site and the Anzac site also indicate zones of high shear strain at this interface. The major principal stresses at this location are rotated approximately 48° from vertical which would reduce the stiffness and strength of the peat mobilized by the peat fibres.

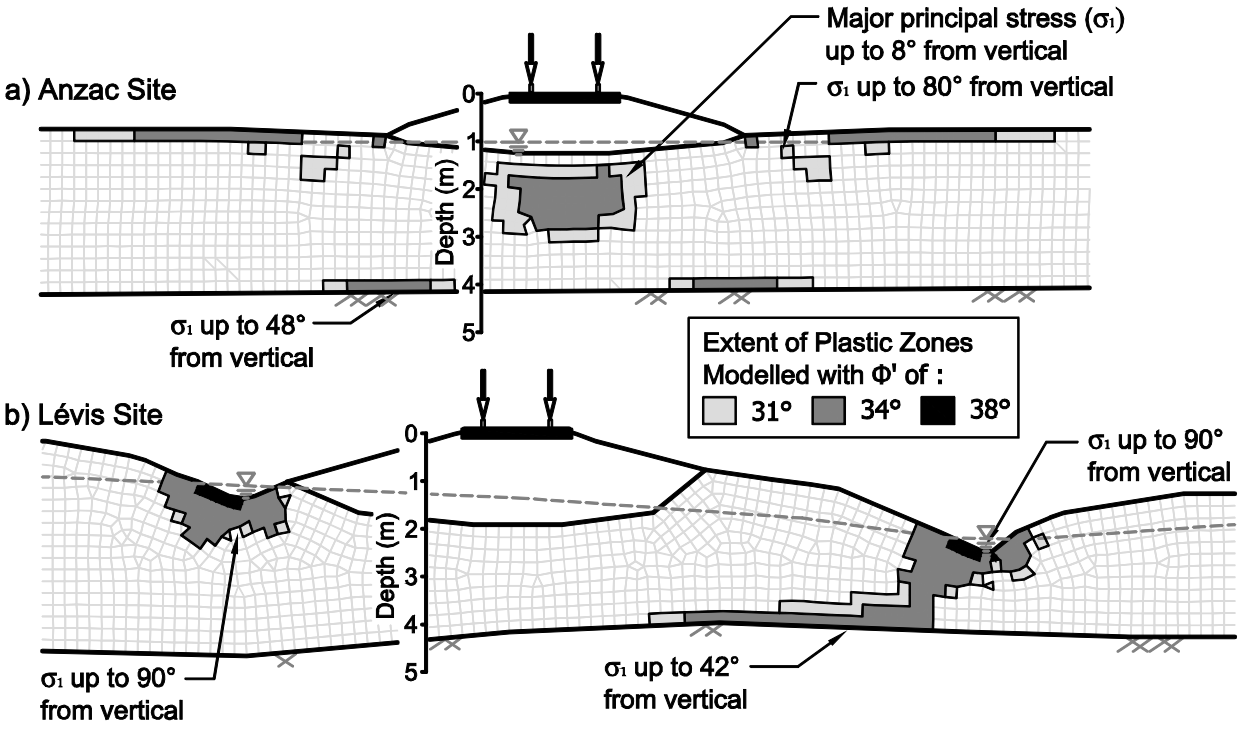

Figure 6.19 : Spatial distribution of plastic zones which are modelled to develop under train loading at (a) the Anzac site and (b) the Lévis site with the peat model simplified to isotropic.

To explore the effect of the very soft transition material found beneath the peat layer at the Edson site the and the high shear stresses at the this interface the lower boundary condition was allowed to move freely in the horizontal direction. The result of this change in boundary condition was an increase in the magnitude of the deviatoric stresses and a reduction of the mean total stress beneath the embankment. Due to the width and gradual slope of the embankment at the Edson site the modelled change in deviatoric stress was still not enough to simulate plastic yielding.

The modelled distribution of the deviatoric stress generated within the peat foundation at the Lévis site was similar to that at the other sites, the differences in the surface geometry and the resulting mean effective stresses resulted in a different distribution of plastic strains. The ditches

on either site of the embankment create the potential for large plastic strains, especially the north –east ditch constructed since the 1999 failure. These locations also correspond to a rotation of the major principal stresses into the horizontal plane causing the peat to reach its softest and weakest state. The interaction between the soft peat and the stiffer underlying material (shale) develops a concentration of shear stresses which also results in the potential for plastic yielding. This distribution of modelled yielding may be a strong indicator of the mechanism of failure of this embankment in 2004.

Even though the model is not able to directly incorporate the anisotropic constitutive model developed previously for the peat the model results do provide three useful insights into the behaviour at these three sites. First, the major deviatoric stresses are concentrated beneath the centreline of the embankment; this suggests that for symmetrical embankment structures this is the key location at which to monitor the peat. Second, large changes in geometry near an embankment, such as digging ditches and placing berms, may result in changes in the stress state of the peat which may lead to a greater potential for yielding of the peat foundation. Finally, the interface between the soft peat and the stiffer underlying material may generate concentrations of shear stress which result in the large shear strains measured with the SAAs at the Edson and Anzac sites.

6.6.3 Stresses and strength from measured *in situ* response

The orientation of principal stresses and strains with respect to the fibre orientation directly beneath the axle loads is the same as those that occur in CU laboratory tests, with the major principal (axial) stress is perpendicular to the horizontal plane of the fibres (Hendry et al 2011a and Hendry et al. 2011b). The magnitude and distribution of stresses directly under the axle loads can be estimated from the measured *in situ* strain and pore pressure response and the laboratory measured response. The calculation is presented graphically in Figure 6.20. The deviatoric and mean effective stresses (p'_0 and q_0) at each site under the embankment were modelled using finite element software based on the geometry of the embankments and the density of the materials. The effective stress paths (ESP) within the peat during application of the axle loads at all three sites were assumed to follow that of the undrained effective stress path determined in the laboratory as defined by a pore pressure parameter *a* of 0.3. The magnitude of the change in pore pressure (Δu) generated directly below the axle loading was based on the field

measurements. The distribution of horizontal strain was determined from the SAA horizontal displacements and an assumption of undrained loading. The change in deviatoric stress (Δq) was then determined from these strains and an assumed modulus of 2.0 MPa (Hendry et al. 2011c). The total stress path (TSP) and the change in mean total stress (Δp) can be estimated from the known stress path (Δq and Δu) (Figure 6.20). These changes in stress and pore pressure generation are plotted for the Edson and Anzac in Figure 6.21.

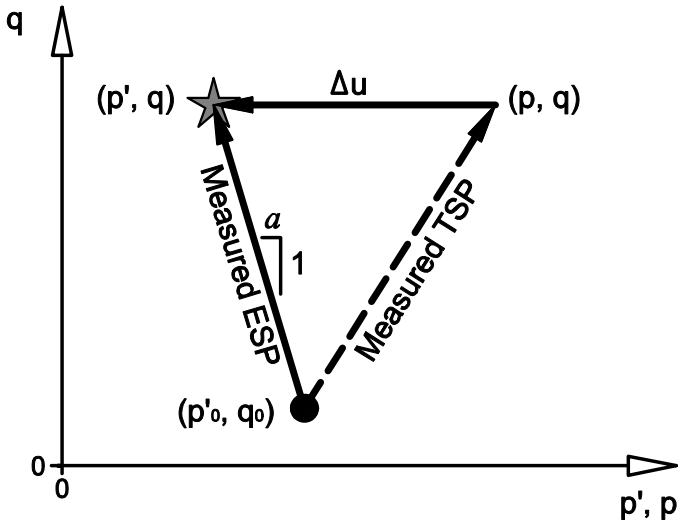

Figure 6.20 : Plot of the calculation of the effective stress path from the measured in situ response and the undrained laboratory response.

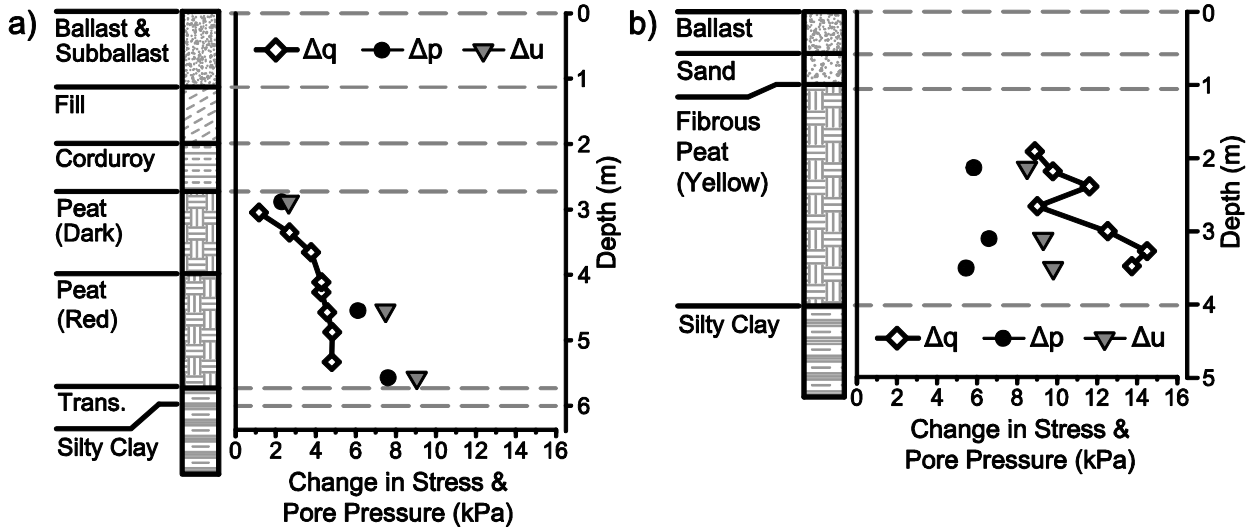

Figure 6.21 : The *in situ* change in stresses due to heavy axle loads calculated from the field and laboratory data for (a) the Edson site and (b) the Anzac site.

There were no horizontal displacement measurements at the Lévis site to calculate the distribution of strain. For the Lévis site the stress state can be estimated from the measured

excess pore pressure and the vertical displacement. The embankment construction at the Anzac and Lévis sites are similar though the magnitude of vertical strain at the Lévis site is double. Estimating the maximum strain within the embankment as twice that found beneath the Anzac site results in a maximum strain of 1.4%. For a generated pore pressure of 10.7 kPa (as measured) or less the laboratory defined effective stress path would require a *negative* change in horizontal total stresses. Thus, the *maximum* possible strains were limited to 0.84% which corresponds to a generated pore pressure (Δp) of 5.66 kPa and deviatoric stress (Δq) of 43.8 kPa with an assumed zero change in horizontal stresses.

The result of the heavy train axle loads on peat foundation is strongly influenced by the structure of the embankment. At the Edson site the increase in stress is predominantly an increase in Δp, and the component of Δu due to shear stress is 16%. At the Anzac site there is a similar increase in Δp as at the Edson site however the Δq was much higher. The component of Δu due to the shear stress is also higher at 35%. The higher strains at the Lévis site result in a higher estimation of Δq (28 kPa), with the component of Δu due to the shear stress at 78%.

These estimates can be used to evaluate the proximity of the *in situ* stress to yielding, even without defining a failure mechanism. This will be quantified by comparing the ratio the mobilized shear stress to the strength of the material. The stress mobilization factor (SM) is defined as the ratio of the change in deviatoric stress (Δq) due to loading to the change in deviatoric stress which would result in yielding (Equation 5.3). The change in deviatoric stress (Δq) resulting from train loading can be determined from the effective stress path of the peat and in situ measurements (Figure 6.21). The change in deviatoric stress which would result in yielding is estimated from the intersection of the stress path with the yield surface (Δq_{yield}) (Figure 6.22).

$$SM = \Delta q \Big/ \Delta q_{yield} \qquad (5.3)$$

The SM for all three sites calculated using the maximum fibre reinforced yield surface is plotted with depth in Figure 6.23. The estimated maximum SM is 15%, 43 % and 51 % for the Edson, Anzac and Lévis sites respectively. The much lower SM value for the Edson site is attributed to the impact of the corduroy construction in spreading the load and reducing the intensity of the deviatoric stress under the embankment. If the SM for the three sites were calculated using the

frictional strength the maximum SM would be 23%, 46% and 78% for the Edson, Anzac and Lévis sites respectively.

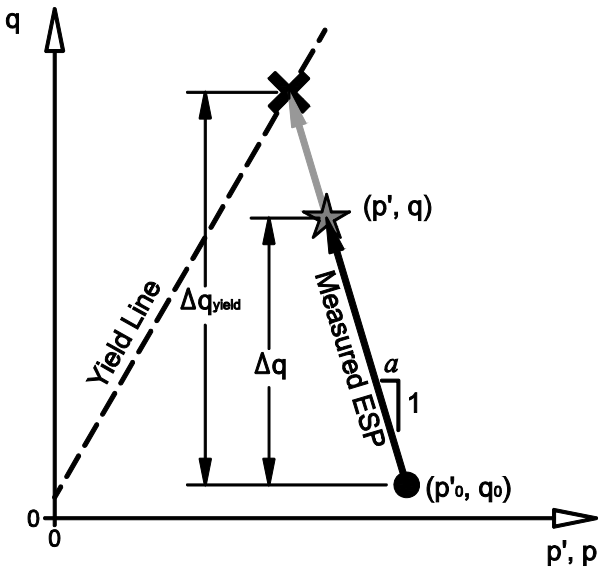

Figure 6.22 : Graphical depiction of parameters used in the calculations for Stress Mobilisation factor.

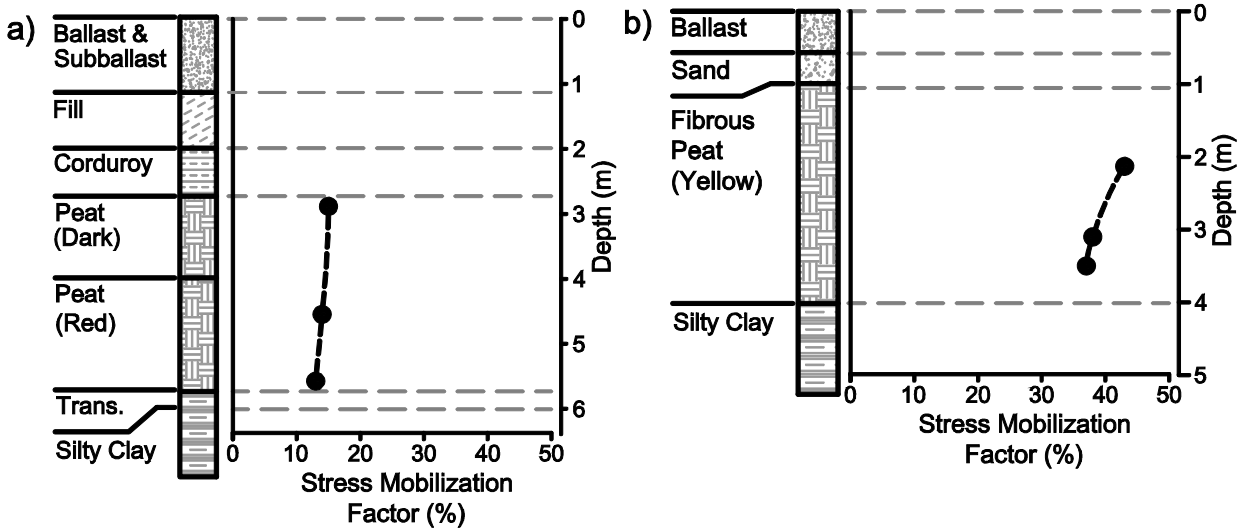

Figure 6.23 : The Stress Mobilization Factor (SM*)* due to in situ stresses under heavy axle loads for (a) the Edson site and (b) the Anzac site.

6.7 Conclusions

Several conclusions can be drawn as to the effect of heavy axle loads on the response of a peat foundation, specifically as it pertains to the generation and dissipation of excess pore pressure, and the spatial distribution of strain and strength of the structures.

The peak pore pressures in a peat foundation were found to be coincident with the passing of the heavy axle loads. The magnitude of the peak cyclic pore pressure was constant under repeated applications of axle loads indicating an undrained response. The exception to the constant magnitude and peak pore pressure is from the measurement taken just below the base of the embankment at the Edson site. These measurements show a decrease in pore pressure due to drainage. However, the rate of this drainage is slow relative to the duration of the axle loading cycle and thus the peat response is approximated as undrained. The measured residual pore pressure following train passage was small indicating that the response of the peat is predominantly elastic, undrained and recoverable. This predominantly elastic behaviour was confirmed by the vertical displacement measurements which also showed the recovery of the embankment.

The distributions of cyclic pore pressures were not consistent with depth. At the Edson and Anzac sites there was an increase in pore pressure with depth which corresponded to a similar distribution of measured cyclic horizontal displacement. At the Lévis site, the greatest increase in pore pressure was near the middle of the peat layer. The lower pore pressure generation at the toe of the Anzac embankment shows a reduction in the change in mean total stress due to the horizontal stiffness of the peat being very low. The small magnitude of the pore pressure generation despite the large magnitude of shear stress demonstrates that there is minimal shear induced pore pressure near the toe of the embankment due to the near horizontal orientation of the major principal stress at this location.

The effect of the construction of the embankment structures is apparent in the relative magnitudes of the horizontal displacements in the perpendicular direction versus the parallel direction and in the magnitude and type of stresses. The effect of the rail to spread the load along the length of the embankment and confine the foundation soil in that direction is apparent in the horizontal cyclic displacement at the Anzac site; where the displacements in the perpendicular direction are twice that in the parallel direction. The effect of the corduroy at the base of the Edson embankment is evident as the horizontal cyclic displacements in both directions are very similar in shape and magnitude, due to the corduroy spreading the load perpendicular to the embankment. The corduroy construction results in a reduction in the magnitude of shear stresses

developed under train loading and a decrease in the ratio of deviatoric to mean total stress due to the distance over which the load is spread.

The distribution of plastic strains within the foundation was simulated for all three sites and was interpreted based on measurements of pore pressure and shear strain obtained from each site. The deviatoric stresses were modelled to be concentrated beneath the centreline of the embankment for symmetrical embankments and terrain. Thus, the calculated stress mobilization factors beneath the embankments at the Edson and Anzac sites, based on the measured response of the peat beneath the centreline of the embankment are good estimates of the stability of the structures. The stress mobilization factors of 15 % at the Edson site and 43 % at the Anzac sites show the strength of the peats exceeds the stresses developed due to the train loading. The simulated plastic yielding at the Lévis site does not occur beneath the embankment, and the stress mobilization factor is not a good estimate of the stability of the embankment.

The result of the interaction between the soft peat and the stiffer underlying material is apparent in the concentration of shear stresses at this interface in the simulations and the horizontal displacements measured with the SAA. The low modulus of the peat results in large areas of peat being affected by the shear stresses resulting from train loading. This distribution is visible in the SAA measurements at the toe of the embankment at Anzac site which showed very similar results as those measured near the track.

From the modelling of plastic yielding at the Lévis site the extent of the plastic zone is a result of two factors. First, the north-east ditch acts to further concentrate the shear stresses at the interface between the soft peat and the fractured shale. Second, this concentration of shear stresses is at a location at which the principal stress orientation corresponds to a reduced strength of peat. From observations of yielding peat specimens in the laboratory, over stressing of the peat within these peats foundation would take the form of plastic shearing over a large volume this could result in a progressive settlement and failure beneath a railway embankment.

Further development of a constitutive model and modelling methods need to be developed so that the full dimensionality of stress and pore-pressure response with peat foundations as a result of rail loading can be characterized. These models can then be used to evaluate failure mechanisms and further explore the potential impact of alternative methods of remediation.

6.8 Acknowledgements

The writers would like to acknowledge the contribution of Canadian National Railways for providing both the project and funding. The authors also thank Tom Edwards for his support of this project. This research was made possible through the Railway Ground Hazard Research Program, funded by the Natural Sciences and Engineering Research Council of Canada (NSERC), CP Rail, CN, and Transport Canada.

6.9 References

GeoSlope International, Ltd. (GeoSlope) (2007). GeoStudio 2007: SIGMA/w (Version 7.17) [Computer software]. Calgary, Alberta, Canada. Available from http://www.geo-slope.com/

Graham, J. and Houlsby, G.T. (1983) "Elastic Anisotropy of a Natural Clay", Géotechnique, 33, No. 2: 165-180

Hall, L. 2003. Simulations and analyses of train-induced ground vibrations in finite element models. Soil Dynamics and Earthquake Engineering, 23: 403-413.

Hendry, M. 2007. Measurement and Analysis of the Train-induced Dynamic Response of Railway Track and Embankments Constructed over Soft Peaty Foundations. MSc. Thesis, University of Saskatchewan, Saskatoon.

Hendry, M., Martin, C.D., Barbour, S.L., and Edwards, T. 2008. Monitoring cyclic strain below a railway embankment overlying a peaty foundation using novel instrumentation. In 61st Canadian Geotechnical Conference, Edmonton, Alberta, Canada.

Hendry, M., Hughes, D., Barbour, L. 2010. Track displacement and energy loss in a railway embankment. Proceeding of the Institution of Civil Engineers Geotechnical Engineering Vol. 162 n.1 pp. 3-12

Hendry, M.T., Barbour, S. and Martin, C.D. 2011a. An evaluation of real-time deformation monitoring using motion capture instrumentation and its application in monitoring railway foundations, Geotechnical Testing Journal, **34**(6), 1-11.

Hendry, M., Sharma, J., Martin, D., Barbour, L., 2011b. Laboratory investigation of the fibre content and in situ structure on the anisotropic strength and stiffness of fibrous peats. ***Submitted to Canadian Geotechnical Journal.***

Hendry, M., Barbour, L., Martin, D., 2011c. The variability and net effect of the stiffness and strength derived from the fibrous nature of peat. ***To be submitted to Journal of Geotechnical and Geoenviromental Engineering.***

Hobbs, N.B. 1986. Mire Morphology and the Properties and Behaviour of some British and Foreign Peats. Quarterly Journal of Engineering Geology, 19: 7-80.

Konrad, J.-M., Grenier, S., and Garnier, P. 2007. Influence of Repeated Heavy Axle Loading on Peat Bearing Capacity. In 60th Canadian Geotechnical Conference. Ottawa, pp. 1551-1558.

Konrad, J-M. ., Grenier, S., and Garnier, P.2006. Heavy Axle Load over Muskeg Déraillement de l'Ultratrain a St-Henri-de-Lévis. Presentation at the Railway Ground Hazard Research Program annual workshop, Kingston, Ontario.

Kumar, A., Wailia, B.S. and Mohan, J. 2006. Compressive strength of fiber reinforced highly compressible clay. Construction and Building Materials, 20: 1063-1068.

Landva, A.O. and Pheeney, P.E. 1980. Peat fabric and structure. Canadian Geotechnical Journal, **17**: 416-435.

Lekarp, F., and Dawson, A. 1998. Modelling permanent deformation behaviour of unbound granular materials. Construction and Building Materials, 12(1): 9-18.

Lester, G. 2005. *Atlas of Alberta Railways*. University of Alberta Press, Edmonton, Canada. Available on-line at http://railways.library.ualberta.ca/ [Accessed January 27, 2011]

Li, J. and Ding, D.W. 2002, Nonlinear elastic behaviour of fiber-reinforced soil under cyclic loading. Soil dynamics and earthquake engineering, 22: 977-983.

MacFarlane, I.C. 1969. Muskeg Engineering Handbook. University of Toronto Press, Toronto.

Madshus, C. 2001. Modelling, Monitoring and controlling the behaviour of Embankments Under High Speed Train Loads. In Geotechnics for Roads, Rail Tracks and Earth Structures: Outcome of ETC (European Technical Committee No.11). Edited by A.G. Correia and H. Brandl. January, 2001. Taylor & Francis, pp. 225-238.

Mesri, G. and Ajlouni, M. 2007. Engineering properties of fibrous peats. ASCE Journal of Geotechnical and Geoenvironmental Engineering, 133(7): 850-866.

Michalowski, R. L., and Čermák, J., 2002. Strength anisotropy of fiber-reinforced sand. Computers and Geotechnics, 29: 279-299

The Transportation Safety Board of Canada (TSB), 1999. Railway Investigation Report R99Q0019.

The Transportation Safety Board of Canada (TSB), 2008. Railway Investigation Report R04Q0040. Cat. No. TU3-6/04-2E, ISBN 978-0-662-47573-6

Wong, R.C.K., Thomson, P.R., and Choi, E.S.C. 2006. In Situ Pore Pressure Responses of Native Peat and Soil under Train Load: A Case Study. Journal of Geotechnical and Geoenviromental Engineering, 132(10): 1360-1369.

Wood, D.M. 2004. Soil Behaviour and Critical State Soil Mechanics. Cambridge University Press

Yamaguchi, H., Ohira, Y., Kogure, K. and Shigeru, M. 1985. Undrained shear characteristics of normally consolidated peat under triaxial compression and extension conditions. Soil and Foundations, 25(3):1-18.

Chapter Seven: Conclusions & Recommendations

7.1 General Conclusions

The Canadian railways have always experienced problems with embankments built over peat foundations. More recently, the performance of these structures has become a critical concern due to recent failures on the Lévis subdivision in southern Quebec and CN's acquisition of northern railways with large stretches of peat crossings. This thesis is a component of a recent research program focussed on effect of heavy axle loads on peat foundations which began following the Transportation Safety Board investigation into the catastrophic failure at the Lévis subdivision (TSB 2008). That investigation highlighted our limited understanding of the response of peat foundations to heavy axle loads. This has generated concerns that increasing traffic and axle loads on the railway network may result wide spread problems with peat foundation failures.

The global objectives of the research presented in this thesis were as follows: to develop an understanding of the mechanisms that govern the spatial and temporal distribution of stress, strain and pore pressure within the cyclically loaded peat foundation of a railway embankment; and to determine the implications of these mechanisms on the strength and stability of these structures. Three areas of study were required to address these objectives: the unique elastic behaviour and yield characteristics of peat had to defined; a comprehensive set of pore pressure and displacement measurements under cyclic loading had to obtained from multiple study sites; and finally, a conceptual model for the behaviour of peat foundation subjected to cyclic heavy axle load loading had to be developed to explain the measured responses of the peat from the study sites.

7.1.1 Yield Characteristics and Elastic Response of Peat

Laboratory testing was used to establish that the properties of peat are governed by the combination of fibre reinforcement and its matrix properties. The composition of the peat investigated in these studies was composed predominantly of organic fibres (Chapter 4 & 5, Manuscript # 2 & 3) which develop tension with expansive strains. This tension acts to reinforce the peat increasing both its strength and stiffness. The peat fibres are oriented predominantly in a horizontal plane as a result of deposition and the large vertical strains experienced during the consolidation following fibre deposition. This horizontal fibre alignment results in the cross-anisotropic strength and stiffness properties of peat.

The strength can be divided into two components: the first component is the interphase friction between the solid phases of the fibres and particles which compose peat; and the second is the tension in the fibres and the resulting reinforcement of the peat. The sum of these components is the effective fibre reinforced strength (Chapter 4, Manuscript #2). The frictional strength is a fundamental property of the surfaces of the fibres and particles; whereas the fibre reinforcement component is dependent on the fibre content, fibre length and fibre orientation with respect to the principal stresses. Thus, the cross-anisotropic nature of the strength properties is derived from the fibre reinforcement component. The yielding of peat was found to not occur in the same manner as soft mineral soils such as clays, as failure planes do not form in peat. In CU tests it continued to deform plastically even at very high (>20%) axial strains while in direct shear tests the specimens appeared to tear throughout the whole specimen (Chapter 4, Manuscript #2).

The cross-anisotropic stiffness of the peat occurs as a result of the tensile stresses generated within the horizontally oriented fibres. This causes the peat to behave several times stiffer in the horizontal direction than in the vertical direction. This stiffness cross-anisotropy is only apparent when the fibres are in tension and thus does not occur during compression. The impact of this stiffness cross-anisotropy is an increase in the pore pressure response during loading as a shear induced component of pore pressure develops that is a function of the orientation of the fibres with respect to the principal stresses (Chapter 5, Manuscript #3).

The resulting characteristics of the fibre reinforcement have contradictory effects on the undrained strength of the material. The shear induced pore pressures generated during undrained loading result in a reduction of the undrained strength while the reinforcing effect of the fibres

increases the effective strength. A comparison of strength developed within a hypothetical peat without fibres and one with horizontally oriented fibres found that the mobilized strength was dependent on the initial preconsolidation pressure and deviatoric stress. Initial stress paths for which the net effect of fibre reinforcement may be detrimental to strength occurred at high preconsolidation pressures with low initial deviatoric stress. These stress states would not apply to the embankment structures peat foundations at the sites investigated (Chapter 5, Manuscript #3).

7.1.2 Observed Response of Peat under Railway Embankments

An instrumentation system was designed and installed to obtain detailed observations of the distribution of pore pressure and strain within the peat foundations under the railway embankments during heavy axle loading. The innovation in this instrumentation was the addition of the SAAs which provided an accurate high resolution measurement of the temporal and spatial distribution of displacement (Chapter 3, Manuscript #1). The instrumentation provided a clear picture of the effects of cyclic loading, embankment construction, soil profile and peat fibre reinforcement on displacement and pore pressure.

The vertical displacements and pore pressure generation measured during this study (Chapter 6, Manuscript #4) show increases in magnitude due to a visco-elastic response, not due to the generation of excess cyclic pore pressure or a dynamic response (Chapter 2). The behaviour of the peat foundation was observed to be predominantly elastic, undrained and recoverable based on the observations of recovery of the vertical displacements, horizontal displacements and pore pressure after each train load. The cyclic pore pressures and strain at both the Edson and Anzac sites increased with depth to the base of the peat layer.

The effect of the construction of the embankment structures is apparent in the relative magnitudes of the horizontal displacements in the perpendicular direction versus the parallel direction and in the nature of the estimated stress. At the Anzac site the rail spreads the load along the length of the embankment and resulting in a confinement of the foundation soil in that direction. This creates similar patterns of deformation with depth in both horizontal directions. But, the magnitude of the deformation in the parallel direction is only half of that in the perpendicular direction. At the Edson site the corduroy reinforcement at the base of the

embankment acts to spread the loading in the perpendicular direction, similar to the effect of the rail. This results in a very similar shape and magnitude of displacement in both horizontal directions (Chapter 6, Manuscript #4).

The horizontal displacements and pore pressures generated at the Edson and Anzac sites increase in magnitude with depth. This distribution is not consistent with the response predicted with an infinite elastic half-space which calculates a slight reduction of pore pressure generation, stress and strain with depth. This appears to be due to the development of high shear strains at the interface plane between the peat and the underlying stiffer mineral soils as evident in the measured cyclic horizontal displacements. This high shear strain indicates that the base of the peat layer not laterally fixed to the underlying material increasing the deviatoric stress within the peat (Chapter 6, Manuscript #4).

7.1.3 Conceptual Model for the Response of Peat Foundation

A conceptual model of the undrained elastic behaviour and strength of the peat was developed from the cross-anisotropic response observed during the laboratory testing and correlations to fibre reinforced soil literature. The model assumes that the behaviour of the peat is defined by its cross-anisotropic stiffness (and the resulting pore pressure generation) and strength which are dependent on the orientation and magnitude of the principal stresses with respect to the fibre orientation. (Chapter 5, Manuscript #3)

Directly under the train loading the principal strains are expansive in the horizontal plane. This generates tension in the fibres and a resulting increase in stiffness and pore pressure generation as well as mobilization of the maximum fibre reinforced strength of the peat. The horizontal expansive stiffness can be several times that of the vertical stiffness with ratios of horizontal to vertical stiffness estimated between 2.6 to 2.9 for the peat tested within this study (Chapter 4, Manuscript #2). As a result of the anisotropic stiffness the shear-induced excess pore water pressure is approximately 0.3 (Chapter 5, Manuscript #3).

The effect of the fibre reinforcement is reduced further from the surface load as the major principal stress rotates and is no longer normal to the horizontal plane. With this rotation there is a corresponding reduction in the shear induced pore pressure parameter. Far from the applied load the horizontal strains perpendicular to the track will be compressive and the stiffness tend to

the vertical stiffness. Since the strength of the peat is also dependant on the orientation of the principal stresses the strength will reduce from the maximum effective fibre reinforce strength (38°) *towards* the effective critical state frictional strength (31°) (Chapter 6, Manuscript #4).

7.1.4 Analysis of Stress States of Peat under Railway Embankments

A numerical simulation was used to evaluate the distributions of stress below within the peat foundations. The simulation was unable to fully incorporate the anisotropic constitutive model but did provide valuable insights into the level of strength mobilized at each of the study sites. It was found that for symmetrical embankments with flat surrounding terrain (i.e. Edson and Anzac) there were two areas susceptible to yielding: first, the peat directly beneath the embankment subjected to the maximum deviatoric stresses; and second, peat near the interface with the stiffer underlying mineral soil. This latter case was confirmed with the SAA measurements from the Edson and Anzac sites which show corresponding zones of high shear strain at the interface (Chapter 6, Manuscript #4).

The modelling also helped to illustrate that the loss of frictional strength at the interface would result in an increase in deviatoric stress and plastic deformation directly below the embankment. This shows that the stress state directly beneath the embankment is a critical measurement of the stability of these embankments. A stress mobilization factor was developed to quantify the stability of the peat foundation during train loading. This factor was defined as the ratio of the measured additional undrained shear stress applied to the peat during the passage of a train to the additional undrained shear stress which would result in the yielding of the peat. The stress mobilization factors from the Edson and Anzac sites were found to be 15 % and 43 % respectively. The higher level of stability at the Edson site is attributed to role of the the embankment structure, including the corduroy, in reducing the magnitude of shear stresses developed under train loading (Chapter 6, Manuscript #4).

The modelled results for the Lévis site indicate that the surface geometry resulted in an increased susceptibility to yielding beneath the recently constructed north-east ditch. The extent of the plastic zone was found to be the result of two factors. First, the north-east ditch acts to further concentrate the shear stresses at the interface between the soft peat and the fractured shale. Second, this concentration of shear stresses is at a location at which the principal stress

orientation corresponds to a reduced strength of peat. This distribution of modelled plastic yielding and the factors which contributed to it may be a strong indicator of the mechanism of failure of this embankment in 2004 (Chapter 6, Manuscript #4).

The instrumentation installed at the Anzac site near the track and at the toe of the embankment allowed the spatial distribution of strain and pore pressure generation to be measured. It appears that there is a large reduction in horizontal strain perpendicular to the rail suggesting a limited distribution of horizontal stress and thus generation of mean total stress. This lower mean total stress is also confirmed by the very low generated pore pressures measured beneath the toe of the embankment. The shear strain calculated from the cyclic shape of the SAA indicates that there is very little variation in deviatoric stress between the two locations. This was confirmed by the finite element modelling which showed that the low modulus for peat results in a wide distribution of shear stress. The shear induced pore pressure generation beneath the Anzac embankment was calculated to contribute 35% of the cyclic change in pore pressure. At the toe of the embankment there is a similar magnitude of deviatoric stress as beside the track there is no discernable contribution of shear stress to the generation of pore pressure. This lack of shear induced pore pressure generation is attributed to the orientation of the principal stresses resulting reduction of pore pressure parameter *a towards* zero (Chapter 6, Manuscript #4).

7.2 Implications of Study

The first objective of this research was to determine the mechanisms that govern the spatial and temporal distribution of stress, strain and pore pressure within the cyclically loaded peat foundation of a railway embankment. These mechanisms have been identified as: the unique cross-anisotropic properties of peat arising from its fibrous composition and *in situ* structure; the construction of the embankment; and the boundary conditions imposed on the peat due to its low compressive horizontal stiffness and potential for shearing at the interface between the peat and the underlying mineral soil. This is described in detail above within the conceptual model and the analysis of the measured responses from the study sites. Laboratory testing of samples from all three sites has shown a cross-anisotropic elastic response during undrained loading with similar values of pore pressure parameters, moduli and a common yield surface defined by the effective shear strength (Chapter 5, Manuscript #3). The minimal variation of the properties of the fibrous peats between these sites suggests that, generally, there may be little difference between the

properties of fibrous peats (or at least for peat which has been strong enough to carry railway embankments for nearly a century).

The second objective was to determine the implications of these mechanisms on the strength of stability of these structures. The understanding of the yield strength of the peat has been clearly defined from the laboratory testing and the development of the conceptual model. A full understanding of the stability of the embankments has not been fully realized as the failure mechanism itself is still undefined. Evidence from the laboratory testing suggests that over stressed peat will continue to shear without the development of shear planes. The assessment of the relative strength of the peat foundations provides an initial method of evaluating the impact of increasing traffic and axle loads. The results of the simulation of plastic yielding of the peat foundation at the Lévis site show that it is a result of the geometry and history of the site. Thus, the Lévis site is not necessarily indicative of problem occurring at all peat sites under similar increases in axle loads and traffic. It is also possible that the peat foundation at the Lévis site was close enough to yielding that increased train speed and resulting pore pressure may have triggered the failure in 2004. (Chapter 6, Manuscript #4)

7.3 Recommendations

The research included within this thesis is only an initial part of a larger ongoing program. The following recommendations for additional work will aid in the progression of this program. The continuation of the research should focus on the further development of a constitutive soil model for peat for implementation within a finite element program, the measurement of the effectiveness of alternate remediation methods, the study of long-term deformation characteristics of the peat foundations, the application of the developed understanding of the response of the peat foundations to the broader railway network and further study of the formation of peat boils.

This study produced a conceptual model for the undrained behaviour of peat foundations under heavy axle loads. Development of a numerical model based on the constitutive model proposed in this thesis will enable the full dimensionality of stress and pore-pressure response resulting from the cross anisotropic stiffness of the peat to be explored. This understanding will allow the locations of peak stresses and potential models of failure to be simulated and explored. These

models can then be used to further explore the potential impact of alternative methods of remediation. The first step in the calibration of the peat constitutive model would be to model the response of peat to the CU laboratory testing both from this study and that produced in Yamaguchi et al. (1985). The model could then be used to simulate the performance of the field sites during undrained loading. Further laboratory testing innovations should include the CU testing of remoulded peat specimens created with fibre alignment along the axis of the specimens and specimens with the principal axis lying within the horizontal plane of fibres. This testing would allow for the measurement of the undrained modulus, pore pressure generation and the shear strength of peat with differing effects of fibre reinforcement similar to that conducted for drained fibre reinforced soils. The results would provide further definition of parameters for a constitutive model. This testing would require the development of methods for preparing specimens for CU testing involving one dimensional radial consolidation.

Within the review of the fibre reinforced literature provided within Chapter 2 the effect of the aspect ratio of the fibres on the definition of the mean normal stress on the surface of these fibres is presented. This mean normal stress controls the magnitude of friction that can be developed between the fibres. This is a fundamental change from current soil models which define the mean effective stress as the mean effective normal stress based on a definition derived from the concept of spheroids. This change in the definition of the normal stress combined with the shape the generation of tension within the fibres appear to control the tension generated within the fibres and thus the horizontal stiffness, the reinforced strength and the strain hardening behaviour. The impact of this on the behaviour of fibrous materials needs to be further explored.

CN is pursuing the remediation of identified problem sites. This provides an opportunity to conduct investigations into the effectiveness of different remediation methods for increasing the stiffness and strength of these embankments over peat foundations. Three different remediation methods are being examined at the three study sites included within this thesis. These include the installation of driven timber piles under an existing embankment[7], the construction of berms on

[7] The effect of the installation of the piles was measured at the Edson site and is presented within a conference paper in Appendix E titled: Assessing the Condition of Peat Subgrades Subjected to Heavy Axle Loads: Effectiveness of the use of Piles to Strengthen Embankments.

the sides of embankments, and the installation of foam polymer piles injected under an existing embankment. The investigation into the effectiveness of the driven timber piles was run concurrently with the research presented within this thesis, with the installation of strain-gauge piezometers in a section of the Edson embankment that was remediated with timber piles in 1998. A comparison was made between the measured pore pressure responses of the peat foundation beneath the unremediated section of the embankment (mile 102.0) and that beneath the remediated section of the embankment (mile 102..3) to determine the effect of the timber piles on the amount of stress within the peat. The investigation into the effectiveness of the addition of berms to the side of embankments began in May of 2011 with the installation of instrumentation in an embankment near the existing Anzac site. This instrumentation will be used to measure the pre-remediation response of the peat foundations. The construction of the berm on the side of the embankment is scheduled to be completed in November 2011. The effect of the addition of berms on the peat foundations has undergone initial modelling (Appendix D). The simulated effect of the addition of berms is a reduction in the shear stress within the peat due to the weight of the embankment material. This reduction of shear stress occurs directly below the embankment at the location which bears the bulk of the shear stress developed during train loading. This measurement of the long-term response of the peat due to the construction of the berm will provide valuable insight into the effect of new construction on peat. This should provide usable data to CN, as there are several construction projects proposed to extend sidings in areas over peat formations. The investigation into the effectiveness of injected foam polymer piles will start at the Lévis site in the spring of 2012. An instrumentation package is being designed to measure the magnitude and distribution of stress during train loading before and after the installation of the polymer piles.

The long-term deformation of peat foundations under repeated train loading was identified in the Transportation Safety Board investigation as a contributing factor to the failures at the Lévis site. If the stress state induced in the peat foundation under train loading exceeds the yield strength of the peat the resulting plastic deformations should accumulate over time. Instrumentation to measure the long-term deformation characteristics of the peat was installed at the Anzac site; however, the resulting data sets showed inconsistent results and additional study is required. To meet this task vibrating wire settlement gauges and SAAs will be installed at both the new berm site and the Lévis site. Additional laboratory testing should also be conducted to characterize the

secondary compression and visco-plastic response of peat and determine if there is a correlation between the magnitude and rate of these and the reliance on the tension developed within the fibres**.** The use of physical modelling may provide additional insight the effects of this behaviour and the mechanism by which this may lead to a failure of the embankment and subgrade.

The in-depth investigation of the three sites included in this study has provided insight into the response of peat foundations to heavy axle loads and can provide the basis for the extrapolation of these results to the larger railway network. Current projects being pursued to achieve this goal include the use of Ground Penetrating Radar (GPR) to measure the depth of peat and a newly developed instrumented rail car to measure the vertical deformations inducted under moving axle loads. The data sets from the GPR and the instrumented rail car in combination with aerial photograph and terrain analysis would allow for the network scale mapping of the extent of embankments over peat foundations and the relative stiffness the peat foundations to determine the spatial variation of peat response under the embankments. It may be possible to perform a detailed analysis with the resulting track stiffness map to correlate the measured track stiffness with the susceptibility of the track structure to maintenance issues such as ballast degradation, track geometry degradation, and rail breaks.

The formation of peat boils is a common issue for Canadian railways. The formation of these features beneath the track or in the embankment presents a hazard failure of the track or the embankment. The generation of these peat boils has been consistently related to the generation of excess pore pressure at sites with shallower peat formation. For these to form, higher pore pressures must be generated near the base of the peat than near the surface. Similar pore pressure profiles were measured at the Edson and Anzac sites, a possible cause could be the generation of large deviatoric stresses and associated shear induced pore pressure response at the interface between the base of the peat and the underlying stiffer soil; and the proximity of this increased pore pressure generation to the surface. Further investigation is required to determine the mechanisms and site conditions which result in the formation of these features so that long term prediction, monitoring and remediation methods can be developed.

References

Abdoun, T., and Bennett, V. 2008. A New Wireless MEMS-Based System for Real-Time Deformation Monitoring. Geotechnical News, 26(1): 36-40.

Abdoun, T., Danisch, L., and Bennett, V. 2005. Wireless Remote Monitoring of Geotechnical Systems. Geotechnical Engineering for Disaster Mitigation and Rehabilitation

Abdoun, T., Abe, A., Bennett, V., Danisch, L., Sato, M., Tokimatsu, K., and Ubillia, J. 2007. GeoDenver 2007: New Peaks in Geotechnics, pp. 1-10.

Adams, J.L. 1965. The engineering behaviour of a Canadian Muskeg. In 6th International Conference on Soil Mechanics and Foundation Engineering, Montreal, pp. 3-7.

Alberta Oil Magazine, 2009. CNR rolls out invitation to catch the oil train. Venture Publishin Inc. Edmonton, Canada, Issue April-May 2009

Alobaidi, I., and Hoare, D.J. 1996. The Developement of Pore Water Pressure at the Subgrade-Subbase Interface of a Highway Pavement and its Effect on Pumping Fines. Geotextiles and Geomembranes, 14: 111-135.

Ashrafi, S.A., and Smyth, A.W. 2007. Generalized Masing Approach to Modeling Hysteretic Deteriorating Behavior. Journal of Engineering Mechanics, 133(5): 495–505.

ASTM D854 Standard Test Methods for Specific Gravity of Soil Solids by Water Pycnometer.

ASTM D1997 Standard Test Method for Laboratory Determination of the Fiber Content of Peat Samples by Dry Mass.

ASTM D2434 Standard Test Method for Permeability of Granular Soils (Constant Head).

ASTM D2435 Standard Test Method for One-Dimensional Consolidation Properties of Soils.

ASTM D2974 Standard Test Methods for Moisture, Ash, and Organic Matter of Peat and Other Organic Soils.

ASTM D2976 Standard Test Method for pH of Peat Materials.

ASTM D4318 Standard Test Methods for Liquid Limit, Plastic Limit, and Plasticity Index of Soils.

ASTM D4427 Standard Classification of Peat Samples by Laboratory Testing.

ASTM D4531 Standard Test Methods for Bulk Density of Peat and Peat Products.

ASTM D4767 Standard Test Method for Consolidated Undrained Triaxial Compression Test for Cohesive Soils.

ASTM D5715 Standard Test Method for Estimating the Degree of Humification of Peat and Other Organic Soils (Visual/Manual Method).

Bauer, I.E., Gignac, L.D., and Vitt, D.H. 2003. Development of a peatland complex in boreal western Canada: lateral site expansion and local variability in vegetation succession and long-term peat accumulation. Canadian Journal of Botany, 81: 833–847.

Bishop, A.W. 1954. The use of pore pressure coefficients in practice. Geotechnique, 4(1): 148-152.

Boulanger, R.W., Arulnathan, R., Harder, L.F.J., Torres, R.A., and Driller, M.W. 1998. Dynamic Properties of Sherman Island Peat. Journal of Geotechnical and Geoenviromental Engineering, 124(1): 12-20.

Boylan, N., Jennings, P., and Long, M. 2008. Peat slope failure in Ireland. Quarterly Journal of Engineering Geology and Hydrogeology, 41(1): 93-108.

Brandl, H. 2001. Geotechnics of railtrack structures. In Geotechnics for Roads, Rail Tracks and Earth Structures: Outcome of ETC (European Technical Committee No.11). Edited by A.G. Correia and H. Brandl. January, 2001. Taylor & Francis, pp. 271-287.

Brawner, C.O., and Tessier, G. 1969. Road and Railway Construction. In Muskeg Engineering Handbook. University of Toronto Press, Toronto. pp. 150-208.

Brecciaroli, F., and Kolisoja, P. 2006. Deformation behaviour of railway embankment materials under repeated loading: Literature review. Finnish Rail Administration.

Brown, H.D. Construction of the Hudson Bay Railway. The Canadian Engineer, Vol. 61, p.11, 1931.

Charles, J.L, The Organic Terrain Factor in Northern Railway Construction. -.Proc,.. -Seventh Muskeg Research Conf ., Nat .- Res . Council of Caniida, Assoc. Ctee on Soil and Snow Mech., Tech. Memo. 71, p.126-132, Ottawa, 1961.

Chiang, D.-Y. 1999. The generalized Masing models for deteriorating hysteresis and cyclic plasticity. Applied Mathematical Modelling, 23: 847-863.

Choi, E., 1998, Evaluation of embankment failure at Canadian Pacific Railway mile 34.1 Kaministiguia subdivision. M.Eng Thesis, University of Calgary.

Clifton Associates Ltd (Clifton), 1988. File R719

Crawford, C.B. 1954. Some Engineering Properties of Muskeg, National Research Council of Canada: the Division of Building Research, Ottawa.

Criner, H.E., and McCann, G.D. 1954. Rails on Elastic Foundations Under the Influence of High-Speed Traveling Loads. Journal of Applied Mechanics, 76: 13-22.

Das, B.M. 1983. Fundamentals of Soil Dynamics. Elsevier.

Davidson, L. 2000. Basic mechanics of soils. University of the West of England, Bristol.

DeNie, F.C. Undulation of Railway Embankments on Soft Subsoil During Passing of Trains. Proc., Second International .Conf. on Soil Mechanics and Foundation Engineering, Vol, 2, .8-12, Rotterdam, 1948.

Duncan, J.M., and Chang, C. 1970. Nonlinear Analysis of Stress and Strain in Soils. Journal of Soil Mechanics and Foundation Division, ASCE, 96(SM5): 1629-1653.

Edwards, T. 2007. CN (West) Chief Geotechnical Engineer, Niton Junction, p. personal communication during site visit and site investigation.

Elsayed, A.A. 2003. The Characteristics and Engineering Properties of Peat in Bogs, PhD Thesis, University of Massachuseets Lowell.

Farrell, E.R. and Hebib, S. 1998. The determination of the geotechnical parameters of organic soils. Proceedings of the International Symposium on Problematic Soils, IS-TOHOKU 98, pp 33-36.

Fenwick, T.H. 1992. Electrification of British Railways' East Coast Main Line Civil Engineering Works, Doncaster to Berwick. Proceedings of the Institution of Civil Engineers: Transportation, 95: 227-238.

Frýba, L. 1999. Vibration of Solids and Structures under Moving Loads. Thomas Telford.

GeoSlope International, Ltd. (GeoSlope) (2007). GeoStudio 2007: SIGMA/w (Version 7.17) [Computer software]. Calgary, Alberta, Canada. Available from http://www.geo-slope.com/

Graham, J. and Houlsby, G.T. (1983) "Elastic Anisotropy of a Natural Clay", Géotechnique, 33, No. 2: 165-180

Hall, L. 2000. Simulations and Analyses of Train-Induced Ground Vibrations. Doctoral Thesis, Royal Institute of Technology, Stockholm, Sweden.

Hall, L. 2003. Simulations and analyses of train-induced ground vibrations in finite element models. Soil Dynamics and Earthquake Engineering, 23: 403-413.

Handy, R.L., and Spangler, M.G. 2007. Geotechnical Engineering : Soil and Foundation Principles and Practice. McGraw-Hill, New York.

Hanrahan, E.T. 1954. An Investigation of Some Physical Properties of Peat. Geotechnique, 4(3): 108-123.

Hanrahan, E.T. 1964. A Road Failure on Peat. Geotechnique, 14(3): 185-202.

Hanrahan, E.T. 1986. Mire Morphology and the Properties and Behaviour of some British and Foreign Peats. Quarterly Journal of Engineering Geology, 19: 7-80.

Hanrahan, E.T., and Rogers, M.G. 1981. Road on Peat: Observations and Design. Journal of Geotechnical Engineering Division, Proceedings of the American Society of Civil Engineers, 107(GT10): 1403-1415.

Hebib, S. 2001. Experimental investigation on the stabilisation of Irish peat. Ph.D. thesis, University of Dublin, Trinity College, Dublin, Ireland.

Hebib, S., and Farrell, E.R. 2003. Some experiences on the stabilization of Irish peats. Canadian Geotechnical Journal, 40(1): 107-120.

Hebib, S., and Farrell, E.R. 2004. Stabilisation of Irish Soils. Presented to the Institution of Engineers of Ireland, pp. 1-15.

Heelis, M.E., Chapman, D.N., and Krylov, V. Predicting and Measuring Vertical Track displacements on Soft Subgrades.

Heelis, M.E., Dawson, A.R., Collop, A.C., Chapman, D.N., and Krylov, V. 1999. Resilient Modulus of Soft soil Beneath High-speed Rail Lines. Transportation Research Record, 1687: 39-46.

Heelis, M.E., Collop, A.C., Dawson, A.R., Chapman, D.N., and Krylov, V. 2000. The 'Bow-Wave' Effect in Soft Subgrade Beneath High Speed Rail Lines. "Performance Verification of Constructed Geotechnical Facilities", Geotechnical Engineering Special Publication(94): 338-349.

Hendry, M. 2007. Measurement and Analysis of the Train-induced Dynamic Response of Railway Track and Embankments Constructed over Soft Peaty Foundations. MSc. Thesis, University of Saskatchewan, Saskatoon.

Hendry, M., Hughes, D., Barbour, S.L. and Atkinson, M. (2006a). Train induced dynamic response of railway track and embankments constructed over soft peat embankments constructed over soft peat foundations. In 59th Canadian Geotechnical Conference: Sea to Sky Geotechnique 2006. Vancouver, Canada, pp. 947-954, October 1-4

Hendry, M., Hughes, D., Barbour, S.L. and Atkinson, M. (2006b). Measurement and modelling the train induced dynamic response of a railway track and embankment constructed over a soft peat foundation. In Railway Foundations: RailFound 06 International Conference on Railway Track Foundations, Edited by G.S. Ghataora and M.P.N. Burrow. Birmingham, U.K. University of Birmingham Press., pp. 274-282, September 11-13.

Hendry, M., Martin, D., Barbour, S. and Edwards, T. (2008). Monitoring cyclic strain below a railway embankment overlying a peaty foundation using novel instrumentation, In 61st Canadian Geotechnical Conference, Edmonton, Alberta, September 21-24, Paper No. 443.

Hendry, M., Martin, D. and Barbour, S. (2009). New Investigation Techniques for Hazard Assessment of Heavy Axle Loads over Soft Peat Foundations, The Transportation Research Board 88th Annual Meeting, Washington, D.C., January 11-15, Paper No. 511.

Hendry, M., Hughes, D.A.B. and Barbour, S. (2010). Track Displacement and Energy Loss in a Railway Embankment over Peat, Proceedings of the ICE - Geotechnical Engineering, 163(1), 3-12.

Hendry, M.T., Edwards, T., Martin, C.D. and Barbour, S. (2011). Assessing the Condition of Peat Subgrades Subjected to Heavy Axle Loads: Effectiveness of the use of Piles to Strengthen Embankment, 2011 International Heavy Haul Association Conference - Railroading in Extreme Conditions, Calgary, AB, June 19-22.

Hendry, M.T., Barbour, S. and Martin, C.D. (2011). An evaluation of real-time deformation monitoring using motion capture instrumentation and its application in monitoring railway foundations, Geotechnical Testing Journal, 34(6 (November), GTJ103285), 1-11.

Hendry, M.T., Sharma, J., Martin, D. and Barbour, S. (2011). Effect of fibre content and structure on anisotropic elastic stiffness and shear strength of peat, Canadian Geotechnical Journal. *(Submitted April)*

Hendry, M., Martin, D. and Barbour, S. (2011). An Investigation for the Hazard Assessment of Heavy Axle Loads over Soft Peat Foundations and the Determination of the Effectiveness of Remediation Measures, The Transportation Research Board 90th Annual Meeting, Washington, D.C. January 23-27 (P11-0145)

Hernandez-Martinez, T.G., and Al-Tabbaa, A. 2002. Strength Properties of Stabilised Peat.

Hobbs, N.B. 1986. Mire Morphology and the Properties and Behaviour of some British and Foreign Peats. Quarterly Journal of Engineering Geology, 19: 7-80.

Hogan, J.M., Kamp, G.V.D., Barbour, S.L., and Schmidt, R. 2006. Field methods for measuring hydraulic properties of peat deposits. Hydrological Processes, 20: 3635–3649.

Hsu, C., and Vucetic, M. 2006. Threshold Shear Strain for Cyclic Pore water Pressure in Cohesive Soils. Journal of Geotechnical and Geoenviromental Engineering, 132(10): 1325-1335.

Hungr, O., and Evans, S.G. 1984. An example of a peat flow near Prince Rupert, British Columbia. Canadian Geotechnical Journal, 22: 246-249.

Idriss, I.M. and Seed, H.B., 1970, Seismic response of soil deposits. Journal of Soil Mechanics and Foundations Division ASCE, **96**(2), 631-638.

Kaynia, A.M., Madshus, C., and Zackrisson, P. 2000. Ground Vibrations from High-Speed Trains: Prediction and Countermeasure. Journal of Geotechnical and Geoenviromental Engineering, 126(6): 531-537.

Kerr, A.D. 2000. On the determination of the rail support modulus k. International Journal of Solids and Structures, 37(32): 4335-4351.

Klausner, Y. 1991. Fundamentals of Continuum Mechanics of Soils. Springer-Verlag, London, Great Britain.

Konrad, J-M. ., Grenier, S., and Garnier, P.2006. Heavy Axle Load over Muskeg Déraillement de l'Ultratrain a St-Henri-de-Lévis. Presentation at the 2006 Railway Ground Hazard Research Program annual workshop, Kingston, Ontario.

Konrad, J.-M., Grenier, S., and Garnier, P. 2007. Influence of Repeated Heavy Axle Loading on Peat Bearing Capacity. In 60th Canadian Geotechnical Conference. Ottawa, pp. 1551-1558.

Kramer, S.L. 1996. Geotechnical Earthquake Engineering. Prentice Hall.

Kramer, S.L. 2000. Dynamic Response of Mercer Slough Peat. Journal of Geotechnical and Geoenviromental Engineering, 126(6): 504-510.

Krylov, V. 1995. Generation of Ground Vibrations by Superfast Trains. Applied Acoustics, 44: 149-164.

Krylov, V., Dawson, A.R., Heelis, M.E., and Collop, A.C. 2000. Rail Movement and Ground Waves caused by High-speed Trains Approaching Track-Soil Critical Velocities. Proceedings of the Institution of Mechanical Engineers, Part F: Journal of Rail and Rapid Transit, 214(2): 107-116.

Kumar, A., Wailia, B.S. and Mohan, J. 2006. Compressive strength of fiber reinforced highly compressible clay. Construction and Building Materials, 20: 1063-1068.

Landva, A.O., Korpijaakko, E.O., and Pheeney, P.E. 1983. Geotechnical Classification of Peats and Organic Soils. ASTM Special Technical Publication: 37-51.

Landva, A.O., and La Rochelle, P. 1983. Compressibility and Shear Characteristics of Radforth Peats. In Testing of Peats and Organic Soils. ASTM Special Technical Publication, 820: 157-191.

Landva, A.O. and Pheeney, P.E. 1980. Peat fabric and structure. Canadian Geotechnical Journal, 17: 416-435.

Lekarp, F., and Dawson, A. 1998. Modelling permanent deformation behaviour of unbound granular materials. Construction and Building Materials, 12(1): 9-18.

Lekarp, F., Isaccson, U., and Dawson, A. 2000a. State of the Art. II: Permanent Strain Response of Unbound Aggregates. Journal of Transportation Engineering, 126(1): 76-84.

Lekarp, F., Isaccson, U., and Dawson, A. 2000b. State of the Art. I: Resilient Response of Unbound Aggregates. Journal of Transportation Engineering, 126(1): 66-75.

Lester, G. 2005. Atlas of Alberta Railways. University of Alberta Press, Edmonton, Canada. Available on-line at http://railways.library.ualberta.ca/ [Accessed January 27, 2011]

Li, D., and Selig, E.T. 1995. Wheel/Track Dynamic Interaction: Track Substructure Perspective. Vehicle System Dynamic Supplement, 24: 183-196.

Li, D., and Selig, E.T. 1998a. Method for Railroad Track Foundation Design. II: Applications. Journal of Geotechnical and Geoenviromental Engineering, 124(4): 323-329.

Li, D., and Selig, E.T. 1998b. Method for Railroad Track Foundation Design. I: Development. Journal of Geotechnical and Geoenviromental Engineering, 124(4): 316-322.

Li, J. and Ding, D.W. 2002, Nonlinear elastic behaviour of fiber-reinforced soil under cyclic loading. Soil dynamics and earthquake engineering, 22: 977-983.

Long, M. 2005. Review of peat strength, peat characterization and constitutive modelling of peat with reference to landslides. Studia Geotechnica et Mechanica, 27(3-4): 67-90.

Lui, C., and Evett, J.B. 2004. Soils and Foundations. Pearson - Prentice Hall.

MacFarlane, I . C . The Muskeg Subcommittee - The First Decade. Proc., Tenth Muskeg Research Conf., National Research Council of Canada, Assoc.Ctee. on Soil and Snow Mech., Tech. Memo. 85, p.1-5, Ottawa, 1965.

MacFarlane, I.C. 1969. Engineering Characteristics of Peat. In Muskeg Engineering Handbook. University of Toronto Press, Toronto. pp. 78-126.

MacFarlane, I.C., 1969b. Annotated Bibliography on Engineering Aspects of Muskeg and Peat. National Research Council of Canada Division of Building Research. Bibliography No. 39

MacFarlane, I.C., and Rutka, A. 1959. Evaluation of Road Performance over Muskeg in Ontario. In Proceedings of the Fortieth Convention of the Canadian Good Roads Association, pp. 396-405.

Madshus, C. 2001. Modelling, Monitoring and controlling the behaviour of Embankments Under High Speed Train Loads. In Geotechnics for Roads, Rail Tracks and Earth Structures: Outcome of ETC (European Technical Committee No.11). Edited by A.G. Correia and H. Brandl. January, 2001. Taylor & Francis, pp. 225-238.

Madshus, C., and Kaynia, A.M. 2000. High-Speed Railway Lines on soft Ground: Dynamic Behaviour at Critical Train Speeds. Journal of Sound and Vibration, 231(3): 689-701.

Maki, G., 2002. DST Consulting Engineers Report: Sinkhole Investigation. White River Sub. Mile 035.7

Matasovic, N., and Vucetic, M. 1995. Generalized Cyclic-Degradation-Pore-Pressure Generation Model for Clays. Journal of Geotechnical Engineering, 121(1): 33-42.

Mesri, G., and Ajlouni, M. 2007. Engineering Properties of Fibrous Peats. Journal of Geotechnical and Geoenviromental Engineering, 133(7): 850-866.

Michaels, P. 1996. In situ Determination of Soil Stiffness and Damping. Journal of Geotechnical and Geoenviromental Engineering, 124(8): 709-719.

Michalowski, R. L., and Čermák, J., 2002. Strength anisotropy of fiber-reinforced sand. Computers and Geotechnics, 29: 279-299

Michalowski, R. L., and Čermák, J., 2003. Triaxial compression of sand reinforced with fibers. ASCE Journal of Geotechnical and Geoenvironmental Engineering, 129(2): 125-136

Mikkelsen, E., and Dunnicliff, J. 2008, "Some Views on a Recent Addition to our Instrumentation Tool Box-the ShapeAccelArray (SAA)," In Geotechnical News. pp. 28-30.

Mulungye, R.M., Owendea, P.M.O., and Mellona, K. 2007. Finite element modelling of flexible pavements on soft soil subgrades Materials & Design, 28(3): 739-756.

O'Kelly, B.C. 2007. Compressibility and Permeability Anisotropy of some Peaty Soils. In 60th Canadian Geotechnical Conference. Ottawa, pp. 1934-1939.

Osinov, V.A. 2003. Cyclic shearing and liquefaction of soil under irregular loading: an incremental model for the dynamic earthquake-induced deformation. Soil Dynamics and Earthquake Engineering, 23: 535–548.

Paolucci, R., and Spinelli, D. 2006. Ground Motion Induced by Train Passage. Journal of Engineering Mechanics, 132(2): 201-210.

Pigon, P.T., Hanrahan, E.T., and Somers, N. 1992. Major canal reconstruction in peat areas. In Proceedings of the Institution of Civil Engineers: Water Maritime and Energy. September, 1992., Vol.96, pp. 141-152.

Popp, K., Kruse, H., and Kaiser, I. 1999. Vehicle-track dynamics in the mid-frequency range. Vehicle System Dynamics, 31(5-6): 423-464.

Porbaha, A., Hanzawa, H., and Kishida, T. 2000. Analysis of a Failed Embankment on Peaty Ground. Geotechnical Special Publication, 101.

Radampola, S.S. 2006. Evaluation and Modelling Performance of Capping Layer in Rail Track Substructure. PhD Doctorate, Central Queensland University.

Radforth, J.R. 1969a. Preliminary Engineering Investigations. In Muskeg Engineering Handbook. University of Toronto Press, Toronto. pp. 127-149.

Radforth, N.W. 1969b. Muskeg as an Engineering Problem. In Muskeg Engineering Handbook. University of Toronto Press, Toronto. pp. 3-30.

Radforth, N.W. 1969c. Airphoto Interpretation of Muskeg. In Muskeg Engineering Handbook. University of Toronto Press, Toronto. pp. 53-77.

Radforth, N.W. 1969d. Classification of Muskeg. In Muskeg Engineering Handbook. University of Toronto Press, Toronto. pp. 31-52.

Raoa, S.N., and Pandab, A.P. 1999. Non-linear analysis of undrained cyclic strength of soft marine clay. Ocean Engineering, 26: 241–253.

Ridley, A.M. 2003. Field measurement of pore water pressures. Quality Services, Civil engineering division, Highways Agency: 1 thru 37.

Ridley, A.M., Vaughan, P.R., McGinnity, B., and Brady, K. 2004. Pore pressure measurements in infrastructure embankments. In Advances in Geotechnical Engineering: The Skempton Conference. Thomas Telford.

Rowe, R.K., and Soderman, K.L. 1985. Geotextile Reinforcement of Embankments on Peat. Geotextiles and Geomembranes, 2: 277-298.

Sadek, S., Najjar, S., and Freiha, F. 2010. Shear Strength of Fiber-Reinforced Sands. ASCE Journal of Geotechnical and Geoenvironmental Engineering, 136(3): 490-499

Sassa, K., Wang, G., Fukuoka, H., and Vankov, D.A. 2005. Shear-Displacement-Amplitude Dependent Pore-Pressure Generation in Undrained Cyclic Loading Ring Shear Tests: An Energy Approach. Journal of Geotechnical and Geoenvironmental Engineering, 131(6): 750–761.

Scott, R.F. 1963. Principles of Soil Mechanics. Addison-Wesley Publishing Company Inc.

Sellers, J.B., and Taylor, R. 2008. MEMS Basics. Geotechnical News, 26(1): 32-33.

Selig, E.T. and Waters, J.M. 1994. Track Geotechnology and Substructure Management, Thomas Telford ISBN: 0-07277-2013-9.

Skempton, A.W. 1954. The pore-pressure coefficients A and B. Geotechnique, 4(1): 143-147.

Slope Indicator 2004. Rod Extensometer. Slope Indicator Company, pp. 1-27.

Stokoe, K.H., Bay, J.A., Rosenblad, B.L., Haung, S.-K., and Twede, M.R., 1994. In situ seismic and dynamic laboratory measurements of geotechnical materials at Queensboro Bridge

and Roosevelt Island. Geotechnical Engineering Rep. GR 94-5, Civil Engineering Department, University of Texas, Austin USA

Tan, Y. 2008. Finite element analysis of highway construction in peat bog Canadian Geotechnical Journal, 45(2): 147-160.

Timoshenko, S.P. 1926. Method of Analysis of Statical and Dynamical Stresses in Rail. In 2nd International Conference of Applied Mechanics. Zurick, Switzerland, pp. 407-418.

The Transportation Safety Board of Canada (TSB), 1999. Railway Investigation Report R99Q0019.

The Transportation Safety Board of Canada (TSB), 2008. Railway Investigation Report R04Q0040. Cat. No. TU3-6/04-2E, ISBN 978-0-662-47573-6

Weber, W.G. 1969. Performance of embankments constructed over peat. Journal of geotechnical Division, ASCE, 95(SM1): 53-76.

Wehling, T.H., Boulanger, R.W., Arulnathan, R., Harder, L.F.J., and Driller, M.W. 2003. Nonlinear Dynamic Properties of a Fibrous Organic Soil. Journal of Geotechnical and Geoenviromental Engineering, 129(10): 929-939.

Wong, R.C.K., Thomson, P.R., and Choi, E.S.C. 2006. In Situ Pore Pressure Responses of Native Peat and Soil under Train Load: A Case Study. Journal of Geotechnical and Geoenviromental Engineering, 132(10): 1360-1369.

Wood, D.M. 2004. Soil Behaviour and Critical State Soil Mechanics. Cambridge University Press

Woods, R.D. 1978. Measurement of Dynamic Soil Properties. *In* ASCE Geotechnical Specialty Conference, Vol.1, pp. 91-178.

Yamaguchi, H., Ohira, Y., Kogure, K. and Shigeru, M. 1985. Undrained shear characteristics of normally consolidated peat under triaxial compression and extension conditions. Soil and Foundations, 25(3):1-18.

Yasuhara, K., Oikawa, H., Noto, S. 1994. Large strain cyclic behaviour of peat. *In* Advances in Understanding and Modelling the Mechanical Behaviour of Peat, ed. den Haan, Balkema, Rotterdam, pp. 301-310.

Appendix A: Site Characterization and instrumentation

This appendix provides a record of the site investigations, sampling and instrumentation installation at the Edson and Anzac sites. There were two different installations at the Anzac site; the second was to install additional piezometers. These two installations are referred to as part 1 and part 2 of the Anzac site investigation and instrumentation.

Appendix A: Site Characterization and instrumentation

Edson Subdivision miles 102.0 and 102.9

This section contains a summary of the site investigation conducted at the Edson subdivision site. The data presented below includes the location of the boreholes, the samples collected, and a summary of the installed instrumentation.

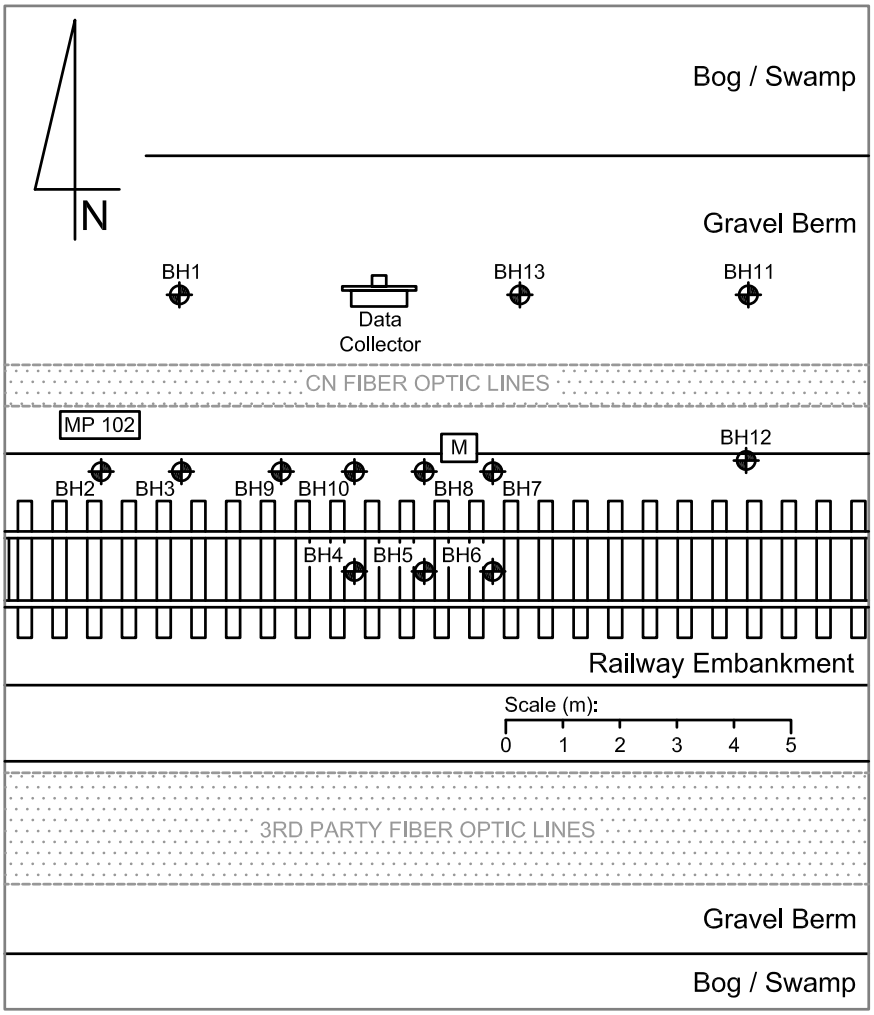

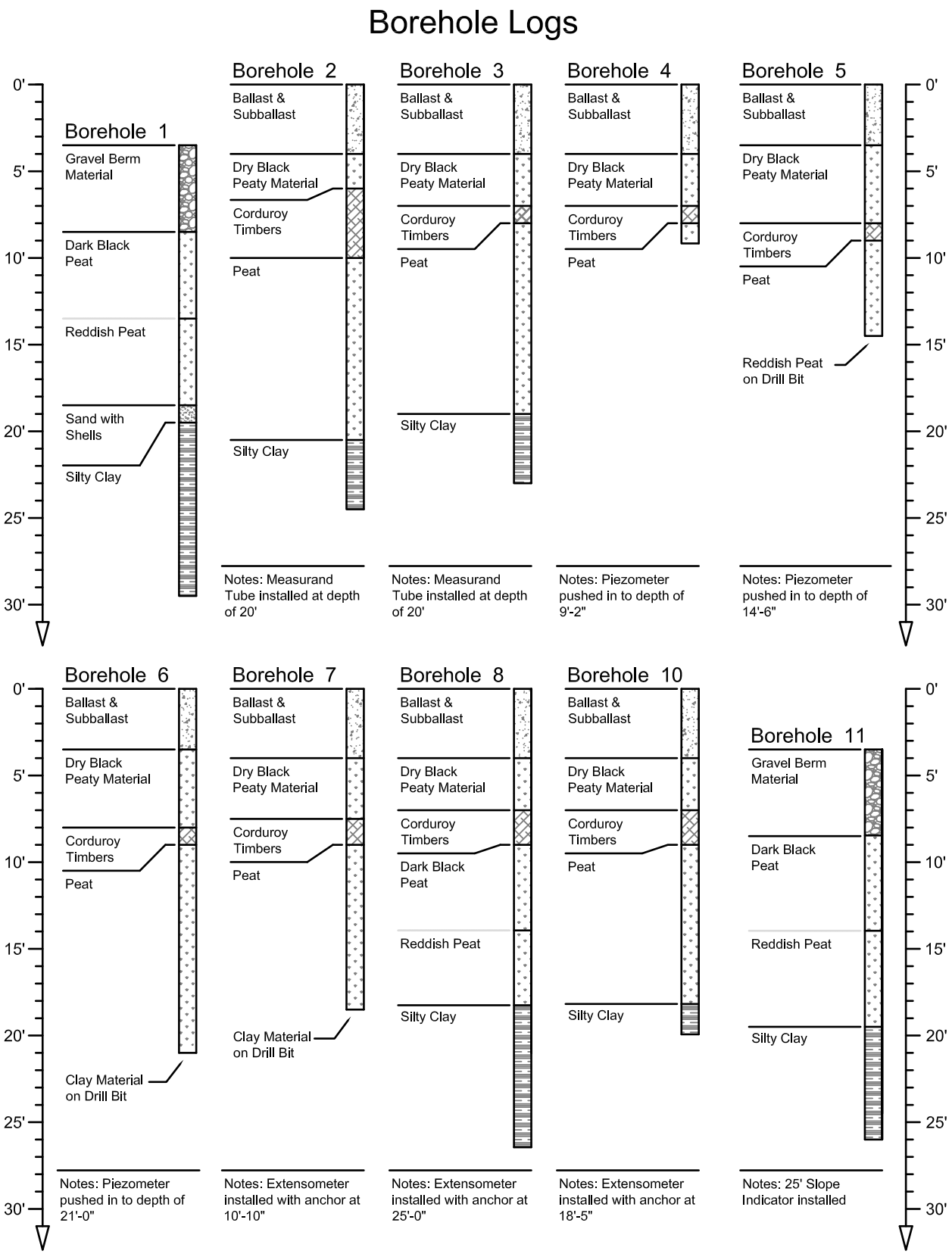
Borehole Logs
Borehole 1
Gravel Berm Material
Dark Black Peat
Reddish Peat
Sand with Shells
Silty Clay
Borehole 2
Ballast & Subballast
Dry Black Peaty Material
Corduroy Timbers
Peat
Silty Clay
Notes: Measurand Tube installed at depth of 20'
Borehole 3
Ballast & Subballast
Dry Black Peaty Material
Corduroy Timbers
Peat
Silty Clay
Notes: Measurand Tube installed at depth of 20'
Borehole 4
Ballast & Subballast
Dry Black Peaty Material
Corduroy Timbers
Peat
Notes: Piezometer pushed in to depth of 9'-2"
Borehole 5
Ballast & Subballast
Dry Black Peaty Material
Corduroy Timbers
Peat
Reddish Peat on Drill Bit
Notes: Piezometer pushed in to depth of 14'-6"
Borehole 6
Ballast & Subballast
Dry Black Peaty Material
Corduroy Timbers
Peat
Clay Material on Drill Bit
Notes: Piezometer pushed in to depth of 21'-0"
Borehole 7
Ballast & Subballast
Dry Black Peaty Material
Corduroy Timbers
Peat
Clay Material on Drill Bit
Notes: Extensometer installed with anchor at 10'-10"
Borehole 8
Ballast & Subballast
Dry Black Peaty Material
Corduroy Timbers
Dark Black Peat
Reddish Peat
Silty Clay
Notes: Extensometer installed with anchor at 25'-0"
Borehole 10
Ballast & Subballast
Dry Black Peaty Material
Corduroy Timbers
Peat
Silty Clay
Notes: Extensometer installed with anchor at 18'-5"
Borehole 11
Gravel Berm Material
Dark Black Peat
Reddish Peat
Silty Clay
Notes: 25' Slope Indicator installed
0'
5'
10'
15'
20'
25'
30'

Appendix A: Site Characterization and instrumentation

Sample Collection

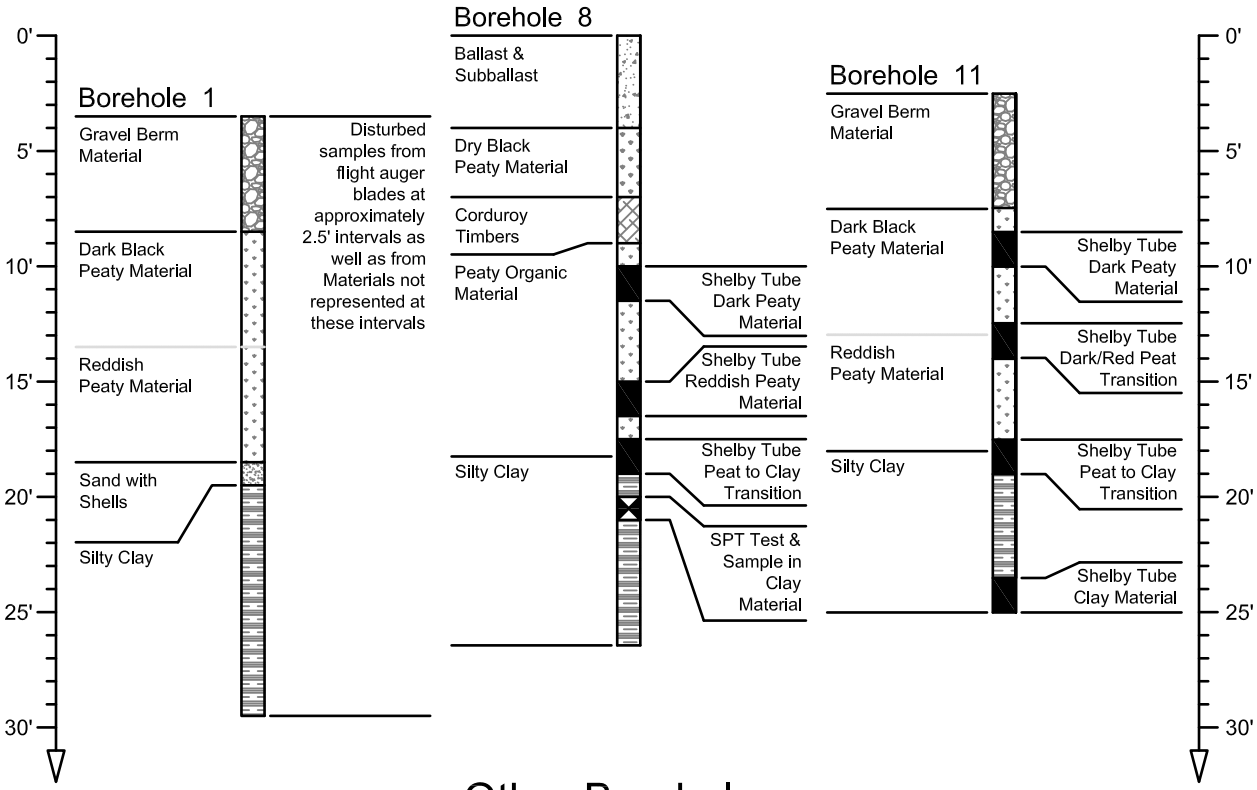

Other Boreholes

Borehole 9

Borehole was started but abandoned partway through.

Borehole 12

No log was written for this borehole.
A 25' Slope indicator installed in this borehole.

Borehole 13

No log was written for this borehole.
A 20' Standpipe was installed in this borehole.

Borehole 14

No log was written for this borehole.
A piezometer was installed in this borehole at a depth of 11'.

Borehole 15

No log was written for this borehole.
A piezometer was installed in this borehole at a depth of 18'.

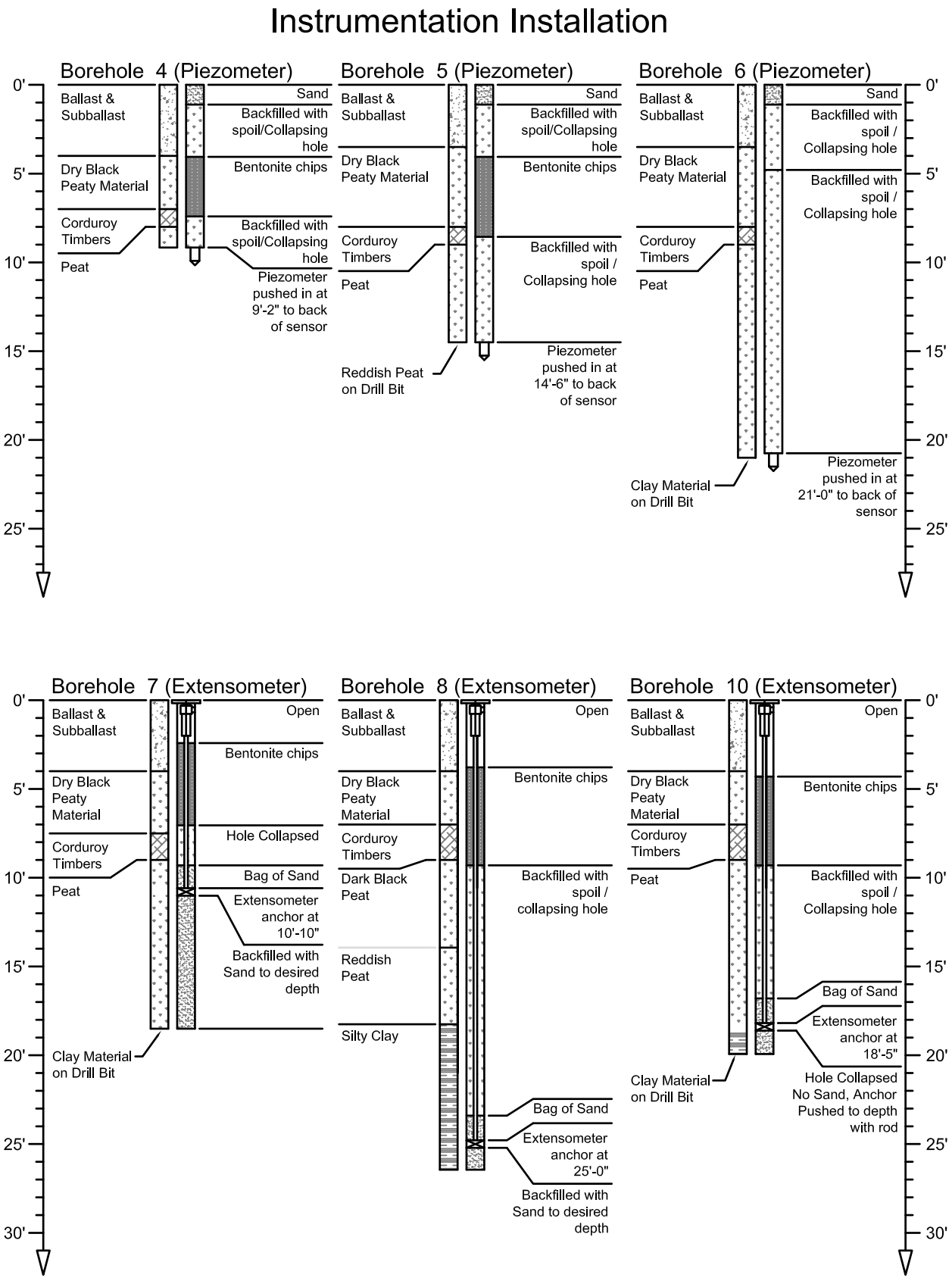
Instrumentation Installation
Borehole 4 (Piezometer)
Ballast & Subballast
Dry Black Peaty Material
Corduroy Timbers
Peat
Sand
Backfilled with spoil/Collapsing hole
Bentonite chips
Backfilled with spoil/Collapsing hole
Piezometer pushed in at 9'-2" to back of sensor
Borehole 5 (Piezometer)
Ballast & Subballast
Dry Black Peaty Material
Corduroy Timbers
Peat
Reddish Peat on Drill Bit
Sand
Backfilled with spoil/Collapsing hole
Bentonite chips
Backfilled with spoil / Collapsing hole
Piezometer pushed in at 14'-6" to back of sensor
Borehole 6 (Piezometer)
Ballast & Subballast
Dry Black Peaty Material
Corduroy Timbers
Peat
Clay Material on Drill Bit
Sand
Backfilled with spoil / Collapsing hole
Backfilled with spoil / Collapsing hole
Piezometer pushed in at 21'-0" to back of sensor
0'
5'
10'
15'
20'
25'
Borehole 7 (Extensometer)
Ballast & Subballast
Dry Black Peaty Material
Corduroy Timbers
Peat
Clay Material on Drill Bit
Open
Bentonite chips
Hole Collapsed
Bag of Sand
Extensometer anchor at 10'-10"
Backfilled with Sand to desired depth
Borehole 8 (Extensometer)
Ballast & Subballast
Dry Black Peaty Material
Corduroy Timbers
Dark Black Peat
Reddish Peat
Silty Clay
Open
Bentonite chips
Backfilled with spoil / collapsing hole
Bag of Sand
Extensometer anchor at 25'-0"
Backfilled with Sand to desired depth
Borehole 10 (Extensometer)
Ballast & Subballast
Dry Black Peaty Material
Corduroy Timbers
Peat
Clay Material on Drill Bit
Open
Bentonite chips
Backfilled with spoil / Collapsing hole
Bag of Sand
Extensometer anchor at 18'-5"
Hole Collapsed No Sand, Anchor Pushed to depth with rod
0'
5'
10'
15'
20'
25'
30'

Appendix A: Site Characterization and instrumentation

Lac-La-Biche Subdivision mile 263.5 (part 1)

This section contains a summary of the first site investigation conducted on the Lac-La-Biche subdivision, at the Anzac site. The data presented below includes the location of the boreholes, the samples collected, and a summary of the installation of the instrumentation.

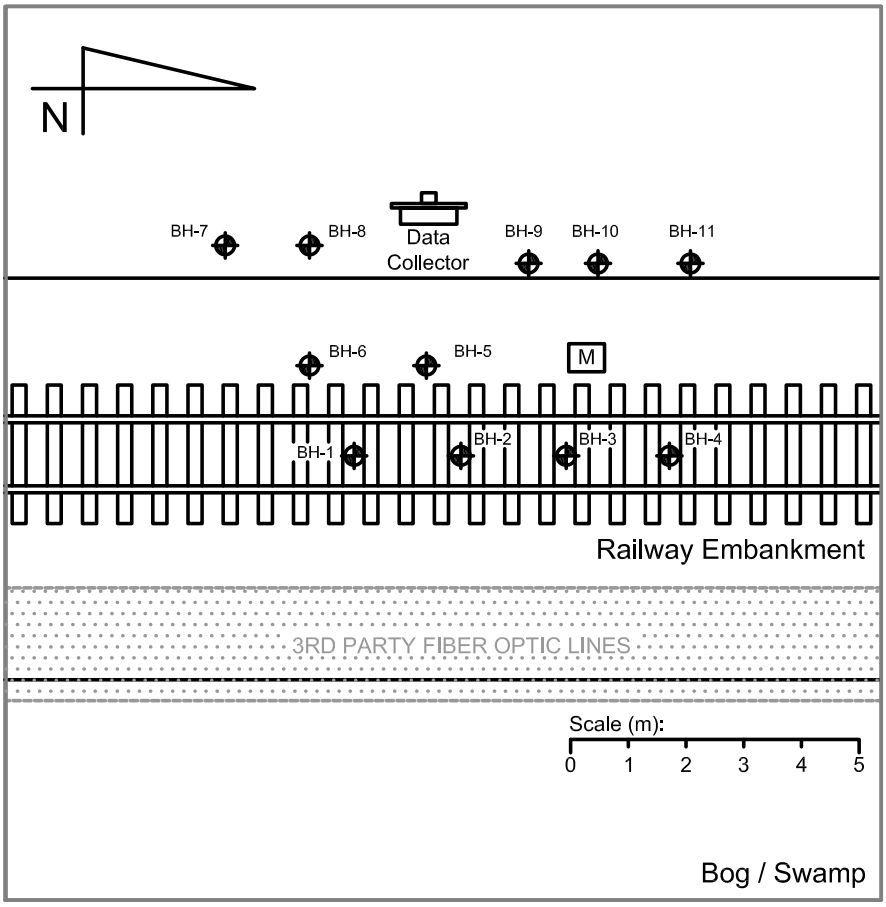

Appendix A: Site Characterization and instrumentation

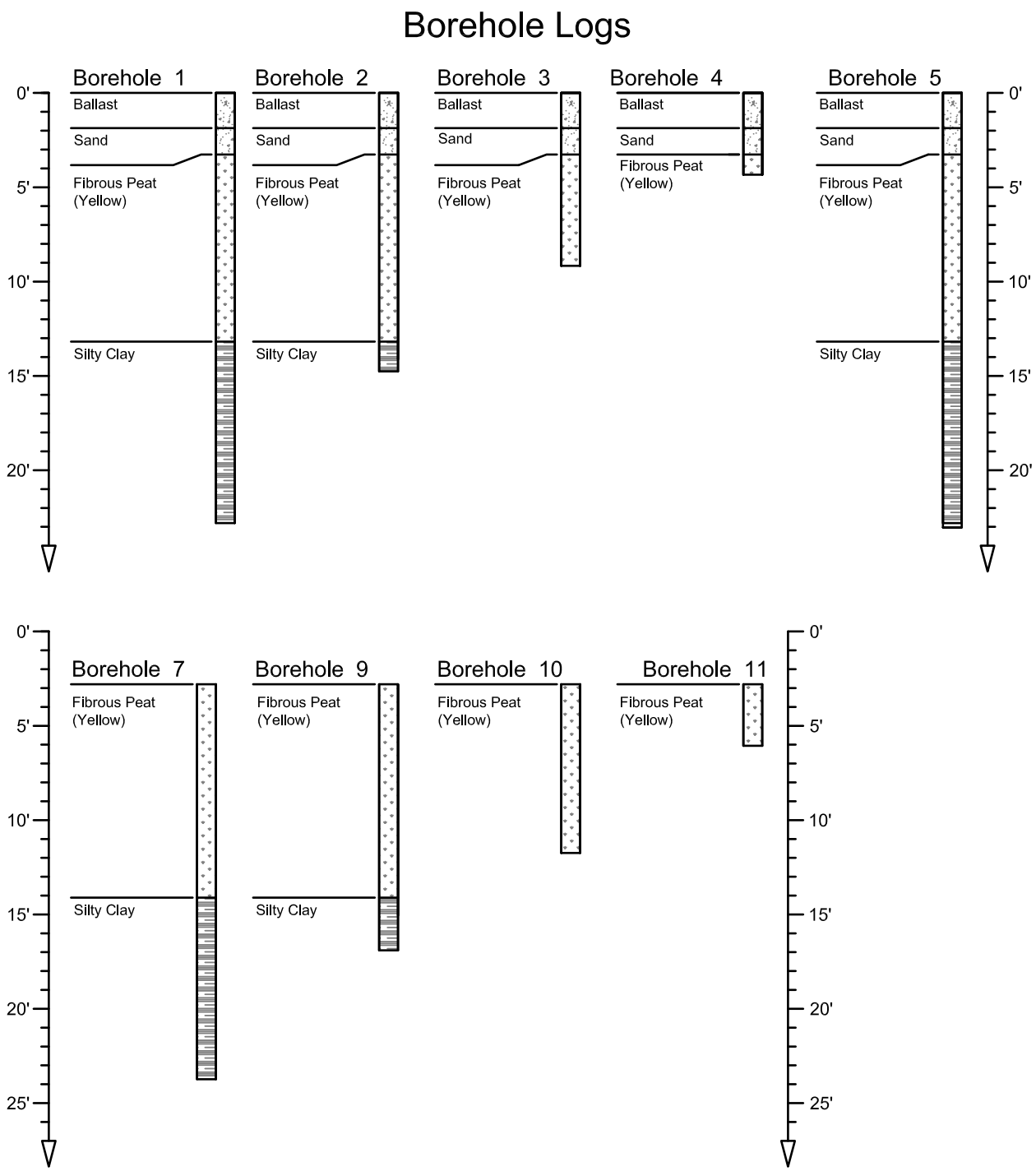

Sample Collection

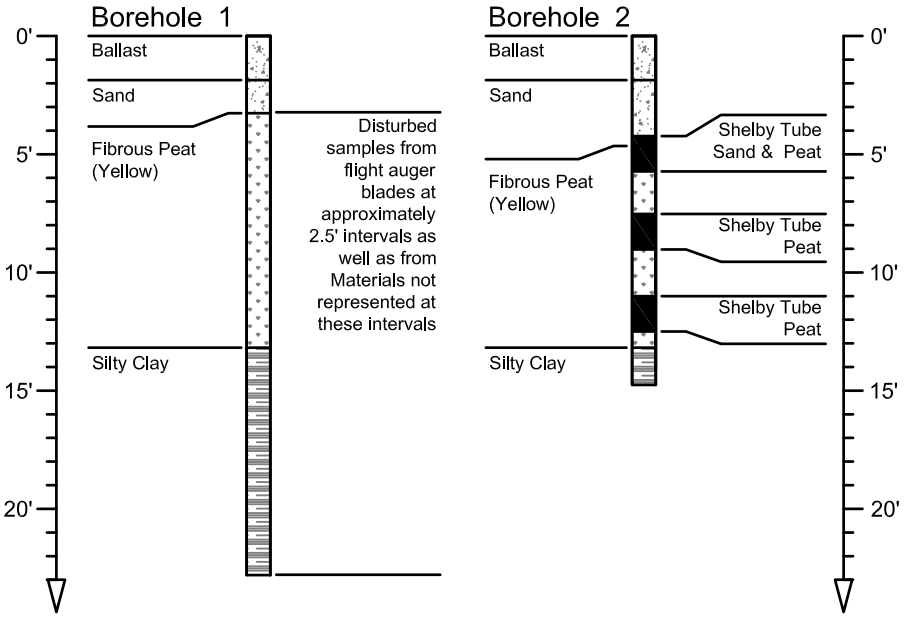

Other Boreholes

Borehole 7

No log was written for this borehole.
24' long 1" diameter PVC access tube installed for ShapeAccelArray

Borehole 8

No log was written for this borehole.
24' long 1" diameter PVC access tube installed for ShapeAccelArray

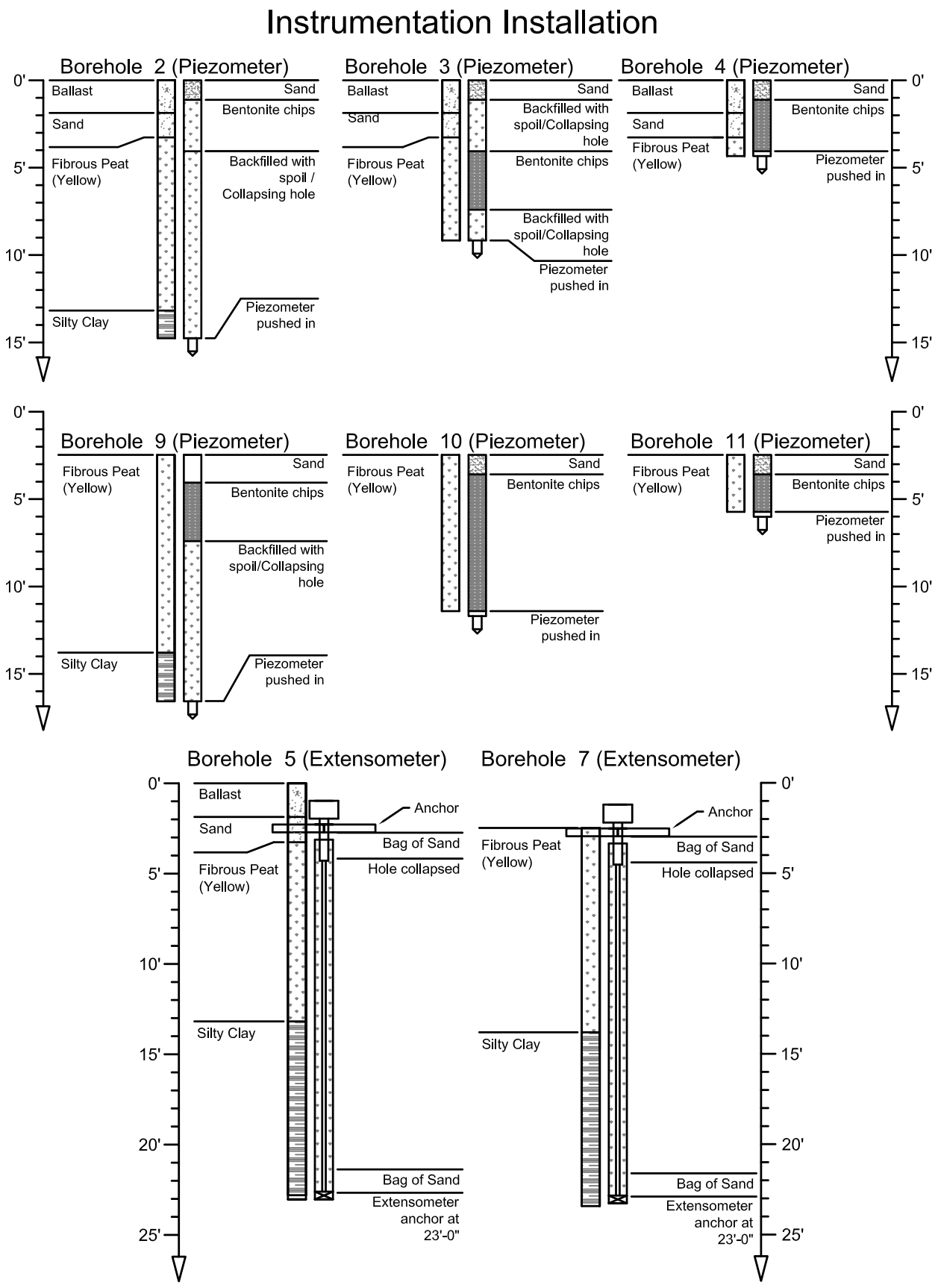
Instrumentation Installation
Borehole 2 (Piezometer)
Ballast
Sand
Fibrous Peat (Yellow)
Silty Clay
Sand
Bentonite chips
Backfilled with spoil / Collapsing hole
Piezometer pushed in
Borehole 3 (Piezometer)
Ballast
Sand
Fibrous Peat (Yellow)
Sand
Backfilled with spoil/Collapsing hole
Bentonite chips
Backfilled with spoil/Collapsing hole
Piezometer pushed in
Borehole 4 (Piezometer)
Ballast
Sand
Fibrous Peat (Yellow)
Sand
Bentonite chips
Piezometer pushed in
Borehole 9 (Piezometer)
Fibrous Peat (Yellow)
Silty Clay
Sand
Bentonite chips
Backfilled with spoil/Collapsing hole
Piezometer pushed in
Borehole 10 (Piezometer)
Fibrous Peat (Yellow)
Sand
Bentonite chips
Piezometer pushed in
Borehole 11 (Piezometer)
Fibrous Peat (Yellow)
Sand
Bentonite chips
Piezometer pushed in
Borehole 5 (Extensometer)
Ballast
Sand
Fibrous Peat (Yellow)
Silty Clay
Anchor
Bag of Sand
Hole collapsed
Bag of Sand
Extensometer anchor at 23'-0"
Borehole 7 (Extensometer)
Fibrous Peat (Yellow)
Silty Clay
Anchor
Bag of Sand
Hole collapsed
Bag of Sand
Extensometer anchor at 23'-0"
0'
5'
10'
15'
20'
25'

Appendix A: Site Characterization and instrumentation

Lac-La-Biche Subdivision mile 263.5 (part 2)

This section contains a summary of the second site instrumentation conducted on the Lac-La-Biche subdivision, at the Anzac site. The data presented below includes the location of the boreholes, the samples collected, and the installation of the instrumentation.

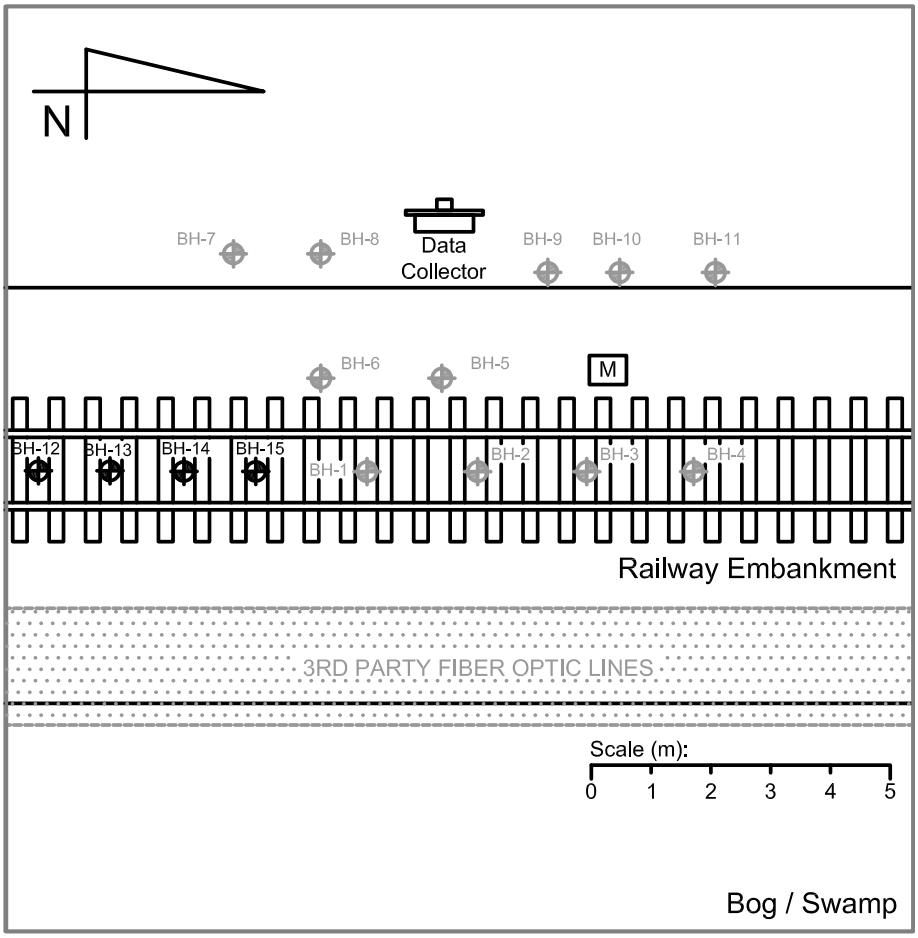

Appendix A: Site Characterization and instrumentation

Borehole Logs

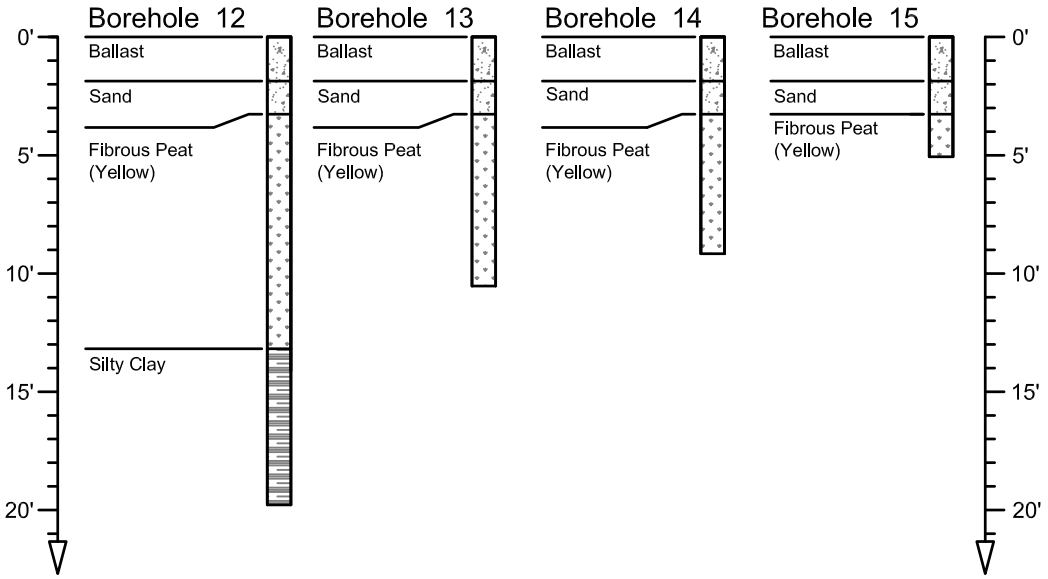

Sample Collection

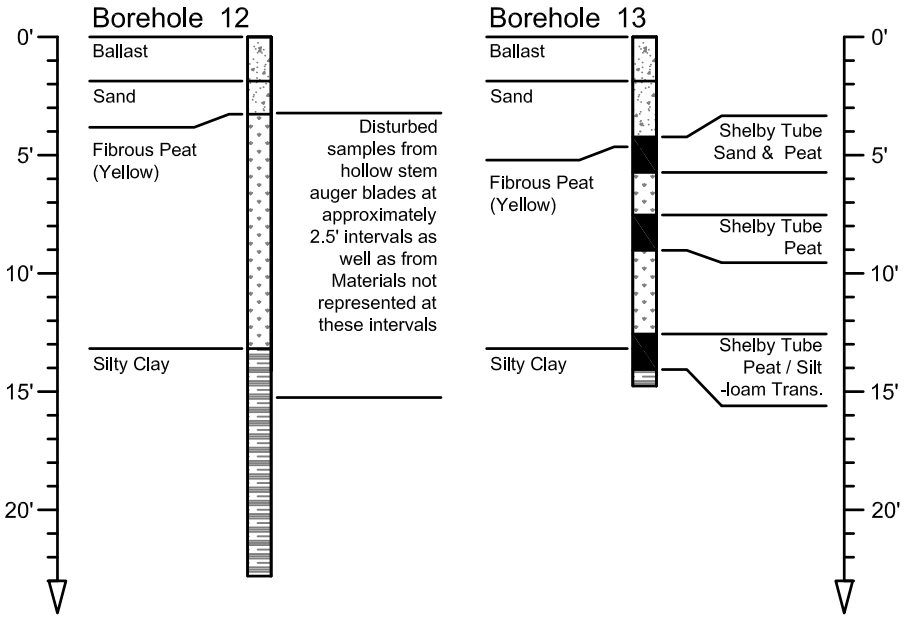

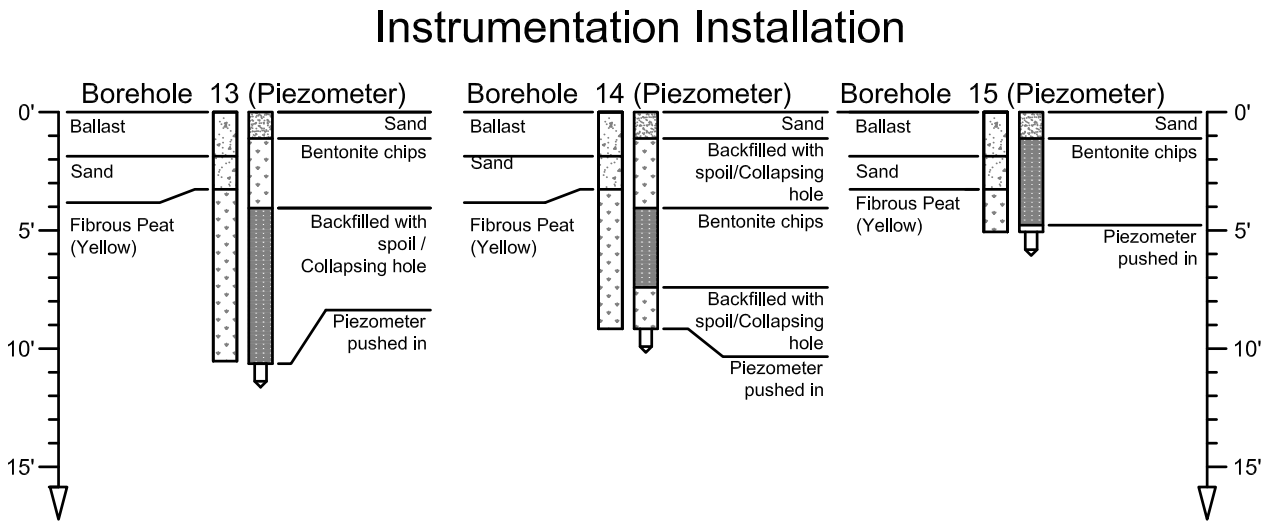
Instrumentation Installation
Borehole 13 (Piezometer)
Ballast
Sand
Fibrous Peat
(Yellow)
Sand
Bentonite chips
Backfilled with
spoil /
Collapsing hole
Piezometer
pushed in
Borehole 14 (Piezometer)
Ballast
Sand
Fibrous Peat
(Yellow)
Sand
Backfilled with
spoil/Collapsing
hole
Bentonite chips
Backfilled with
spoil/Collapsing
hole
Piezometer
pushed in
Borehole 15 (Piezometer)
Ballast
Sand
Fibrous Peat
(Yellow)
Sand
Bentonite chips
Piezometer
pushed in
0'
5'
10'
15'

Appendix B: Example data sets from field instrumentation

This appendix provides a record of the field data collected the three sites included in this study. The data sets provided were selected to illustrate the measured response of the peat foundations to a variety of different axle loads at both the Edson and Anzac sites. A single data set from the Lévis site is provided, this was produced from published data (Konrad et al. 2006; Konrad et al. 2007) and is provided for comparison to the data collected from the other sites.

Presented after the data sets is a brief guide to the types of railcars which passed over the embankments during the collection of the example data sets.

Appendix B: Example data sets from field instrumentation

Edson Subdivision miles 102.0

Data set: 1

Date of collection: October 10, 2007

Train type: Hopper cars full of grain

Length (number of cars): 92

Average train speed: 34.5 km/h (9.58 m/s)

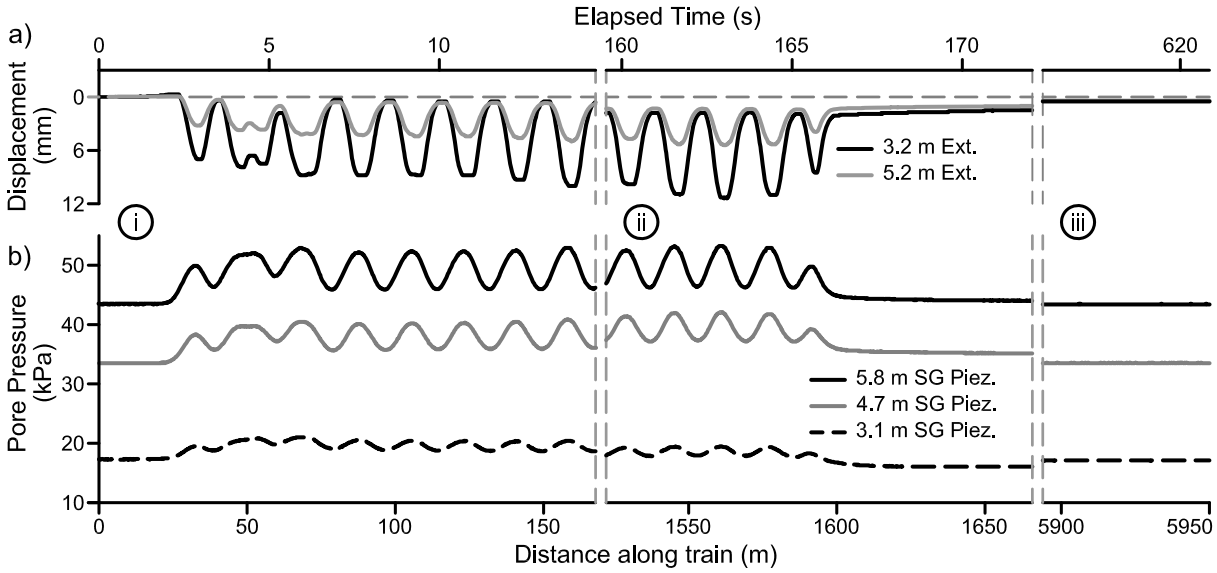

Figure B.1 Edson data set 1, presenting (a) the vertical displacement measured by the extensometers, and (b) the pore pressure as measured by the piezometers during the passage of the train

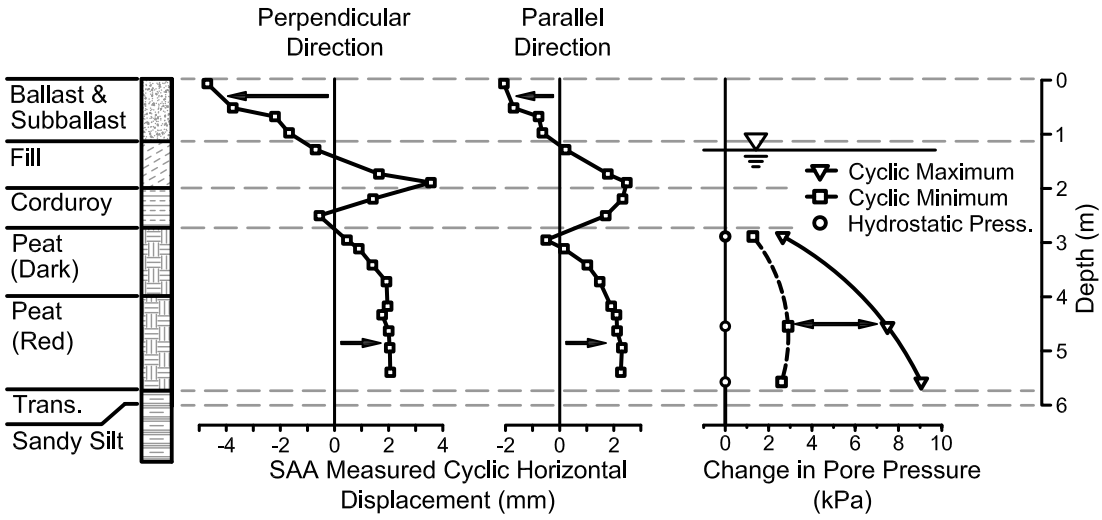

Figure B.2 Edson data set 1, presenting the cyclic horizontal displacement measured by the SAA, and the cyclic change in pore pressure as measured by the piezometers with depth.

Appendix B: Example data sets from field instrumentation

Data set: 2

Date of collection: October 10, 2007

Train type: Empty intermodal cars

Length (number of cars): 89

Average train speed: 42.3 km/h (11.7 m/s)

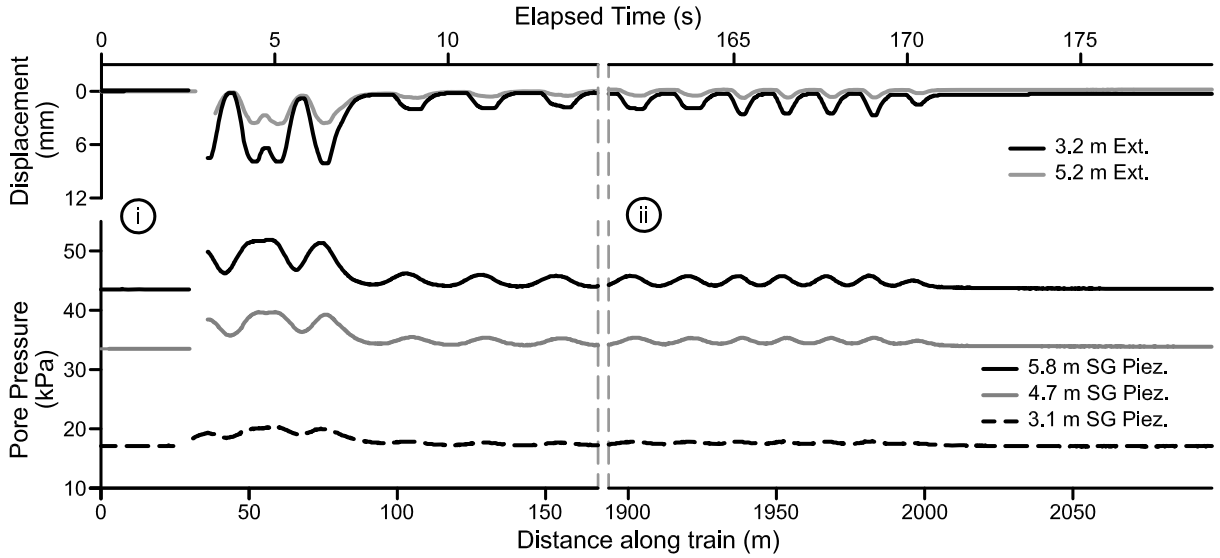

Figure B.3 Edson data set 2, presenting (a) the vertical displacement measured by the extensometers, and (b) the pore pressure as measured by the piezometers during the passage of the train

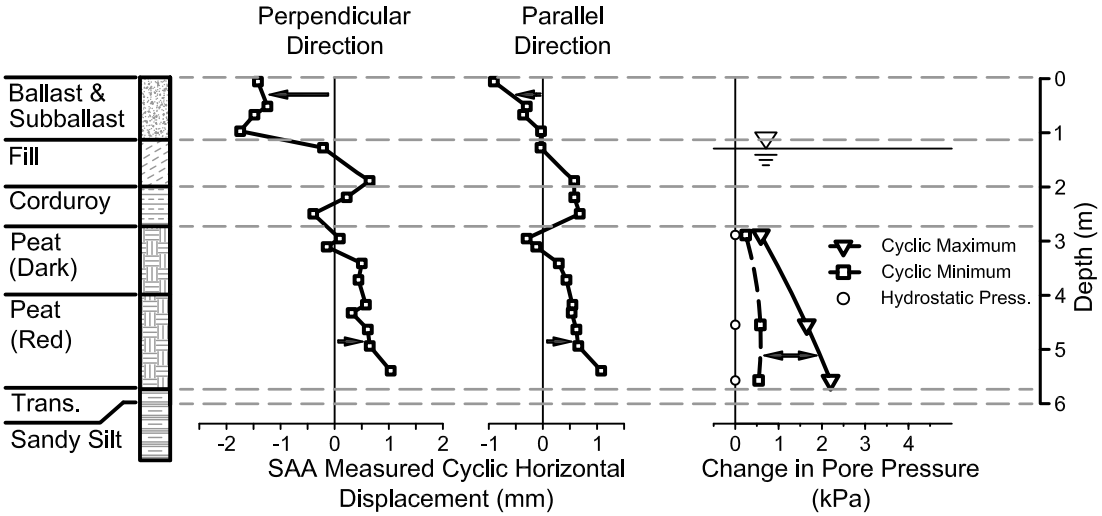

Figure B.4 Edson data set 2, presenting the cyclic horizontal displacement measured by the SAA, and the cyclic change in pore pressure as measured by the piezometers with depth.

Appendix B: Example data sets from field instrumentation

Data set: 3

Date of collection: October 11, 2007

Train type: Loaded flat cars and empty intermodal cars

Length (number of cars):

Average train speed: 44.8 km/h (12.4 m/s)

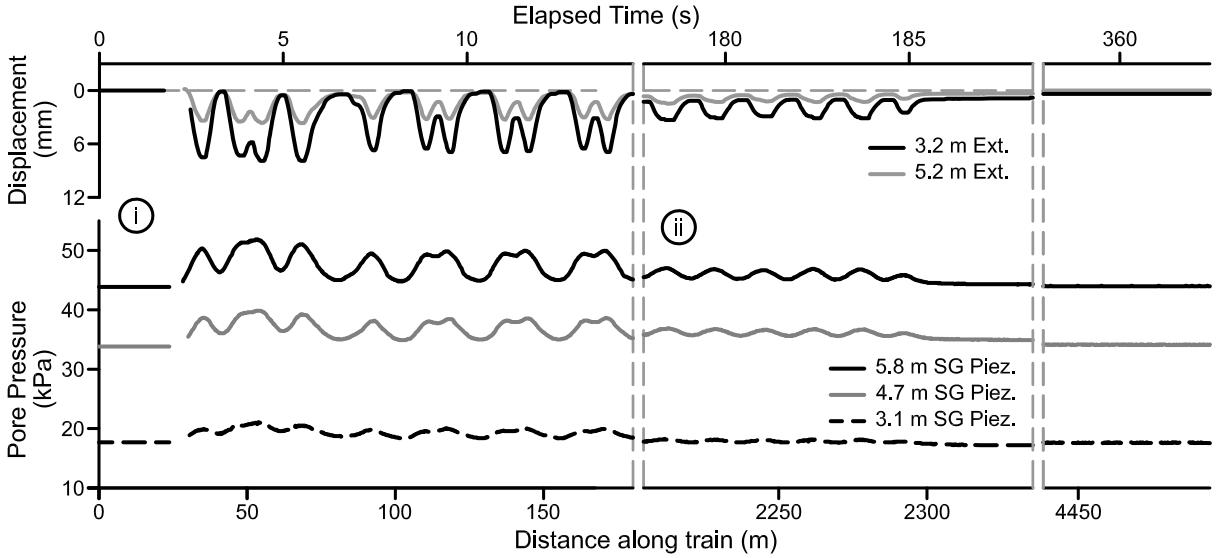

Figure B.5 Edson data set 3, presenting (a) the vertical displacement measured by the extensometers, and (b) the pore pressure as measured by the piezometers during the passage of the train.

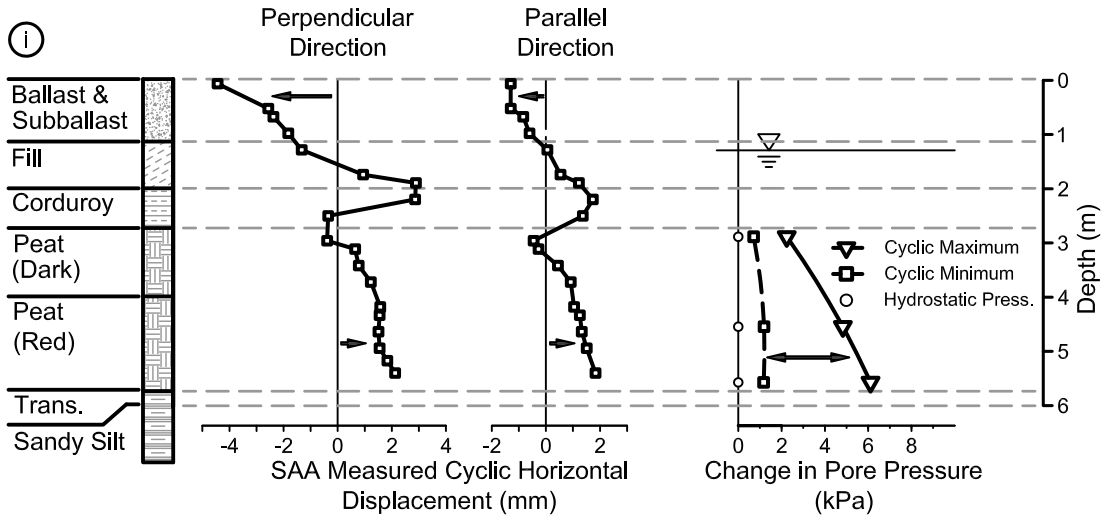

Figure B.6 Edson data set 3, presenting the cyclic horizontal displacement measured by the SAA, and the cyclic change in pore pressure as measured by the piezometers with depth, during the passage of the flatcars.

Appendix B: Example data sets from field instrumentation

Lac-La-Biche Subdivision mile 263.5

Data set: 1

Date of collection: October 22, 2010

Train type: Hopper and tankers cars

Length (number of cars): 31 hopper and 19 tankers

Average train speed: 10 km/h (2.78 m/s)

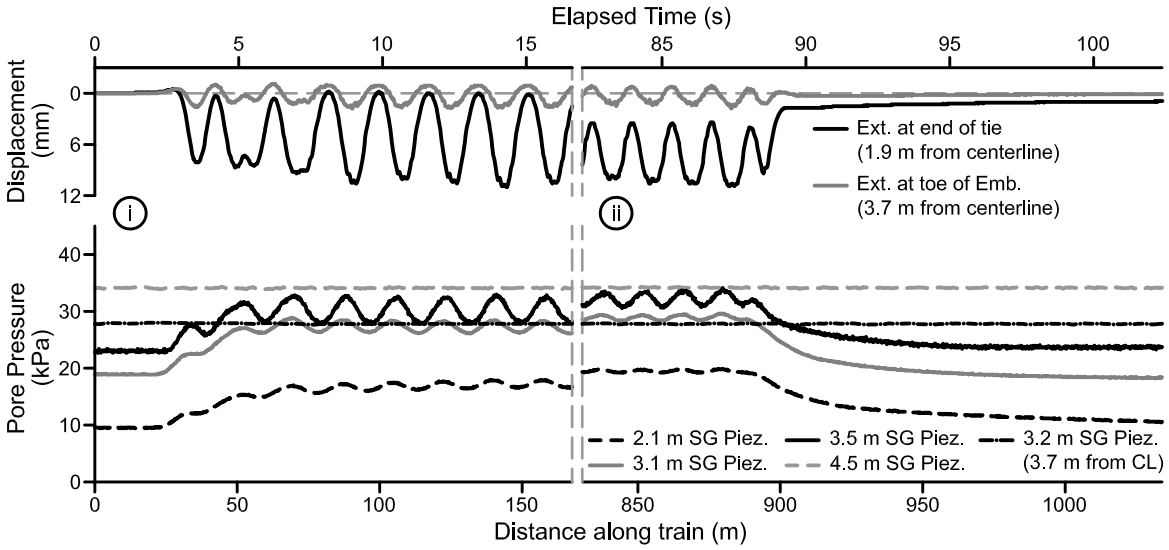

Figure B.7 Anzac data set 1, presenting (a) the vertical displacement measured by the extensometers, and (b) the pore pressure as measured by the piezometers during the passage of the train

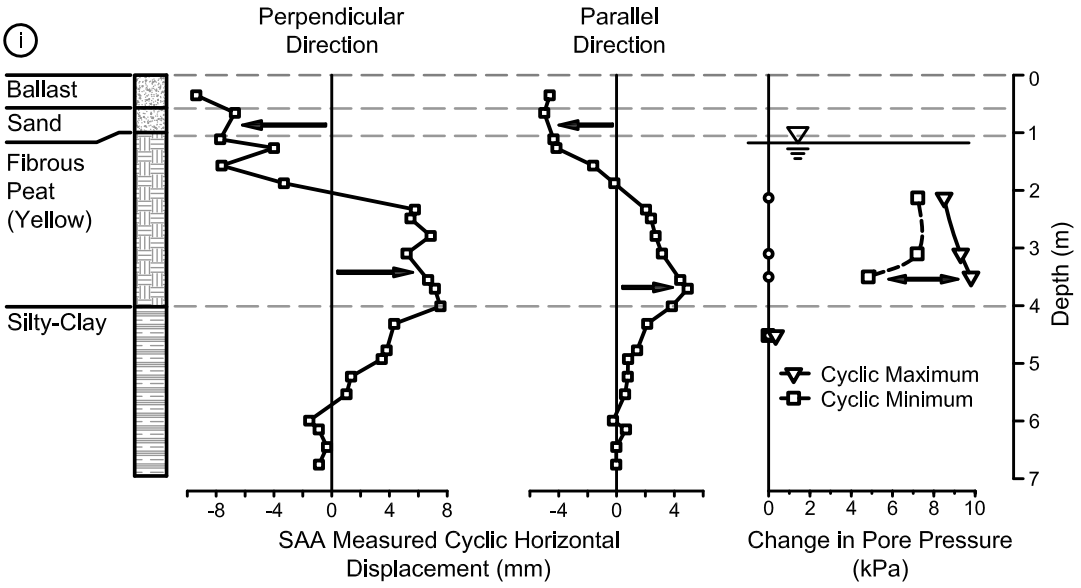

Figure B.8 Anzac data set 1, presenting the cyclic horizontal displacement measured by the SAA, and the cyclic change in pore pressure as measured by the piezometers with depth for the passage of the hopper cars, near the tie.

Appendix B: Example data sets from field instrumentation

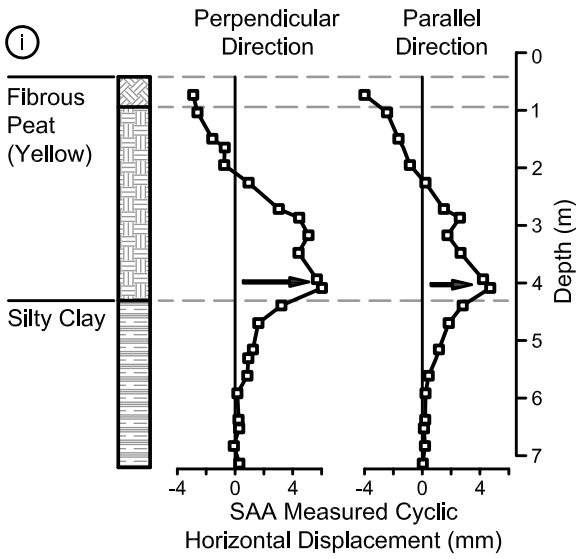

Figure B.9 Anzac data set 1, presenting the cyclic horizontal displacement measured by the SAA, and the cyclic change in pore pressure as measured by the piezometers with depth for the passage of the hopper cars, at the toe of the embankment.

Appendix B: Example data sets from field instrumentation

Data set: 2

Date of collection: July 22, 2009

Train type: Loaded flat cars, hopper cars and tankers

Length (number of cars): 19 flatcars, 26 hopper cars and 11 tankers

Average train speed: 16.9 km/h (4.69 m/s)

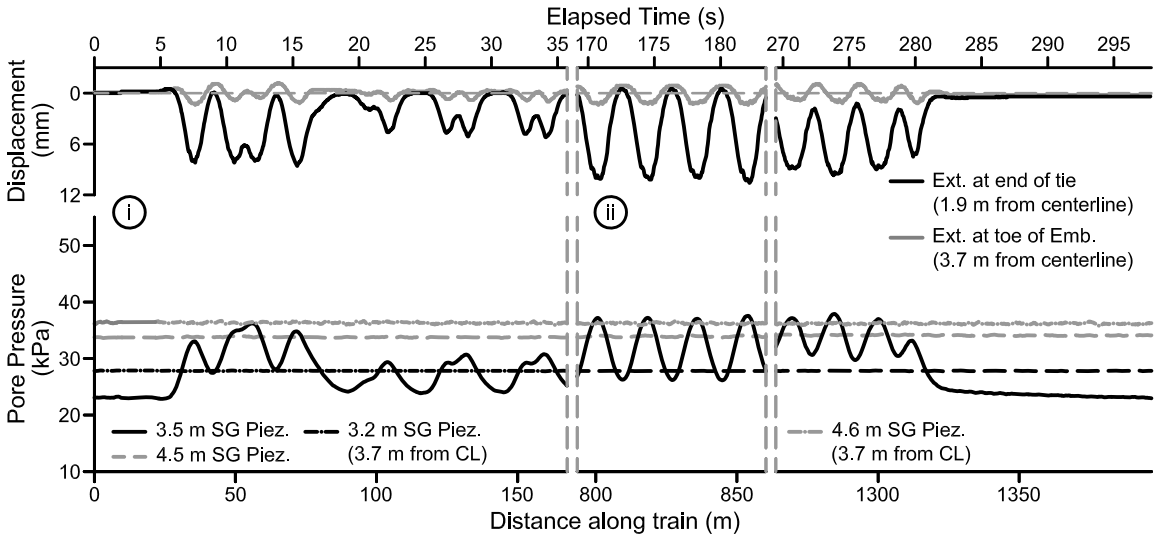

Figure B.10 Anzac data set 2, presenting (a) the vertical displacement measured by the extensometers, and (b) the pore pressure as measured by the piezometers during the passage of the train.

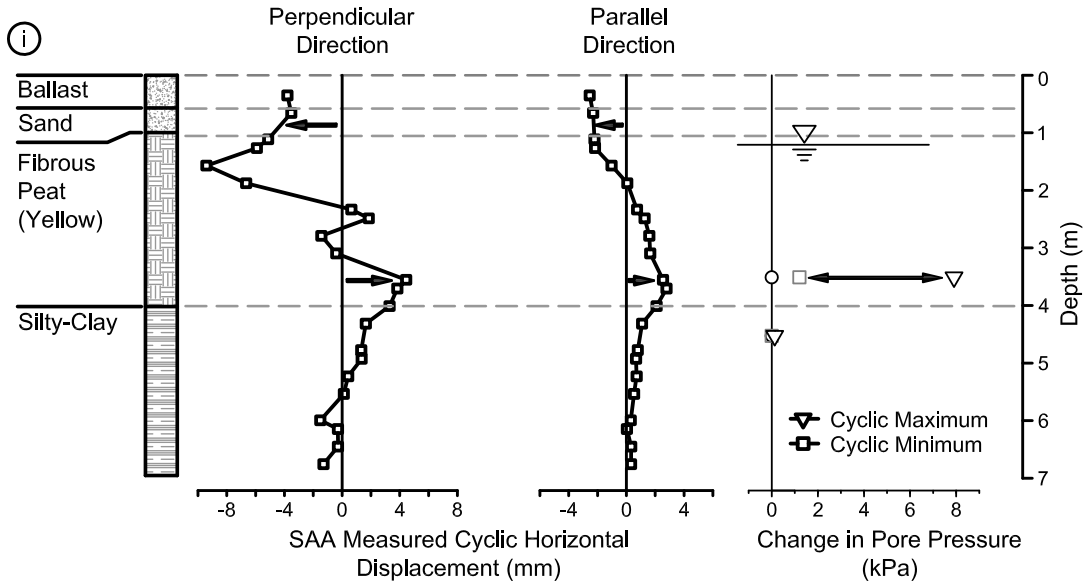

Figure B.11 Anzac data set 2, presenting the cyclic horizontal displacement measured by the SAA, and the cyclic change in pore pressure as measured by the piezometers with depth for the passage of the flatcars, near the tie.

Appendix B: Example data sets from field instrumentation

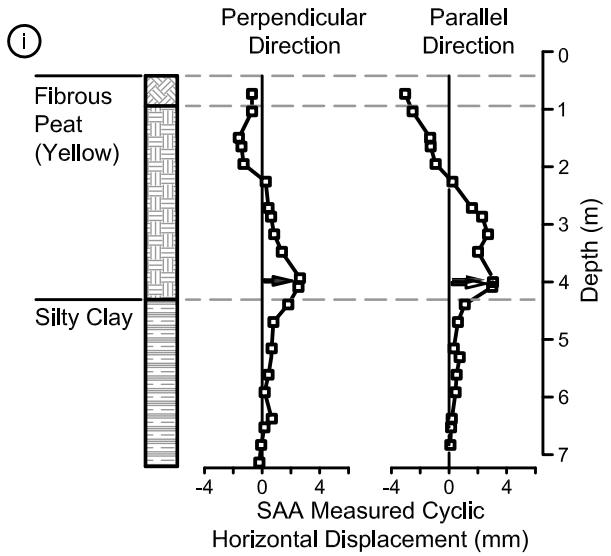

Figure B.12 Anzac data set 2, presenting the cyclic horizontal displacement measured by the SAA, and the cyclic change in pore pressure as measured by the piezometers with depth for the passage of the flatcars, at the toe of the embankment.

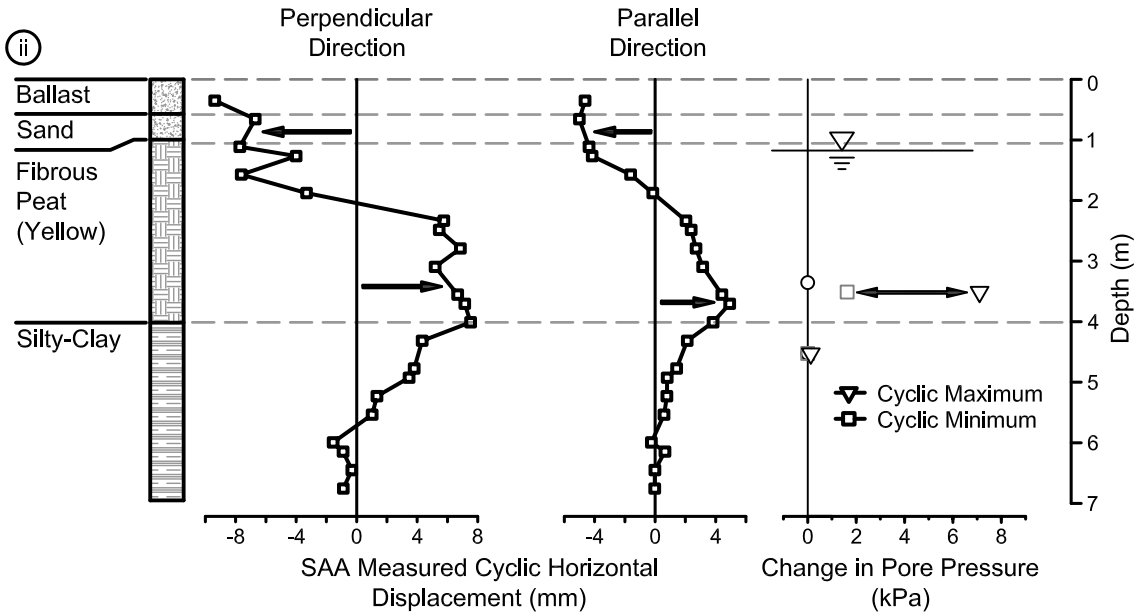

Figure B.13 Anzac data set 2, presenting the cyclic horizontal displacement measured by the SAA, and the cyclic change in pore pressure as measured by the piezometers with depth for the passage of the hopper cars, near the tie.

Appendix B: Example data sets from field instrumentation

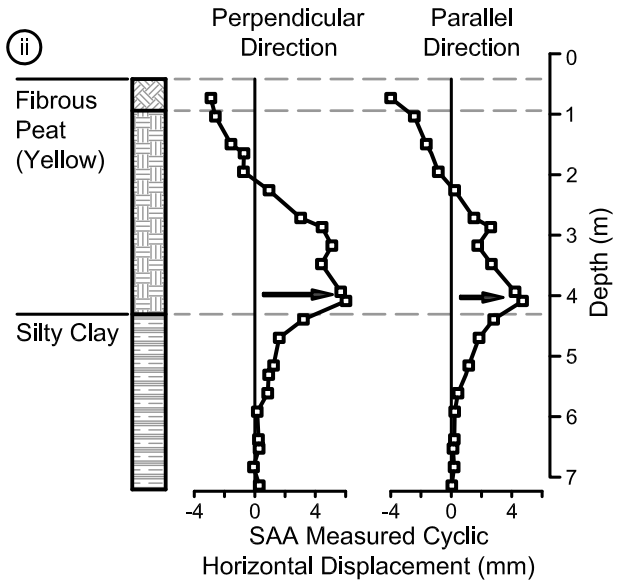

Figure B.14 Anzac data set 2, presenting the cyclic horizontal displacement measured by the SAA, and the cyclic change in pore pressure as measured by the piezometers with depth for the passage of the hopper cars, at the toe of the embankment.

Appendix B: Example data sets from field instrumentation

Data set: 3

Date of collection: August 11, 2009

Train type: Empty tankers

Length (number of cars): 85

Average train speed: 15 km/h (4.17 m/s)

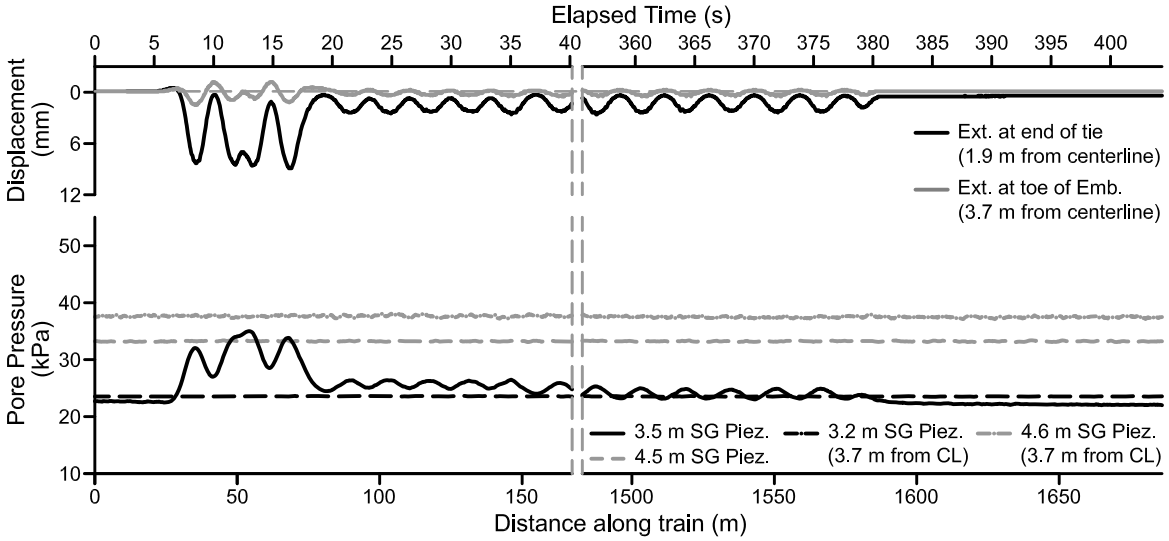

Figure B.15 Anzac data set 3, presenting (a) the vertical displacement measured by the extensometers, and (b) the pore pressure as measured by the piezometers during the passage of the train.

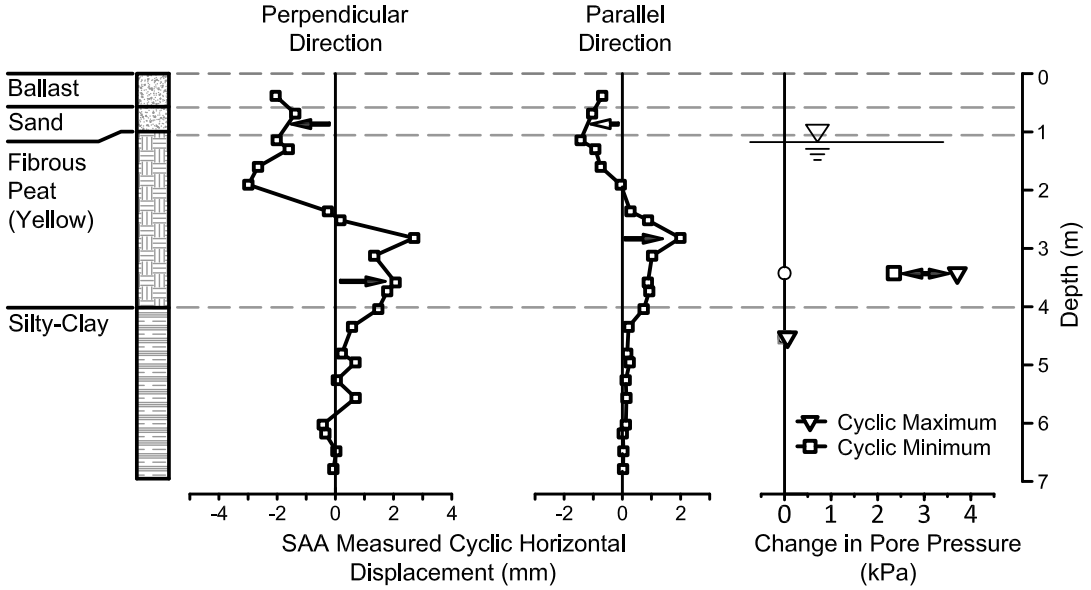

Figure B.16 Anzac data set 3, presenting the cyclic horizontal displacement measured by the SAA, and the cyclic change in pore pressure as measured by the piezometers with depth for the passage of empty tankers, near the tie.

Appendix B: Example data sets from field instrumentation

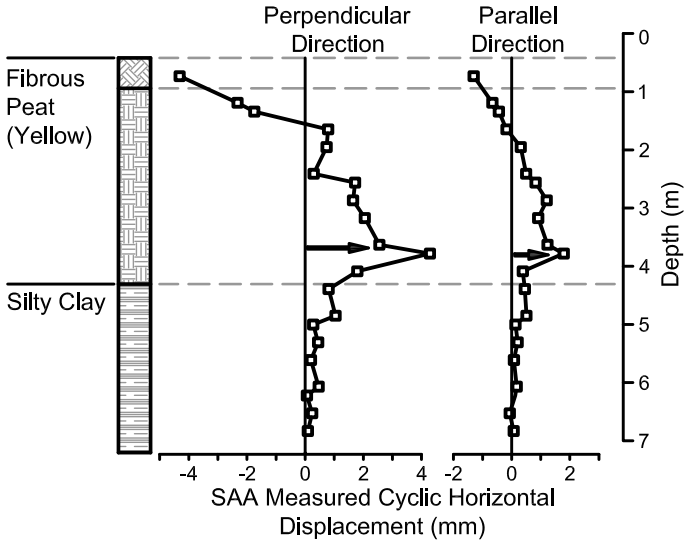

Figure B.17 Anzac data set 3, presenting the cyclic horizontal displacement measured by the SAA, and the cyclic change in pore pressure as measured by the piezometers with depth for the passage of the tankers, at the toe of the embankment.

Appendix B: Example data sets from field instrumentation

Lévis Subdivision mile 3.9

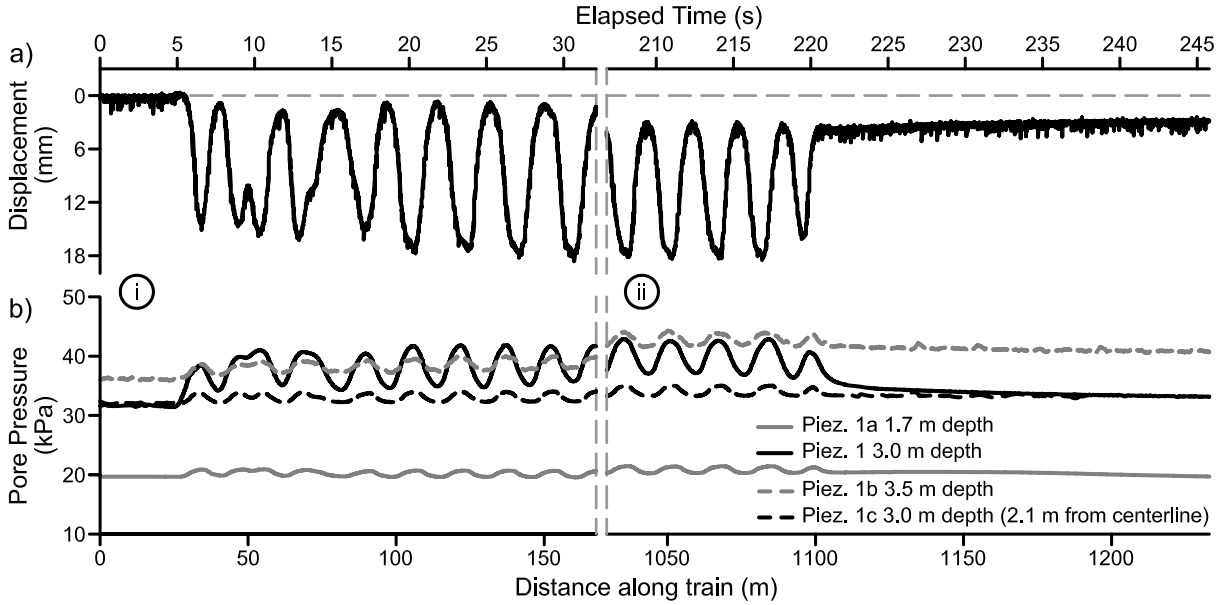

Figure B.18 Lévis data set, presenting (a) the vertical displacement measured by the extensometers, and (b) the pore pressure as measured by the piezometers during the passage of the train (after Konrad et al. 2006 & Konrad et al. 2007).

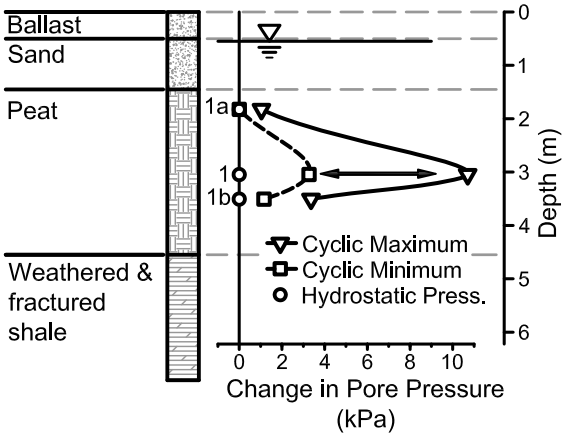

Figure B.19 Lévis data set the cyclic change in pore pressure as measured by the piezometers with depth for the passage of tankers (after Konrad et al. 2006 & Konrad et al. 2007).

Appendix B: Example data sets from field instrumentation

Rail Car Types

Rail car dimensions vary with manufacturer and production year. Both CN and CP own and operate large fleets of rail cars, customers also own and operate their own fleets. Thus, there is a large variety of rail car types with varying dimensions. This section presents a brief explanation of the types of cars referred to above and examples of the dimensions and loads.

Intermodal / Container Stack cars

These cars are designed to carry standard ocean freight containers is various stacking combinations. Different manufacturers provide different configurations; some sets of cars are linked together so that they share common trucks (groupings of axles). The weights of loaded intermodal cars are as varied as the containers they ship, the resulting axle loads and associated deformations from loaded intermodal cars vary greatly. An example of an intermodal car is the Greenbrier Husky-Stack 53' Container Car (Figure B.20): it has dimensions of 23.387 m between the couplers and 19.08 m between the truck centers; the loads are 22,906 kg (56.2 kN/axle) empty or a maximum of 99,790 kg (244.8 kN/axle).

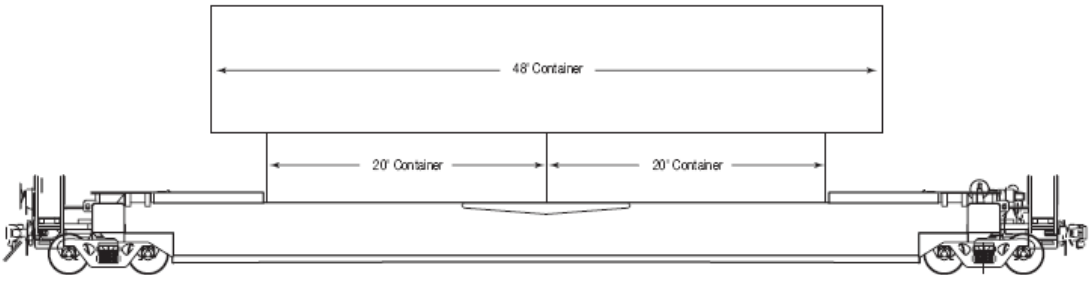

Figure B.20 Example of an intermodal or container stack car (GBRX 2011).

Flatcars

These cars are designed to carry all types of goods, typically oversized goods which must be loaded from the top or side; these can include heavy machinery and steel products. Modifications to the design of these types of cars are extremely varied and common ones include center beams to allow for the stacking of lumber and upright side beams to stack logs from forestry operations. The dimensions of flatcars vary widely, though they typically have trucks further away from the couplers than other types of rail cars. This results in deformation patters which show the effects of individual trucks. An example of a flat car is the Greenbrier Heavy Duty Flatcar (Figure B.21): it has dimensions of 27.59 m between the couplers and 20.12 m between the truck centers;

the loads are 27.216 kg (66.7 kN/axle) empty or a maximum of 129,727 kg (318.1 kN/axle) (GBRX 2011).

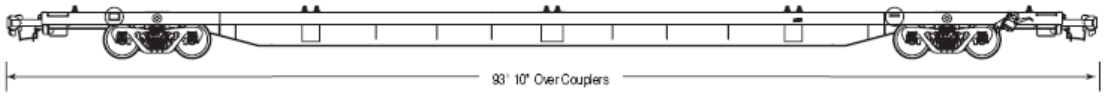

Figure B.21 Example of flatcar.

Tankers

Tankers are designed to carry bulk liquids; these often include refined gasoline, heating oil, alcohol, industrial chemicals, corn syrup and other foodstuffs. The designs of the cars vary, due to special designs for hazardous materials they may contain. An example of a Greenbrier gasoline tanker (Figure B.22): it has dimensions of 18.21 m between the couplers and 17.41 m between the truck centers; the loads are 29.801 kg (73.1 kN/axle) empty or a maximum of 119,295 kg (291.8 kN/axle) (GBRX 2011).

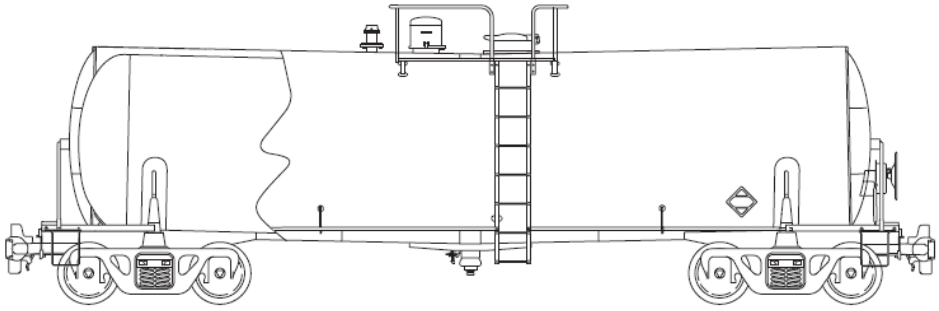

Figure B.22 Example of a tanker car (GBRX 2011).

Hopper Car

Hopper cars are designed to transport dry bulk goods. These cars typically grains, industrial minerals, plastic pellets, crushed rock, coal, gravel and sand. They are designed to allow for loading from the top of the car and unloading from the bottom. An example of a hopper car is the Greenbrier Covered Hopper for Grain Service (Figure B.23): it has dimensions of 17.68 m between the couplers and 16.11 m between the truck centers; the loads are 27,896 kg (68.4 kN/axle) empty or a maximum of 129, 727 kg (318.1 kN/axle).

Appendix B: Example data sets from field instrumentation

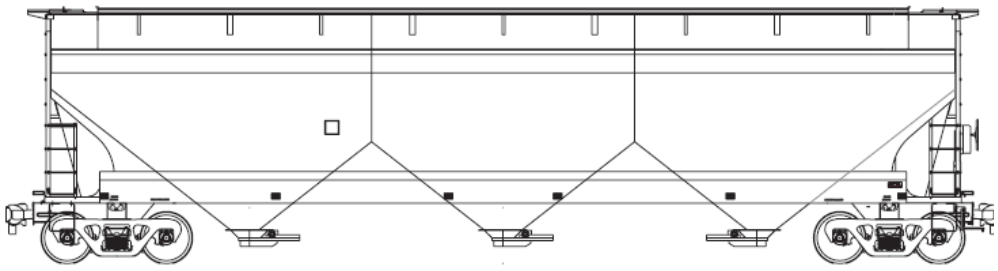

Figure B.23 Example of a hopper car (GBRX 2011).

References

Konrad, J-M. ., Grenier, S., and Garnier, P.2006. Heavy Axle Load over Muskeg Déraillement de l'Ultratrain a St-Henri-de-Lévis. Presentation at the 2006 Railway Ground Hazard Research Program annual workshop, Kingston, Ontario.

Konrad, J.-M., Grenier, S., and Garnier, P. 2007. Influence of Repeated Heavy Axle Loading on Peat Bearing Capacity. In 60th Canadian Geotechnical Conference. Ottawa, pp. 1551-1558.

The Greenbrier Companies (GBRX) 2011. on-line at http://gbrx.com/ [Accessed March 10, 2011]

Appendix C: Results from laboratory testing of peat specimens

This appendix provides a record of the data collected during the course of the laboratory testing of samples retrieved from the Edson and Anzac sites. The CU triaxial testing results for samples retrieved from the Lévis site is provided. This was produced from published data in Konrad et al. (2007) and is provided for comparison to the testing result of the peat from the other sites. For each type of peat tested there is a summary of the strength and stiffness properties determined from the testing, a full discussion of the laboratory data is presented in Chapters 4 and 5 (Manuscripts #2 and #3).

Appendix C: Results from laboratory testing of peat specimens

CU Testing of Remoulded Peat with a p'_0 of 11 kPa

One Dimensional Consolidation & Specimen Preparation

Initial specimen length:	130±3 mm
Mould diameter:	36mm
Applied axial load:	90 kPa
Consolidated length:	90.5 mm

CU Testing

Trimmed Specimen Length:	77.6 mm
Specimen diameter:	36 mm
Specimen mass:	89.9 g
Preconsolidation pressure (p'_0):	11 kPa
Initial Modulus (E_U):	798 kPa
◆ End of Linear Elasticity (p', q):	10.9, 31.1 kPa
Pore pressure parameter a:	-0.023
✖ Fibre Reinforced Critical State (p', q):	80.8, 139 kPa
Critical State Strain Hardening Modulus:	17.3 kPa
● Frictional Critical State (q):	34.0 kPa

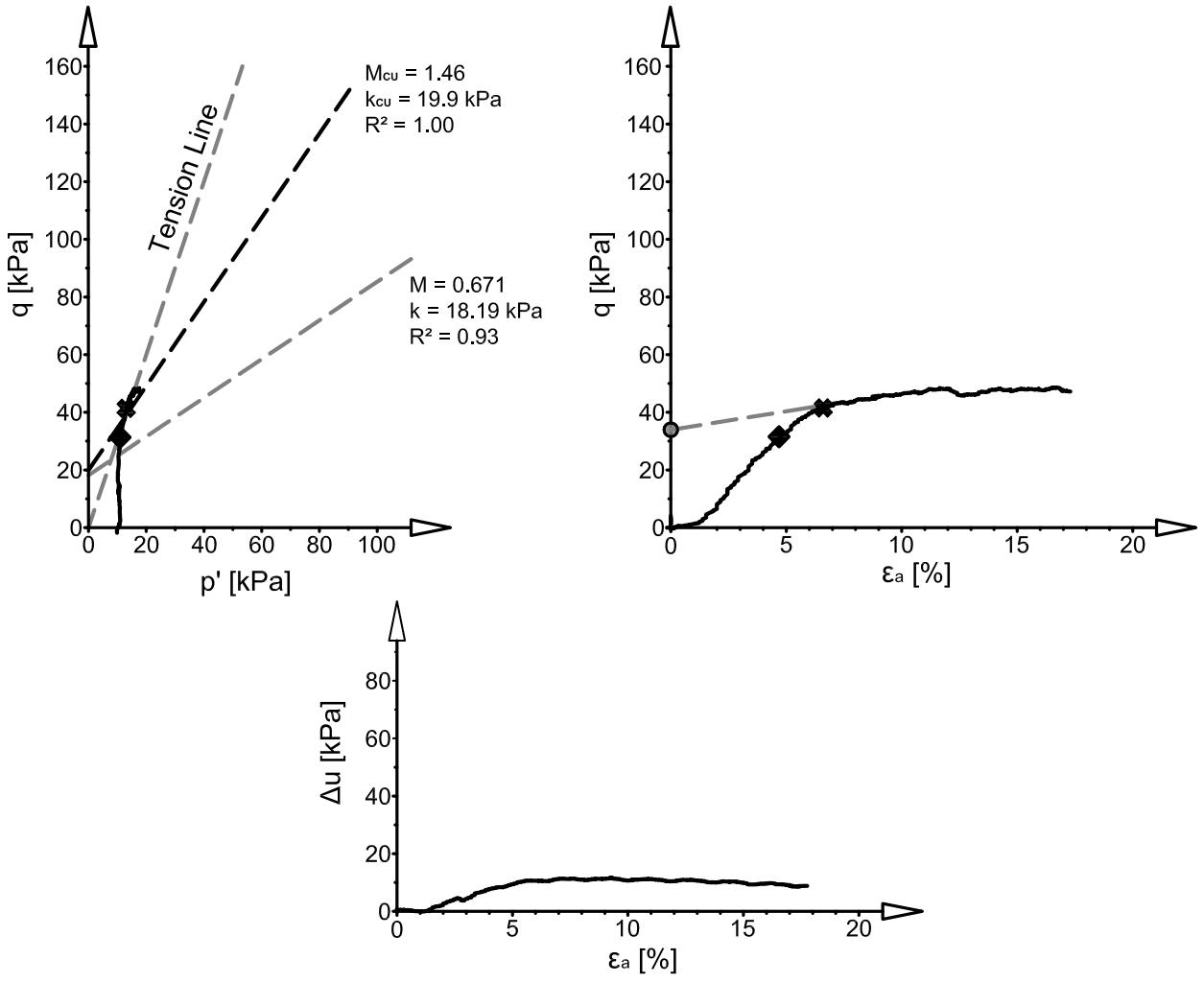

Appendix C: Results from laboratory testing of peat specimens

CU Testing of Remoulded Peat with a p'_0 of 25 kPa

One Dimensional Consolidation & Specimen Preparation

Initial specimen length:	NA
Mould diameter:	36mm
Applied axial load:	90 kPa
Consolidated length:	70.3 mm

CU Testing

Trimmed Specimen Length:	70.3 mm
Specimen diameter:	36 mm
Specimen mass:	85.6 g
Preconsolidation pressure (p'_0):	25 kPa
Initial Modulus (E_U):	1560 kPa
◆ End of Linear Elasticity (p', q):	23.6, 34.3 kPa
Pore pressure parameter a:	0.029
✖ Fibre Reinforced Critical State (p', q):	23.2, 53.0 kPa
Critical State Strain Hardening Modulus:	153 kPa
● Frictional Critical State (q):	45.0 kPa

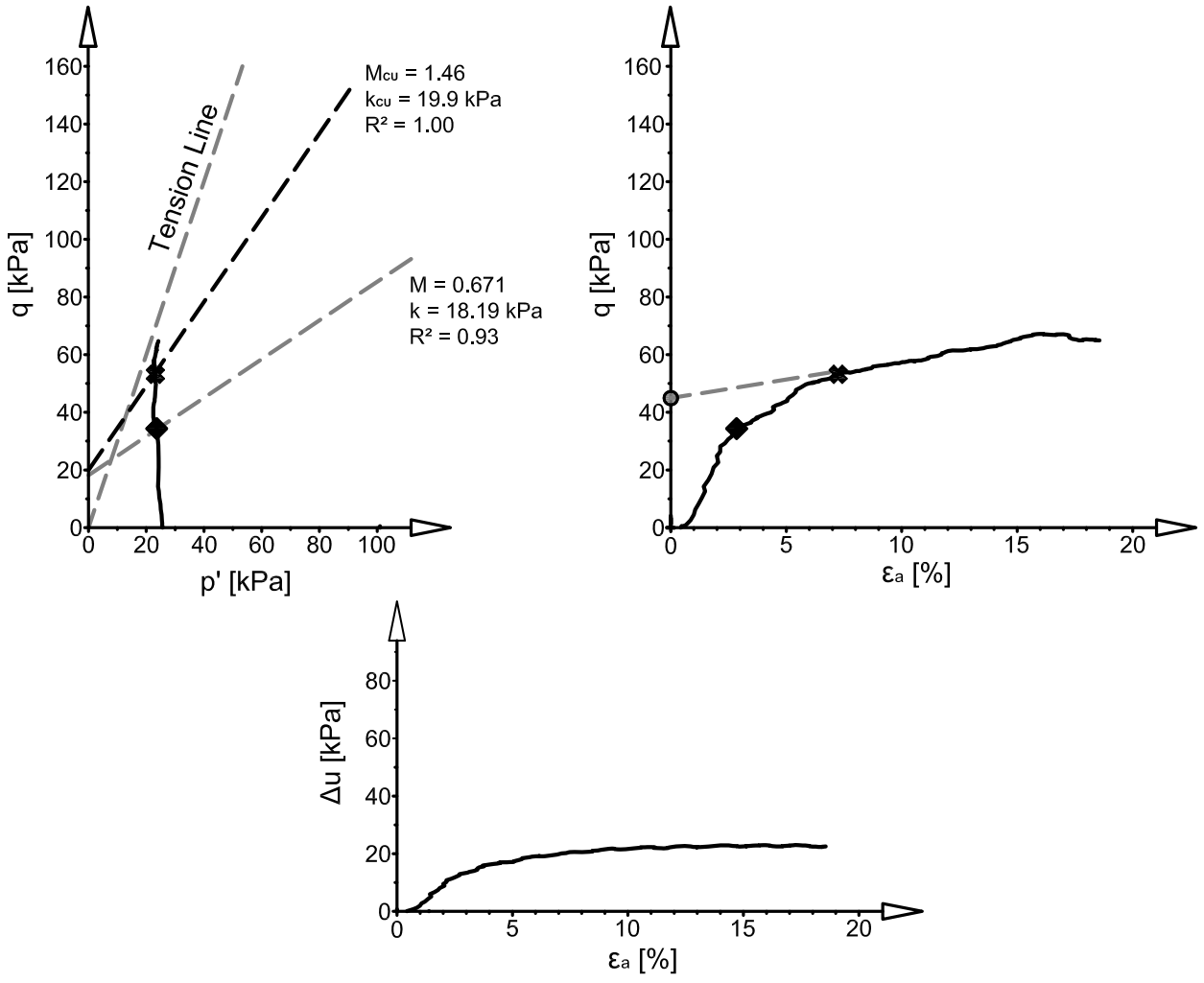

Appendix C: Results from laboratory testing of peat specimens

CU Testing of Remoulded Peat with a p'_0 of 47 kPa

One Dimensional Consolidation & Specimen Preparation

Initial specimen length:	130±3 mm
Mould diameter:	36mm
Applied axial load:	90 kPa
Consolidated length:	94.6 mm

CU Testing

Trimmed Specimen Length:	77.6 mm
Specimen diameter:	36 mm
Specimen mass:	37.4 g
Preconsolidation pressure (p'_0):	47 kPa
Initial Modulus (E_U):	2020 kPa
◆ End of Linear Elasticity (p', q):	44.8, 41.5 kPa
Pore pressure parameter a:	0.146
✖ Fibre Reinforced Critical State (p', q):	39.8, 74.9 kPa
Critical State Strain Hardening Modulus:	-13.5 kPa
● Frictional Critical State (q):	74.0 kPa

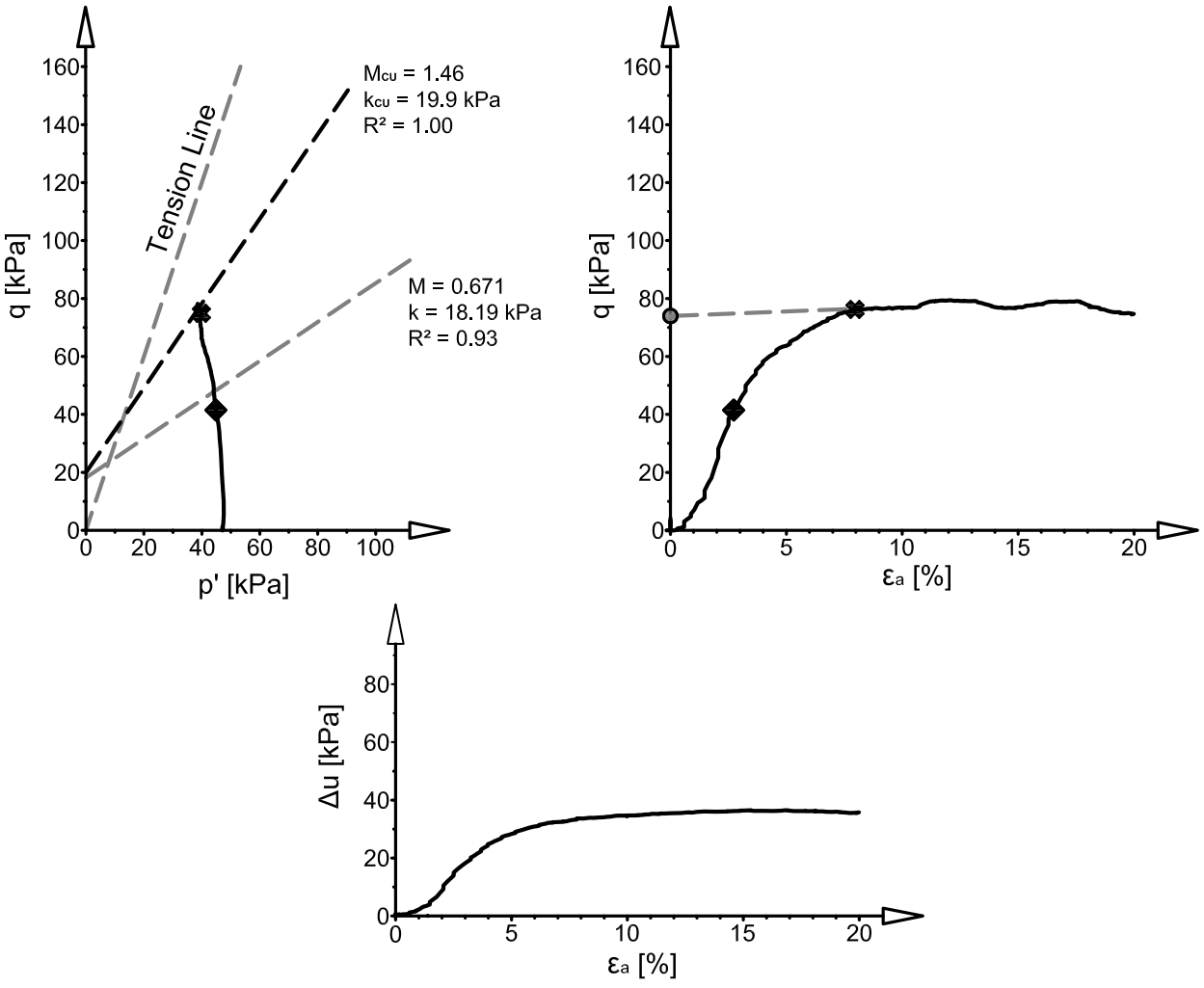

Appendix C: Results from laboratory testing of peat specimens

CU Testing of Remoulded Peat with a p'_0 of 75 kPa

One Dimensional Consolidation & Specimen Preparation

Initial specimen length:	130±3 mm
Mould diameter:	36mm
Applied axial load:	90 kPa
Consolidated length:	96.0 mm

CU Testing

Trimmed Specimen Length:	76.1 mm
Specimen diameter:	36 mm
Specimen mass:	88.5 g
Preconsolidation pressure (p'_0):	75 kPa
Initial Modulus (E_U):	2450 kPa
◆ End of Linear Elasticity (p', q):	69.9, 58.8 kPa
Pore pressure parameter a:	0.234
✖ Fibre Reinforced Critical State (p', q):	50.0, 106 kPa
Critical State Strain Hardening Modulus:	39.6 kPa
● Frictional Critical State (q):	103 kPA

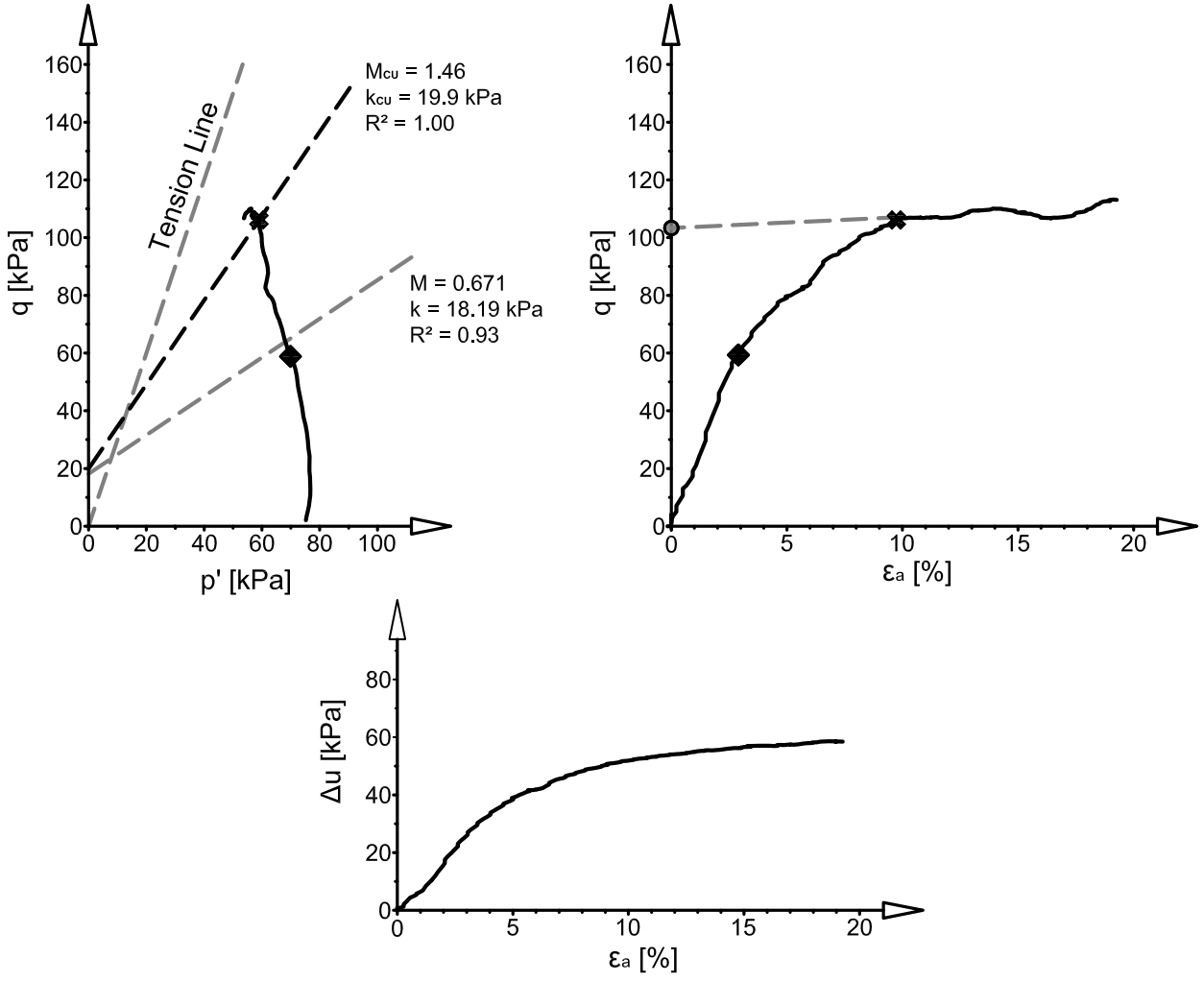

Appendix C: Results from laboratory testing of peat specimens

CU Testing of Remoulded Peat with a p'_0 of 101 kPa

One Dimensional Consolidation & Specimen Preparation

Initial specimen length:	130±3 mm
Mould diameter:	36mm
Applied axial load:	90 kPa
Consolidated length:	96.7 mm

CU Testing

Trimmed Specimen Length:	79.8 mm
Specimen diameter:	36 mm
Specimen mass:	92.3 g
Preconsolidation pressure (p'_0):	101 kPa
Initial Modulus (E_U):	3770 kPa
◆ End of Linear Elasticity (p', q):	96.7, 90.0 kPa
Pore pressure parameter a:	0.249
✖ Fibre Reinforced Critical State (p', q):	80.8, 139 kPa
Critical State Strain Hardening Modulus:	126 kPa
● Frictional Critical State (q):	128 kPa

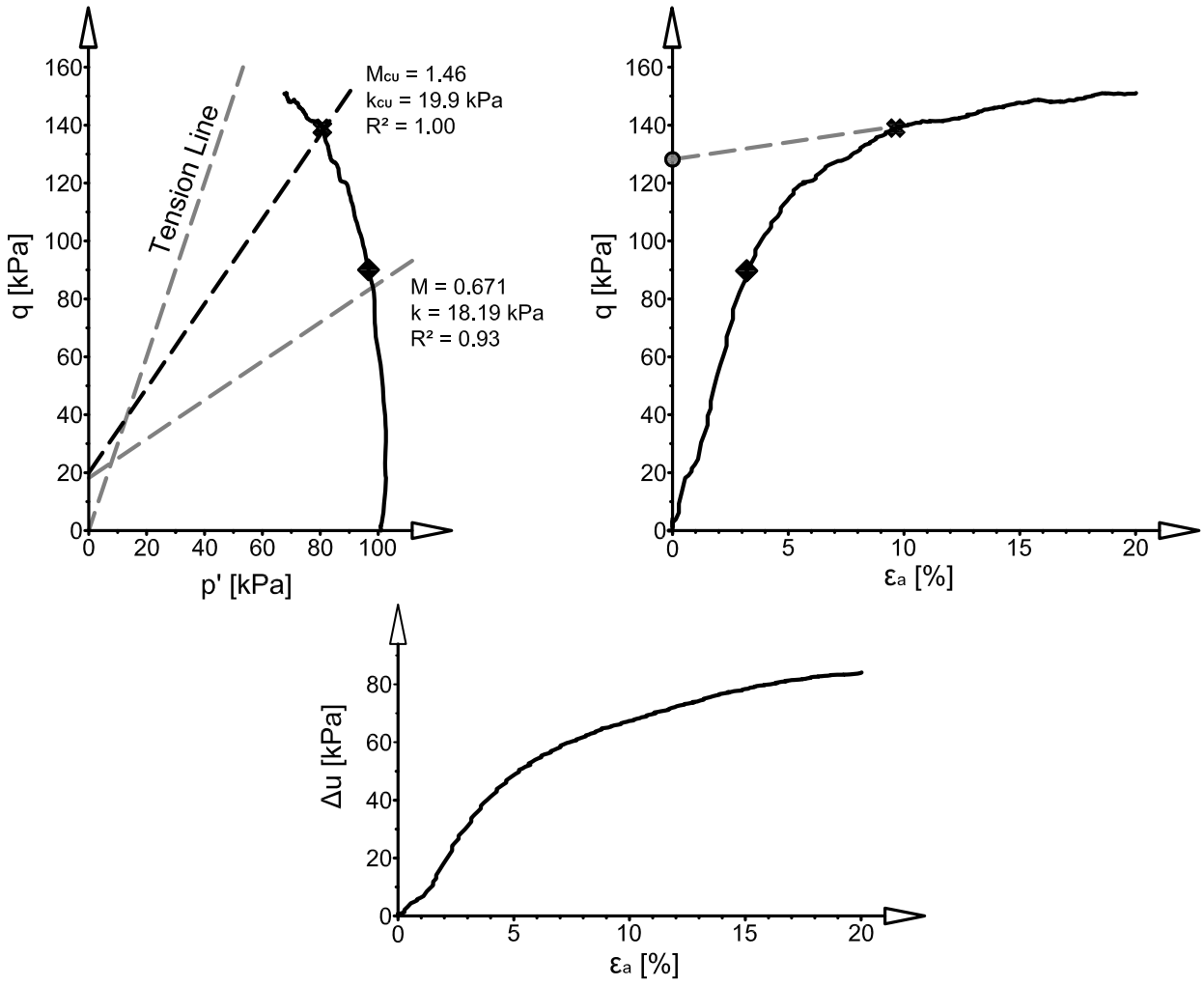

Appendix C: Results from laboratory testing of peat specimens

Summary of CU Testing of Remoulded Peat

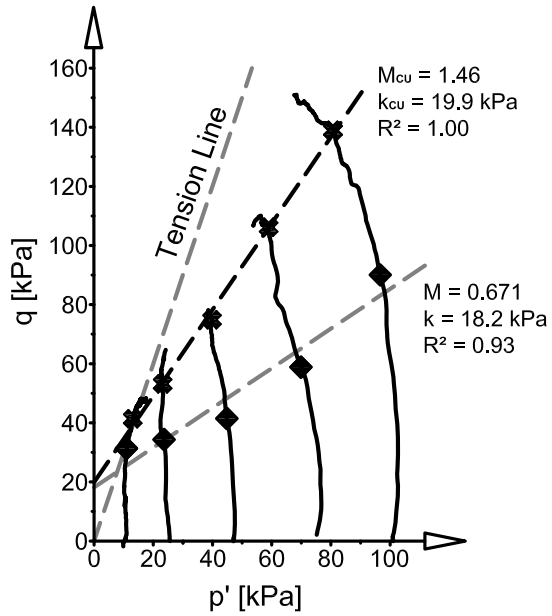

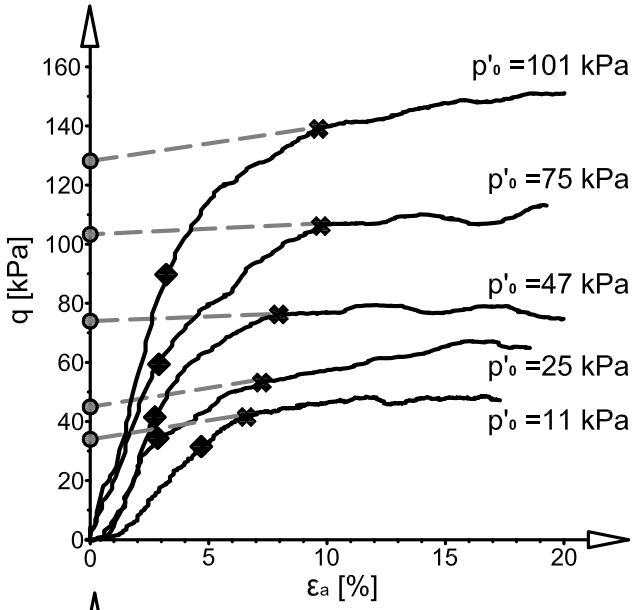

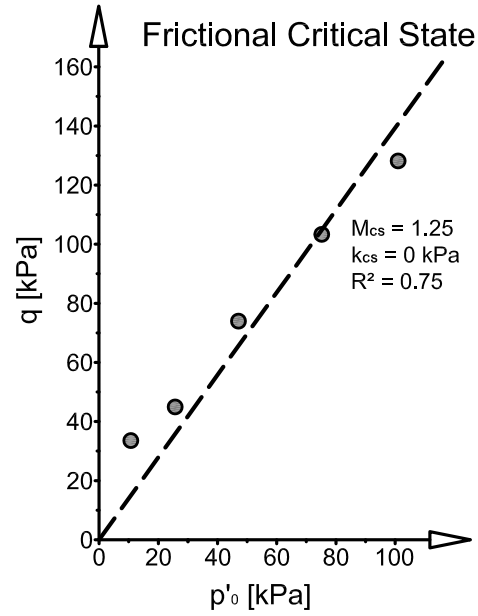

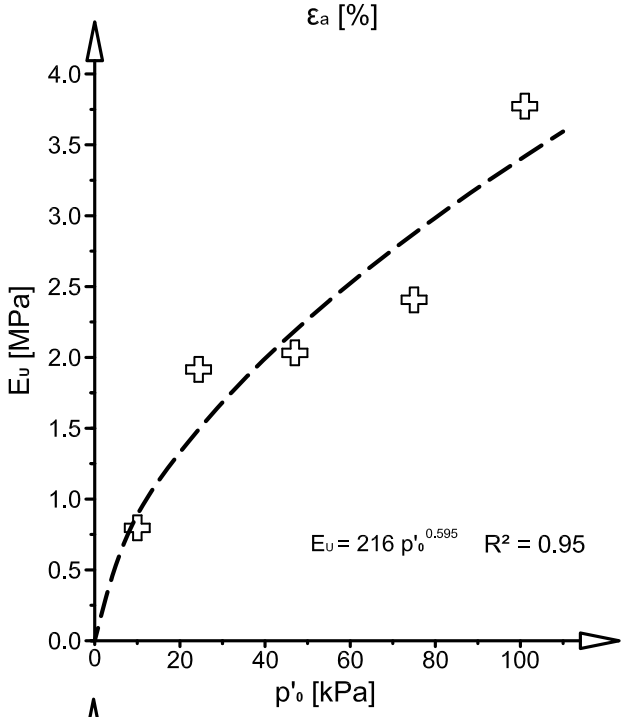

Reinforced Strength	Frictional Strength	End of Linear Elasticity
Mcu : 1.46	Mcs : 1.25	M : 0.67
kcu : 19.9 kPa	kcs : 0.0 kPa	k : 18.2 kPa
Φ'cu : 36°	Φ'cs : 31°	Φ' : 18°
c'cu : 9.89 kPa	c'cs : 0.0 kPa	c' : 8.58 kPa

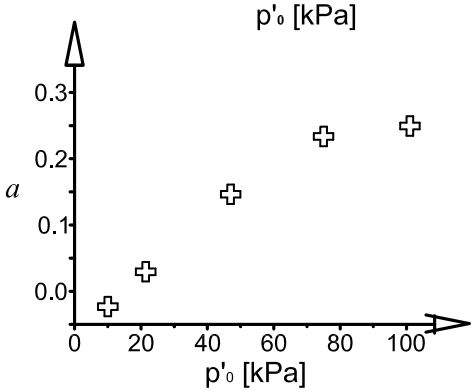

Summary of DS Testing of Remoulded Peat

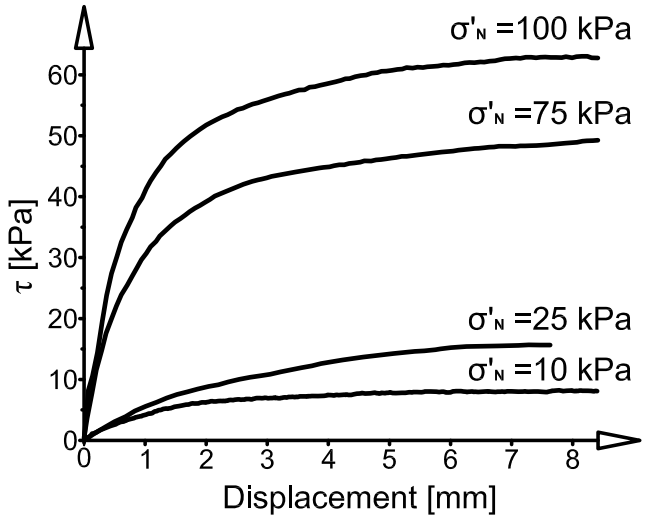

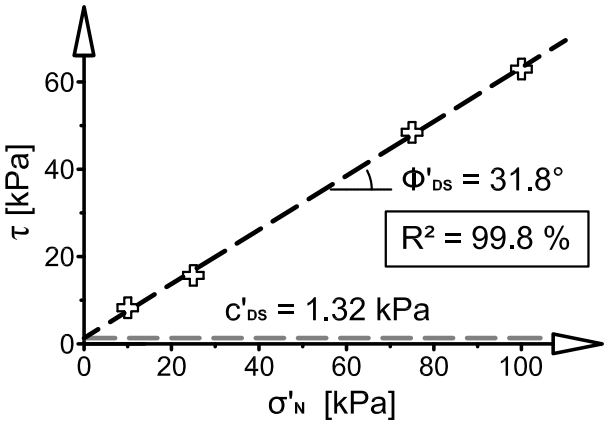

CU Testing of Remoulded Peat Fibre with a p'$_0$ of 11 kPa

One Dimensional Consolidation & Specimen Preparation

Initial specimen length:	130±3 mm
Mould diameter:	36mm
Applied axial load:	90 kPa
Consolidated length:	66.8 mm

CU Testing

Trimmed Specimen Length:	66.8 mm
Specimen diameter:	36 mm
Specimen mass:	78.8 g
Preconsolidation pressure (p'$_0$):	11.0 kPa
Initial Modulus (E$_U$):	1280 kPa
◆ End of Linear Elasticity (p', q):	12.4, 32.8 kPa
Pore pressure parameter a:	0.052
✖ Fibre Reinforced Critical State (p', q):	14.8, 43.3 kPa
Critical State Strain Hardening Modulus:	101 kPa
● Frictional Critical State (q):	40.0 kPa

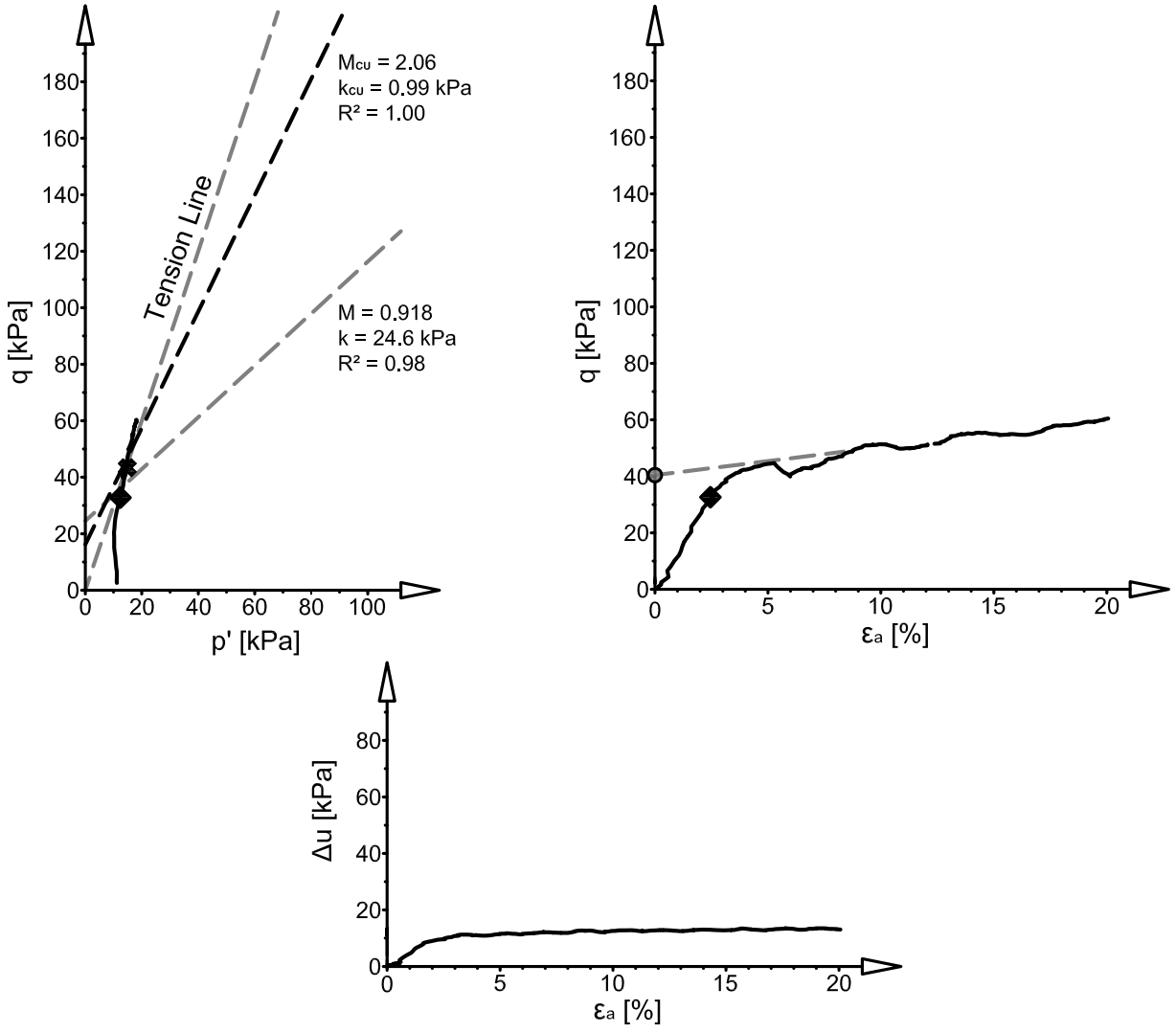

Appendix C: Results from laboratory testing of peat specimens

CU Testing of Remoulded Peat Fibre with a p'_0 of 25 kPa

One Dimensional Consolidation & Specimen Preparation

Initial specimen length:	130±3 mm
Mould diameter:	36mm
Applied axial load:	90 kPa
Consolidated length:	70.3 mm

CU Testing

Trimmed Specimen Length:	70.3 mm
Specimen diameter:	36 mm
Specimen mass:	86.4 g
Preconsolidation pressure (p'_0):	25.0 kPa
Initial Modulus (E_U):	1510 kPa
◆ End of Linear Elasticity (p', q):	22.8, 45.6 kPa
Pore pressure parameter a:	0.102
✖ Fibre Reinforced Critical State (p', q):	19.7, 56.6 kPa
Critical State Strain Hardening Modulus:	237 kPa
● Frictional Critical State (p', q):	46.0 kPa

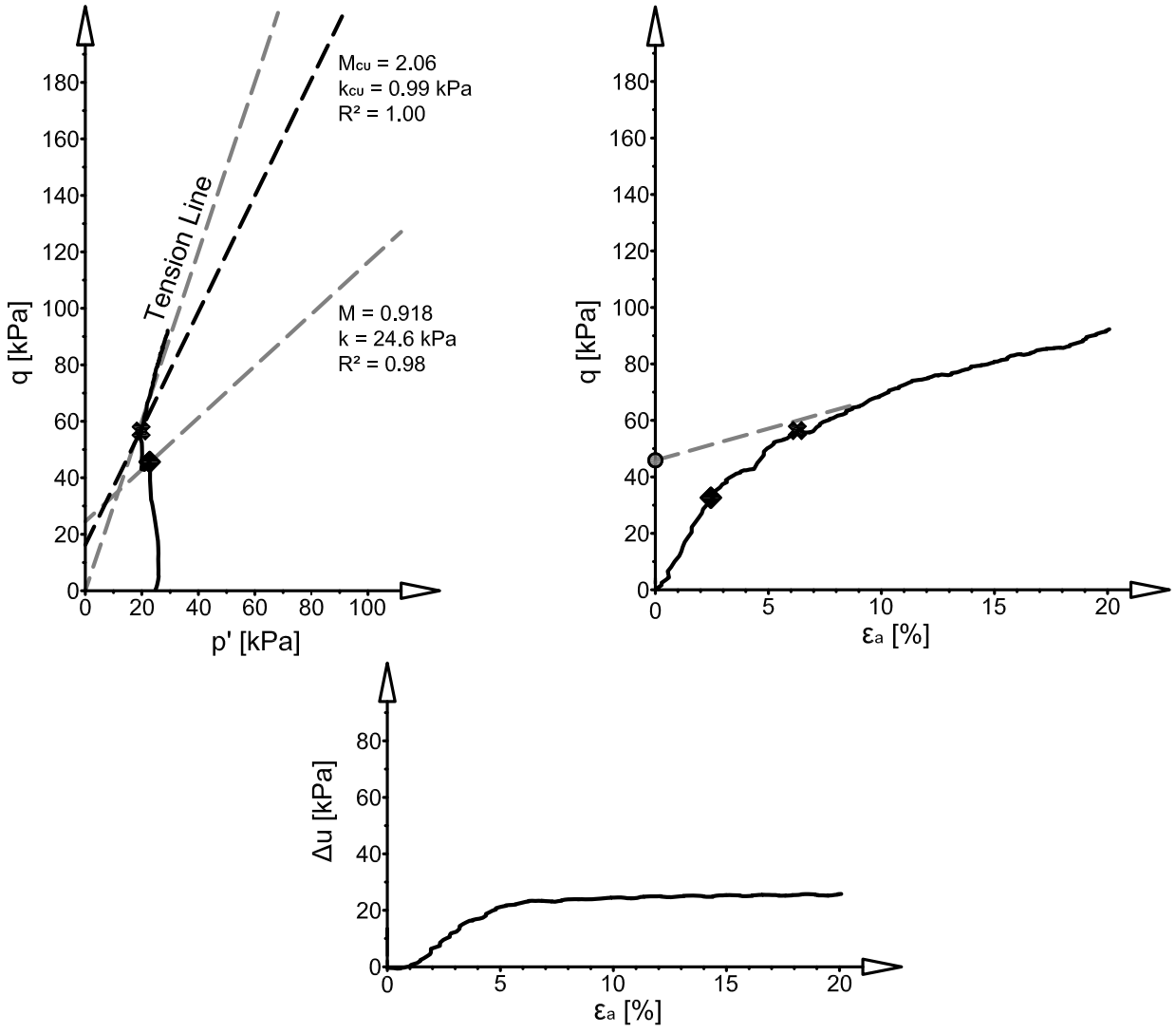

Appendix C: Results from laboratory testing of peat specimens

CU Testing of Remoulded Peat Fibre with a p'_0 of 47 kPa

One Dimensional Consolidation & Specimen Preparation

Initial specimen length:	130±3 mm
Mould diameter:	36mm
Applied axial load:	90 kPa
Consolidated length:	76.3 mm

CU Testing

Trimmed Specimen Length:	76.3 mm
Specimen diameter:	36 mm
Specimen mass:	90.1 g
Preconsolidation pressure (p'_0):	46.7 kPa
Initial Modulus (E_U):	2590 kPa
◆ End of Linear Elasticity (p', q):	42.5, 68.0 kPa
Pore pressure parameter a:	0.131
✖ Fibre Reinforced Critical State (p', q):	41.2, 105 kPa
Critical State Strain Hardening Modulus:	354
● Frictional Critical State (p', q):	81.0 kPa

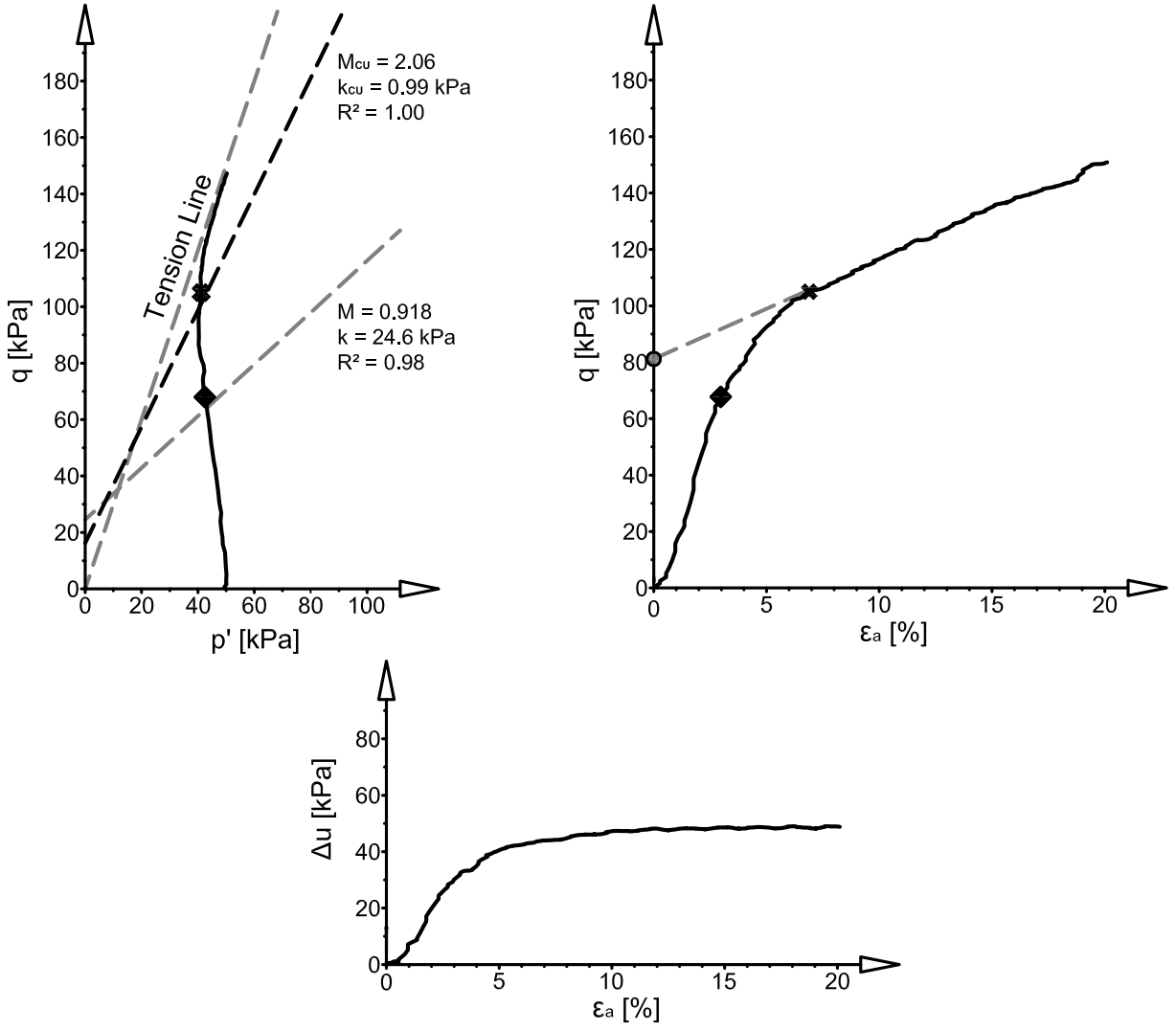

Appendix C: Results from laboratory testing of peat specimens

CU Testing of Remoulded Peat Fibre with a p'_0 of 76 kPa

One Dimensional Consolidation & Specimen Preparation

Initial specimen length:	130±3 mm
Mould diameter:	36mm
Applied axial load:	90 kPa
Consolidated length:	66.7 mm

CU Testing

Trimmed Specimen Length:	66.7 mm
Specimen diameter:	36 mm
Specimen mass:	78.9 g
Preconsolidation pressure (p'_0):	80.0 kPa
Initial Modulus (E_U):	3680 kPa
◆ End of Linear Elasticity (p', q):	58.7, 80.2 kPa
Pore pressure parameter a:	0.200
✖ Fibre Reinforced Critical State (p', q):	50.7, 125 kPa
Critical State Strain Hardening Modulus:	344 kPa
● Frictional Critical State (p', q):	99.0 kPa

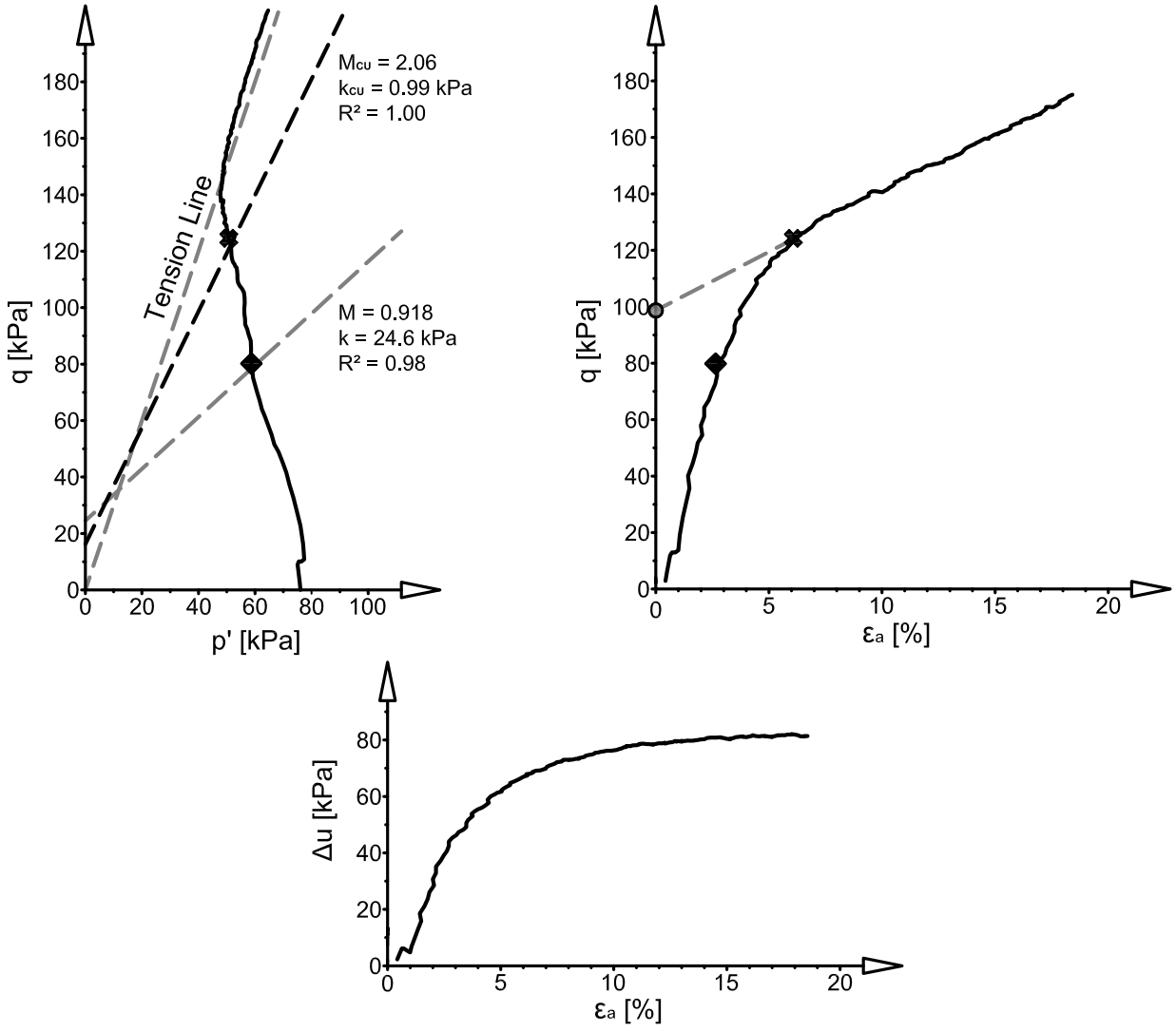

Appendix C: Results from laboratory testing of peat specimens

CU Testing of Remoulded Peat Fibre with a p'_0 of 94 kPa

One Dimensional Consolidation & Specimen Preparation

Initial specimen length:	130±3 mm
Mould diameter:	36mm
Applied axial load:	90 kPa
Consolidated length:	67.9 mm

CU Testing

Trimmed Specimen Length:	67.9 mm
Specimen diameter:	36 mm
Specimen mass:	79.9 g
Preconsolidation pressure (p'_0):	94.0 kPa
Initial Modulus (E_U):	4040 kPa
◆ End of Linear Elasticity (p', q):	81.0, 95.8 kPa
Pore pressure parameter a:	0.167
✖ Fibre Reinforced Critical State (p', q):	69.3, 154 kPa
Critical State Strain Hardening Modulus:	337 kPa
● Frictional Critical State (p', q):	138 kPa

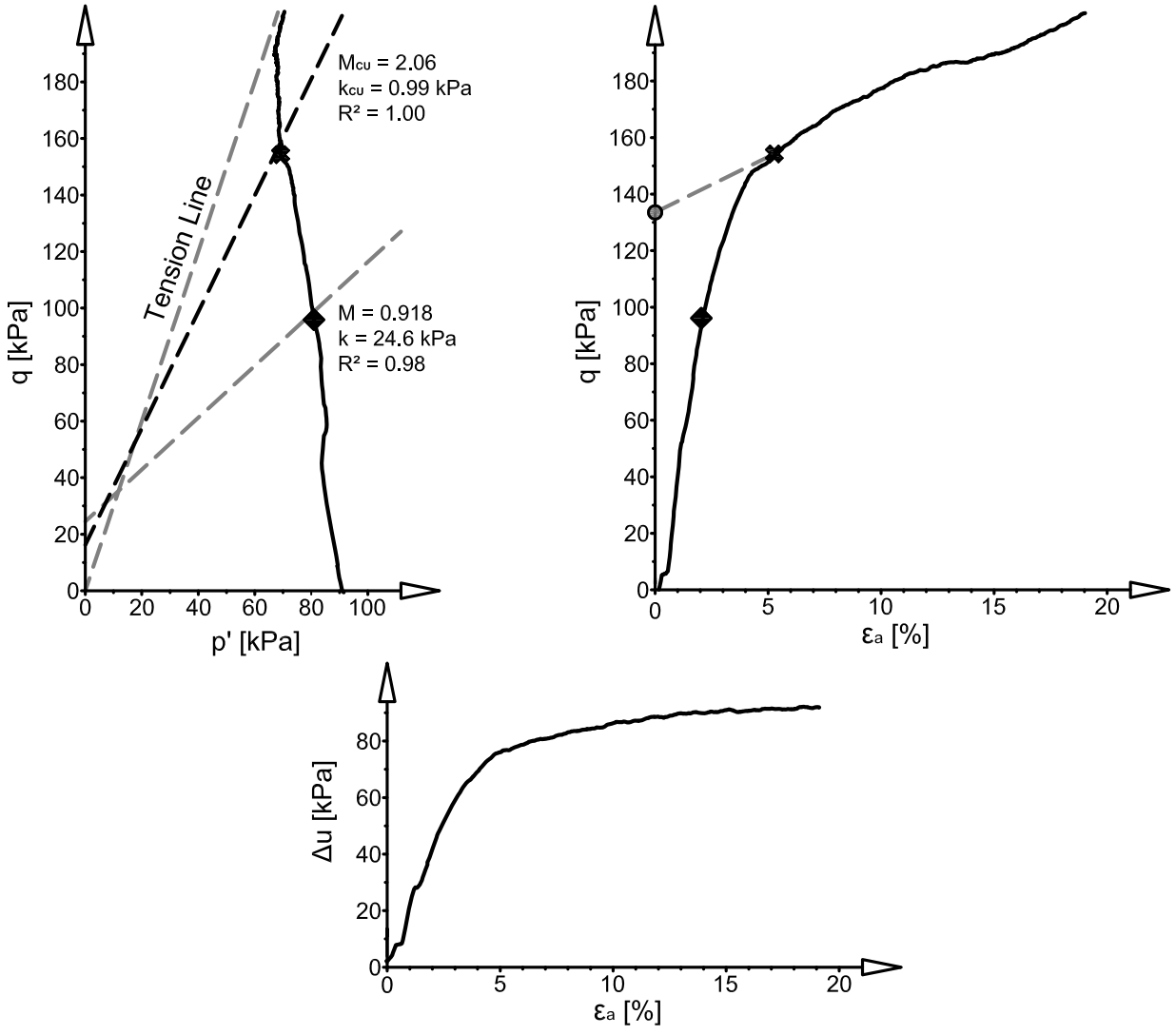

Summary of CU Testing of Remoulded Peat Fibre

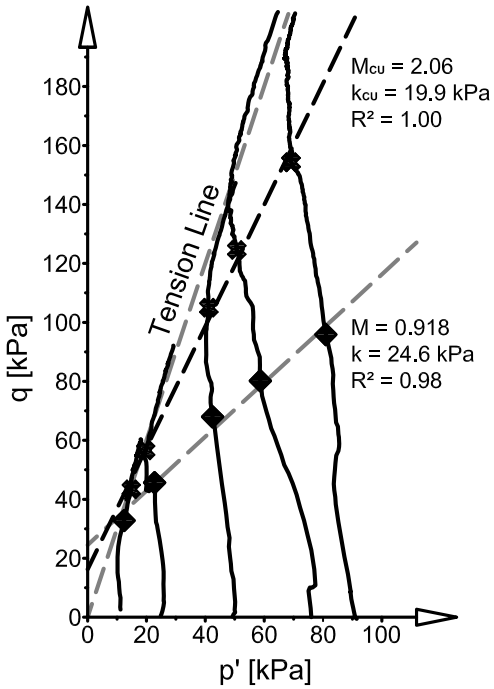

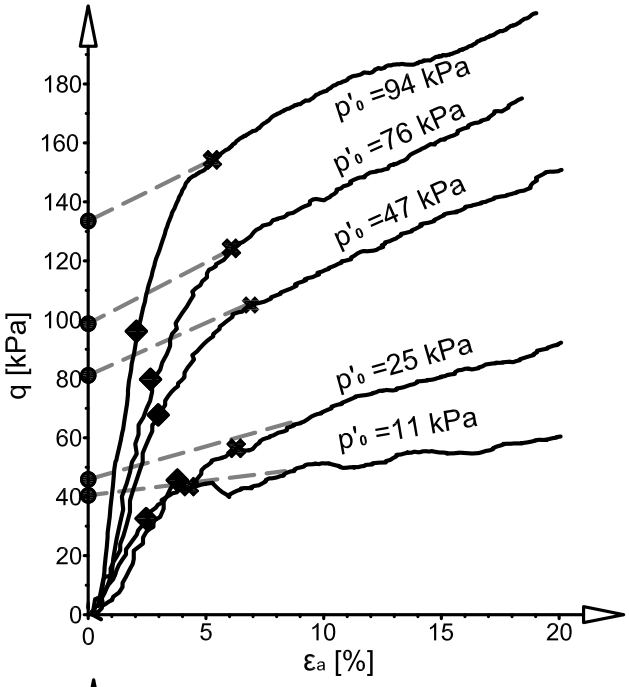

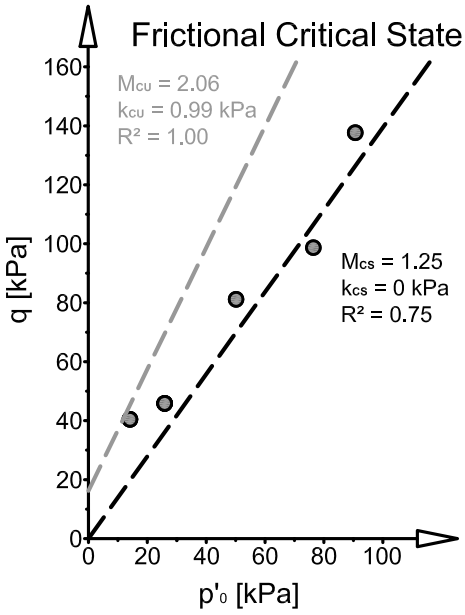

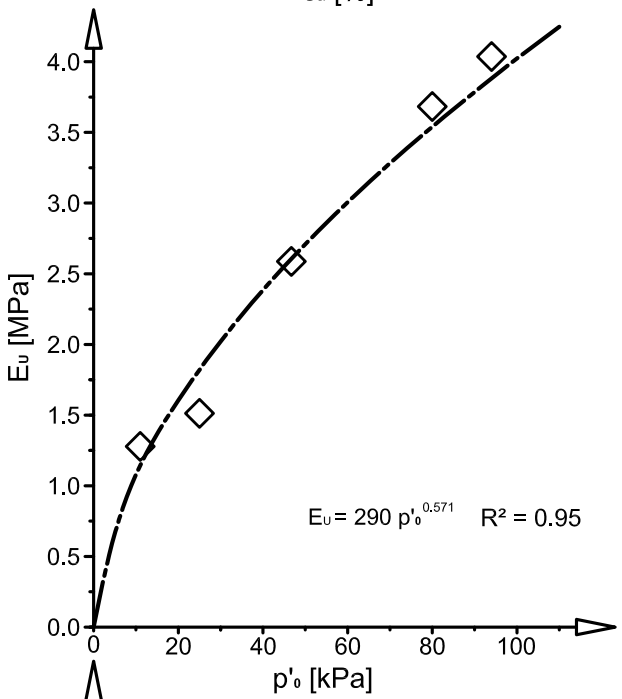

Reinforced Strength	Frictional Strength	End of Linear Elasticity
M_{cu} : 2.06	M_{cs} : 1.25	M : 0.918
k_{cu} : 19.9 kPa	k_{cs} : 0.0 kPa	k : 24.6 kPa
Φ'_{cu} : 50°	Φ'_{cs} : 31°	Φ' : 23°
c'_{cu} : 11.5 kPa	c'_{cs} : 0.0 kPa	c' : 11.6 kPa

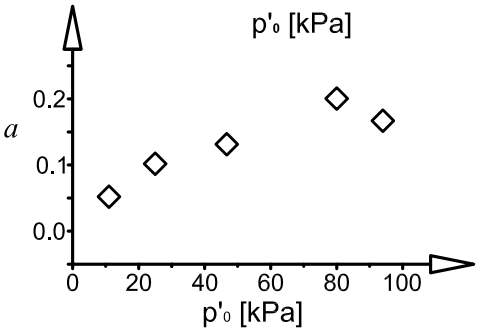

Summary of DS Testing of Remoulded Peat Fibre

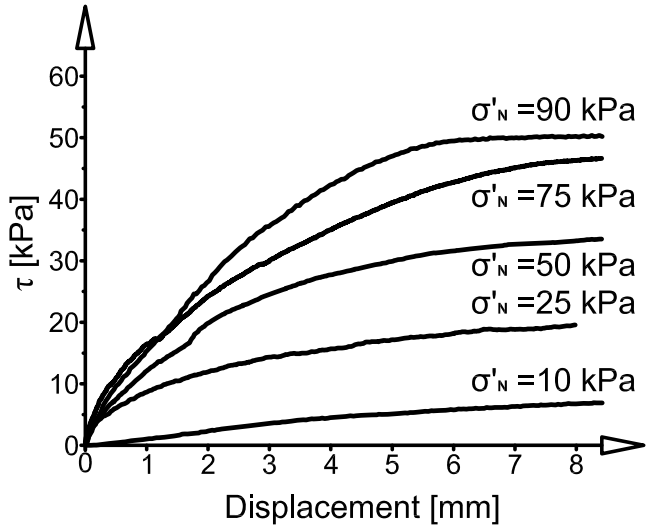

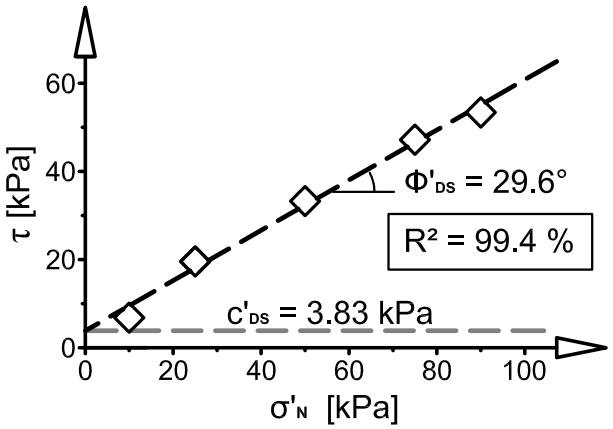

CU Testing of Edson Shelby Specimen with a p'$_0$ of 24 kPa

CU Testing

Sample source:	Bore hole 8; 3 m depth
Trimmed Specimen Length:	159 mm
Specimen diameter:	70.0 mm
Specimen mass:	603 mm
Preconsolidation pressure (p'$_0$):	24 kPa
Initial Modulus (E_U):	2030 kPa
◆ End of Linear Elasticity (p', q):	19.5, 17.6 kPa
Pore pressure parameter a:	0.243
✖ Fibre Reinforced Critical State (p', q):	17.0, 36.4 kPa
Critical State Strain Hardening Modulus:	147 kPa
● Frictional Critical State (q):	32.0 kPa

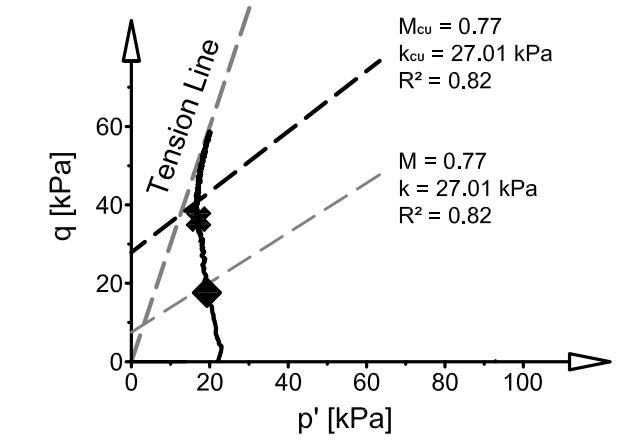

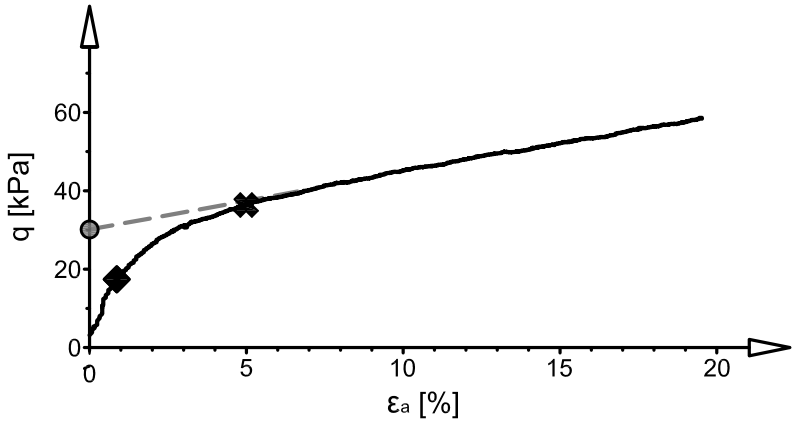

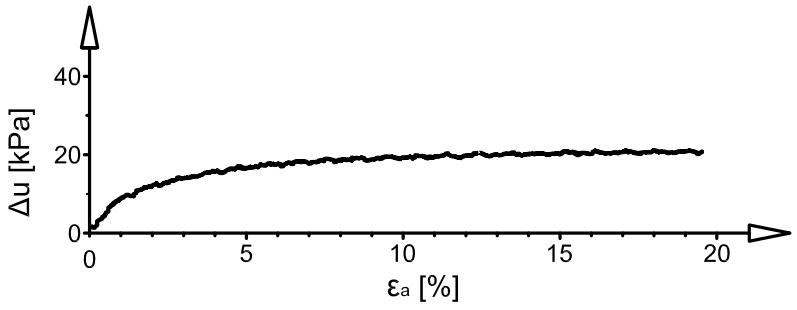

CU Testing of Edson Shelby Specimen with a p'_0 of 47 kPa

CU Testing

Sample source:	Bore hole 8; 3 m depth
Trimmed Specimen Length:	165 mm
Specimen diameter:	71.7 mm
Specimen mass:	658 g
Preconsolidation pressure (p'_0):	47.3 kPa
Initial Modulus (E_U):	2330 kPa
◆ End of Linear Elasticity (p', q):	19.5, 17.6 kPa
Pore pressure parameter a:	0.326
✖ Fibre Reinforced Critical State (p', q):	17.0, 36.4 kPa
Critical State Strain Hardening Modulus:	66.6 kPa
○ Frictional Critical State (q):	49.0 kPa

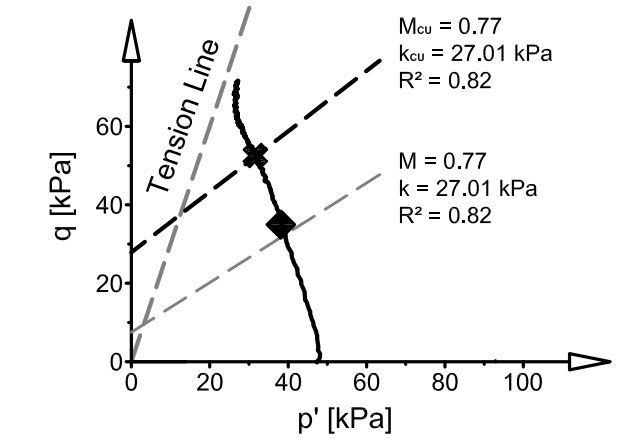

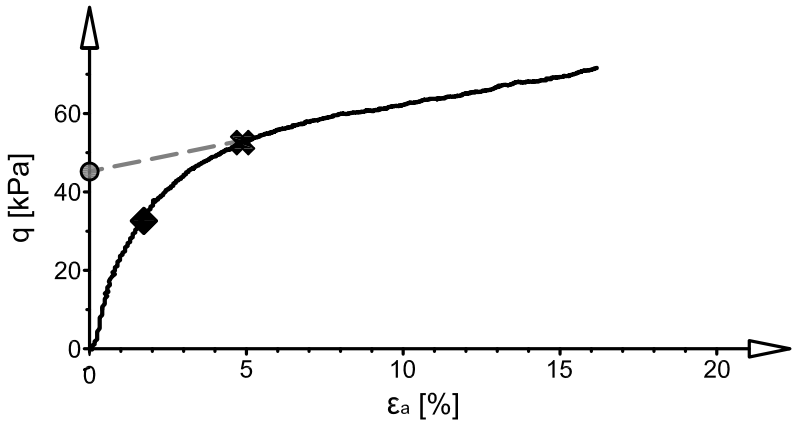

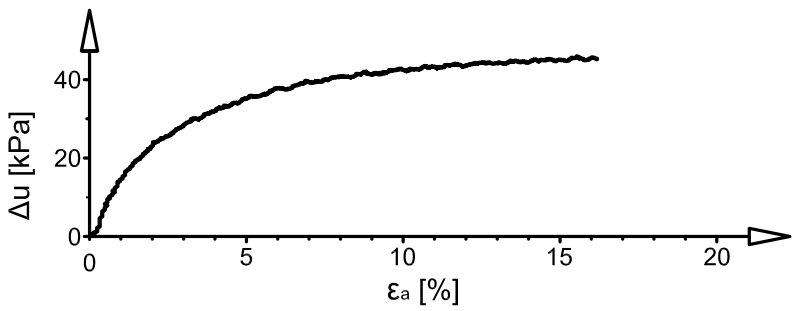

CU Testing of Edson Shelby Specimen with a p'_0 of 49 kPa

CU Testing

Sample source:	Bore hole 8; 4.6 depth
Trimmed Specimen Length:	130 mm
Specimen diameter:	68.8 mm
Specimen mass:	460 mm
Preconsolidation pressure (p'_0):	48.7 kPa
Initial Modulus (E_U):	2750 kPa
◆ End of Linear Elasticity (p', q):	38.4, 35.0 kPa
Pore pressure parameter a:	0.319
✖ Fibre Reinforced Critical State (p', q):	31.5, 59.3 kPa
Critical State Strain Hardening Modulus:	65.9 kPa
● Frictional Critical State (q):	54.0 kPa

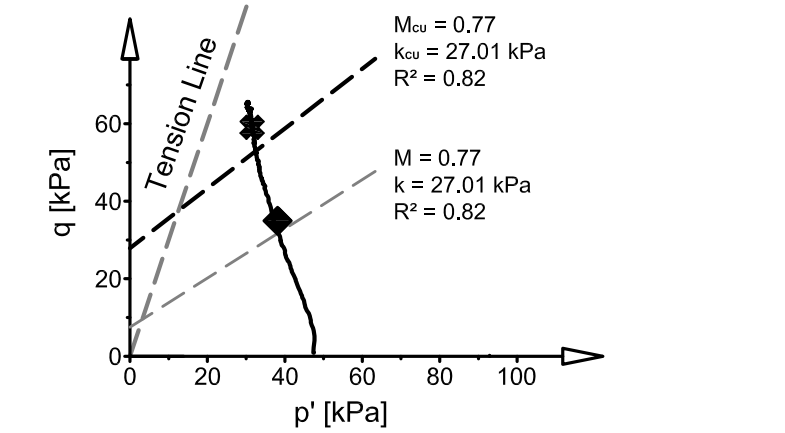

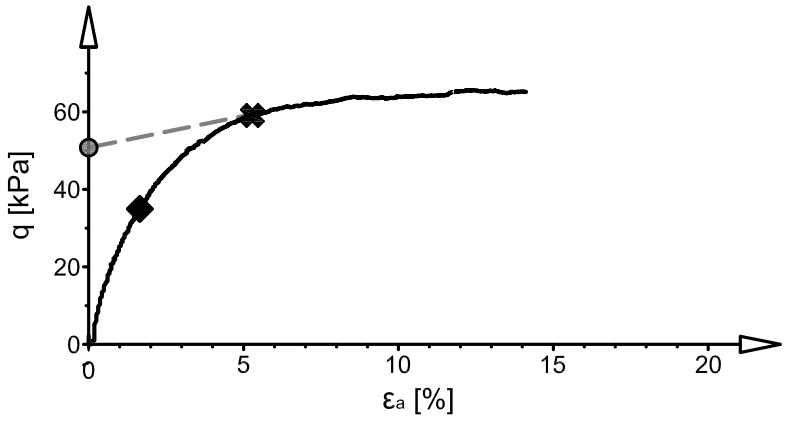

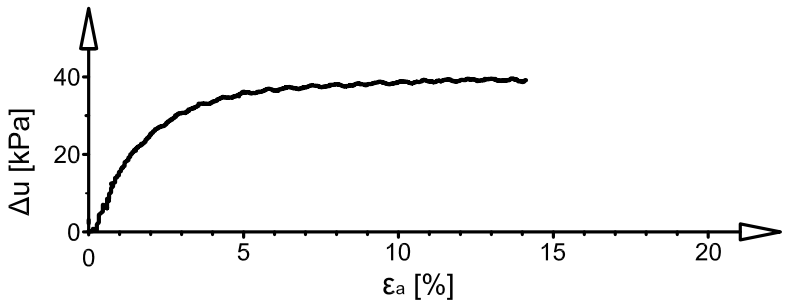

CU Testing of Edson Shelby Specimen with a p'_0 of 73 kPa

CU Testing

Sample source:	Bore hole 8; 4.6 m depth
Trimmed Specimen Length:	131 mm
Specimen diameter:	70.3 mm
Specimen mass:	436 g
Preconsolidation pressure (p'_0):	72.5 kPa
Initial Modulus (E_U):	2790 kPa
◆ End of Linear Elasticity (p', q):	58.2, 42.3 kPa
Pore pressure parameter a:	0.312
✖ Fibre Reinforced Critical State (p', q):	52.6, 65.3 kPa
Critical State Strain Hardening Modulus:	151 kPa
● Frictional Critical State (q):	63.0 kPa

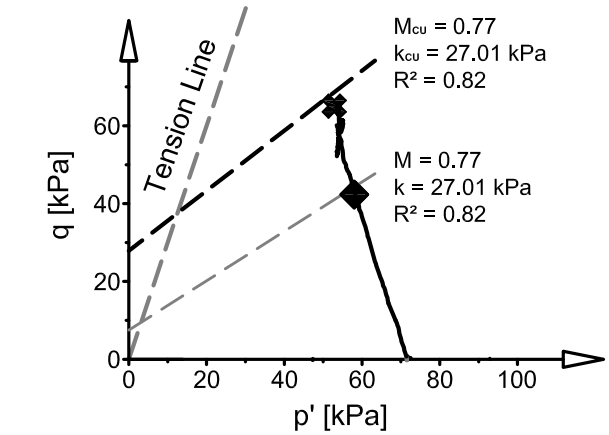

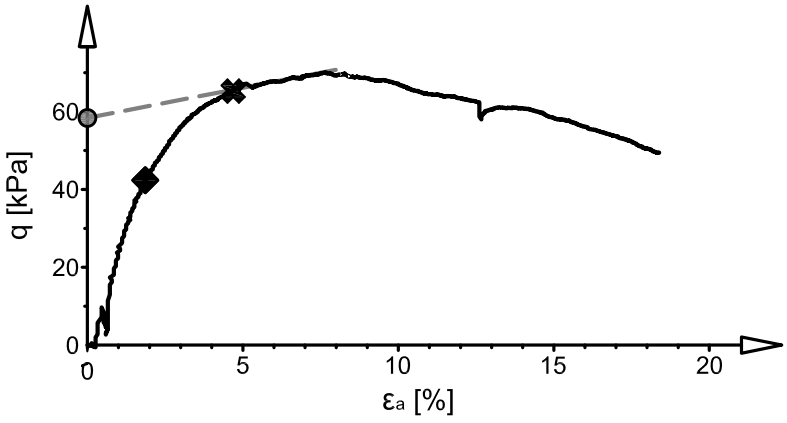

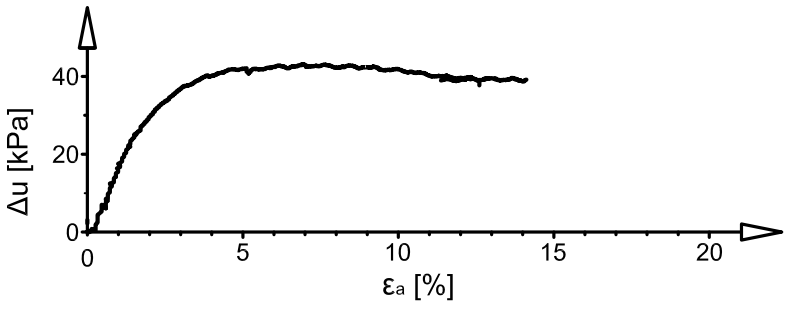

Appendix C: Results from laboratory testing of peat specimens

Summary of CU Testing of Edson Shelby Specimens

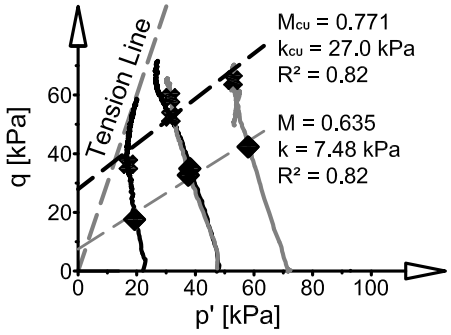

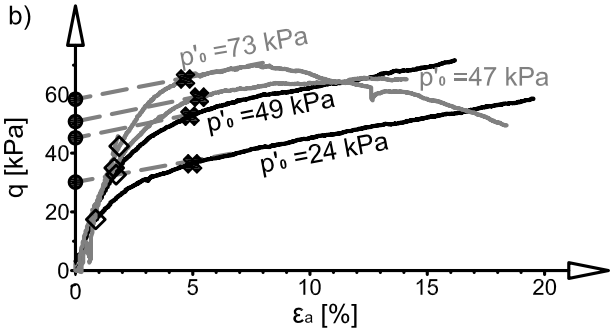

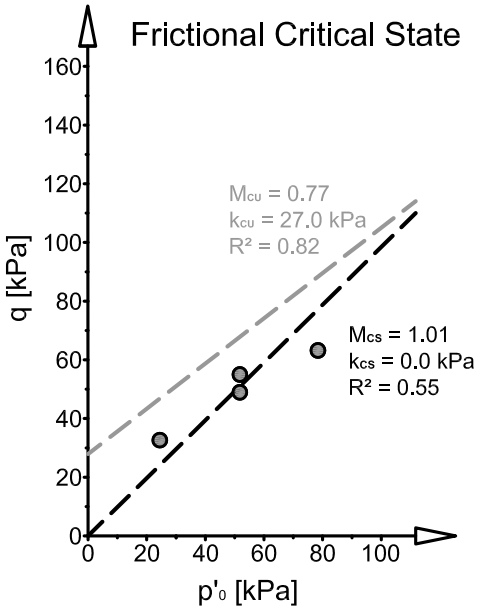

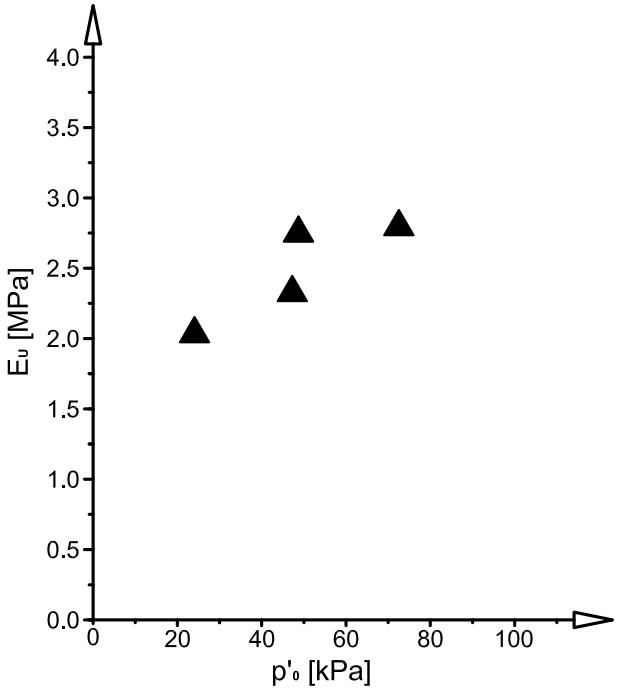

Reinforced Strength	Frictional Strength	End of Linear Elasticity
Mcu : 0.771	Mcs : 1.01	M : 0.735
kcu : 27.0 kPa	kcs : 0.0 kPa	k : 7.48 kPa
Φ'cu : 20°	Φ'cs : 26°	Φ' : 19°
c'cu : 12.7 kPa	c'cs : 0.0 kPa	c' : 3.53 kPa

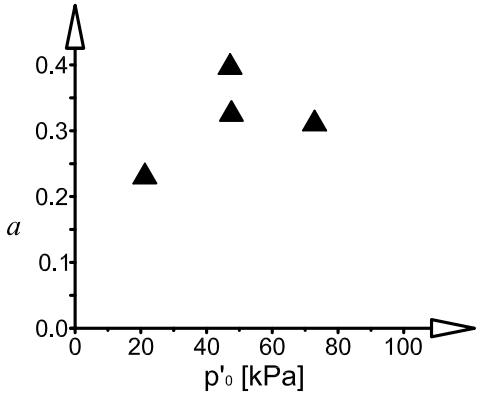

CU Testing of Anzac Shelby Specimen with a p'_0 of 29 kPa

CU Testing

Sample source:	Bore hole 2; 2.3 m depth
Trimmed Specimen Length:	152 mm
Specimen diameter:	71.7 mm
Specimen mass:	465 g
Preconsolidation pressure (p'_0):	29.0 kPa
Initial Modulus (E_U):	1800 kPa
◆ End of Linear Elasticity (p', q):	21.1, 28.0 kPa
Pore pressure parameter a:	0.250
✖ Fibre Reinforced Critical State (p', q):	20.1, 36.8 kPa
Critical State Strain Hardening Modulus:	244 kPa
● Frictional Critical State (q):	31.0 kPa

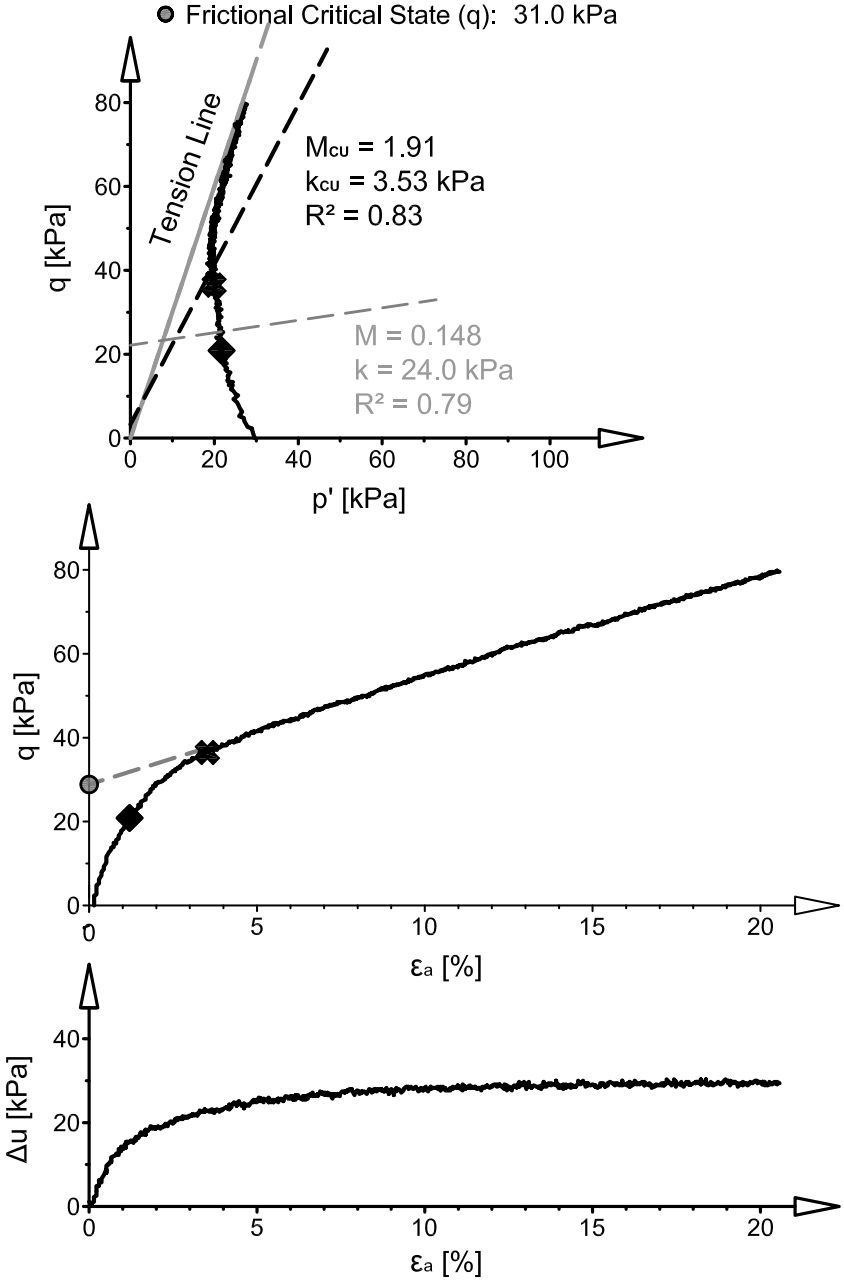

CU Testing of Anzac Shelby Specimen with a p'_0 of 41 kPa

CU Testing

Sample source:	Bore hole 2; 2.3 m depth
Trimmed Specimen Length:	149 mm
Specimen diameter:	72.1 mm
Specimen mass:	578 g
Preconsolidation pressure (p'_0):	40.7 kPa
Initial Modulus (E_U):	2870 kPa
◆ End of Linear Elasticity (p', q):	35.1, 27.7 kPa
Pore pressure parameter a:	0.286
✖ Fibre Reinforced Critical State (p', q):	28.0, 66.0 kPa
Critical State Strain Hardening Modulus:	236 kPa
● Frictional Critical State (q):	42.0 kPa

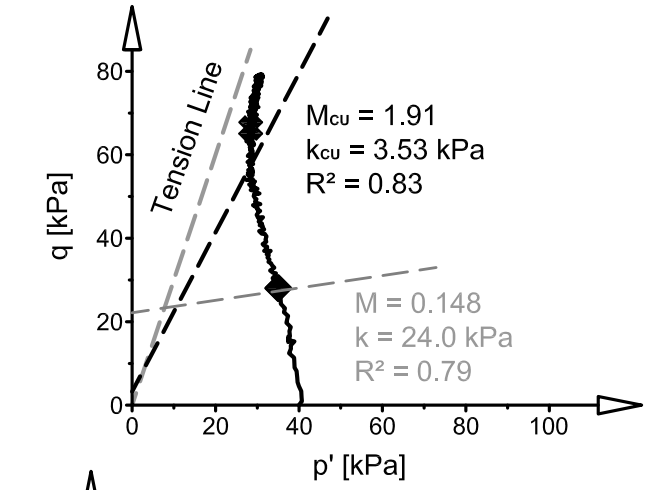

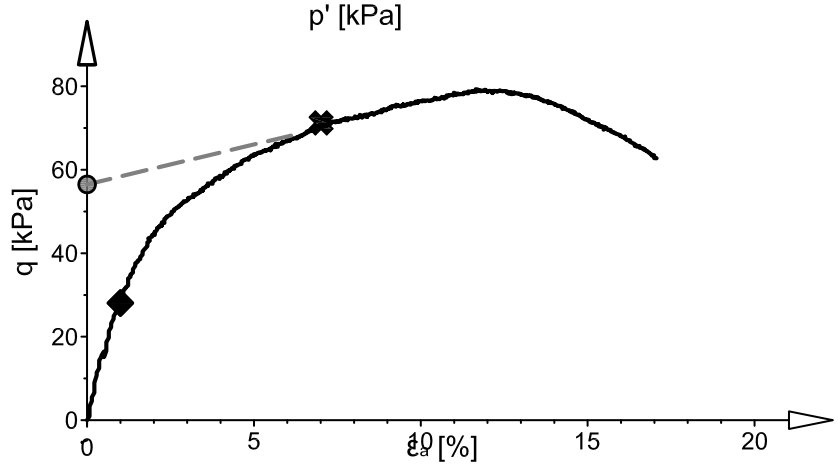

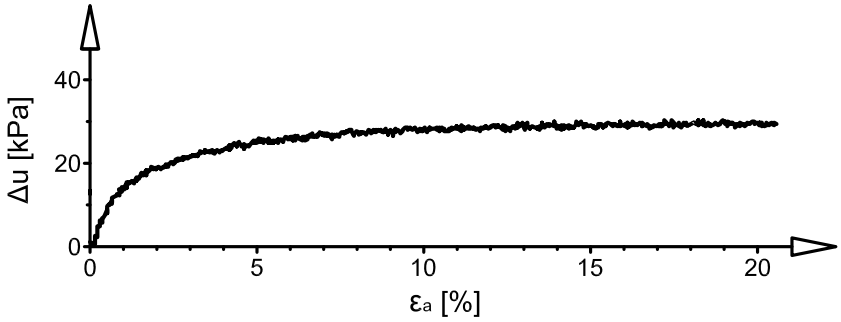

CU Testing of Anzac Shelby Specimen with a p'_0 of 51 kPa

CU Testing

Sample source:	Bore hole 2; 3.3 m depth
Trimmed Specimen Length:	156 mm
Specimen diameter:	71.9 mm
Specimen mass:	601 g
Preconsolidation pressure (p'_0):	50.6 kPa
Initial Modulus (E_U):	2950 kPa
◆ End of Linear Elasticity (p', q):	55.3, 32.8 kPa
Pore pressure parameter a:	0.385
✖ Fibre Reinforced Critical State (p', q):	38.0, 72.0 kPa
Critical State Strain Hardening Modulus:	65.6 kPa
● Frictional Critical State (q):	69.0 kPa

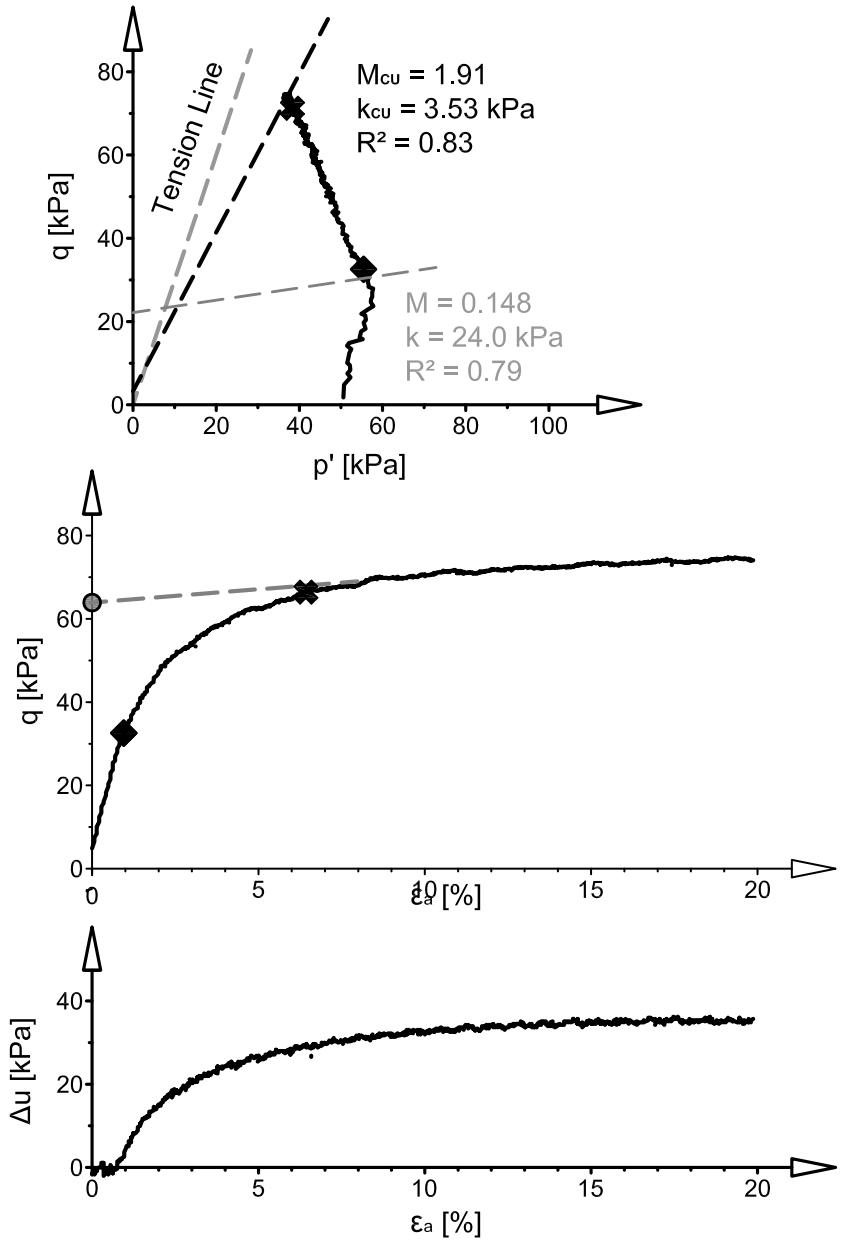

Appendix C: Results from laboratory testing of peat specimens

Summary of CU Testing of Anzac Shelby Specimens

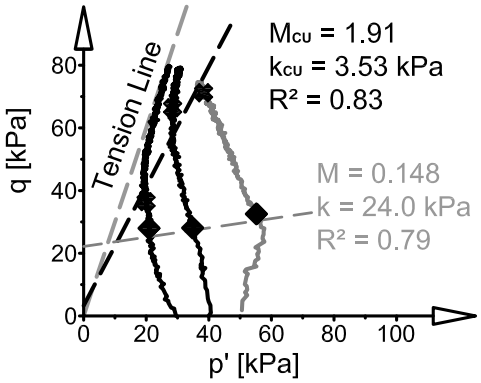

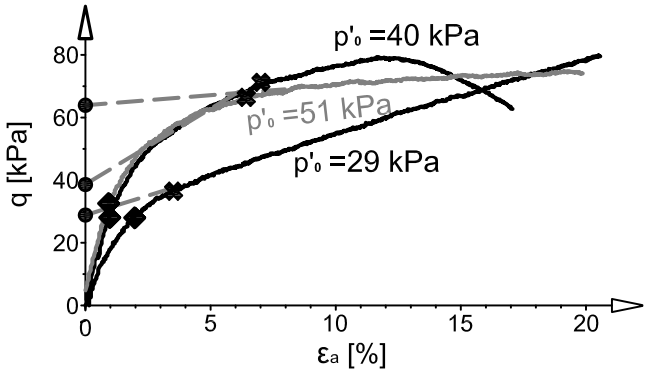

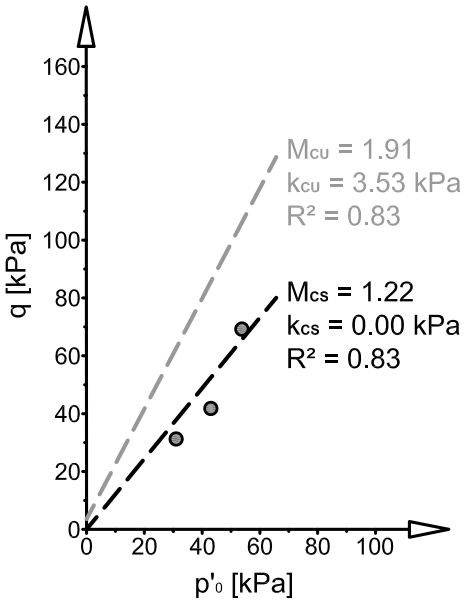

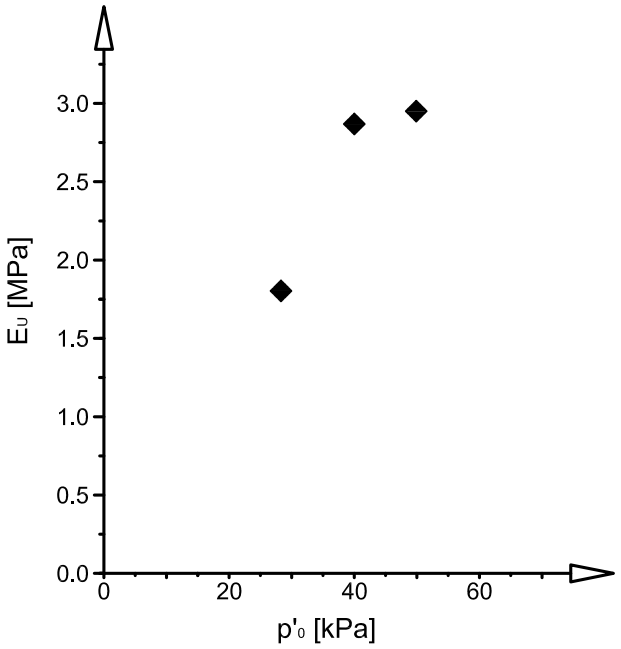

Reinforced Strength	Frictional Strength	End of Linear Elasticity
Mcu : 1.91	Mcs : 1.22	M : 0.148
kcu : 3.53 kPa	kcs : 0.00 kPa	k : 24.0 kPa
Φ'cu : 46°	Φ'cs : 30°	Φ' : 4°
c'cu : 1.94 kPa	c'cs : 0.00 kPa	c' : 11.74 kPa

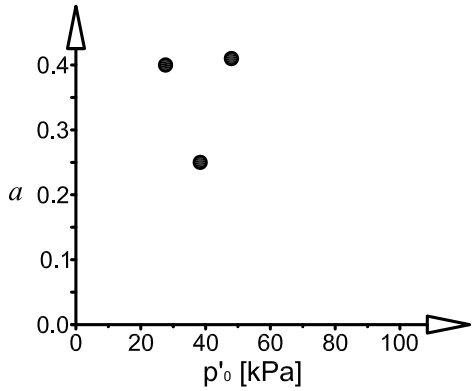

Appendix C: Results from laboratory testing of peat specimens

Summary of CU Testing of Lévis Shelby Specimens

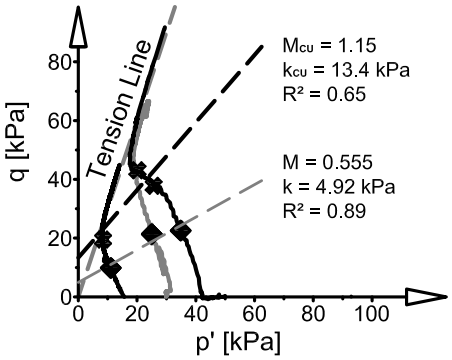

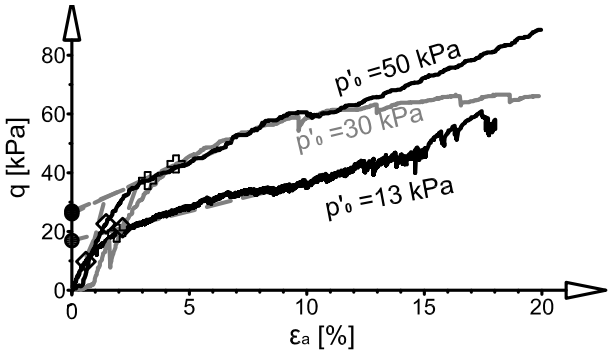

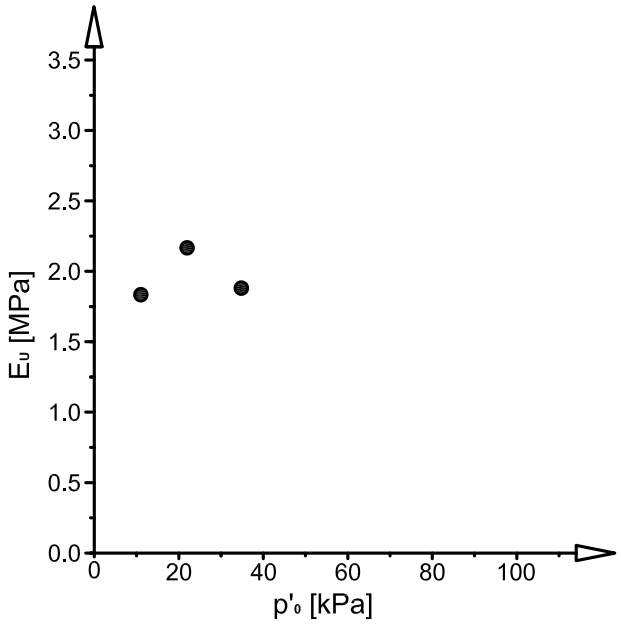

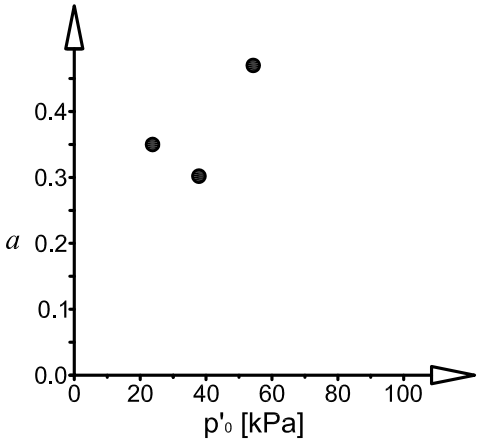

Reinforced Strength	End of Linear Elasticity
M_{cu} : 1.15	M : 0.555
k_{cu} : 13.4 kPa	k : 4.92 kPa
Φ'_{cu} : 29°	Φ' : 15°
c'_{cu} : 6.42 kPa	c' : 2.33 kPa

Appendix D: Finite element modelling of embankments

This appendix provides a record of the Finite Element Modelling conducted during the course of this study. This modelling includes: the calculation of the *in situ* stresses under the embankment without train loading used in Chapter 5 (Manuscript #3) and in the calculation of the stress mobilization factor for each embankment in as presented in Chapter 6 (Manuscript #4); the elastic deformation modelling to verify the pattern of deformation measured by the ShapeAccelArrays during the passage of trains as presented in Chapter 3 (Manuscript #1); and modelling of the effect of the addition of the berms to the Edson embankment on the strength of the structure.

Appendix D: Finite element modelling of embankments

D.1. Modelling of *In situ* Stresses

The *in situ* stresses were modelled using the GeoSlope software Sigma/W (GeoSlope 2007). The specific gravity used for the ballast and sand were estimated from typical values of 2.6. The specific gravity of the peat, and the peaty fill (in the Edson site Embankment) was estimated as 1.3, as was determined from the results of the laboratory testing of peat specimens retrieved from the Edson and Anzac sites (Chapter 4 and 5, Manuscripts #2 and #3). A presentation of the magnitude and spatial distribution of the mean total, mean effective and deviatoric stresses as modelled under the embankments are presented for all three sites below.

D.1.1. Edson site embankment

A model for the Edson embankment (Figure D.1) was developed from surface measurements taken at the site with GPS surveying equipment, and the stratigraphy was estimated from borehole logs (Appendix A). The water table is located at or very near the surface of the peat; this was evident from the ponded water on the surface and measurements from the strain gauge piezometers installed at the site.

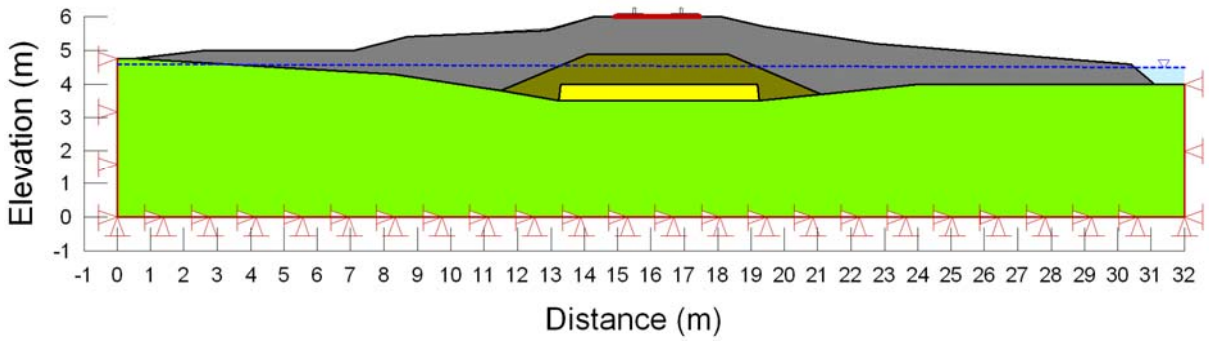

Figure D.1 : Model of the Edson embankment developed in the GeoSlope software Sigma/W.

The *in situ* initial (without train loading) stresses under the embankment were calculated in terms of the mean total stress (p) (Figure D.2), the mean effective stress (p') (Figure D.3), and the deviatoric stress (q) (Figure D.4). A plot of these stresses versus depth under the centreline of the embankment is shown in Figure D.5a. From Figure D.5a and the contour plots it is apparent that there is very little increase in mean effective stress and deviatoric stress with depth within the peat foundation. The mean effective stress and deviatoric stress range from 22 to 37 kPa and 7 to 12 kPa respectively. For the mean effective stress this is due to the very low specific gravity of

the peat, and for the deviatoric stress this is due to the width of the embankment and berms. The effect of the berms is modelled later in this Appendix in Section D.3. The stresses within the foundation are predominantly due to the weight of the embankment material.

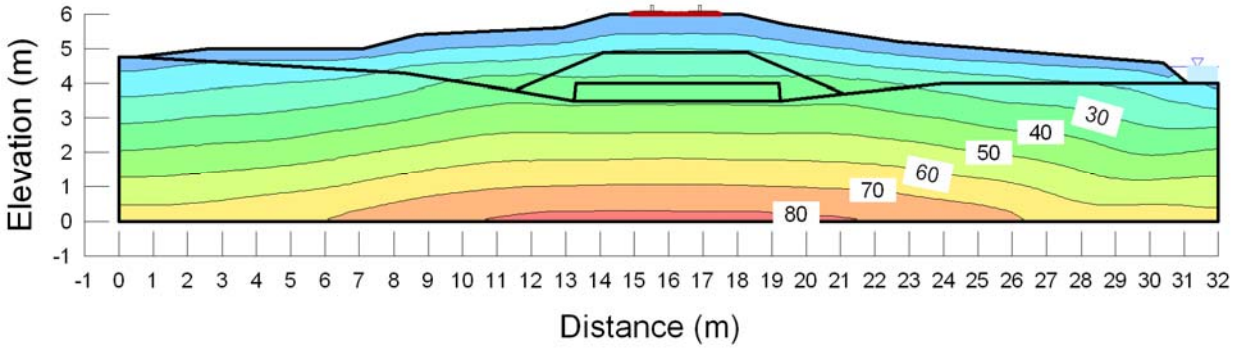

Figure D.2 : Modelled initial mean total stress (p) contours under the Edson embankment.

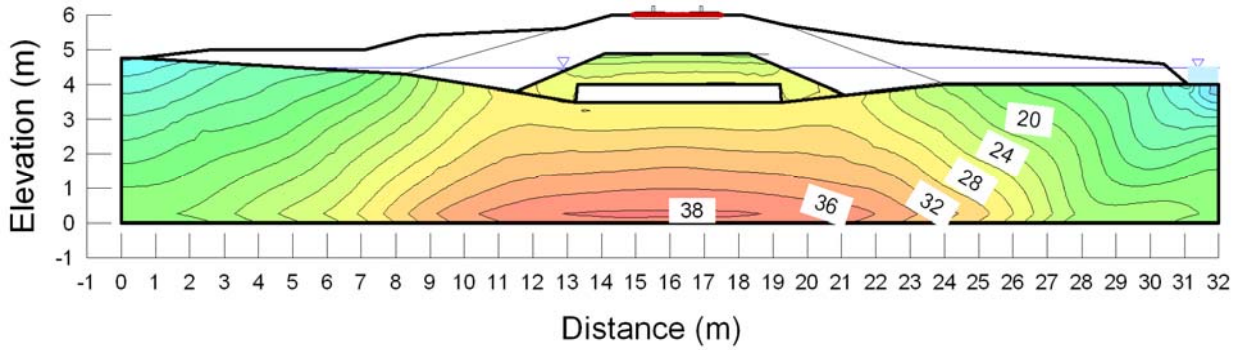

Figure D.3 : Modelled initial mean effective stress (p') contours under the Edson embankment.

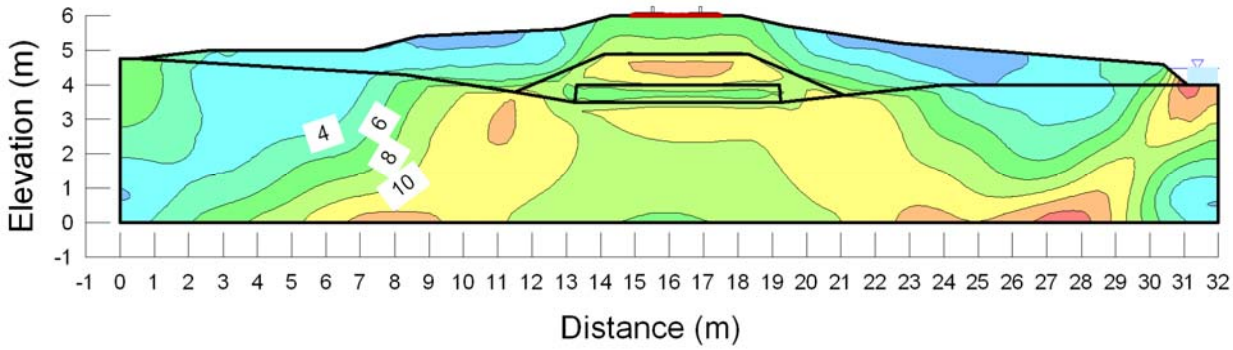

Figure D.4 : Modelled initial deviatoric stress (q) contours under the Edson embankment.

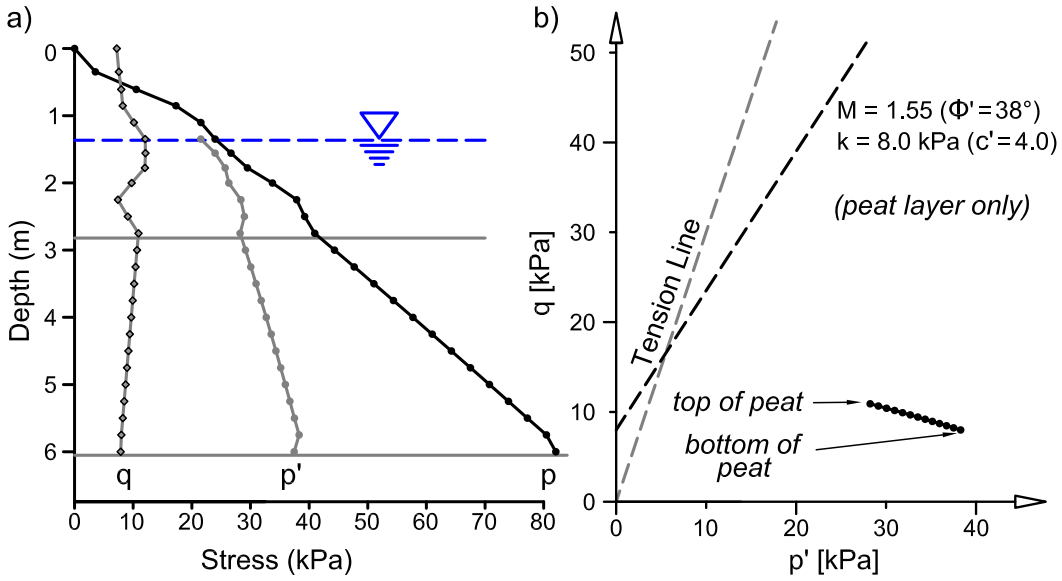

Figure D.5 : Modelled initial mean effective, mean total and deviatoric stresses (p', p, q) under the centerline of the Edson embankment plotted versus depth.

As presented in Chapter 5, the major principal stress directly under the train load is vertical and perpendicular to the horizontally orientated fibres and the resulting principal strains are expansive in the horizontal plane and will create tension in the reinforcing elements. This orientation of principal stresses and strains corresponds to the laboratory testing of the specimens from the site presented in Chapter 4 and 5. Thus the analysis of the stresses *in situ* relative to the strength of the peat developed in the laboratory can only be conducted directly under the axle loads, under the center line of the track. The *in situ* initial stress state modelled for the embankment and underlying peat foundation at the centerline of the embankment are presented in Figure D.5a, and are plotted in the p'q stress space with the yield surface in Figure D.5b.

D.1.2. Anzac site embankment

A model for the Anzac embankment (Figure D.6) was developed from measurements taken at the site, and the stratigraphy was estimated from borehole logs (Appendix A). The water table is located at or very near the surface of the peat; this was evident from the ponded water on the surface and measurements from the strain gauge piezometers installed at the site. As with the Edson embankment, the *in situ* initial (without train loading) stresses under the embankment were calculated in term of the mean total stress (p) (Figure D.7), the mean effective stress (p')

(Figure D.8), and the deviatoric stress (q) (Figure D.9). A plot of these stresses versus depth under the centreline of the embankment is shown in Figure D.10a. From Figure D.10a, and the contour plots, it is apparent that there is very little increase in mean effective stress with depth within the peat foundation. This is due to the very low specific gravity of the peat. The mean effective stress ranges from 20 to 26 kPa. The deviatoric stress has a higher variation than that found under the Edson site embankment, with a range of 6 to 14 kPa respectively.

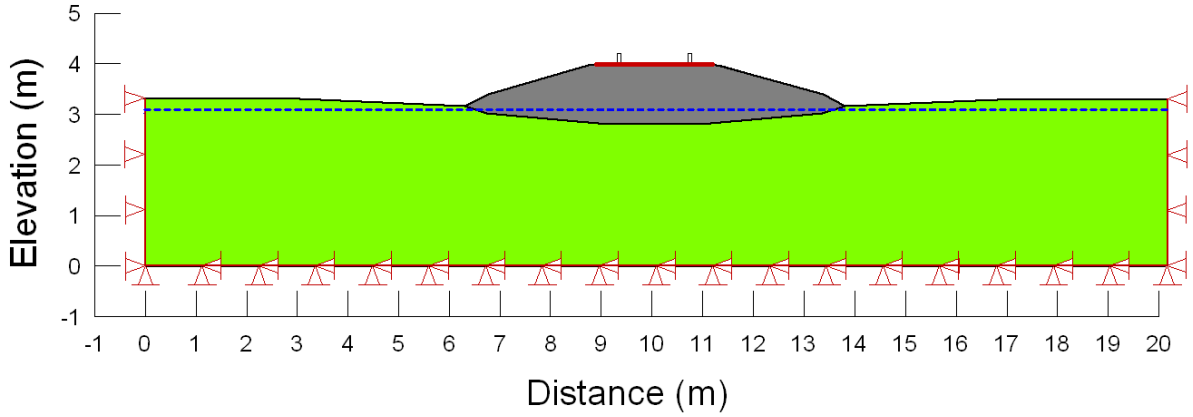

Figure D.6 : Model of the Anzac site embankment developed in the GeoSlope software Sigma/W.

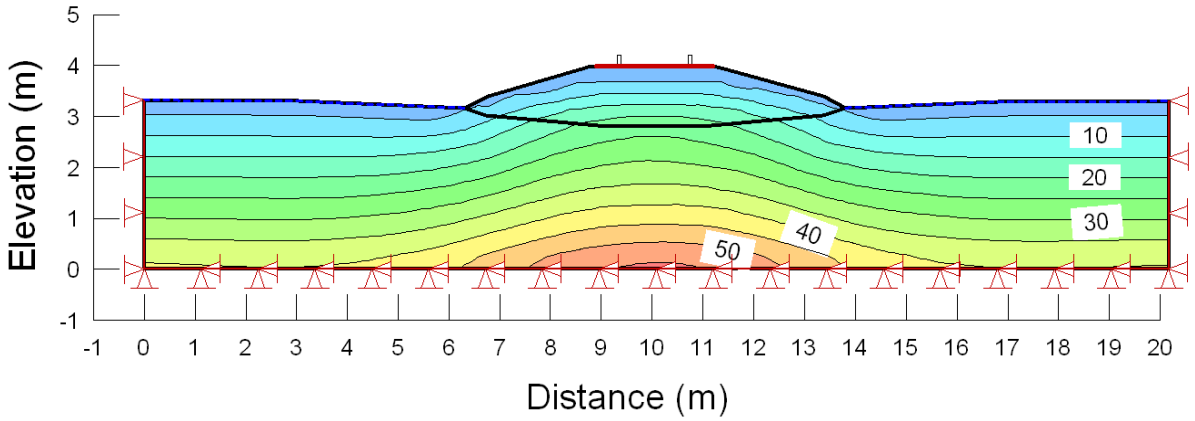

Figure D.7 : Modelled initial mean total stress (p) contours under the Anzac site embankment.

As was presented above in section D.1.1, the analysis of the stresses *in situ* relative to the strength of the peat developed in the laboratory can only be conducted directly under the axle loads, under the center line of the track. The *in situ* initial stress state modelled for the embankment and underlying peat foundation at the centerline of the embankment are presented in Figure D.10a, and are plotted in the p'q stress space with the yield surface in Figure D.10b.

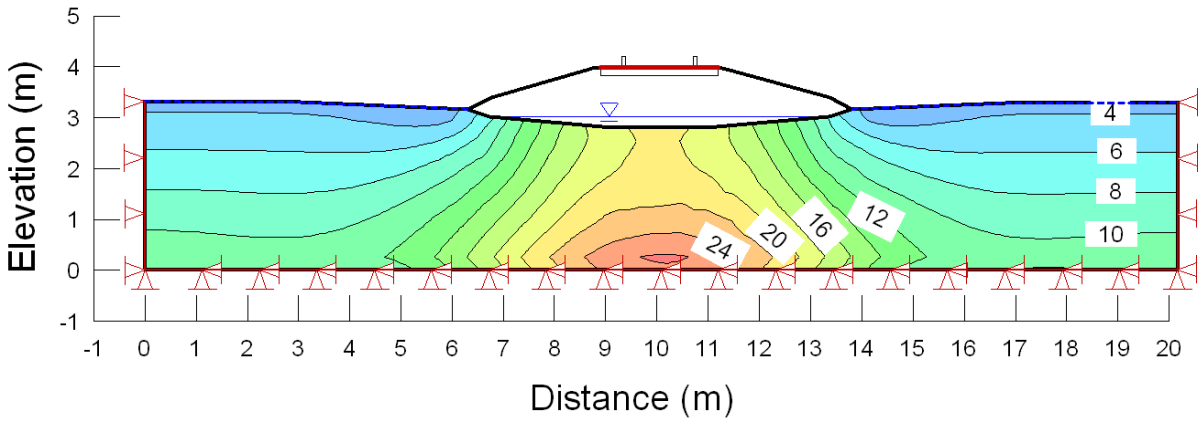

Figure D.8 : Modelled initial mean effective stress (p') contours under the Anzac site embankment.

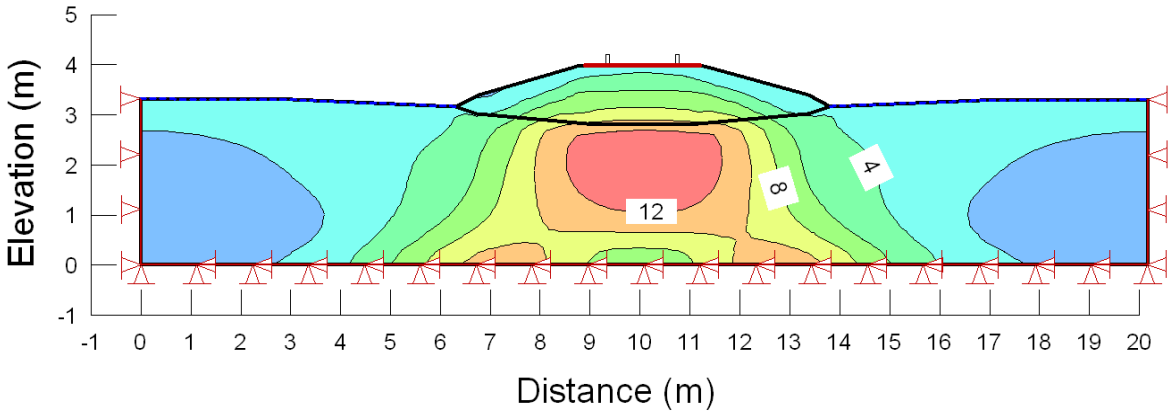

Figure D.9 : Modelled initial deviatoric stress (q) contours under the Anzac embankment.

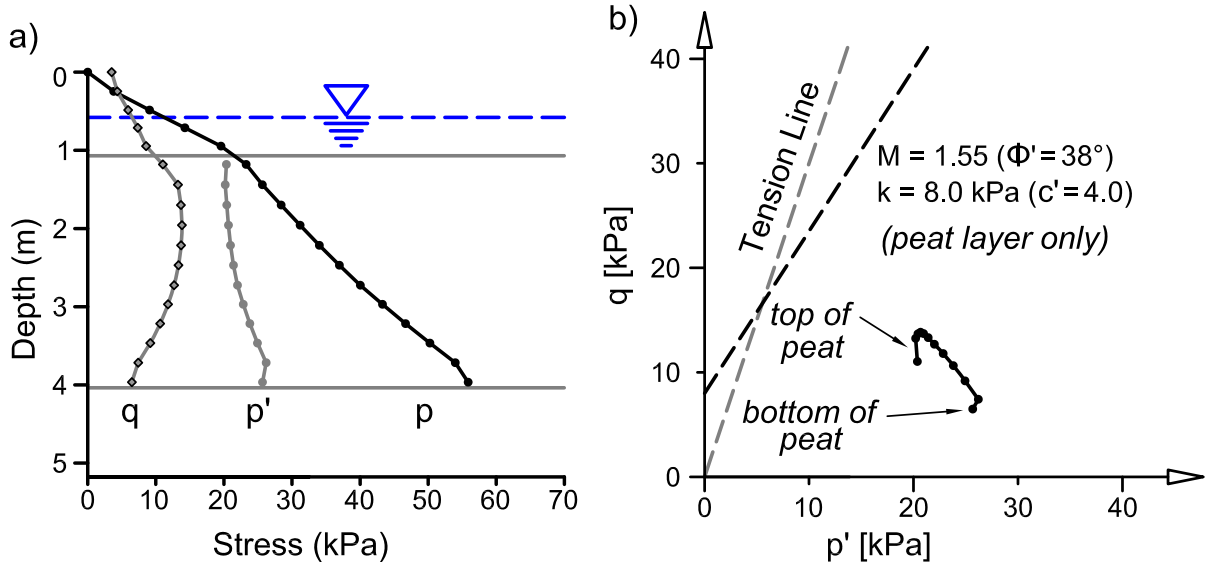

Figure D.10 : Modelled initial mean effective, mean total and deviatoric stresses (p', p, q) under the centerline of the Anzac site embankment plotted versus depth.

D.1.3. Lévis site embankment

A model for the Lévis embankment (Figure D.11) was developed from the cross-section presented in Konrad et al. (2007). As with the Edson embankment, the *in situ* initial (without train loading) stresses under the embankment were calculated in terms of the mean total stress (p) (Figure D.12), the mean effective stress (p') (Figure D.13), and the deviatoric stress (q) (Figure D.14). A plot of these stresses versus depth under the centreline of the embankment is shown in Figure D.15a. From Figure D.15, and the contour plots, it is apparent that there is very little increase in mean effective stress with depth within the peat foundation. This is due to the very low specific gravity of the peat. The mean effective stress ranges from 34 to 40 kPa. The deviatoric stress has a higher variation than that found under the Edson and Anzac embankments, with a range of 10 to 22 kPa respectively.

As was presented above in section D.1.1, the analysis of the stresses *in situ* relative to the strength of the peat developed in the laboratory can only be conducted directly under the axle loads, under the center line of the track. The *in situ* initial stress state modelled for the embankment and underlying peat foundation at the centerline of the embankment are presented in Figure D.15a, and are plotted in the p'q stress space with the yield surface in Figure D.15b.

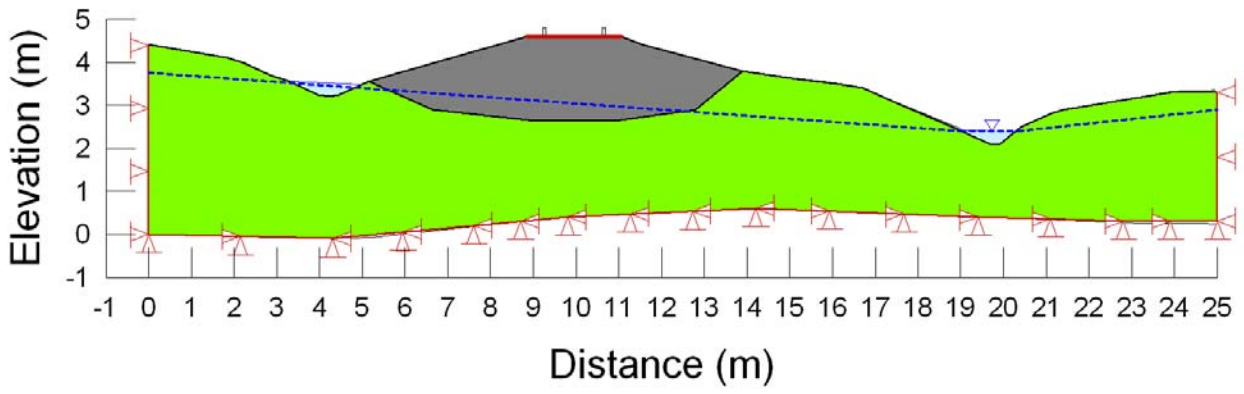

Figure D.11 : Model of the Lévis site embankment developed in the GeoSlope software Sigma/W.

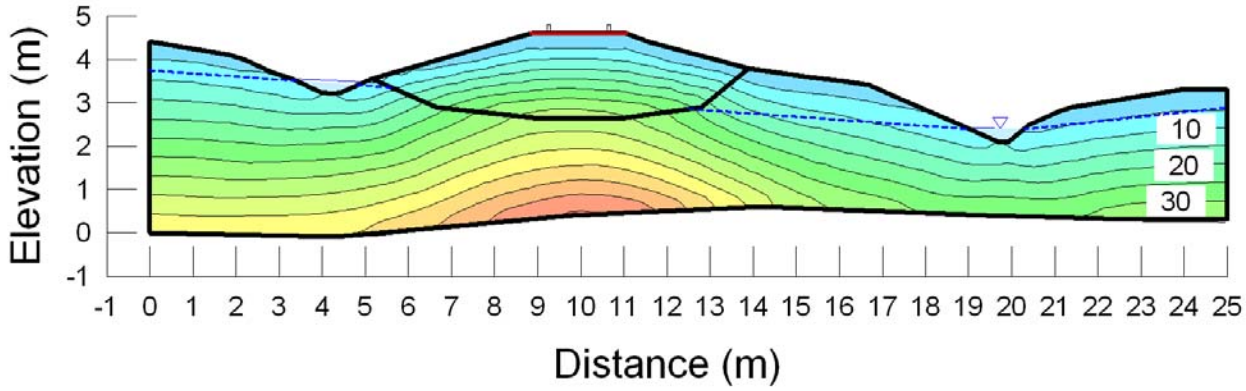

Figure D.12 : Modelled initial mean total stress (p) contours under the Anzac site embankment.

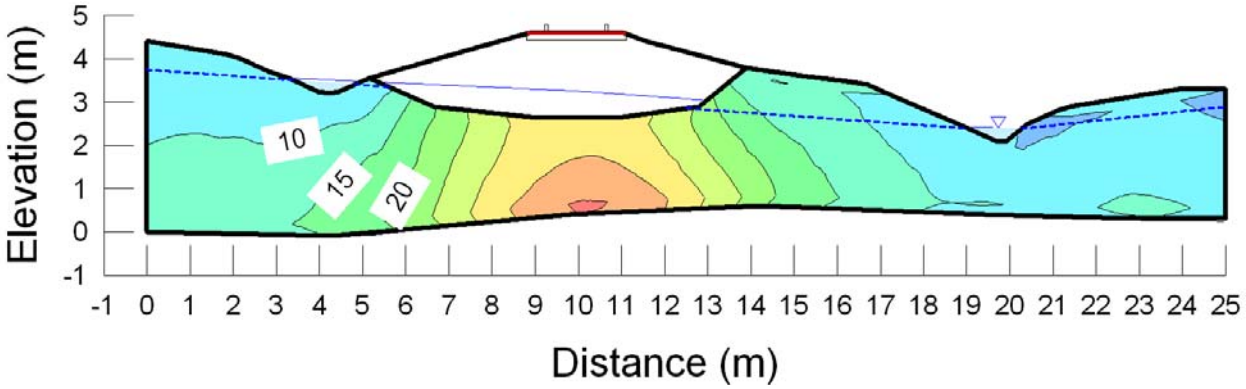

Figure D.13 : Modelled initial mean effective stress (p') contours under the Anzac site embankment.

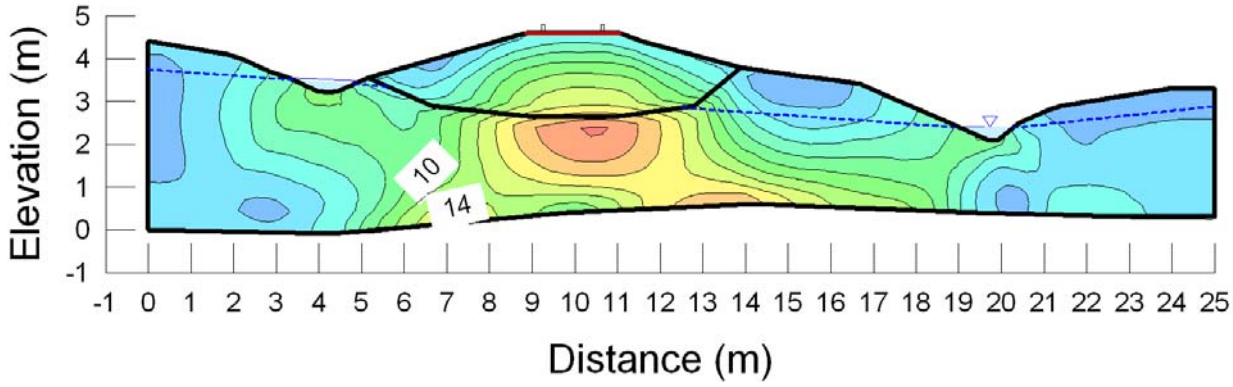

Figure D.14 : Modelled initial deviatoric stress (q) contours under the Lévis site embankment.

Appendix D: Finite element modelling of embankments

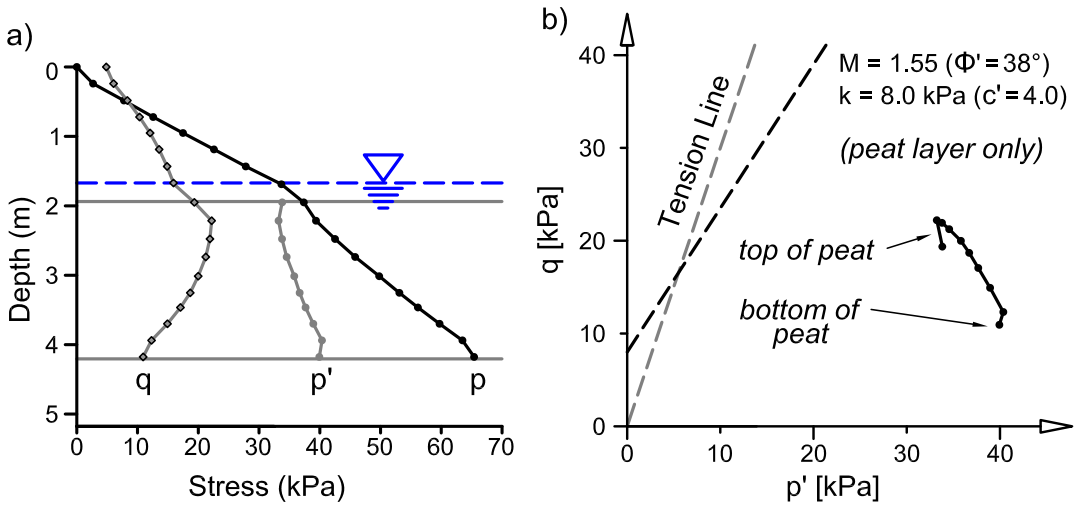

Figure D.15 : Modelled initial mean effective, mean total and deviatoric stresses (p', p, q) under the centerline of the Lévis site embankment plotted versus depth.

D.2. Modelling of Horizontal Displacements

The horizontal displacements due to train loading were modelled for the Edson site embankment and peat foundation. This modelling was restricted to very simple linear isotropic elastic models to explore the nature of the displacement profile with depth as measured by the ShapeAccelArrays (SAA) installed at both sites. This was presented within Chaper 3 (Manuscript #1). The elastic anisotropic behaviour of the peat is not included in this analysis, thus the distribution of pore pressure generation and stresses are not modelled completely. There is further reduction of the accuracy of the results from the use of a two dimensional plane strain model for the calculation of the stress distribution in an essentially three dimensional problem, as modelled in Hall (2000) and shown in the SAA measurement from both instrumented sites. Thus, the results of this analysis are limited to verify the plausibility of the measurements obtained from the SAA in the field, and to explaining the shape of the profile and the boundary conditions required for this shape.

The model used for the embankment at the Edson site was developed from the model described above for the modelling of the *in situ* initial stresses. The train loading was applied as a distributed stress boundary condition. From a Winkler model of the displacements from the measured axle loads, the maximum load distributed to the surface of the embankment from the rail track structure is 43 kPa (Figure D.16). The modulii for the ballast, subballast and gravel

berms was approximated as 160 MPa. Beam elements were used to model the effect of the ties and the corduroy timbers. The moduli of the peat and peaty fill material were determined by fitting the magnitude of the displacements to that measured by the SAA. These modulii were found to be approximately 3 MPa for the peat and 1.5 MPa for the peaty fill material.

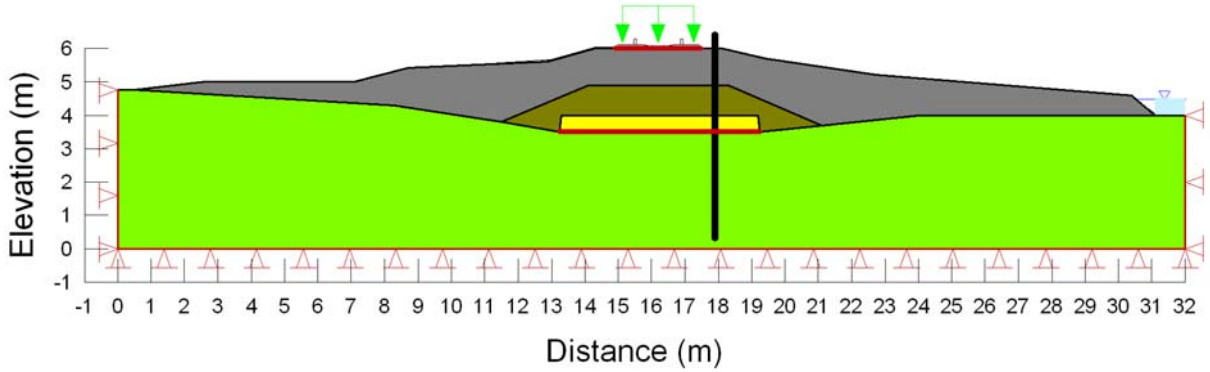

Figure D.16 : Model of the Edson embankment developed in the GeoSlope software Sigma/W with train load applied as a distributed load on surface of embankment.

The pattern of cyclic displacement measured with the SAA is consistent with results from finite element modelling of the Edson site embankment (Figure D.17) using a simple linear elastic soil. The lower peat foundation material was found to spread laterally during the undrained (fast) loading, consistent with an undrained soil acting as an elastic solid. The embankment materials were measured and modelled to be rotating inwards with the formation of a deflection bowl on the surface. The near linear displacement with depth within the ballast layer is due to the stiffness of the ballast material, and the contrast between this stiffness and that of the peat fill material. The measured peat responses in both perpendicular and parallel directions are very similar both in shape and magnitude. Considering the stiffness and negligible vertical strain (as measured with the extensometers) of the silty clay base, the cyclic displacement of the deepest MEMS accelerometer suggests that there is a zone of significant shear at or near the interface between the peat layer and the underlying silty clay. This is represented in the model by allowing the base of the peat to move freely in the horizontal direction.

D.3. Modelling of Effect of Berm Addition to Edson Embankment

Part of the 1998 remediation of the embankment conducted on the Edson site embankment was the installation of berms along the full length of the embankment. From personal conversations

with senior geotechnical engineers at both CN and CP this is a common and historically used method for the remediation of unstable embankments over peat foundations. These increases in the stability and stiffness of the embankments due to the addition of berms has been attributed to the consolidation of the peat material and the resulting increase in the strength and stiffness properties of the peat. This is explanation is strongly based on experience with construction over peat (presented in Chaper 2). An alternative explanation as to the effect of the addition of the berms has on the stability and stiffness of the peat foundations may be due to the resulting change in initial *in situ* stresses.

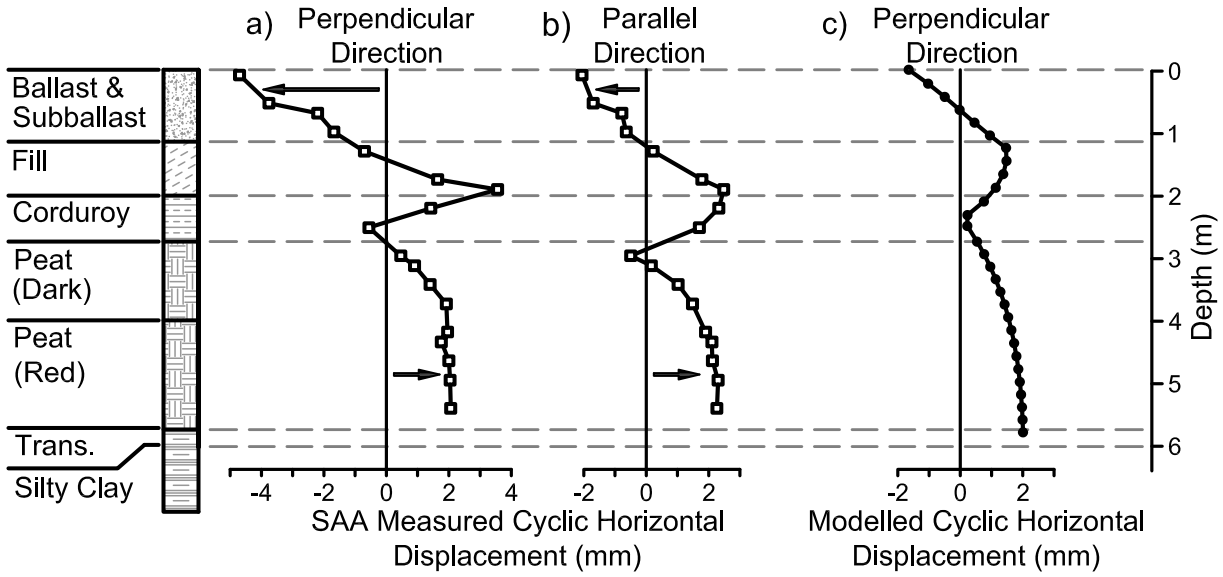

Figure D.17 : Model of the Edson embankment developed in the GeoSlope software Sigma/W.

This change in initial stresses was modeled using GeoSlope software Sigma/W for the Edson site embankment. The basis of the modelling was to determine the effect of the initial stresses and the stress mobilization factor under the Edson embankment before the addition of the berms and compare this to the stresses and the stress mobilization factor under the Edson embankment after the installation of the berms. For this analysis the model used for determining the stresses under the Edson site embankment in Section D.1.1 was modified by removing the berms on either side of the embankment as shown in Figure D.18. The *in situ* initial stresses under the embankment were re-calculated in terms of the mean total stress (p) (Figure D.19), the mean effective stress (p') (Figure D.20), and the deviatoric stress (q) (Figure D.21).

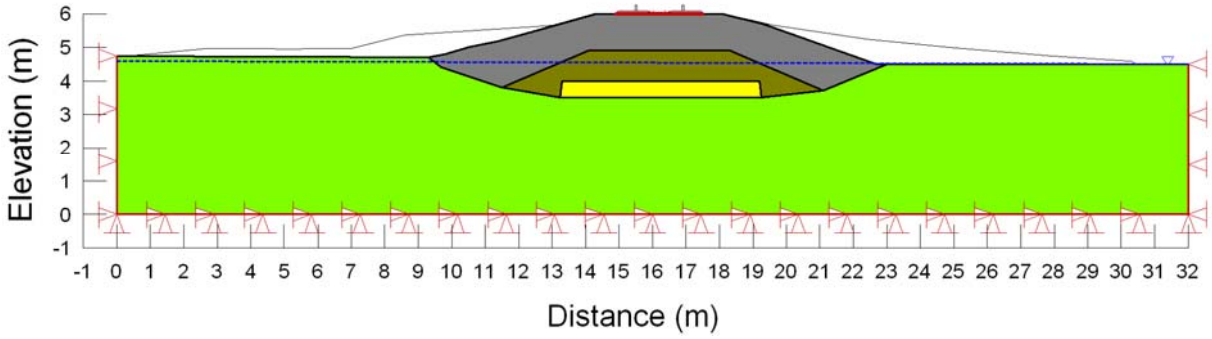

Figure D.18 : Model of the Edson embankment developed in the GeoSlope software Sigma/W with berm removed.

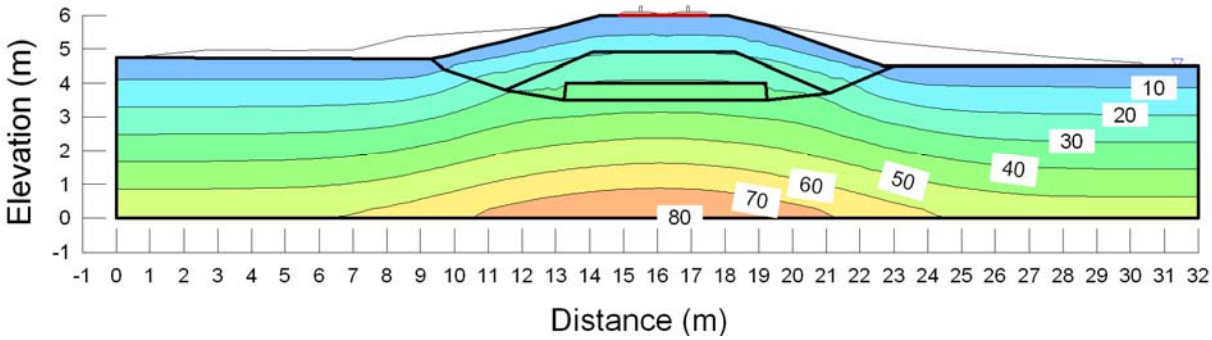

Figure D.19 : Modelled initial mean total stress (p) contours under the Edson embankment before the addition of the berms.

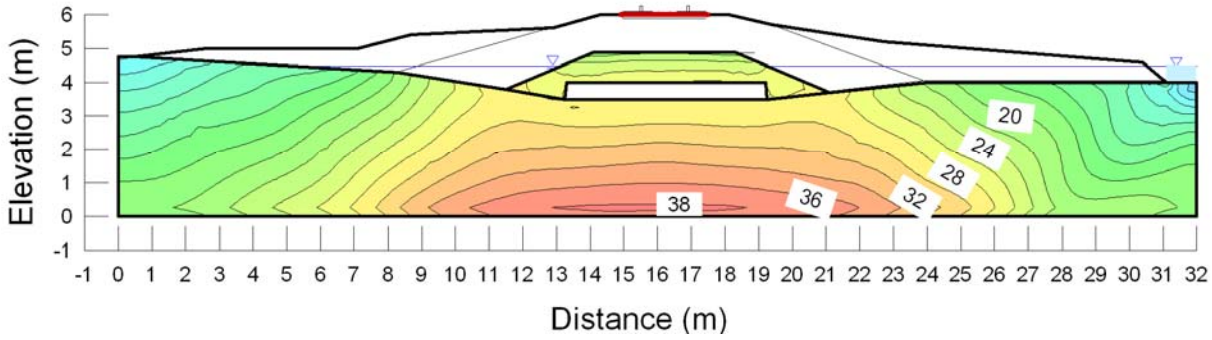

Figure D.20 : Modelled initial mean effective stress (p') contours under the Edson embankment before the addition of the berms.

As presented in above in section D.1.1, the major principal stress directly under the train load is vertical and perpendicular to the horizontally orientated fibres and the resulting principal strains are expansive in the horizontal plane and will create tension in the reinforcing elements. This orientation of principal stresses and strains corresponds to the laboratory testing of the specimens

from the site presented in Chapter 4. Thus the analysis of the stresses relative to the strength of the peat developed in the laboratory can only be conducted directly under the axle loads, under the centerline of the track. The *in situ* initial stress state modelled for the Edson embankment without the berms is plotted alongside the modelled stress state for the Edson embankment with berms in Figure D.22.

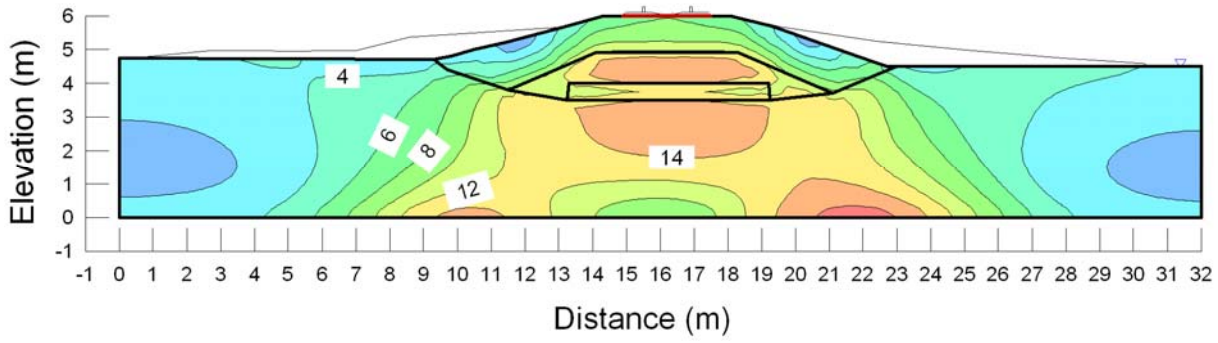

Figure D.21 : Modelled initial deviatoric stress (q) contours under the Edson embankment before the addition of the berms.

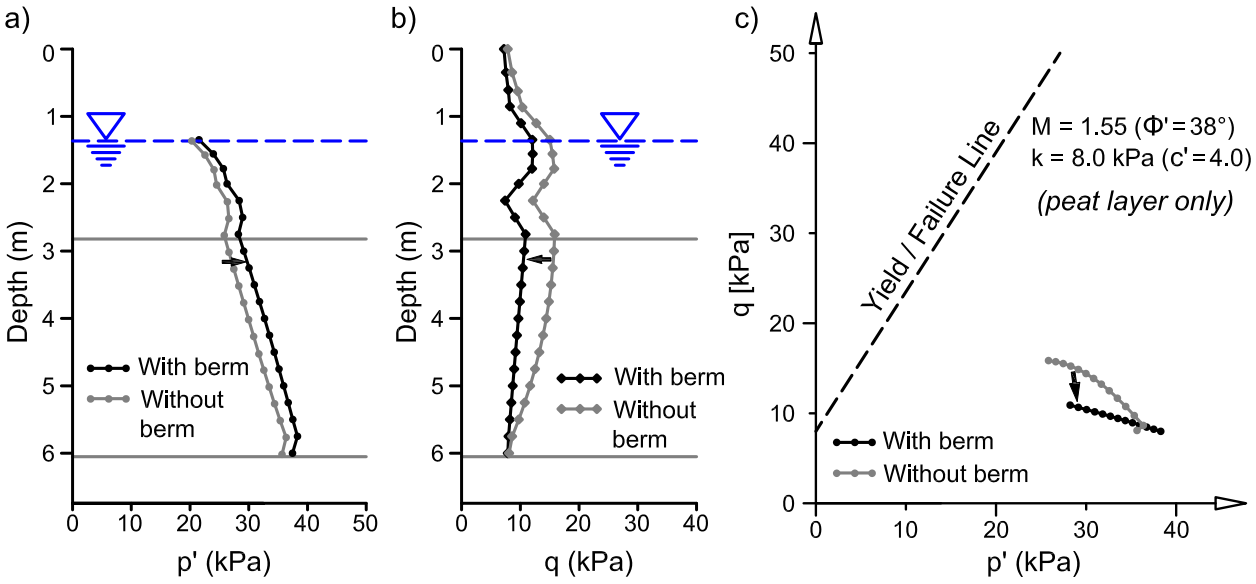

Figure D.22 : Plots showing the modeled change in initial stress state of the peat under the Edson embankment due to the addition of the berms; a) showing the mean effective stress; b) shows the deviatoric stress; c) shows the change in stress state in relative to the yield surfaces from the laboratory testing of the Edson peat.

The modelled result of the addition of the berms to the Edson embankment is a reduction of the initial shear (deviatoric) stresses by up to 33% (Figure D.22a) within the peat layer, accompanied

by an increase in mean effective stress up to 9.0% (Figure D.22b). The addition of the berm is estimated to have decreased the stress mobilization factor (SM) by 38 %; from 18 % for the embankment without a berm to 11 % with the berm.

References

GeoSlope International, Ltd. (GeoSlope) (2007). GeoStudio 2007: SIGMA/w (Version 7.17) [Computer software]. Calgary, Alberta, Canada. Available from http://www.geo-slope.com/